Report Prepared for:

National Oceanic and Atmospheric Administration/National Ocean Service
Coast Survey Development Laboratory, Office of Coast Survey

Mesh Development, Tidal Validation, and Hindcast Skill Assessment of an ADCIRC Model for the Hurricane Storm Surge Operational Forecast System on the US Gulf-Atlantic Coast

Global Science Solutions

Submitted by:

RIVERSIDE
global science solutions

In Association With:

AECOM

Riverside Technology, inc.
2950 E. Harmony Road, Suite 390
Fort Collins, Colorado 80528
970.484.7573
www.riverside.com

TABLE OF CONTENTS

Table of Contents i

List of Figures iv

List of Tables ix

List of Acronyms and Abbreviations x

1. Executive Summary 11

2. Introduction 12

3. Mesh Development 13

3.1 Model Boundary 13

3.2 Topography and Bathymetry Data Sources 14

3.3 ADCIRC Mesh 15

3.4 Elevation Assignment 17

3.5 Datum Conversion 17

4. ADCIRC Model Development 19

4.1 Fort.15 Model Control File 19

4.2 Fort.13 Nodal Attribute File 21

4.2.1 Primitive Weighting in Continuity Equation 21

4.2.2 Formulation of Land Use-Dependent Parameters 21

4.2.3 Land Use Data Sources 22

4.2.4 Manning's n at Sea Floor 23

4.2.5 Surface Canopy Coefficient 23

4.2.6 Surface Directional Effective Roughness Length (z_0) 23

5. Astronomical Tide Scenario 26

5.1 Harmonic Forcings and Validation Data 26

5.2 Astronomical Tide Validation 26

5.2.1 Harmonic Constituent Amplitude Skill 26

5.2.2 Harmonic Constituent Phase Skill 29

5.2.3 Effect of Advection Terms 31

5.3 Overall Tidal Skill 33

6. Storm Hindcast Validation 35

6.1 Typical Model Setup 35

6.2 Ike (2008) 38

6.2.1 Model Setup 38

6.2.2 Results and Skill Assessment 39
6.3 Katrina (2005) 47
6.3.1 Model Setup 47
6.3.2 Results and Skill Assessment 48
6.4 Dennis (2005) 52
6.4.1 Model Setup 52
6.4.2 Results and Skill Assessment 53
6.5 Charley (2004) 58
6.5.1 Model Setup 58
6.5.2 Results and Skill Assessment 59
6.6 Hugo (1989) 64
6.6.1 Model Setup 64
6.6.2 Results and Skill Assessment 65
6.7 Floyd (1999) 71
6.7.1 Model Setup 71
6.7.2 Results and Skill Assessment 74
6.8 Isabel (2003) 78
6.8.1 Model Setup 78
6.8.2 Results and Skill Assessment 79
6.9 Sandy (2012) 84
6.9.1 Model Setup 84
6.9.2 Results and Skill Assessment 85
6.10 Long Island Express (1938) 92
6.10.1 Model Setup 92
6.10.2 Results and Skill Assessment 93
6.11 Perfect Storm (1991) 98
6.11.1 Model Setup 98
6.11.2 Results and Skill Assessment 99
7. Results for All Hindcast Events 104
8. Conclusions and Recommended Next Steps 110
9. Acknowledgments 114
10. References 115
11. APPENDIX A – Model Domain Development 117

11.1 ADCIRC Mesh Boundary Data Sources 118
11.2 ADCIRC Mesh Boundary Development and Modification 119
11.3 Connections with River Models 127
12. APPENDIX B – Development of Topo-Bathy Data and of Mesh 135
12.1 Data Sources 135
12.2 Datum Conversion 139
12.3 Meshing Methodology 141
12.4 Base Meshes 141
12.5 Flow Path Guidance 147
12.6 Flow Barrier Guidance 152
12.7 Topographic Peak Elevation Assignment 152
12.8 General Elevation Assignment 153
12.9 Final Mesh 153
12.9.1 NOMAD mesh topo-bathymetry 154
12.9.2 NOMAD mesh node spacing 161
13. APPENDIX C – List of Stations for Skill Assessment 167
14. APPENDIX D – Non-Zero Mean Elevation Trend 172

LIST OF FIGURES

Figure 3-1: Final mesh boundary in green with approximate 10-meter contour along US inland boundary and EC2012 Mesh boundary elsewhere. 14
Figure 3-2: Overview of final NOMAD mesh topo-bathymetry (feet MSL) 16
Figure 3-3: Detail of NOMAD mesh topo-bathymetry (feet MSL) for US coastline. 17
Figure 3-4: EC2012 mesh nodes shown in yellow and red. Red mesh nodes are those within the extent of the extended VDatum conversion grid. 18
Figure 5-1: Geographic distribution of M_2 constituent amplitude error. 27
Figure 5-2: Modeled versus predicted harmonic amplitudes for seven primary harmonic constituents. 28
Figure 5-3: Sorted relative amplitude error for seven primary harmonic constituents at stations with M_2 amplitude greater than 0.1 meters. 28
Figure 5-4: Geographic distribution of phase error for M_2 harmonic constituent. 29
Figure 5-5: Correlation of modeled versus predicted harmonic phases. 30
Figure 5-6: Sorted phase error for individual harmonic constituent phases. 30
Figure 5-7: Water elevation solution at one time step 4 days before fatal instability. 31
Figure 5-8: Correlation of M_2 constituent amplitude comparing predicted and simulated results from simulations with non-linear advection terms turned on (blue points) and off (red points). 32
Figure 5-9: A pseudo-geographic depiction of the effect of modification of the non-linear advection; results from simulations with non-linear advection terms turned on are plotted as blue points and off as red points. 33
Figure 5-10: Geographic distribution of water level time series RMSE at 398 tide gages, highlighting points exceeding the 0.2 meter RMS error metric. 34
Figure 6-1: Approximate landfall locations of hindcast validation events. 37
Figure 6-2: Storm track of Hurricane Ike. Dots denote 6-hour intervals and landfall. 38
Figure 6-3: Ike maximum wind speeds (top, mph) and maximum modeled surge (bottom, ft MSL); NOAA gage sites marked by pinwheels (bottom). 39
Figure 6-4: Geographic distribution of NOAA gage peak surge error (feet, modeled minus measured). 40
Figure 6-5: Geographic distribution of NOAA gage time series RMSE (feet). 41
Figure 6-6: Galveston area NOAA gage time series peak water level error (left, feet, modeled minus measured) and RMSE (right, feet). 41
Figure 6-7: Alongshore plot of time series RMSE at NOAA stations; selected stations named for reference, red line indicates target RMSE, green line gives gage mean RMSE, and the purple line is mean RMSE from all storms. 42
Figure 6-8: Difference in peak surge for 1.04x winds from 1.09x winds (feet). 43
Figure 6-9: Measured and modeled time series at Galveston Pleasure Pier, Texas. 44
Figure 6-10: Measured and modeled time series at Bay Waveland, Mississippi. 44
Figure 6-11: Measured and modeled time series at Galveston Bay Entrance, Texas. 45
Figure 6-12: Measured and modeled time series at Galveston Pier, Texas. 45
Figure 6-13: Ike advection-on minus advection-off peak surges (feet). 46
Figure 6-14: Storm track of Hurricane Katrina. Dots denote 6-hour intervals and landfall. 47
Figure 6-15: Katrina maximum wind speeds (top, mph) and maximum modeled surge (bottom, feet MSL); NOAA gage sites marked by pinwheels (bottom). 48

Figure 6-16: Geographic distribution of peak water level error (left) and time series RMSE (right) at NOAA stations. Peak surge errors are only shown for gages with a distinct surge signal.....49
Figure 6-17: Alongshore plot of time series RMSE at NOAA stations; selected stations named for reference; red line indicates target RMSE, green line gives gage mean RMSE, and the purple line is mean RMSE from all storms. 49
Figure 6-18: Measured and modeled time series at Waveland, Mississippi.....50
Figure 6-19: Measured and modeled time series at Dauphin Island, Alabama. 50
Figure 6-20: Katrina advection-on minus advection-off peak water level (feet).....51
Figure 6-21: Storm track of Hurricane Dennis. Dots denote 6-hour intervals and landfall.....52
Figure 6-22: Dennis maximum wind speeds (top, mph) and maximum modeled surge (bottom, feet MSL); NOAA gage sites marked by pinwheels (bottom).....53
Figure 6-23: Geographic distribution of peak water level error (left) and time series RMSE (right) at NOAA stations. Peak surge errors are only shown for gages with a distinct surge signal.....54
Figure 6-24: Alongshore plot of time series RMSE at NOAA stations; selected stations named for reference, red line indicates target RMSE, green line gives gage mean RMSE, and the purple line is mean RMSE from all storms. 55
Figure 6-25: Measured and modeled time series at Cedar Key, Florida. 55
Figure 6-26: Measured and modeled time series at Apalachicola, Florida.....56
Figure 6-27: Measured and modeled time series at Panama City, Florida. 56
Figure 6-28: Comparison of measured HWMs vs. FEMA study modeled peak water level] (left) and the same HWMs vs. NOMAD modeled peak water levels (right). The NOMAD results shown are from a test run using with 1.09x scaled winds for more direct comparison to the FEMA results.....57
Figure 6-29: Dennis advection-on minus advection-off peak surges (feet).....57
Figure 6-30: Storm track of Hurricane Charley. Dots denote 6-hour intervals and landfall. 58
Figure 6-31 Charley maximum wind speeds (left, mph) and maximum modeled surge (right, feet MSL); NOAA gage sites marked by pinwheels (right). 59
Figure 6-32 Geographic distribution of peak water level error (left) and time series RMSE (right) at NOAA stations. Peak surge errors are only shown for gages with a distinct surge signal.....60
Figure 6-33 Measured and modeled time series at Loggerhead Key, Florida. 60
Figure 6-34 Measured and modeled time series at Fort Meyers, Florida. 61
Figure 6-35 Hurricane Charley surveyed post-storm HWMs (left) and HWM error (right).....62
Figure 6-36: Charley advection-on minus advection-off peak surges (feet). 63
Figure 6-37: Storm track of Hurricane Hugo. Dots denote 6-hour intervals. 64
Figure 6-38 Hugo maximum wind speeds (left, mph) and maximum modeled surge (right, feet MSL); NOAA gage sites marked by pinwheels (right). 65
Figure 6-39 Geographic distribution of peak water level error (left) and time series RMSE (right) at NOAA stations. Peak surge errors are only shown for gages with a distinct surge signal.....65
Figure 6-40 Alongshore plot of time series RMSE at NOAA stations; selected stations named for reference; red line indicates target RMSE, green line gives gage mean RMSE, and the purple line is mean RMSE from all storms. 66
Figure 6-41 Measured and modeled time series at Wilmington, North Carolina. 67

Figure 6-42 Measured and modeled time series at Charleston, South Carolina. 67
Figure 6-43: Post-storm HWM data error, modeled minus measured. 68
Figure 6-44 Comparison of NOMAD vs. FEMA model skill to measured surge height. 69
Figure 6-45 Peak water level difference (feet) showing NOMAD modeled minus FEMA modeled values 69
Figure 6-46: Hugo advection-on minus advection-off peak surges (feet). 70
Figure 6-47: Storm track of Hurricane Floyd. Dots denote 6-hour intervals 71
Figure 6-48: Floyd H*Wind and Best track maximum wind speed (left and right, respectively, kilometers per hour) 72
Figure 6-49: H*Wind maximum modeled surge (bottom left and bottom right, respectively, meters MSL) 73
Figure 6-50: Differences between advection-on and advection-off simulations using the H*Wind forcing data for Floyd. 73
Figure 6-51: Geographic distribution of peak water level error (left) and time series RMSE (right) at NOAA stations. Peak surge errors are only shown for gages with a distinct surge signal 74
Figure 6-52: Alongshore plot of time series RMSE at NOAA stations; selected stations named for reference; red line indicates target RMSE, green line gives gage mean RMSE, and the purple line is mean RMSE from all storms. 75
Figure 6-53: Observed and simulated water levels during Floyd at Money Point, VA. Green is observed (obs); dark blue is advection-off H*Wind (flr01); light blue is advection-on H*Wind (flr02); black is best track (flr03) 76
Figure 6-54: Observed and simulated water levels during Floyd at Cape Hatteras, NC. Green is observed (obs); dark blue is advection-off H*Wind (flr01); light blue is advection-on H*Wind (flr02); black is best track (flr03) 76
Figure 6-55: Observed and simulated water levels during Floyd at Atlantic Beach, NC. Green is observed (obs); dark blue is advection-off H*Wind (flr01); light blue is advection-on H*Wind (flr02); black is best track (flr03) 76
Figure 6-56: Observed and simulated water levels during Floyd at Wilmington, NC. Green is observed (obs); dark blue is advection-off H*Wind (flr01); light blue is advection-on H*Wind (flr02); black is best track (flr03) 77
Figure 6-57: Observed and simulated water levels during Floyd at Springmaid Pier, SC. Green is observed (obs); dark blue is advection-off H*Wind (flr01); light blue is advection-on H*Wind (flr02); black is best track (flr03) 77
Figure 6-58: Observed and simulated water levels during Floyd at St. Simons Island, GA. Green is observed (obs); dark blue is advection-off H*Wind (flr01); light blue is advection-on H*Wind (flr02); black is best track (flr03) 77
Figure 6-59: Storm track of Hurricane Isabel. Dots denote 6-hour intervals and landfall. 78
Figure 6-60: Isabel maximum wind speeds (left) and maximum modeled surge (left); NOAA gage sites marked by pinwheels (right). 79
Figure 6-61: Geographic distribution of peak water level error (left) and time series RMSE (right) at NOAA stations. Peak surge errors are shown only for gages with a distinct surge signal 80
Figure 6-62: Alongshore plot of time series RMSE at NOAA stations; selected stations named for reference; red line indicates target RMSE, green line gives gage mean RMSE, and the purple line is mean RMSE from all storms. 80

Figure 6-63: Measured and modeled time series at Washington, DC. 81
Figure 6-64: Measured and modeled time series at Newbold, Pennsylvania. 82
Figure 6-65 Measured and modeled time series at Oregon Inlet Marina, North Carolina. 82
Figure 6-66: Measured and modeled time series at Cape Hatteras Fishing Pier, North Carolina. 83
Figure 6-67: Storm track of Hurricane Sandy. Dots denote 6-hour intervals, extratropical transition, and landfall. 84
Figure 6-68 Sandy maximum wind speeds (top, mph) and maximum modeled surge (bottom, feet MSL); NOAA gage sites marked by pinwheels (bottom). 85
Figure 6-69 Geographic distribution of peak water level error (left) and time series RMSE (right) at NOAA stations. HWM errors are limited to gages with a distinct surge signal 86
Figure 6-70 Alongshore plot of time series RMSE at NOAA stations; selected stations named for reference; red line indicates target RMSE, green line gives gage mean RMSE, and the purple line is mean RMSE from all storms. 86
Figure 6-71: Measured and modeled time series at Providence, Rhode Island. 87
Figure 6-72: Measured and modeled time series at New Haven, Connecticut. 87
Figure 6-73 Measured and modeled time series at Kings Point, New York. 88
Figure 6-74: Measured and modeled time series at The Battery, New York. 88
Figure 6-75: Measured and modeled time series at Bergen Point, New York. 89
Figure 6-76: Measured and modeled time series at Sandy Hook, New Jersey. 89
Figure 6-77 Measured and modeled time series at Atlantic City, New Jersey. 90
Figure 6-78 Measured and modeled time series at Cape May, New Jersey. 90
Figure 6-79 Measured and modeled time series at Ocean City, Maryland. 91
Figure 6-80: Storm track of the Long Island Express. Dots denote 6-hour intervals and landfall. 92
Figure 6-81 Long Island Express maximum wind speeds (top, mph) and maximum modeled surge (bottom, feet MSL; NOAA gage sites marked by pinwheels (bottom) 93
Figure 6-82 Geographic distribution of peak water level error (left) and time series RMSE (right) at NOAA stations. HWM errors are limited to gages with a distinct surge signal 94
Figure 6-83: Geographic distribution of peak water level error from additional high water marks. 94
Figure 6-84 Alongshore plot of time series RMSE at NOAA stations; selected stations named for reference; red line indicates target RMSE, green line gives gage mean RMSE, and the purple line is mean RMSE from all storms. 95
Figure 6-85 Measured and modeled time series at Willets Point, New York. 96
Figure 6-86 Measured and modeled time series at The Battery, New York. 96
Figure 6-87: Long Island Express advection-on minus advection-off peak surges (feet). 97
Figure 6-88: Storm track of the Perfect Storm. Dots denote 6-hour intervals. 98
Figure 6-89: Perfect Storm maximum wind speeds (top, mph) and maximum modeled surge (bottom, feet MSL); NOAA gage sites marked by pinwheels (bottom) 99

Figure 6-90: Geographic distribution of peak water level error (left) and time series RMSE (right) at NOAA stations. HWM errors are limited to gages with a distinct surge signal.....100
Figure 6-91: Alongshore plot of time series RMSE at NOAA stations; selected stations named for reference; red line indicates target RMSE, green line gives gage mean RMSE, and the purple line is mean RMSE from all storms. 101
Figure 6-92: Measured and modeled time series at Woods Hole, Massachusetts. 101
Figure 6-93: Measured and modeled time series at Montauk, New York. 102
Figure 6-94 Comparison of NOMAD (top) to FEMA (bottom) time series at Atlantic City, New Jersey. 103
Figure 7-1: NOAA gage time series RMSE for all storms. 105
Figure 7-2: NOAA gage mean water level difference for all storms. 105
Figure 7-3: Along-shore NOAA gage time series RMSE for all storms. 106
Figure 7-4: Along-shore NOAA gage time series mean difference for all storms. 106
Figure 7-5 Peak water level error and surveyed HWM error for all storms. Data points labeled ‘extra’ are surveyed HWM datasets for the corresponding events 107
Figure 7-6: Along-shore NOAA gage peak water level error. 107
Figure 7-7: Peak water level and surveyed HWM comparison for all storms. Data points labeled ‘extra’ are surveyed HWM datasets for the corresponding events. 108
Figure 7-8 Sorted RMSEs from all NOAA gages (excluding gages which failed during the event) across all validation storm simulations. Gages used in multiple storms have multiple points. 109
Figure 7-9 Sorted HWM errors from all NOAA gages (excluding gages which failed during the event) across all validation storm simulations. Gages used in multiple storms have multiple points. 109

LIST OF TABLES

Table 4-1: ADCIRC Control File Parameters....20
Table 4-2: Mapping of Spatial Parameters to CCAP Classes....24
Table 4-3: NLCD Land Use Classifications....25
Table 6-1: Summary of tropical and extratropical cyclone hindcast validation simulations....36
Table 6-2: Comparison of HWM Error. 102
Table 12-1: Sources of topo-bathymetric data for development of the HSSOFS mesh node elevations....136
Table 14-1 Stations with identified non-zero mean elevation trend. 173

LIST OF ACRONYMS AND ABBREVIATIONS

ADCIRC	ADvanced CIRCulation model
CO-OPS	Center for Operational Oceanographic Products and Services
CSDL	Costal Survey Development Laboratory
ETSS	Extratropical Storm Surge
ESTOFS	Extratropical Surge and Tide Operational Forecast System
FEMA	Federal Emergency Management Agency
GFS	Global Forecast System
EC2012	East Coast 2012 Tidal Constituent Project
HWM	High Water Mark
MSL	Mean Sea Level
MLLW	Mean Lower Low Water
NCEP	National Centers for Environmental Prediction
NHC	National Hurricane Center
NOS	National Ocean Service
NOAA	National Oceanic and Atmospheric Administration
NWS	National Weather Service
NAVD 88	North American Vertical Datum of 1988
OCS	Office of Coast Survey
OPC	Ocean Prediction Center
RMSE	Root Mean Square Error
SLOSH	Sea Lake and Overland Surge from Hurricanes
USACE	United States Army Corps of Engineers
USGS	United States Geological Survey

1. EXECUTIVE SUMMARY

The Coast Survey Development Laboratory (CSDL) of the National Ocean Service (NOS) previously developed an Extratropical Surge and Tide Operational Forecast System (ESTOFS) for the US coastal waters (Funakoshi et al. 2013). Now, to extend the capability of ESTOFS to include tropical storm event simulation and ensemble prediction, CSDL is preparing a prototype Hurricane Storm Surge Operational Forecast System (HSSOFS). Under direction from CSDL, a technical team led by Riverside Technology, inc. has developed a hydrodynamic model of the US East Coast and Gulf of Mexico and has validated the model for 10 major tropical and extratropical events. Eventually, this model will form the basis for an operational system on National Centers for Environmental Prediction (NCEP) computers. The prototype model described in this document is called NOMAD: NOAA Operational Model with ADCIRC.

The hydrodynamic model employed for NOMAD is the ADvanced CIRCulation (ADCIRC) finite element model (Luettich et al. 1992; Luettich and Westerink 2004). The ADCIRC hydrodynamic model has demonstrated to be effective at predicting tidal circulation and storm surge propagation in complex coastal systems.

For the development of NOMAD, the project team constructed a new model grid covering all of the US Atlantic and Gulf coasts. Two model-run scenarios were tested: 1) astronomical tide and 2) model hindcast. The model results from each scenario are compared with observations using NOS' standard skill assessment software. The skill assessment demonstrated that NOMAD generally predicts the surge reasonably well, considering the meteorological forcing.

The target error metric was 0.2 meters RMSE (0.66 feet). With no adjustment for mean water level differences, the mean RMSE for all storms is about 0.26 meters (0.85 feet) with a range from approximately 0.1-0.7 meters (0.3-2.3 feet). At least some of the model error is due to mean water level differences from effects not modeled, such as seasonal water level variations. CSDL may achieve improved results by using a seasonal correction during operational implementation to account for steric effects and annual tidal signals.

2. **INTRODUCTION**

Impacts of storm surge from extratropical and tropical events can be far-reaching and catastrophic along the coast of the United States. The Office of Coast Survey/CSDL (OCS/CSDL) of the NOS and the Environmental Modeling Center (EMC) of NCEP have previously collaborated to establish an ESTOFS for the Atlantic and Gulf of Mexico (Funakoshi et al. 2013).

Continuing in the path of the ESTOFS development, CSDL has established an objective to further improve operational storm surge guidance for Eastern and Gulf US coasts. The objective includes providing guidance during both extratropical and tropical surge events, providing ensemble forecasts, and preparing to address the effects of combined coastal and river flooding by expanding into key areas of interest for coupled river-ocean modelling. To accomplish these goals, CSDL is developing a new hydrodynamic model which will be implemented for operational simulations of storm surge and ocean water levels due to both tropical and extratropical storm events.

The hydrodynamic model code employed will be the ADvanced CIRCulation (ADCIRC) finite element model (Luettich et al. 1992; Luettich and Westerink 2004). ADCIRC has proven effective at predicting tidal circulation and storm surge propagation in complex coastal systems. Its unstructured grid methodology allows for representation of complex shorelines and bathymetry.

CSDL tasked a team ('the Project Team' or 'the Team') from Riverside Technology, inc. (Riverside) and AECOM (formerly URS Group, Inc.) to:

- Develop a preliminary ADCIRC mesh based on best-available bathymetry and overland topography.
- Validate the preliminary model mesh using tidal harmonics.
- Execute hindcast simulations of 10 significant historical tropical and extratropical storm events.
- Evaluate model hindcast performance using both the NOS standard skill assessment program (Zhang et al. 2006) and criteria (Hess et al. 2003), as well as comparison to observed high water marks.

This report describes the work performed to develop and validate the preliminary ADCIRC model, which is referred to herein as the NOAA Operational Model with ADCIRC (NOMAD). When implemented operationally with appropriate meteorological forcing, and following additional testing and verification by CSDL, the new model is expected to be called the Hurricane Storm Surge Operational Forecast System (HSSOFS).

The overall skill assessment results for NOMAD presented in this report show that the model is providing useful simulated water levels for tropical and extratropical events in all areas tested.

3. MESH DEVELOPMENT

CSDL will use the NOMAD mesh as a basis for HSSOFS to provide operational surge and tide predictions for the US East Coast and Gulf of Mexico. The ADCIRC unstructured mesh allows simulation for such a large domain, while still providing resolution of local coastal features. Given that the application of interest includes overland flooding, both topographic and bathymetric data sources were collected to prepare the model. The final mesh averages node spacing of 500 meters along the coast with some areas decreasing to a node spacing of approximately 150 meters. There are a total of approximately 1.8 million nodes.

CSDL provided mesh datasets which were used for various purposes during this project including various versions of the East Coast tidal constituent simulation meshes (EC2001, EC2001Ex, and EC2012). CSDL also provided access to a detailed mesh developed by researchers at University of Notre Dame for storm surge studies in Puerto Rico and the US Virgin Islands. Finally, a set of mesh datasets for coastal Louisiana and Mississippi were provided by CSDL from inland surge models developed in collaboration with the Southeastern Universities Research Association (SURA) and the Integrated Ocean Observation System (IOOS). Additional detail and references for datasets used to define the model boundary and facilitate mesh development are contained in Appendix A and Appendix B.

3.1 Model Boundary

The inland mesh boundary was developed following these general guidelines:

- At most locations, the mesh extends inland to a smoothed version of the 10-meter topographic contour.
- In some areas with major population centers, the mesh was extended inland beyond the 10-meter topographic contour to include the entire developed area in the final mesh.
- Except for significant rivers to be considered for coupled modeling, the boundary extends into coastal river inlets only to the point where the channel width decreases below approximately 1,500 meters.
- In some areas where the 10-meter contour was significantly inland of the Federal Emergency Management Agency (FEMA) determined 0.2-percent-annual-chance flood elevation, the amount of modeled inland area was reduced.
- The SURA-IOOS mesh for portions of Texas, Louisiana, and Mississippi provided the mesh boundary in those areas.
- Portions of the Everglades, though well below the 10-meter contour, were specifically excluded from the mesh because of low population, complex flow dynamics, and the presence of levees.
- Non-US overland areas are excluded from the mesh. Coastal boundaries outside of the United States are from the EC2012 Mesh boundary.
- All of the ESTOFS-modeled area is included in the new mesh.

Understanding the long-term objective of integrating the water level forecast from HSSOFS with riverine water level forecasts, the team reviewed a number of areas along the Atlantic and Gulf coasts where the NWS is developing riverine HEC-RAS models. The following river inlets were identified for inclusion in the NOMAD mesh: the Atchafalaya, Mississippi, St. John's, Waccamaw, Tar, Potomac, Hudson, and Connecticut rivers.

The open ocean boundary location for the model coincides with the EC2001 extended mesh developed by the University of Oklahoma. This selection allowed for direct application of a number of existing datasets developed for that boundary and provided by NOAA for this project. The mesh model boundary is seen in Figure 3-1.

Figure 3-1: Final mesh boundary in green with approximate 10-meter contour along US inland boundary and EC2012 Mesh boundary elsewhere.

3.2 Topography and Bathymetry Data Sources

Two primary data sources provided the majority of mesh node elevations: the USGS 1/3 arc-second (nominally 10 meter) National Elevation Dataset (NED) digital elevation model (DEM) supplied overland topography, and the NOAA EastCoast2012 (EC2012) tidal constituent database mesh nodes constituted the primary bathymetry data source. High-resolution topography was derived from the 1/9 arc-second USGS NED (approximately 3 meter), which provides lidar-sourced elevations for nearly all of the Gulf Coast, Florida, North Carolina, the Delmarva Peninsula, and most of New England. Riverside obtained lidar data to fill gaps in the 1/9 arc-second NED coverage from the NOAA Coastal Services Center (CSC) for the following areas: Boston area, Massachusetts; Long Island, New York City, and the Hudson riverbank, New York; Norfolk and Virginia Beach, Virginia; portions of coastal South Carolina in Colleton and Jasper counties, as well as Chatham County in Georgia. Along the South Carolina coast, where neither 1/9 arc-second NED nor lidar data were available, AECOM provided several gridded elevation datasets from in-house archives to improve topographic elevation estimates for five South Carolina counties.

3.3 **ADCIRC Mesh**

Attention to mesh quality is essential to produce a geometry that not only accurately represents the terrain and bathymetry, but also produces stable and consistent results when run with the ADCIRC model. The ADCIRC model runs on a triangulated mesh with varying element sizes. Each node has an associated elevation. Additional spatial parameters can also be associated with each node. Due to the large geographic extent of this project including the Atlantic and Gulf of Mexico, the mesh was constructed in separate sections by different team members using a guiding methodology to maintain consistency throughout the study domain.

One key mesh development constraint, derived from the intended operational implementation of the model, included maintaining a total node count of less than 2,000,000 nodes. An average spacing was defined in the US near shore and onshore areas of around 400 to 500 meters with a nominal minimum spacing around 200 meters for smaller channels, specifically where flow paths tie together large water bodies, or provide a conduit to extensive inland flooding behind major flow barriers. Some highly populated areas were also modeled with a finer-scale mesh.

The mesh extent was generated from several sources, including developing much of the over-land mesh in-house. For this task, the high-resolution topographic data sources referenced in Section 3.2 were carefully examined to identify locations of critical flow pathways and flow barriers. The technical team traced break lines along these features and provided the break lines to the meshing algorithm to explicitly include the features in the mesh. In addition, the team examined data extracted from the National Levee Database to confirm the location of levees were properly represented within the study area. CSDL provided the technical team with several mesh geometries including the NOAA EastCoast 2012 (EC2012) tidal constituent database mesh and the Extended EastCoast2001 (ExEC2001) mesh. Both geometries cover the entire deep-ocean domain. The EC2012 mesh has more than two million nodes while the ExEc2001 mesh has approximately 258,000 nodes.

In addition, CSDL provided the Gulf Coast-focused SURA-IOOS mesh developed for round one of the Coastal Ocean Modeling Testbed project. Generally, the SURA-IOOS mesh had less dense node spacing than what was developed for other areas on the Gulf and Atlantic coasts, but it remains useful because it was specifically designed and tested for storm surge studies in the Louisiana and Mississippi coasts. Because of the lower node spacing of this mesh (lower than other meshes used in Louisiana), it is also referred to as the Ultralite mesh, referring to the relatively lightweight computational load required for simulating larger node spacing.

The team also examined a mesh developed for detailed storm surge studies in Puerto Rico and the US Virgin Islands. The mesh, developed by Joannes Westerink and Juan Gonzales-Lopez from the University of Notre Dame, was more detailed than necessary for this project due to a minimum node spacing of 14 meters.

The final mesh incorporated all of the geometries detailed above, combined and edited to the appropriate resolution for the current modeling task. The node and element configuration from the on-shore and near-shore areas of the SURA-IOOS mesh for Louisiana and Mississippi was incorporated with minor modifications. The Puerto Rico mesh was indirectly incorporated, as the inland boundary was extracted and then smoothed using a large node-to-node spacing. This boundary was used to develop the overland portion of the mesh for Puerto Rico and the US Virgin Islands. The smaller node count ExEC2001 mesh was used directly for the deep ocean boundary, and the EC2012 mesh nodes were used as a bathymetry data source for the near shore as explained below.

The final mesh comprises 1.813 million nodes with the smallest node spacing approximately 160 meters (in the SURA-IOOS mesh in Louisiana) to a maximum of 46 kilometers at the open boundary in the

Atlantic. Figure 3-2 gives an overview of the final mesh topo-bathymetry followed by Figure 3-3 showing greater detail for the US coast. Additional detail images showing bathymetry and mesh node spacing for select areas are found in Appendix B.

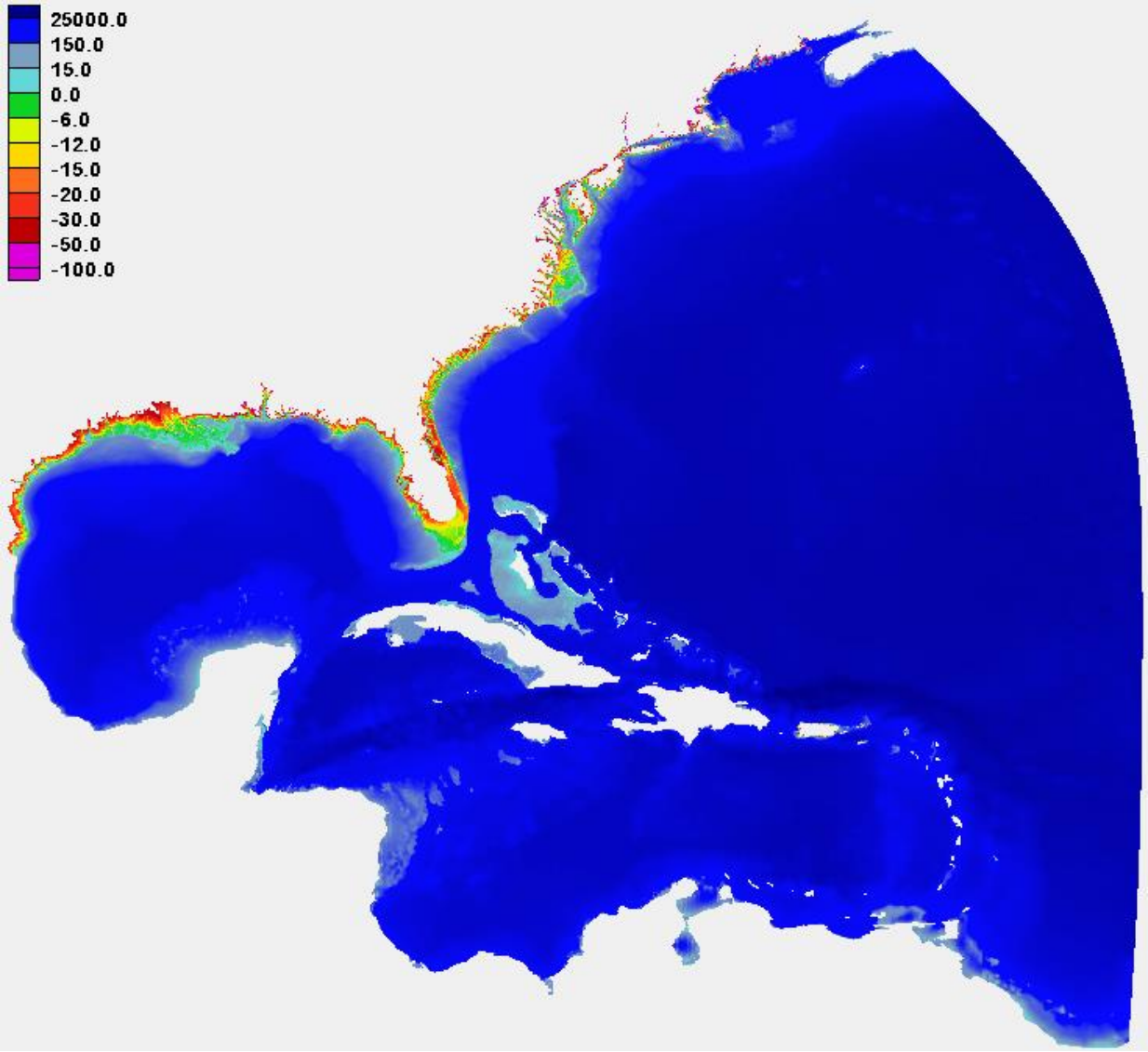

Figure 3-2: Overview of final NOMAD mesh topo-bathymetry (feet MSL)

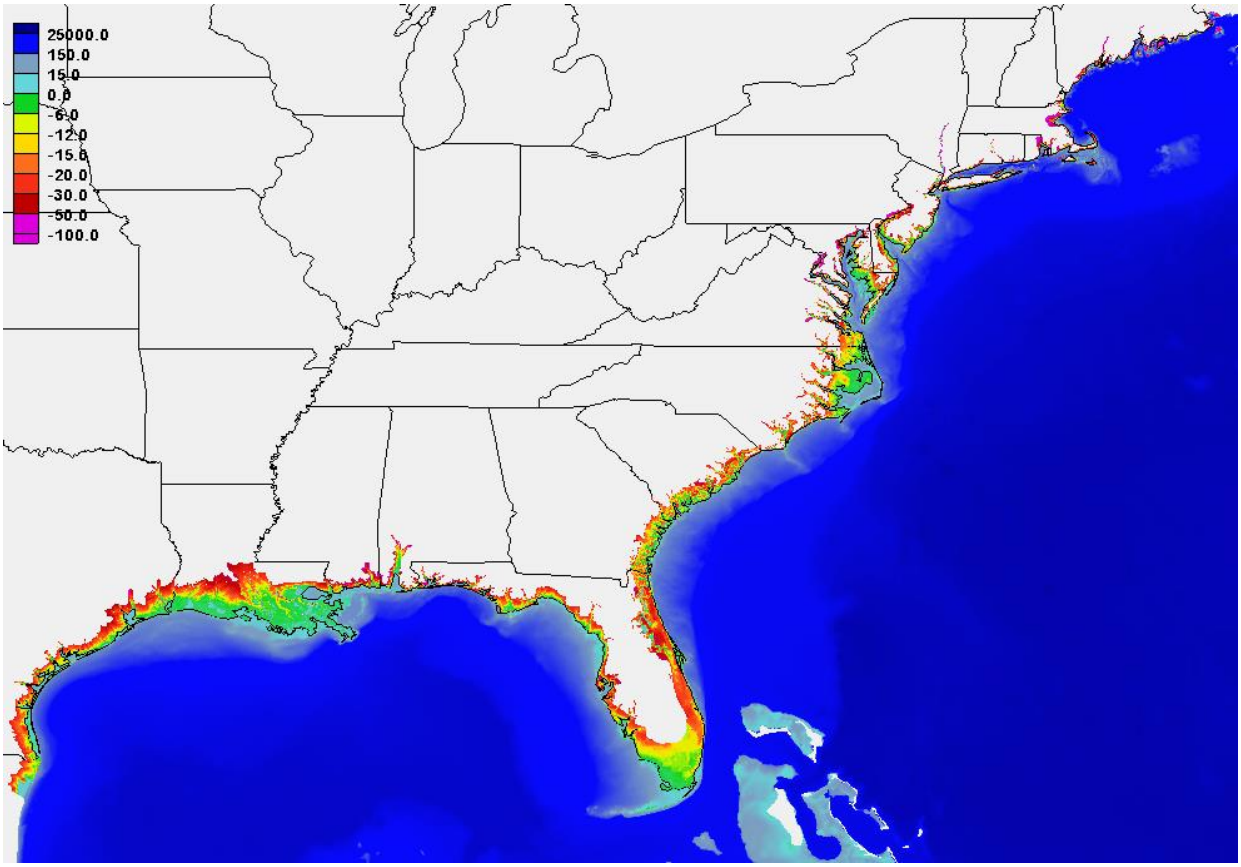

Figure 3-3: Detail of NOMAD mesh topo-bathymetry (feet MSL) for US coastline.

3.4 Elevation Assignment

For broad overland areas exclusive of explicit barriers or channels, the topographic data was smoothed using a circular averaging window with a radius of 100 to 300 meters via ArcGIS focal statistics. A Fortran program was then used to assign elevations from the closest elevation data point in the smoothed topographic DEM to each mesh node

3.5 Datum Conversion

As previously noted, the EC2012 mesh node elevations are the primary source for bathymetric data for building the storm surge modeling mesh. It was necessary to convert the node elevations from MSL to NAVD88 in order to combine them with topographic data from the USGS. Normally, a translation of this type would be performed using the NOS-provided tool, VDatum. However, the VDatum application provided on the NOS website[1] uses a translation grid with several key areas missing, including Pamlico Sound and the Indian River inlet.

CSDL provided an updated bathymetric translation grid that extends beyond the publicly available VDatum grid into all coastal waters within the model area of interest (Figure 3-4). The translation grid uses the TCARI interpolation technique (Hess et al. 2004) to allow extrapolation of the datum conversion field a significant distance over land and into the deep ocean. Where they overlap, the extended conversion is identical to the VDatum grid conversion. Using CSDL code provided with the extended grid, a complete set of MSL-to-NAVD88 conversion values was generated for the entire near-shore bathymetric dataset from the EC2012 grid nodes.

[1] VDatum software is provided via download links on this site: http://vdatum.noaa.gov/

A similar process was applied to convert the combined storm surge modeling mesh nodes back to MSL for use in modeling. When simulation results have been obtained, these conversion values will be applied as needed to compare to verification datasets in either MSL or NAVD88. The CSDL code was extremely efficient for converting the large point datasets represented by the mesh nodes.

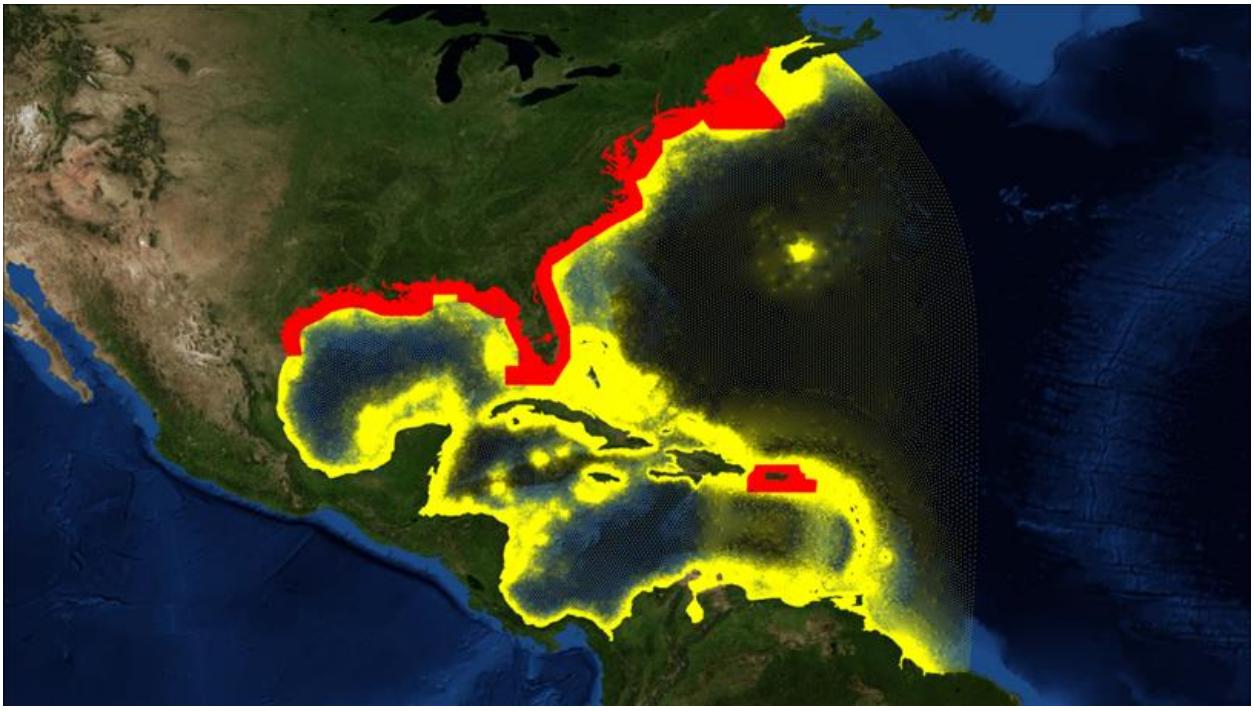

Figure 3-4: EC2012 mesh nodes shown in yellow and red. Red mesh nodes are those within the extent of the extended VDatum conversion grid.

4. ADCIRC MODEL DEVELOPMENT

Each ADCIRC model is constructed with various control files to represent the mesh and forcing characteristics for a particular simulation. Except where specifically noted otherwise, all tidal and hindcast simulations for the NOMAD model reported here used fort.15 control files and fort.13 nodal attribute files conforming to the descriptions in the following sections.

4.1 Fort.15 Model Control File

The fort.15 file is the model control file used for setting physical parameters and determining how the model runs. Table 4-1 shows the parameters, their values and rationale for these values in the fort.15 ADCIRC control file. The parameter values were chosen to accurately represent system physics while ensuring simulations were stable.

Tidal forcing is applied as an elevation-specified boundary condition at the model's oceanic boundary along the offshore boundary and as a body force on all nodes in the domain. Tidal forcing constituents were obtained from CSDL who specified them on the extended EC2001 mesh (whose boundary was adapted from the EC2012 mesh). The K_1, K_2, M_2, N_2, O_1, Q_1, S_2, P_1, Mf, Mm, M_4, Ms_4, and Mn_4 constituents were used.

The ADCIRC model land boundary conditions prevent normal flow, but they do not restrict tangential flow. No river boundary conditions are specified in the study region, although several rivers, including the Potomac, Hudson, Mississippi, and Atchafalaya Rivers, are represented up to the mesh's inland boundary.

Under the chosen model setup, bottom drag in ADCIRC is applied by a depth-dependent quadratic friction law, with a drag coefficient set by the Manning's n value, which is defined for each node using land use data. See Section 4.2.3 for more information on the land use and Manning's n values.

Table 4-1: ADCIRC Control File Parameters

Parameter	Description	Value	Explanation
NOLIBF	Parameter controlling the type of bottom stress parameterization used in a two-dimensional depth-integrated (2DDI) ADCIRC run. 1 = quadratic bottom friction law.	1	Standard value. This value is necessary for using the "mannings_n_at_sea_floor" nodal attribute in the fort.13 file.
NOLIFA	Parameter controlling the finite amplitude terms in ADCIRC. 2 = finite amplitude terms are included in the model run and wetting and drying of elements is enabled.	2	Recommended value. This value has been used in previous studies, including the Big Bend study.
NOLICA	Parameter controlling the advective terms in ADCIRC (with the exception of a time derivative portion that occurs in the GWCE form of the continuity equation). 1 = advective terms are included in the computations.	0 or 1	1 when possible, though some simulations were unstable.
NOLICAT	Parameter controlling the time derivative portion of the advective terms that occurs in the GWCE form of the continuity equation in ADCIRC. 1 = the time derivative portion of the advective terms that occur in the GWCE continuity equation are included in the computations.	0 or 1	1 when possible, though some simulations were unstable.
NCOR	Parameter controlling whether the Coriolis parameter is spatially varying as computed from the y-coordinates of the nodes in the grid. 1 = compute a spatially variable Coriolis parameter.	1	Standard recommended value. This value is most representative of the system physics.
TAU0	Generalized Wave Continuity Equation (GWCE) weighting factor that weights the relative contribution of the primitive and wave portions of the GWCE. A value of -3 indicates that the value varies in space and time according to the nodal attribute "primitive_weighting_in_continuity_equation."	-3	Standard value. See Section 4.2.1 for more information.
DTDP	ADCIRC time step (in seconds).	2	Model was also generally stable at 4 seconds.
A00, B00, C00	Time weighting factors (at time levels k+1, k, k-1, respectively) in the GWCE.	0.35, 0.3, 0.35	Standard value.
H0	Nominal water depth for a node (and the accompanying elements) to be considered dry (in meters).	0.05	Value within the recommended range of 0.01 to 0.1 m.
VELMIN	Minimum velocity for wetting (in meters per second).	0.05	Standard recommended value.
CF	Minimum value of the equivalent quadratic friction coefficient determined by Manning's n value.	0.0025	Standard value used in other studies, including the Big Bend study.
ESLM	Spatially constant horizontal eddy viscosity for the momentum equations (units of length^2/time).	10	Standard value.

4.2 Fort.13 Nodal Attribute File

The ADCIRC model is capable of applying multiple spatially varying parameters (nodal attributes), many of which alter wind and bottom drag using land use data. The following subsections detail the nodal parameters and the land use data used for the spatial attributes. All Fortran utilities used to create the various nodal attributes can be found on the ADCIRC website[2].

4.2.1 *Primitive Weighting in Continuity Equation*

The "primitive weighting in continuity equation" attribute sets the τ_0 parameter, controlling the relative contribution of the primitive and wave portions of the GWCE, which is a reformulation of the shallow water equation used by the ADCIRC model. This balance is such that for τ_0, a value of 0 is the pure wave equation and a value greater than 1 behaves like a pure primitive continuity equation.

The program *tau0_gen.f* from the ADCIRC website was used to create the "primitive weighting in continuity equation" attribute. The parameter was set by finding the average distance between a node and its neighbors (as determined by the element connectivity between nodes). If the average distance between neighboring nodes was less than 1,750 meters, the τ_0 parameter was set to 0.03. Otherwise, the value was set to 0.005 for depths greater than 10 meters and 0.02 for depths less than or equal to 10 meters. A value of 0.03 causes the ADCIRC model to calculate the τ_0 parameter for each node at each time step throughout the simulation using a hard-coded scheme. Details on the scheme are provided at the ADCIRC website[3].

4.2.2 *Formulation of Land Use-Dependent Parameters*

The effect of spatially variable land cover and land use types enter into the computations via three coefficients. Three spatial variable parameters are applied in the bottom and surface stress terms in the depth averaged momentum equations:

$$\frac{\partial u}{\partial t} + u\frac{\partial u}{\partial x} + v\frac{\partial u}{\partial y} - fu = -g\frac{\partial}{\partial x}\left(\frac{P}{g\rho} + \zeta\right) - \frac{\tau_{bx}}{\rho H} + \frac{\tau_{sx}}{\rho H} + \frac{1}{H}(M_x + D_x - B_x)$$

in the x-direction and

$$\frac{\partial v}{\partial t} + u\frac{\partial v}{\partial x} + v\frac{\partial v}{\partial y} + fv = -g\frac{\partial}{\partial y}\left(\frac{P}{g\rho} + \zeta\right) - \frac{\tau_{by}}{\rho H} + \frac{\tau_{sy}}{\rho H} + \frac{1}{H}(M_y + D_y - B_y)$$

in the y-direction, where:

t = time
x and y = horizontal spatial coordinates
u and v = horizontal velocity vectors
f = Coriolis parameter
P = pressure
ζ = free surface departure from the geoid
H = total water column height
M = vertically integrated later stress gradient
D = momentum dispersion
B = vertically integrated baroclinic pressure gradient
g = the acceleration due to gravity
ρ = water density (1,000 kilograms/m^3, about 1.94 slug/ft^3)
τ_b = bottom stress
τ_s = the surface stress

The bottom stress terms are approximated as:

[2] http://adcirc.org/home/related-software/adcirc-utility-programs/.
[3] http://adcirc.org/home/documentation/users-manual-v50/parameter-definitions/

$$\frac{\tau_{bx}}{\rho H} = g\frac{n^2}{H^{\frac{1}{3}}}\frac{\sqrt{u^2+v^2}}{H}u$$
$$\frac{\tau_{by}}{\rho H} = g\frac{n^2}{H^{\frac{1}{3}}}\frac{\sqrt{u^2+v^2}}{H}v$$

where *n* is the Manning's n parameter, which is specified for every ADCIRC node as the "Manning's n at sea floor" attribute. This parameter is applied to every node under the assumption that nodes anywhere in the mesh can become submerged as the storm surges propagate inland.
The surface stress terms are approximated as:

$$\frac{\tau_{sx}}{\rho H} = \frac{C_d}{H}\frac{\rho_{air}}{\rho}|W_{10}|W_{10x}$$
$$\frac{\tau_{sy}}{\rho H} = \frac{C_d}{H}\frac{\rho_{air}}{\rho}|W_{10}|W_{10y}$$

where C_d is a standard drag coefficient defined by Garratt's drag formula (Garratt 1977) for wind stress, ρ_{air} is the density of air (1.15 kilograms/m^3, about 0.00223 slug/ft^3), and W_{10} is the wind velocity at a 10-meter height sampled at a 10-minute period (Hsu 1988). The W_{10} value is the wind velocity for full marine conditions as provided by an appropriate wind model (Powell et al. 1996). To account for the effect of land roughness, the 10-meter wind velocity is replaced by a reduced W_{land} velocity. The W_{land} velocity is found by:

$$W_{land} = f_d \cdot W_{10}$$

where f_d is the ratio of marine roughness to the roughness of the land surface and is expressed as:

$$f_d = \left(\frac{z_{marine}}{z_0}\right)^{0.0706}$$

where z_{marine} and z_0 are the marine and land roughness lengths, respectively; z_{marine} is defined as:

$$z_{marine} = \frac{0.018}{g}C_d{W_{10}}^2$$

The z_0 length scale is specified at every node as the "surface directional effective roughness length" attribute. This length scale varies with land cover and has been determined for a variety of standardized land use classifications.

In addition to the Manning's n and z_0 parameters, a third parameter is used to represent the effects of tall and dense vegetation on the wind stress term. It has been shown that little wind momentum transfers through heavily forested canopies. The effect of forested vegetative canopies is included by reducing W_{land} to zero in the presence of land use classes that contain trees and thick shrubs, and is specified as the "surface canopy coefficient" nodal attribute. This attribute represents the assumption that the branches, leaves, and trunks absorb the momentum of the wind, thereby preventing momentum transfer to the underlying water column.

4.2.3 *Land Use Data Sources*

The Manning's n, surface roughness length and canopy coefficient parameters all depend on local land use information. It is standard practice to evaluate these parameters using land use classification data. The Coastal Change Analysis Program (CCAP) regional land cover data are a recent NOAA product[4] and have been chosen to develop the frictional parameters. CCAP data define 22 land cover classes and

[4] CCAP data may be obtained on-line from http://coast.noaa.gov/digitalcoast/data/ccapregional/

provide the spatial distribution of these classes across the study region at a resolution of 30 meters. Last updated in 2006, CCAP data are the most recent available source at the required resolution. The CCAP data were therefore chosen to help define model spatial attributes in the study area.

USGS National Land Cover Database (NLCD) data is also often used in surge modeling studies. NLCD data has a well-established set of values for the z_0 parameter derived from Hazus (FEMA 2014; Vickery et al. 2006). Like NOAA's CCAP data, the USGS Gap Analysis Program (GAP) land use data identify local habitat and biodiversity and have more accurate local detail and well-defined vegetation subdivisions than the nationally uniform NLCD set. Standard hydraulic texts have helped establish bottom friction Manning's n values for all the classifications in the GAP data. Each point in the CCAP data set has a class, and each class has an associated value for the needed parameters (Table 4-2). The spatially variable attributes for each ADCIRC node were obtained by interpolating parameter values from nearby CCAP data set points. The standard NLCD land use classification mapping is provided in Table 4-3 for comparison.

4.2.4 *Manning's n at Sea Floor*

Manning's n at sea floor is an isotropic scalar parameter used to approximate resistance to flow from a variety of physical mechanisms, including form drag and skin friction. For the depth-averaged ADCIRC model, the Manning's n correlates to roughness of the land surface at the spatial scale of the computed flow. The Fortran code *mannings_n_finder_v10.f* was downloaded from the ADCIRC website to interpolate the CCAP dataset to the ADCIRC nodes. Modifications to the Fortran code were made to correlate the Manning's n values with the CCAP data descriptions. These correlations between CCAP classes and Manning's n are listed in Table 4-2.

4.2.5 *Surface Canopy Coefficient*

The surface canopy coefficient parameter accounts for an additional wind adjustment. The coefficient was determined in previous studies using only the NLCD classes, but the CCAP datasets were used for this study. Modifications were made to the program *surface_canopy_v5.f*, which is available on the ADCIRC website (as noted in Section 4.2), to incorporate the CCAP land use codes.

4.2.6 *Surface Directional Effective Roughness Length (z_0)*

The local surface roughness length z_0 can be affected by upwind transitions in wind speed due to localized roughness in those areas. For instance, when transitioning in the downwind direction from a forest to an area with shrubs, the effective roughness affecting the wind drag just downstream of the forest edge in the shrub area will be larger than that associated with just the shrub area. This effect can depend on the instantaneous wind direction, and therefore the roughness length is specified by 12 values each representing a 30 degree "upwind" directional bin. The modified roughness parameter is referred to as the *surface directional effective roughness length* and is assigned 12 values at each mesh node.
The program *surface_roughness_calc_v16.f*, available on the ADCIRC website, was used to create the z_0 parameter. For each direction, the upwind land use data up to 6.21 miles (10 kilometers) away are used in a spatial Gaussian weighting scheme to determine the appropriate roughness value. This program was originally designed to map various NLCD types to surface roughness lengths. Modifications were made to the source code to include the CCAP land use classes.

Table 4-2: Mapping of Spatial Parameters to CCAP Classes

CCAP Class	Land Cover Description	Manning's n^	z_0 (m) Parameter	Canopy*
2	High Intensity Developed	0.120	0.300	1
3	Medium Intensity Developed	0.120	0.300	1
4	Low Intensity Developed	0.070	0.300	1
5	Developed Open Space	0.035	0.300	1
6	Cultivated Land	0.100	0.060	1
7	Pasture/Hay	0.055	0.060	1
8	Grassland	0.035	0.040	1
9	Deciduous Forest	0.160	0.650	0
10	Evergreen Forest	0.180	0.720	0
11	Mixed Forest	0.170	0.710	0
12	Scrub/Shrub	0.080	0.120	1
13	Palustrine Forested Wetland	0.200	0.600	0
14	Palustrine Scrub/Shrub Wetlands	0.075	0.110	1
15	Palustrine Emergent Wetland	0.070	0.300	1
16	Estuarine Forested Wetland	0.150	0.550	0
17	Estuarine Scrub/Shrub Wetland	0.070	0.120	1
18	Estuarine Emergent Wetland	0.050	0.300	1
19	Unconsolidated Shore	0.030	0.090	1
20	Bare Land	0.030	0.050	1
21	Open Water	0.020	0.001	1
22	Palustrine Aquatic Bed	0.035	0.040	1
23	Estuarine Aquatic Bed	0.030	0.040	1

^ Implementation of Manning's n values depends on the units being used; a conversion of units' time/length$^{1/3}$ should be applied to the n value if units other than meters and seconds are used.
* A canopy value of 0 denotes no wind stress applied. A canopy value of 1 denotes wind stress will be applied.

Table 4-3: NLCD Land Use Classifications

NLCD Code	Land Cover Description	Manning's n^	z_0 (m) Parameters	Canopy*
11	Open Water	0.02	0.001	1
12	Perennial Snow/Ice	0.01	0.012	1
21	Developed, Open Space	0.02	0.1	1
22	Developed, Low Intensity	0.05	0.3	1
23	Developed, Medium Intensity	0.1	0.4	1
24	Developed, High Intensity	0.15	0.55	1
31	Barren Land	0.09	0.04	1
32	Unconsolidated Shore	0.04	0.09	1
41	Deciduous Forest	0.1	0.65	0
42	Evergreen Forest	0.11	0.72	0
43	Mixed Forest	0.1	0.71	0
51	Dwarf Scrub	0.04	0.1	1
52	Shrub/Scrub	0.05	0.12	1
71	Herbaceous	0.034	0.04	1
72	Sedge/Herbaceous	0.03	0.03	1
73	Lichens	0.027	0.025	1
74	Moss	0.025	0.02	1
81	Hay/Pasture	0.033	0.06	1
82	Cultivated Crops	0.037	0.06	1
90	Woody Wetlands	0.1	0.55	0
91	Palustrine Forested Wetland	0.1	0.55	0
92	Palustrine Scrub/Shrub Wetland	0.048	0.12	0
93	Estuarine Forested Wetland	0.1	0.55	0
94	Estuarine Scrub/Shrub Wetland	0.048	0.12	1
95	Emergent Herbaceous Wetlands	0.045	0.11	1
96	Palustrine Emergent Wetland (Persistent)	0.045	0.11	1
97	Estuarine Emergent Wetland	0.045	0.11	1
98	Palustrine Aquatic Bed	0.015	0.03	1
99	Estuarine Aquatic Bed	0.015	0.03	1

^ Implementation of Manning's n values depends on the units being used; a conversion of units' time/length$^{1/3}$ should be applied to the n value if units other than meters and seconds are used.
* A canopy value of 0 denotes no wind stress applied. A canopy value of 1 denotes wind stress will be applied.

5. ASTRONOMICAL TIDE SCENARIO

Astronomical tide simulations are a means to validate the model's skill under tidal forcing and assist in determining if the model accurately simulates hydrodynamics in preparation for carrying out hindcast and forecast simulations. In the tidal simulation, the model has no meteorological forcing but is forced only with harmonically predicted astronomical tides for the open boundary water levels and tidal potential within the domain. While it is anticipated that river flux forcing will be part of later operational simulations, no flow boundaries were simulated as part of the tidal validation. In addition, no steric terms were included. The harmonic tidal simulation was conducted for the 120 day period beginning August 1, 2013.

5.1 Harmonic Forcings and Validation Data

The open ocean boundary forcing was developed based on Oregon State University (OSU) TOPEX/Poseidon Global Inverse Solution version 7.2 (TPXO7.2) (Egbert and Erofeeva 2002) with 13 tidal constituents (M_2, S_2, N_2, K_2, K_1, O_1, P_1, Q_1, Mf, Mm, M_4, Ms_4, and Mn_4). Body forcing is applied using eight principal constituents (M_2, S_2, N_2, K_2, K_1, O_1, P_1, and Q_1). The nodal factors and equilibrium arguments are created using the *tide_fac.f* routine available from the ADCIRC website[5].

The CSDL skill-assessment software was used to acquire the harmonic constituents from the Center for Operational Oceanographic Products and Services (CO-OPS) website for comparison with the modeled constituents. A database obtained from Chris Szpilka at the University of Oklahoma gave 404 stations that are being used for validation of the EC2012 mesh—this list was used as a starting point under the assumption that any station represented in the NOMAD mesh would also be in the EC2012. This list was reduced to 398 stations which are covered by the NOMAD mesh.

5.2 Astronomical Tide Validation

Tidal validation was performed with a 120-day simulation consisting of a 30-day warmup period including a 20-day ramping function followed by 10 days of full strength forcing. Harmonic analysis was executed on the remaining 90 days of simulation results for days 30 through 120. ADCIRC was run in implicit mode for these simulations with a two-second time step. The simulation was executed using 1,200 cores for roughly seven hours (approximately 93 core-hours per simulation day).

After resolving issues with the skill assessment software and updating ADCIRC code to the current production version (50.99.14), a set of final tidal skill assessment was performed and the results of the analysis are provided in Figure 5-1 through Figure 5-6. The harmonic constituents obtained from the analysis were compared to values published for the NOAA CO-OPS stations. In the analysis, 398 stations were used out of the original 404 available in the Szpilka database. Additional stations were removed because they were not well-resolved within the mesh.

The following sections present harmonic constituent skill assessment for the simulated tidal time series based on analysis with the CSDL-developed skill assessment software described in Zhang et al.(2006, 2010).

5.2.1 *Harmonic Constituent Amplitude Skill*

Individual harmonics correlated well to predicted harmonic amplitudes, with greatest deviations in the Gulf of Maine. Other areas with error included points in the wetlands on Florida's west coast; inland Florida and Georgia; secluded parts of the Chesapeake Bay; the Delaware River; the East River, NY; and in western Long Island Sound. Figure 5-1 shows the geographic distribution of M_2 amplitude error

[5] *Tide_fac.f* available on-line here: http://unc.edu/ims/adcirc/utility_programs/tide_fac.f

highlighting the difficulty in the Gulf of Maine. Figure 5-2 shows correlation of modeled and predicted harmonic amplitudes with a good fit to the 1:1 line, excluding the large amplitude tides from the Gulf of Maine. Figure 5-3 shows the relative magnitude-sorted amplitude error for modeled vs. predicted harmonic constituents larger than 0.1 meters.

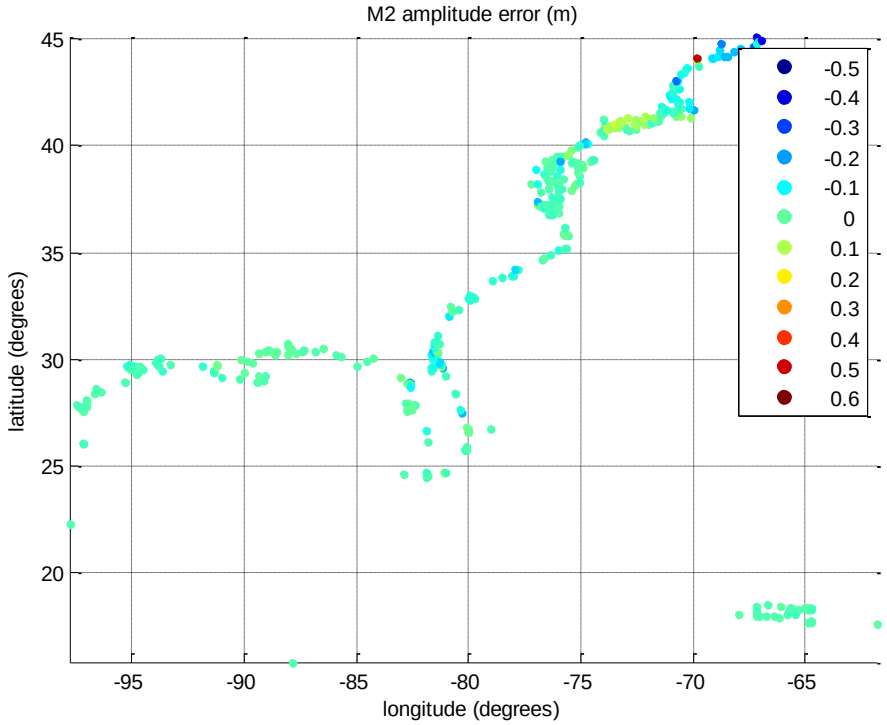

Figure 5-1: Geographic distribution of M_2 constituent amplitude error.

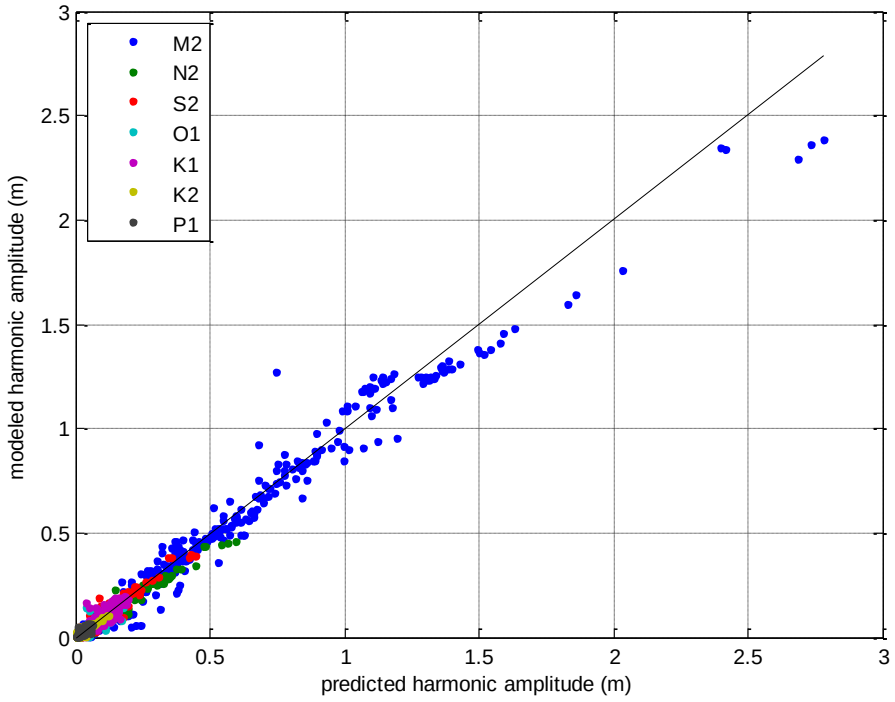

Figure 5-2: Modeled versus predicted harmonic amplitudes for seven primary harmonic constituents.

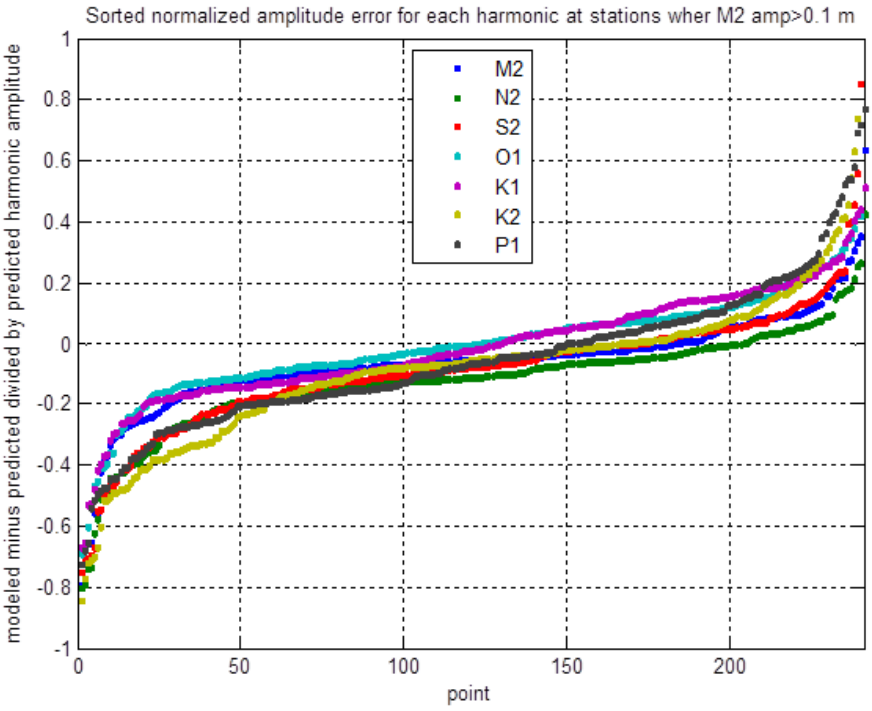

Figure 5-3: Sorted relative amplitude error for seven primary harmonic constituents at stations with M_2 amplitude greater than 0.1 meters.

5.2.2 *Harmonic Constituent Phase Skill*

Phase errors show difficulty particularly in the Chesapeake Bay and Potomac River, as well as in the riverine stations represented in the Louisiana portion of the mesh. The phase error reflects the channel influence on tide wave propagation. Finally, in these simulations, Puerto Rico exhibits significant phase error. Tidal phase changes rapidly around the island, and the University of Notre Dame has previously indicated that accurately modeling the tidal phase requires resolving fine-scale features such as the reef systems around the island (Gonzalez-Lopez 2014). Figure 5-4, Figure 5-5, and Figure 5-6 show the geographic distribution, correlation, and sorted distribution of the phase errors, respectively.

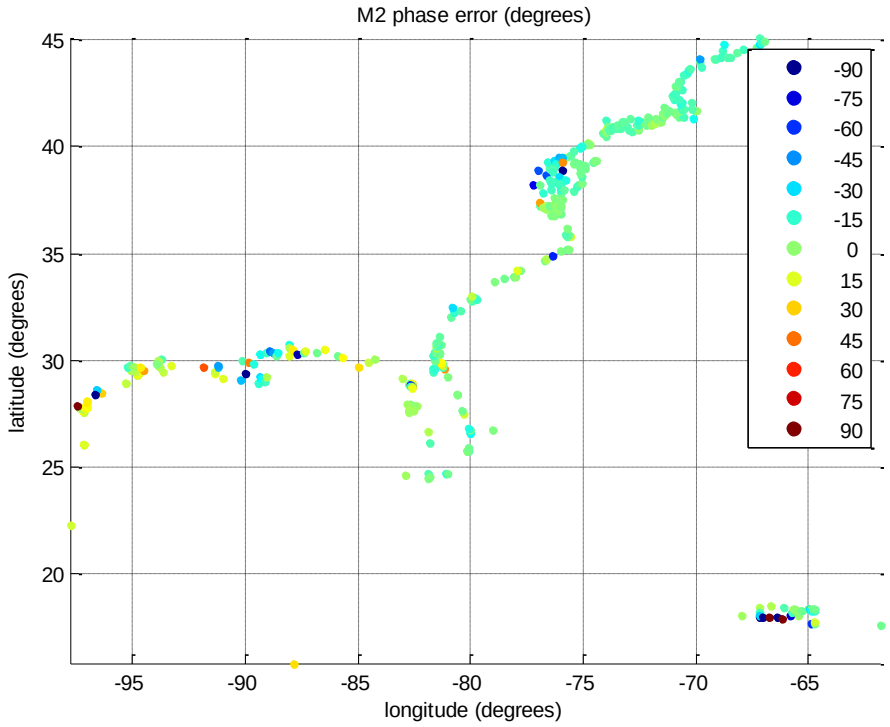

Figure 5-4: Geographic distribution of phase error for M_2 harmonic constituent.

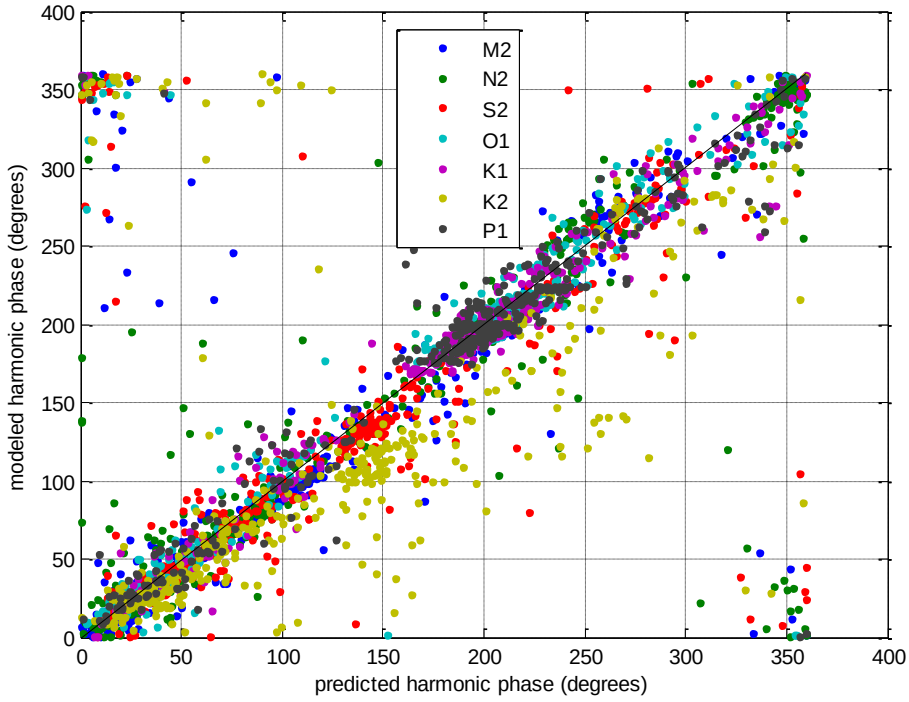

Figure 5-5: Correlation of modeled versus predicted harmonic phases.

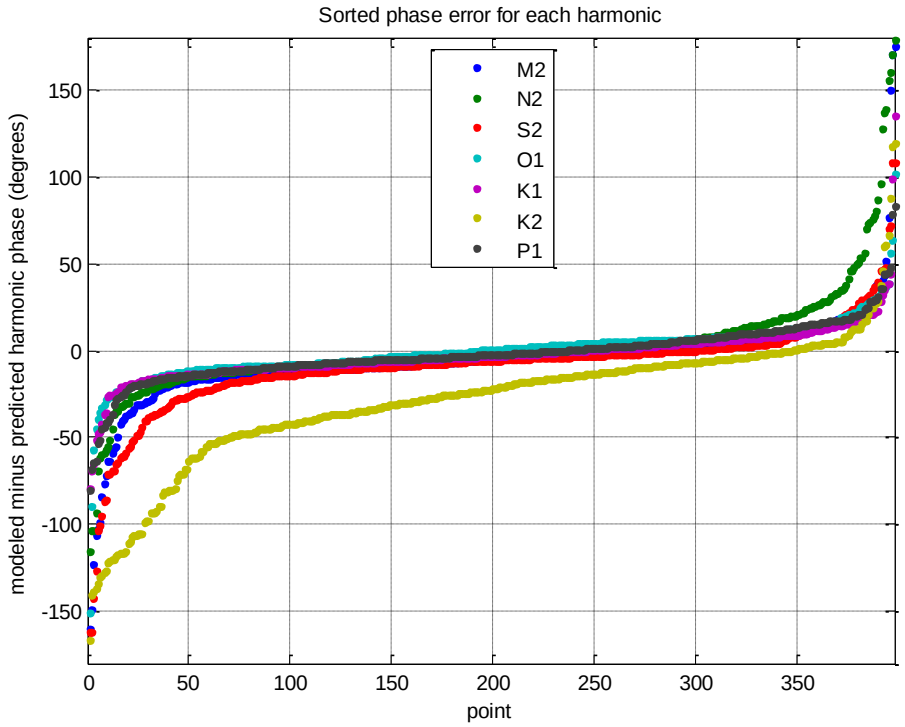

Figure 5-6: Sorted phase error for individual harmonic constituent phases.

5.2.3 *Effect of Advection Terms*

Initial tidal validation runs were attempted using all advective transport terms in the water level solution. However, completing a 120-day simulation without significant mesh instabilities proved extremely difficult, and we developed the final tidal validation results using simulations without consideration for the advective transport terms NOLICA and NOLICAT.

Instabilities consistently formed after a period of 20-110 days near the offshore boundary, either near the southern end (south of roughly 13 degrees latitude) or around the same latitude as Bermuda. Mesh modifications near the locations of the instabilities only delayed the formation of the instability. Modifications made attempting to prevent the instability included changing the number of nodes along and near the boundary, smoothing bathymetry, modifications to the Bay of Fundy to deal with bathymetric issues, turning off boundary forcing of several smaller tidal harmonics, moving the boundary to -60 longitude (the location of the boundaries in the EC95 and EC2001 meshes), increasing the horizontal eddy viscosity (ESLM) up to 50, and turning off wetting and drying and the time derivative of the advection term (NOLICAT).

Manual reviews were also carried out on the water elevation and velocity solutions at dozens of time steps for various runs, and on the boundary forcing amplitudes and phases to verify their smoothness. The only tide simulation that completed without a fatal instability and without any of the above-mentioned modifications was a 90-day simulation with nodal factors set to 1 and equilibrium arguments set to 0. Though, this same run failed if extended to 120 days. Close inspection shows the instability east of Bermuda to be periodic, seemingly appearing at certain tide phases. The nascent instability could be seen weeks or even months before suddenly growing large and crashing the simulation, as shown in Figure 5-7.

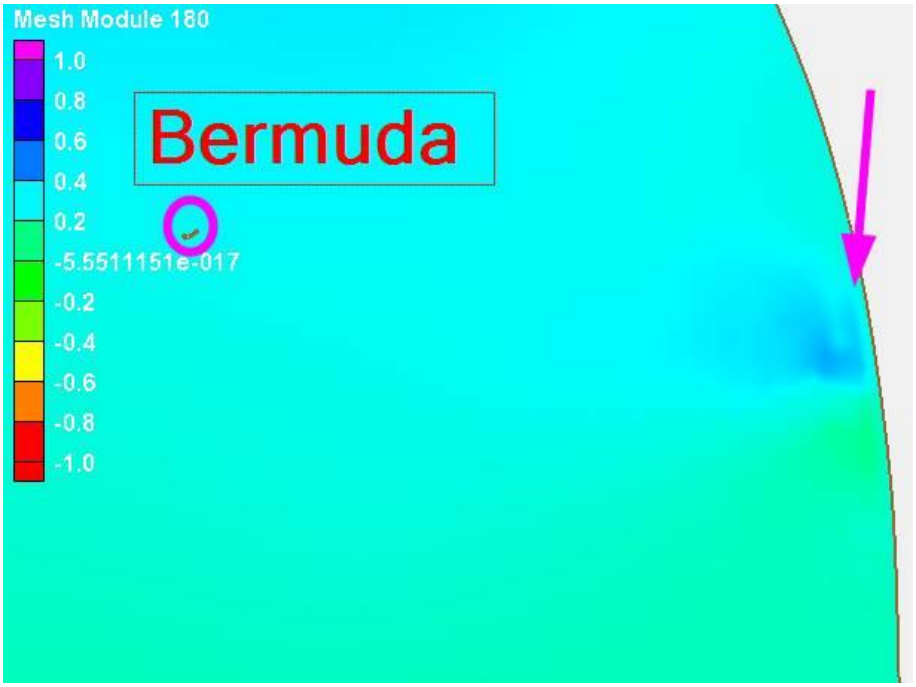

Figure 5-7: Water elevation solution (MSL, meters) at one time step 4 days before fatal instability.

Figure 5-8 and Figure 5-9 show the effects of having the advection terms turned on/off for the tidal simulation. Many improvements in amplitudes of the advection-off run are because they were done with a later version of the mesh and with an improved set of stations, i.e. station positions were changed as necessary to get them within the model domain. These changes can be seen to tighten up the model performance for several other stations (e.g. ones in the 0.5-1 m amplitude range). In both plots, the greatest deviations are found at stations in the Gulf of Maine (all stations with observed amplitudes above 1.2 m) and other areas in the northeast US. At Boston, the differences are on the order of 0.10 meters and in the northern Gulf of Maine, the differences reach 0.20 meters with the results with advection on being greater in both cases. In Long Island Sound, the sense of the deviation is reversed with M_2 amplitudes being smaller for advection-on simulations. Differences between simulations with advection on and off are insignificant in the rest of the East Coast and Gulf of Mexico portions of the mesh.

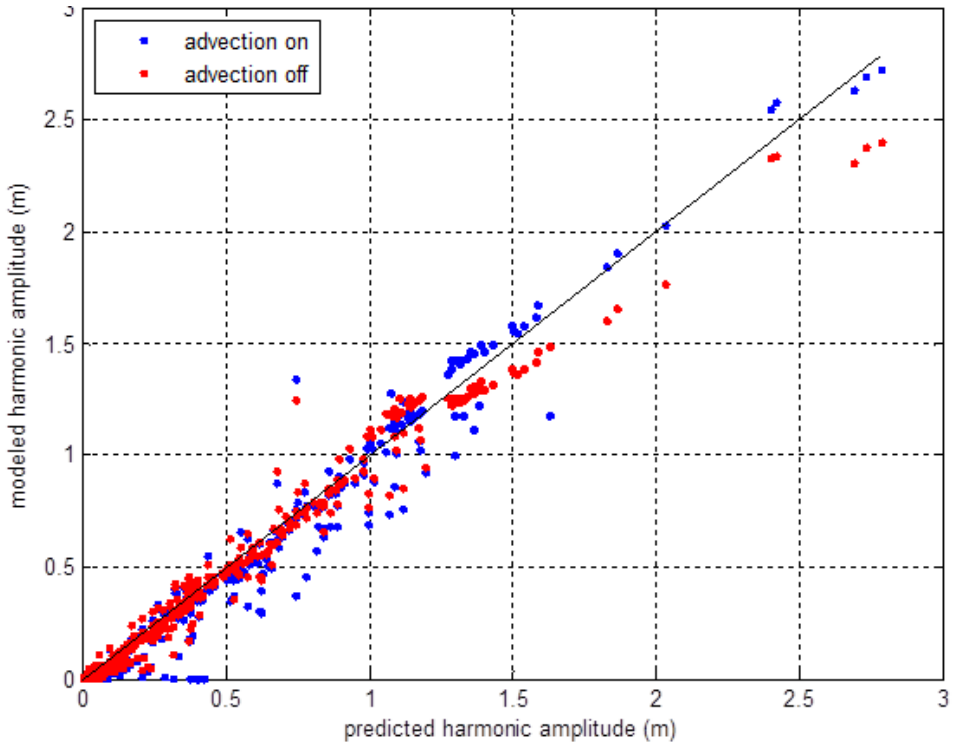

Figure 5-8: Correlation of M_2 constituent amplitude comparing predicted and simulated results from simulations with non-linear advection terms turned on (blue points) and off (red points).

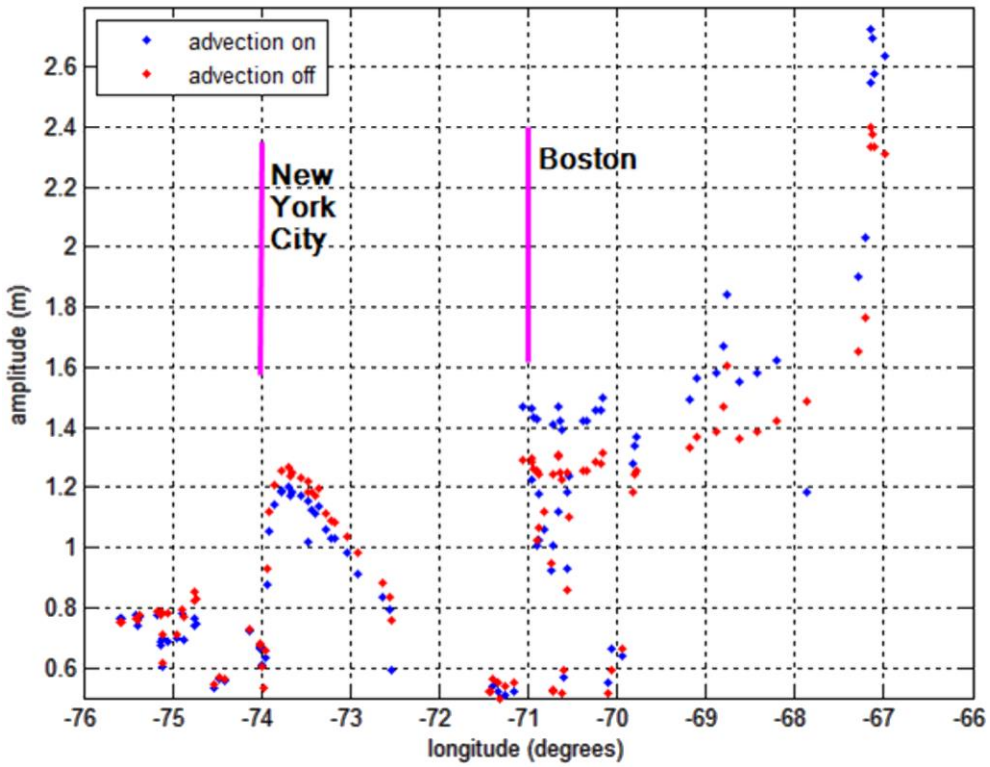

Figure 5-9: A pseudo-geographic depiction of the effect of modification of the non-linear advection; results from simulations with non-linear advection terms turned on are plotted as blue points and off as red points.

5.3 Overall Tidal Skill

Of the 398 stations, 324 meet the target error metric of 0.2 meter root mean squared error (RMSE). Of 74 stations not meeting the target error metric, only 18 are located outside of the Gulf of Maine. The 56 points not meeting the skill metric in the Gulf of Maine owe their poor performance to the effect of disabling the advection terms in the model and to the large tide ranges characteristic of the region. The other stations exceeding the error metric are also in challenging locations, including two points located in wetlands on Florida's west coast; six points in inland parts of Florida and Georgia; four points in secluded parts of the Chesapeake Bay; three points up the Delaware River; one point in the East River; and one point in western Long Island Sound.

The inland points in Florida and Georgia were affected by a problem endemic to the wetting and drying algorithm within ADICIRC. The problem is associated with the factors which are included in the ADCIRC solution to prevent instabilities when elements are periodically wetting and drying. Essentially under certain conditions, the model will artificially produce water over broad, slow draining areas surrounded by steep drop-offs, such as in the Georgia tidal flats. This creates an artificially high water level on the tidal flats. Additional detail regarding this issue is documented in Appendix D.

Figure 5-10 shows the geographic distribution of the gage errors, highlighting gages that exceed the error criteria.

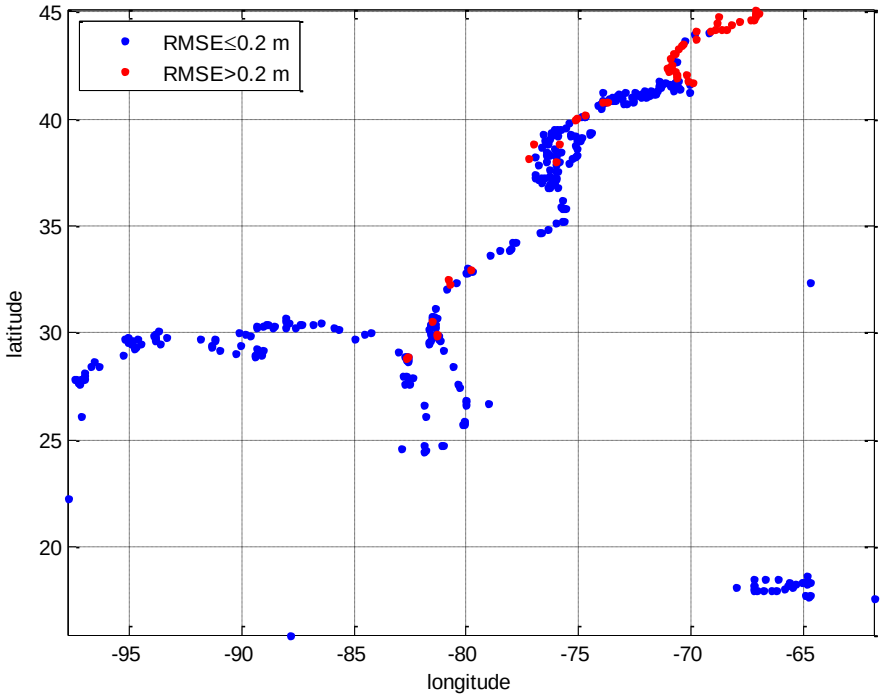

Figure 5-10: Geographic distribution of water level time series RMSE at 398 tide gages, highlighting points exceeding the 0.2 meter RMS error metric.

6. STORM HINDCAST VALIDATION

Surge responses during a total of ten tropical and extratropical storms were evaluated, covering a spectrum of landfalls across the US Gulf of Mexico and East coasts. The target error metric was 0.2 meters (0.66 feet) RMSE for time series data at NOAA gages as computed by the CSDL Skill Assessment Software[6]. Simulated peak surges were compared to both NOAA time series data and to post-storm surveyed High Water Mark (HWM) datasets, where these datasets were available. Storms whose meteorological forcing came from a FEMA Flood Insurance Study (FIS) have model skill comparisons to those studies to give a sense of baseline performance that can be expected with the same meteorological data. However, the FEMA studies use much higher resolution meshes and (in most cases) a coupled wave model.

Model skill suffered most from differences in initial water level (model simulations were run without a starting water level anomaly adjustment) and from missing wave setup contributions. As a result, most storms' modeled results are biased low. Some storms, particularly Ike, the 1991 Perfect Storm, and Dennis, showed poor performance for other reasons as explained in the sections below. The quality of the wind forcing was a significant factor in the overall skill of the models. For this reason, the FEMA-sourced hindcast forcing created by Ocean Weather, Inc. (OWI) was used where available because it provided the best opportunity to test the performance of the mesh. For events where OWI meteorology was not available, the model skill suffered as a result.

The CSDL Skill Assessment reported RMSE for all gages evaluated for all storms was 0.26 meters, 30% greater than the target. Modifications suggested in Section 0, specifically making some accommodation for the un-simulated mean water level effects, could bring the mean error within the target. Additional analysis and discussion are given for the individual storms in this section and for the entire set of storms as a group in Section 7.

6.1 Typical Model Setup

All storm simulations began with a 15-day tidal simulation, during which the tidal forcing was ramped up using a hyperbolic tangent ramping function for the first 10 days. Storm simulations were then hot-started from the tide ramp runs, with the duration of the storm forcing varying by storm. A separate ramping of the meteorological forcing was applied at hot-start time, which lasted 0.5 days for most storms. Following the meteorological ramping period, the simulation was completed within the actual event period, going from as little as 1.25 days up to 8 days depending on the length of the event.

All storms were modeled at their historical time by use of proper tidal harmonic phasing. The *tide_fac.f*[7] Fortran routine was used to generate boundary and body forcing values for 13 harmonic constituents. Further details on tidal forcing are supplied in Section 5.1. All simulations were attempted with advection both on and off. Information about how this affected results is included in the sections below. Details on bottom friction, wind drag, and other spatially varying parameters are supplied in Section 4.2.

Surface forcing fields consisting of wind velocities and atmospheric pressure were provided from a variety of sources, including: 1) quality controlled high resolution wind fields created by Ocean Weather, Inc. (OWI) as part of FEMA FIS studies and provided by FEMA to NOAA for this project; 2) Hurricane Weather Research and Forecast System (HWRF) hindcasts from NOAA; 3) NOAA's Atlantic Oceanographic & Meteorological Laboratory (AOML) Hurricane Research Division (HRD) Surface

[6] The skill assessment software provided by CSDL was modified to prevent clipping of observed surge data. By default, the software is set to remove downloaded data points more than three standard deviations from the rest of the data. This value was extended include all valid water level measurements including the surge crest.
[7] Available on the ADCIRC website http://adcirc.org/home/related-software/adcirc-utility-programs/

Wind Analysis System (H*Wind)[8] real-time analysis fields; and 4) NHC best-track data driving the parametric hurricane vortex model included within the ADCIRC model. The storms used for hindcast analysis are shown in Table 6-1, along with an indication of the source for the wind forcings for the simulation. In the table and throughout Section 6, the storms are presented in geographic order, from west to east along the Gulf of Mexico, then south to north along the East coast, as shown in Figure 6-1.

Table 6-1: Summary of tropical and extratropical cyclone hindcast validation simulations.

Coastal Impact Area	Name	Year	Month	Wind Data Source(s)	Wind Scaling	Advection
North Central Texas, Western Louisiana.	Ike	2008	Sept	OWI/FEMA Region 6: Texas study	1.04	On
Eastern Louisiana, Mississippi	Katrina	2005	Aug	OWI/FEMA Region 4: Mississippi, Panhandle studies	1.09	On
Panhandle and northwestern Florida.	Dennis	2005	July	OWI/FEMA Region 4: Big Bend, Panhandle studies	1.04	On
Southwestern Florida	Charley	2004	Oct	OWI/FEMA Region 4: Southwest Florida study	1.04	On
South Carolina	Hugo	1989	Sept	OWI/FEMA Region 4: South Carolina study	1.04	Off
North Carolina	Floyd	1999	Sept	H*Wind; ADCIRC parametric with NHC best track (Holland)		
Virginia., Washington D.C., Maryland., Delaware.	Isabel	2003	Sept	OWI/FEMA Region 3: Region 3 study	1.04	On
New England	Sandy	2012	Oct	HWRF	1.0	On
New England	Long Island Express or Great New England Hurricane	1938	Sept	OWI/FEMA Region 2: New Jersey/New York study	1.04	On
New England	Perfect Storm or Halloween Nor'easter	1991	Oct	OWI/FEMA Region 2: New Jersey/New York study	1.04	Off

[8] H*Wind data may be obtained from: http://www.aoml.noaa.gov/hrd/data_sub/wind.html.

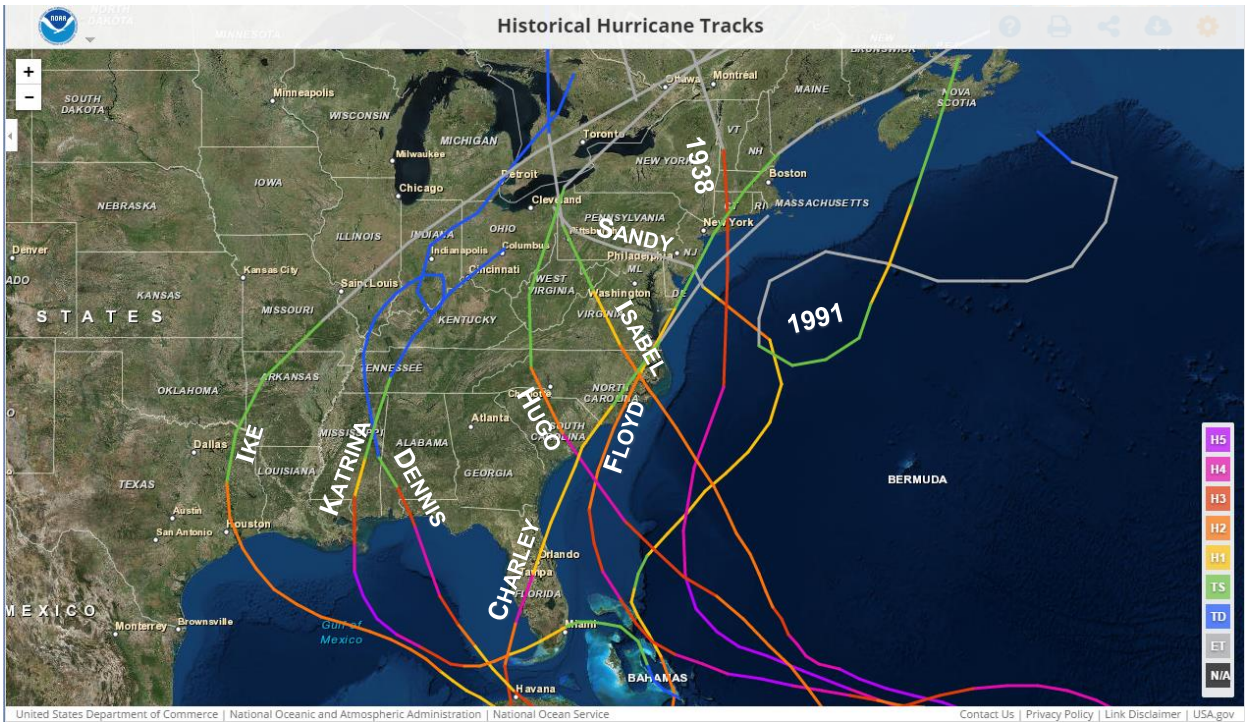

Figure 6-1: Approximate landfall locations of hindcast validation events.

The majority of the simulations used OWI wind and pressure forcing obtained from FEMA studies. OWI provides 30-minute averaged marine-equivalent winds at 10 meter elevation. All storms using OWI wind forcing had their winds scaled by a factor of 1.04 (except for Hurricane Katrina), due to the differences between 10 and 30-minute wind averaging as seen in prior modeling projects and different values used in FEMA studies, including 1.00, 1.04, and 1.09. Hurricane Katrina's OWI winds were a special case due to the way in which they were developed, which is detailed for that storm in Section 6.3. Early test simulations for Ike, Sandy, and Floyd were made with H*Wind real-time analysis fields as they initially lacked OWI windfields, but these simulations yielded poor model skill. Alternative forcing data sources were sought for these events. HWRF fields improved the model performance for Sandy and OWI winds were eventually obtained and also improved the model skill for Ike. The only alternative source found for Floyd was the best-track + ADCIRC internal parametric wind model which did not improve the overall skill for the event.

Skill assessment for all simulations described in this section were carried out using the CSDL-developed software described in Zhang et al. (2006, 2010). Hurricane track plots shown in Figure 6-1 above and in the following sections were obtained from the NOAA Historical Hurricane Tracks tool (Office of Coastal Management[9]).

[9] The NOAA Office of Coastal Management on-line archive and map of hurricane tracks is available here: http://coast.noaa.gov/hurricanes/

6.2 **Ike (2008)**

Hurricane Ike was a Category 4 hurricane that devastated Texas. Ike made landfall on September 13, 2008 at Galveston, Texas as a Category 2 hurricane. Storm surge was most prominent in Texas and Louisiana, although an appreciable surge signal was present throughout the Gulf of Mexico.

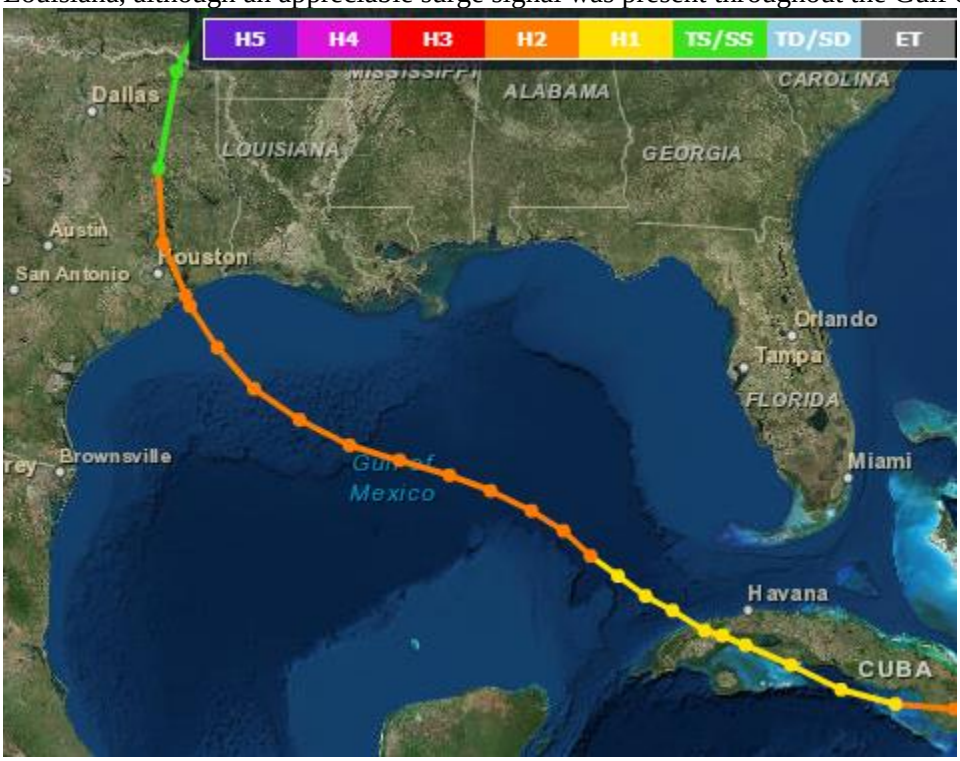

Figure 6-2: Storm track of Hurricane Ike. Dots denote 6-hour intervals and landfall.

6.2.1 ***Model Setup***

The model simulation was 22.25 days long, with an 8.75-day storm run. Meteorological forcing was supplied by OWI wind files, and the winds were scaled up by a factor of 1.04 for consistency with other validation storms. However, it should be noted the Texas FEMA study scaled these OWI winds by a factor of 1.09. Wind/pressure forcing was supplied at 15-minute intervals. The simulation was executed with advection terms both on and off, and peak surge differences were found to be within +/- 0.15 meters (0.5 feet).

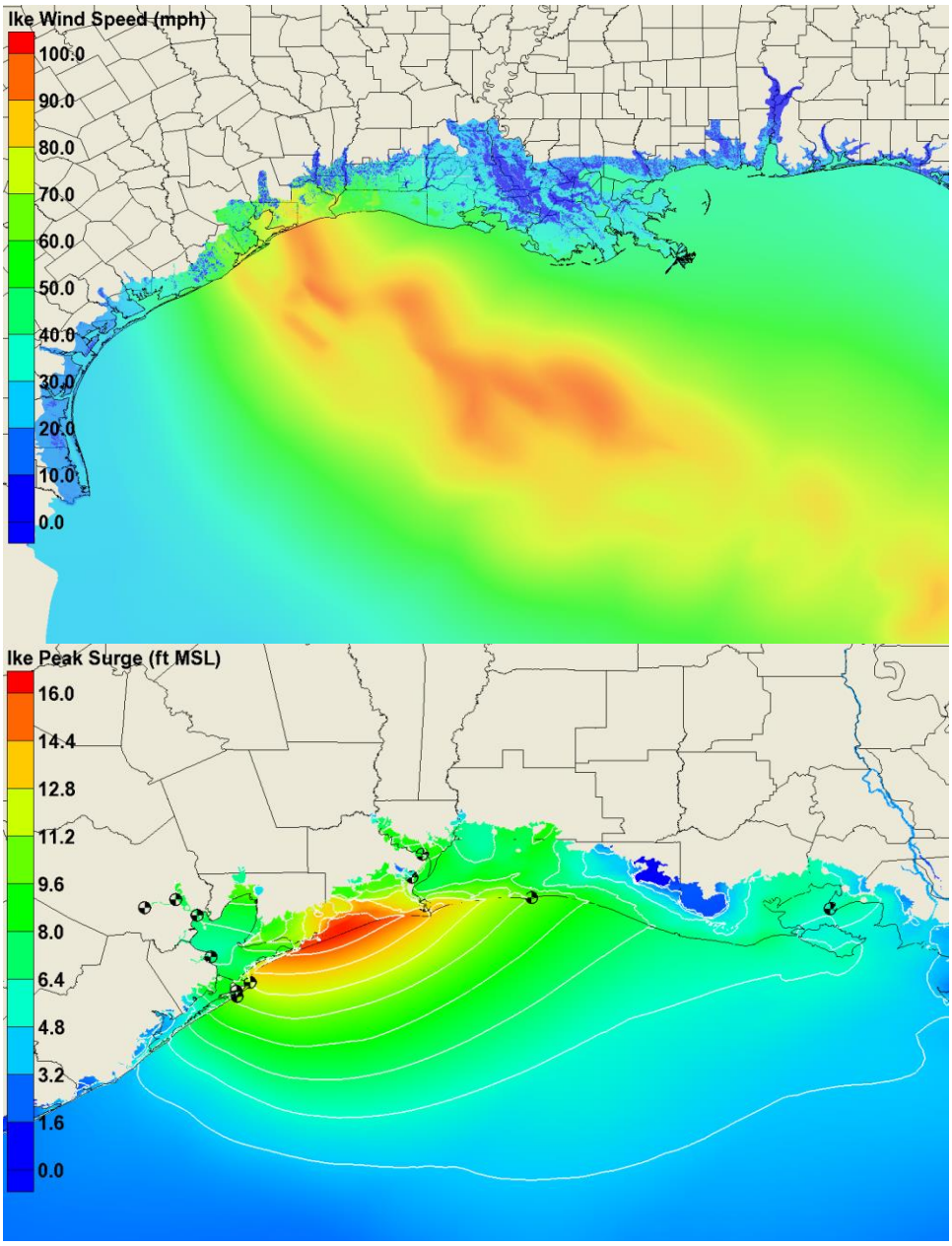

Figure 6-3: Ike maximum wind speeds (top, mph) and maximum modeled surge (bottom, ft MSL); NOAA gage sites marked by pinwheels (bottom).

6.2.2 *Results and Skill Assessment*

Model skill for Ike was generally poor with most RMSE errors greater than 1 foot as shown in Figure 6-5. Time series (Figure 6-9 to Figure 6-12) clearly indicate that surge did not effectively penetrate behind the barrier islands, largely due to an under-prediction of a forerunner surge. Kennedy et al. (2011) estimated the magnitude of the forerunner surge at 1.4 meters.

Prior studies, including the FEMA and IOOS studies, have indicated that alterations to the bottom friction along the muddy Louisiana-Texas shelf strongly assist the FEMA model performance in this regard. Details on the modifications to the bottom friction are not well documented, however Hope et al. (2013)

indicates that the Manning's n value used for bottom friction was reduced to 0.012 for most of the continental shelf in the LA-TX region, as compared to 0.02 in the NOMAD model. Although not mentioned explicitly in their paper, discussions with modelers involved in the studies also indicated that the minimum bottom friction (CF in the fort.15 file) was set to 0. This reduction in CF is critical because without it, the effect on bottom friction of reducing Manning's n over the domain would be relatively minor. For instance, a typical minimum bottom friction of 0.0025 (used in the NOMAD model) will be reached at 3.9 m depth for Manning's n = 0.02 and at 0.18 m depth for Manning's n = 0.012. So, if the minimum bottom friction wasn't lowered, the reduction in friction would only affect areas shallower than 3.9 m depth, i.e. almost none of the continental shelf in the Louisiana – Texas area.

The FEMA study (and possibly also the IOOS study) also sought improved representation of the forerunner surge by increasing the wind field by a factor of 1.09. However, based on guidance from CSDL[10], this study maintained a wind scaling factor of 1.04 for consistency across reported results for all storms.

Most gages around the peak surge in the Galveston area failed, as shown in Figure 6-4 and Figure 6-6. The greater detail in Figure 6-6 makes apparent that the surge was severely under-estimated within Galveston Bay. The NOMAD simulation did not represent the forerunner surge (see Figure 6-11, Figure 6-12, and especially Figure 6-9) but this phenomenon with its long duration preceding the storm provided time for the bay to fill with water. Without this additional water in the bay accounted for, the primary surge was underestimated.

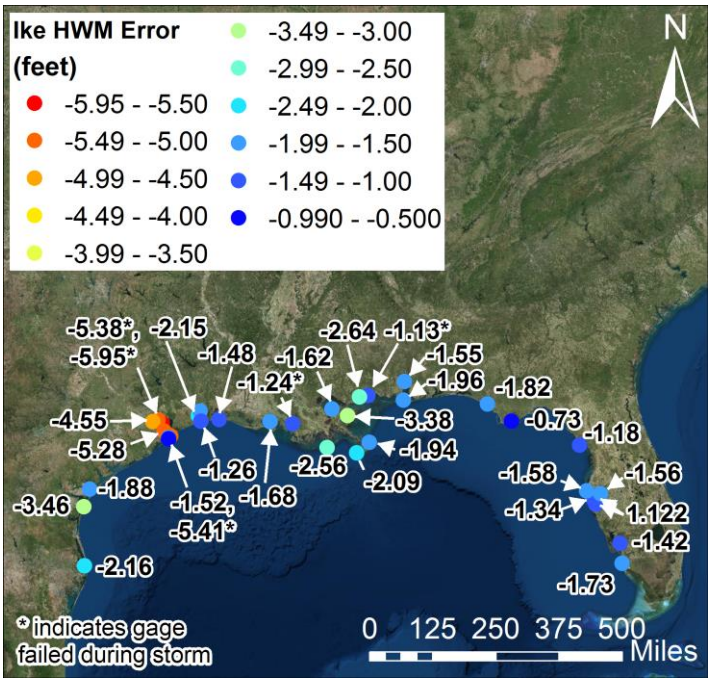

Figure 6-4: Geographic distribution of NOAA gage peak surge error (feet, modeled minus measured).

[10] The CSDL guidance is based at least partially on the fact that in the operational forecasting environment, dynamic modifications to scaling factors will be difficult to implement or justify.

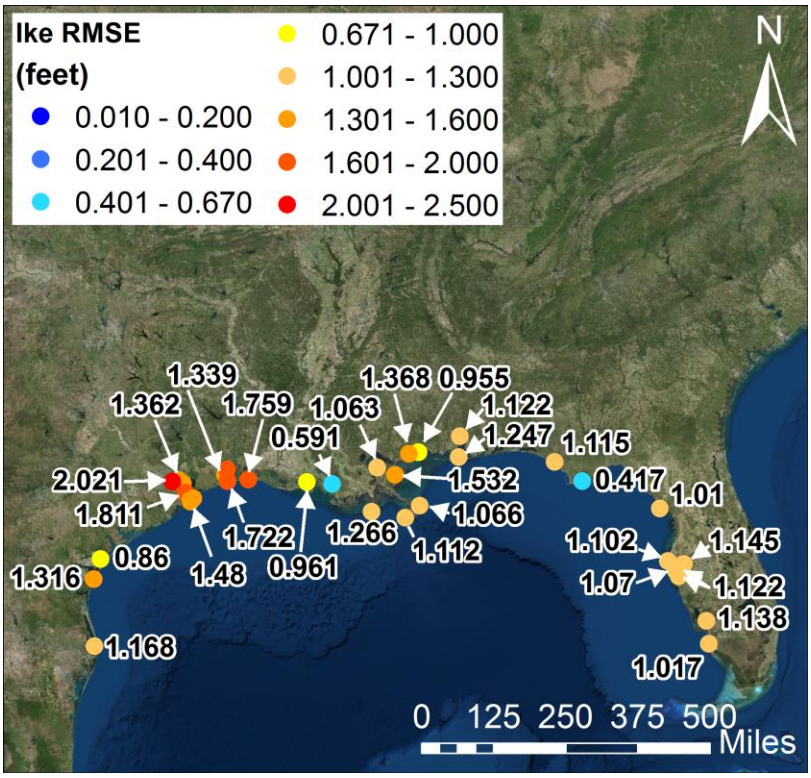

Figure 6-5: Geographic distribution of NOAA gage time series RMSE (feet).

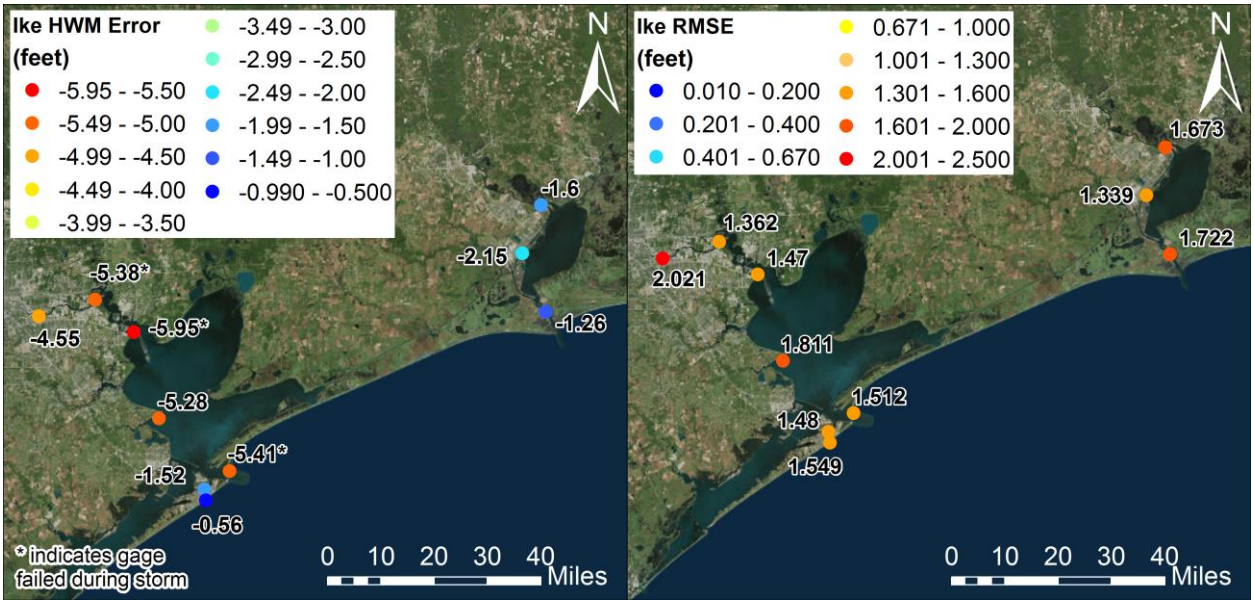

Figure 6-6: Galveston area NOAA gage time series peak water level error (left, feet, modeled minus measured) and RMSE (right, feet).

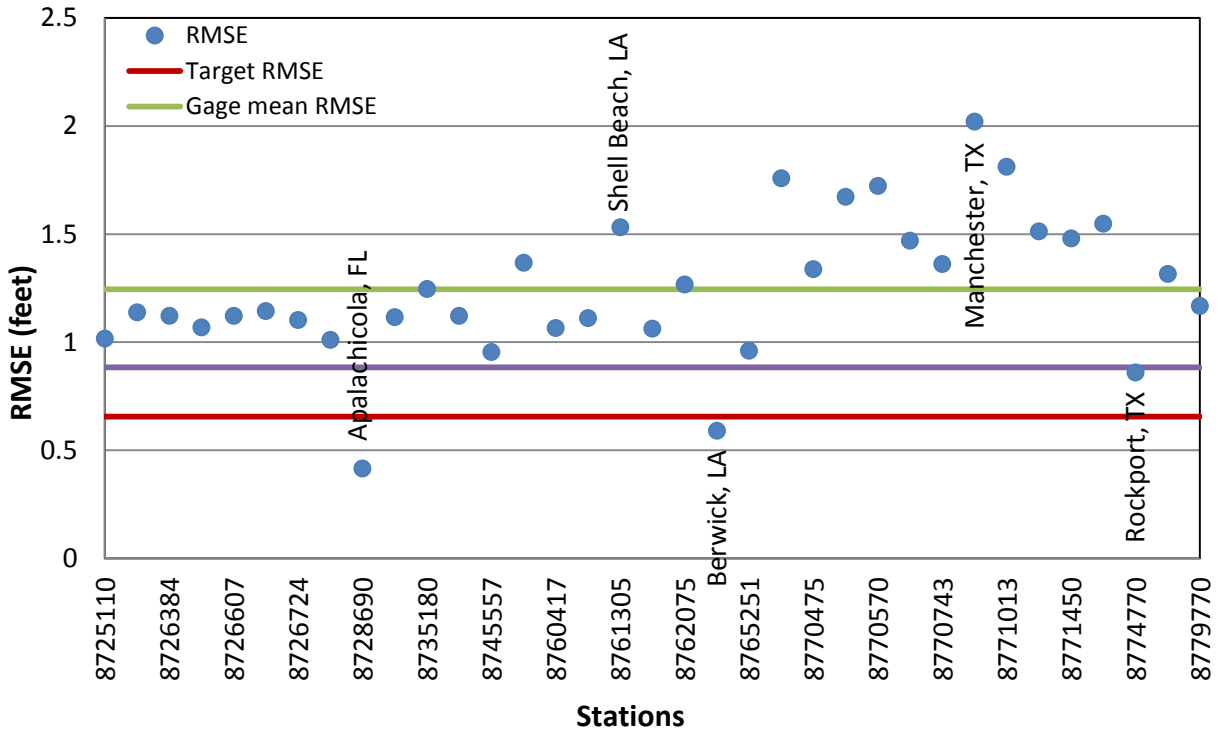

Figure 6-7: Alongshore plot of time series RMSE at NOAA stations; selected stations named for reference, red line indicates target RMSE, green line gives gage mean RMSE, and the purple line is mean RMSE from all storms.

As a test, Ike was simulated on the NOMAD mesh with 1.09x winds (which is based on the FEMA model setup for this area) to evaluate how much this changed modeled results. As shown in Figure 6-8, this has a large effect on the surge. Attempts to test the NOMAD mesh with reduced bottom friction failed with model instabilities mid-way through the simulation.

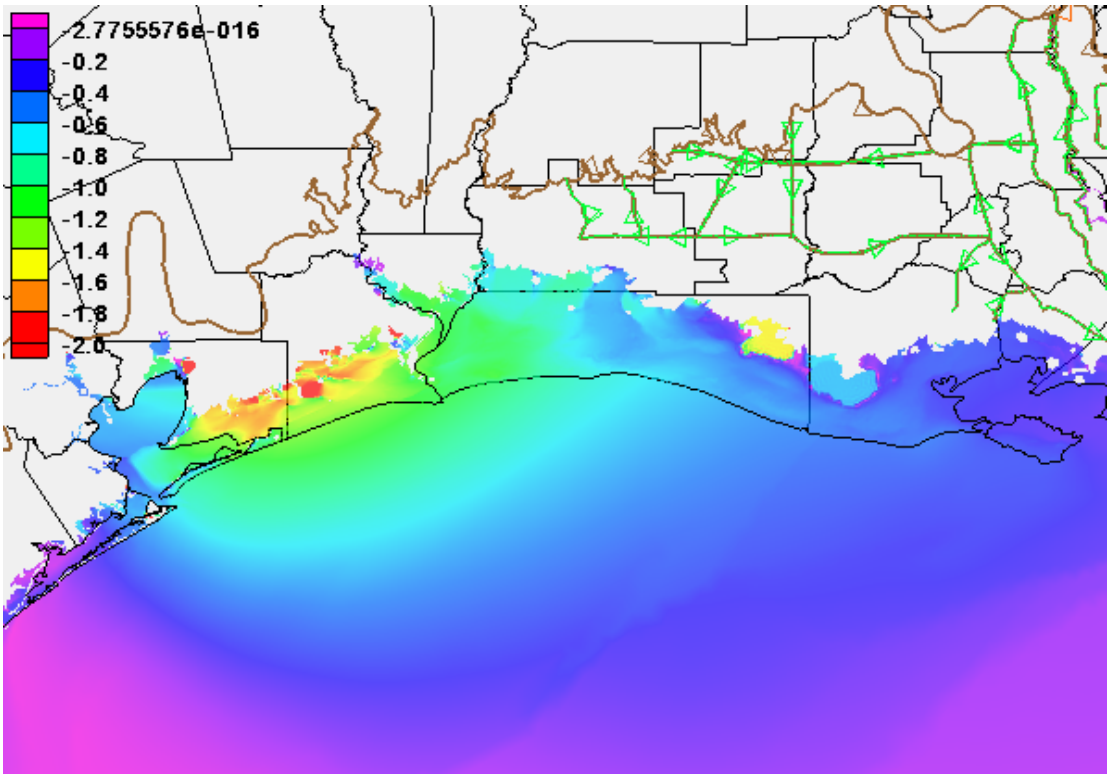

Figure 6-8: Difference in peak surge for 1.04x winds from 1.09x winds (feet).

The only open coast gage in the area that did not fail, Galveston Pleasure Pier, nearly matches the peak surge (Figure 6-9). The average water level (i.e. before the storm arrives) is low at all gages because the model does not account for seasonal water level changes, such as the steric effect. Interestingly, the model also shows a low bias in peak surges across all the gages checked, not just those in the Louisiana-Texas region. The model wind fields were developed for the Texas area and they may not be as accurate outside of that region; however, the consistent low bias in peak modeled surges even in the Texas area where the wind fields are considered accurate is noteworthy and may be worth further investigation by CSDL.

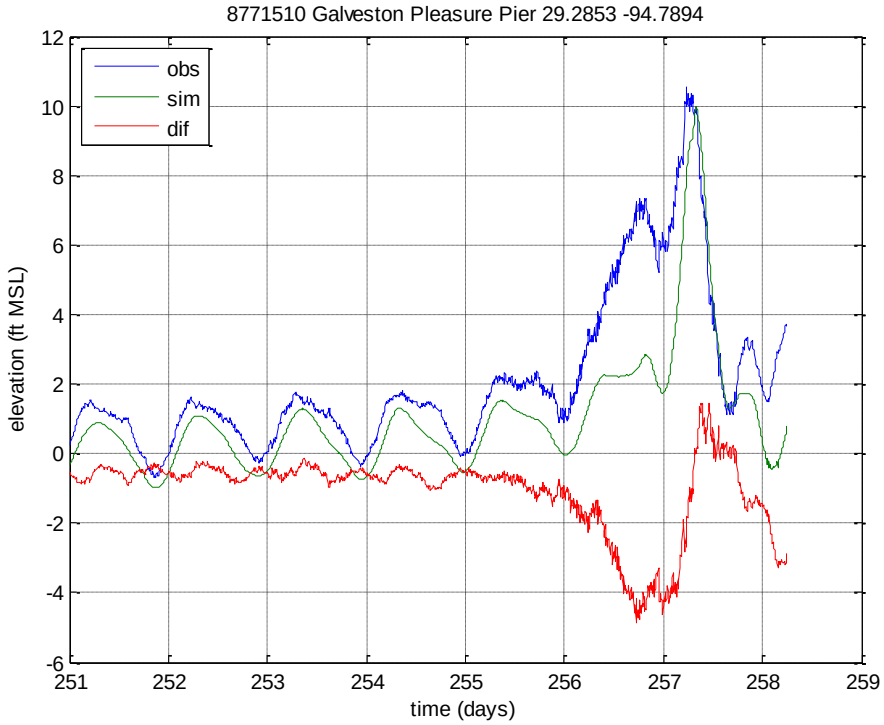

Figure 6-9: Measured and modeled time series at Galveston Pleasure Pier, Texas.

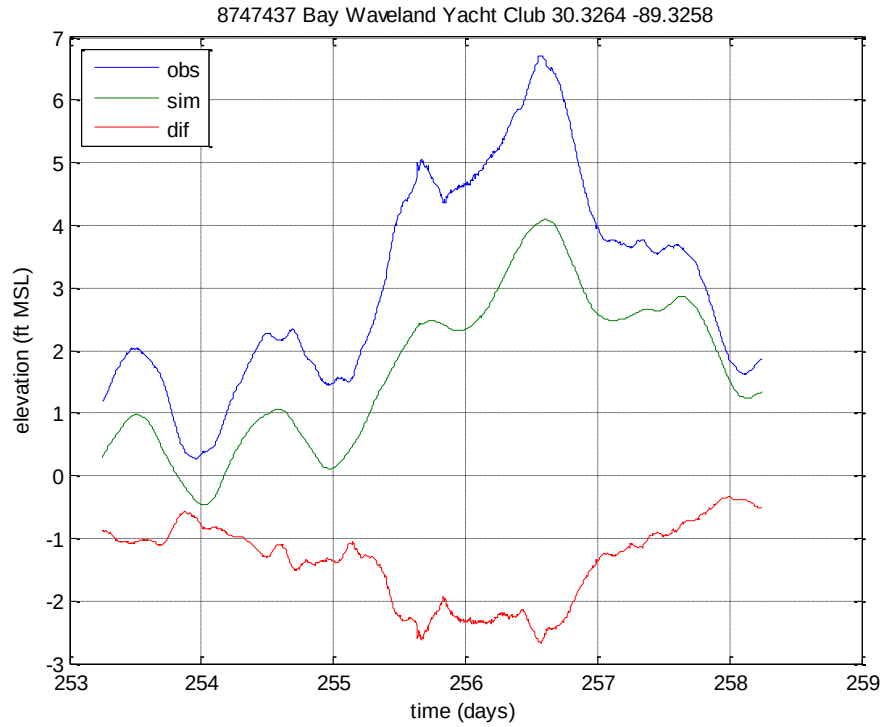

Figure 6-10: Measured and modeled time series at Bay Waveland, Mississippi.

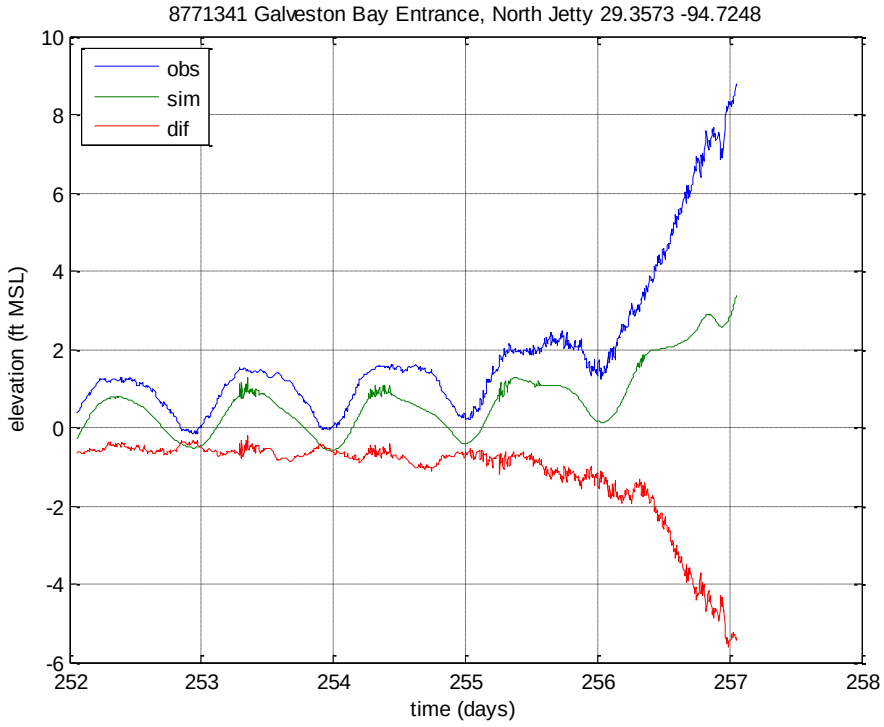

Figure 6-11: Measured and modeled time series at Galveston Bay Entrance, Texas.

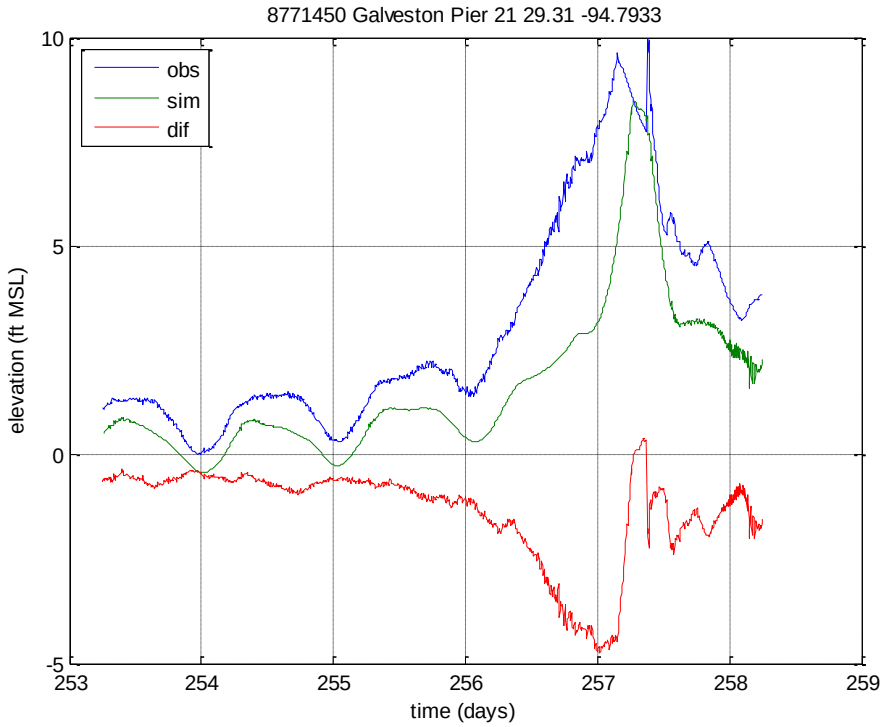

Figure 6-12: Measured and modeled time series at Galveston Pier, Texas.

Advection's effect was small except for a few locations, as shown in Figure 6-13. These areas are mostly around the peak surge, as expected. The half-foot effect from advection is typically less than three percent of the peak surge amplitude.

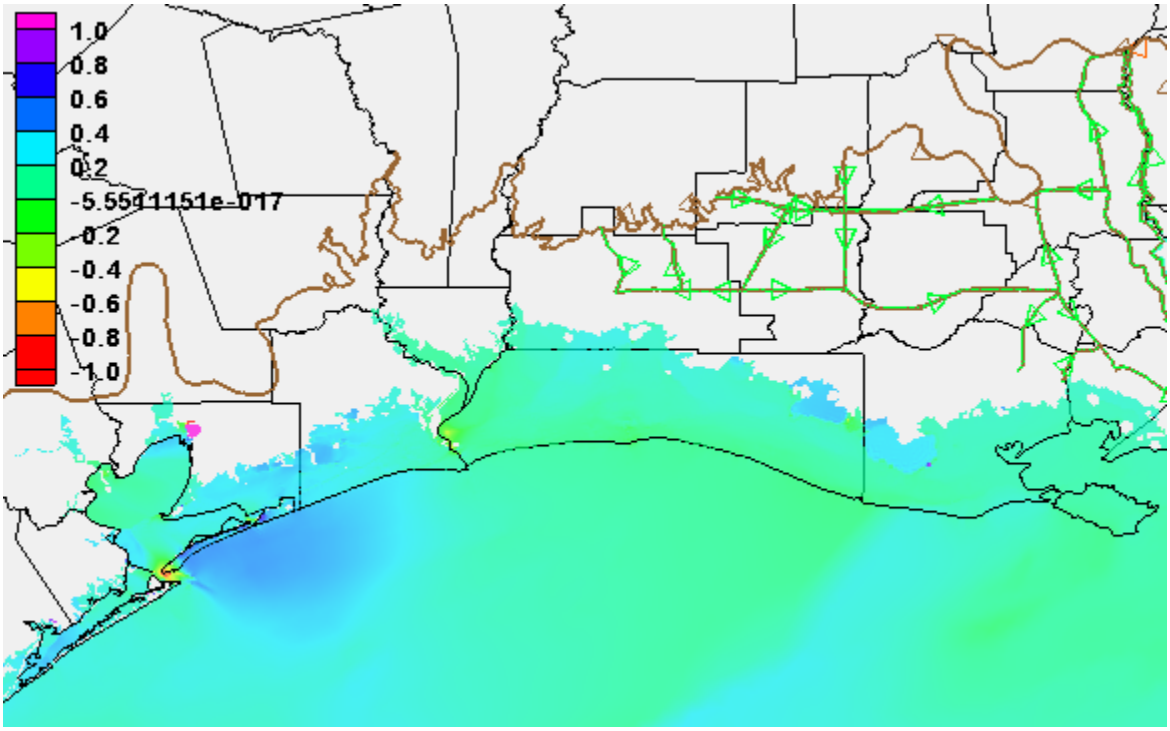

Figure 6-13: Ike advection-on minus advection-off peak surges (feet).

6.3 **Katrina (2005)**

Hurricane Katrina was a Category 5 hurricane that caused unprecedented damage to Louisiana and Mississippi. Katrina made landfall August 29, 2005 in southeast Louisiana as a Category 3 hurricane. Storm surge was most prominent in Louisiana and Mississippi, although an appreciable surge signal was present in Alabama and Florida.

Figure 6-14: Storm track of Hurricane Katrina. Dots denote 6-hour intervals and landfall.

6.3.1 ***Model Setup***

The model simulation was 19.5 days long, with a 4.5-day storm run. Meteorological forcing was supplied by OWI-formatted wind files, and the winds were scaled up by a factor of 1.09, as in the Mississippi and Panhandle FEMA studies that supplied the meteorological inputs. The winds for Katrina were scaled up more than other runs due to a peculiarity in how the wind fields were developed, in which an incorrectly used gust factor was applied to the H*Wind data that served the core of the OWI wind model. This resulted in the OWI-produced wind fields being off by a factor of roughly 1.09. The OWI wind fields were pieced together from multiple FEMA studies, which did not have the same spatial frames. This resulted in one piece of the wind field being smeared, as can be seen in Figure 6-15; however this does not appear to have any effect on the results. Wind/pressure forcing was supplied at 15-minute intervals. The simulation was executed with advection terms both on and off, and differences were found to be generally within +/-0.30 meters (1 foot).

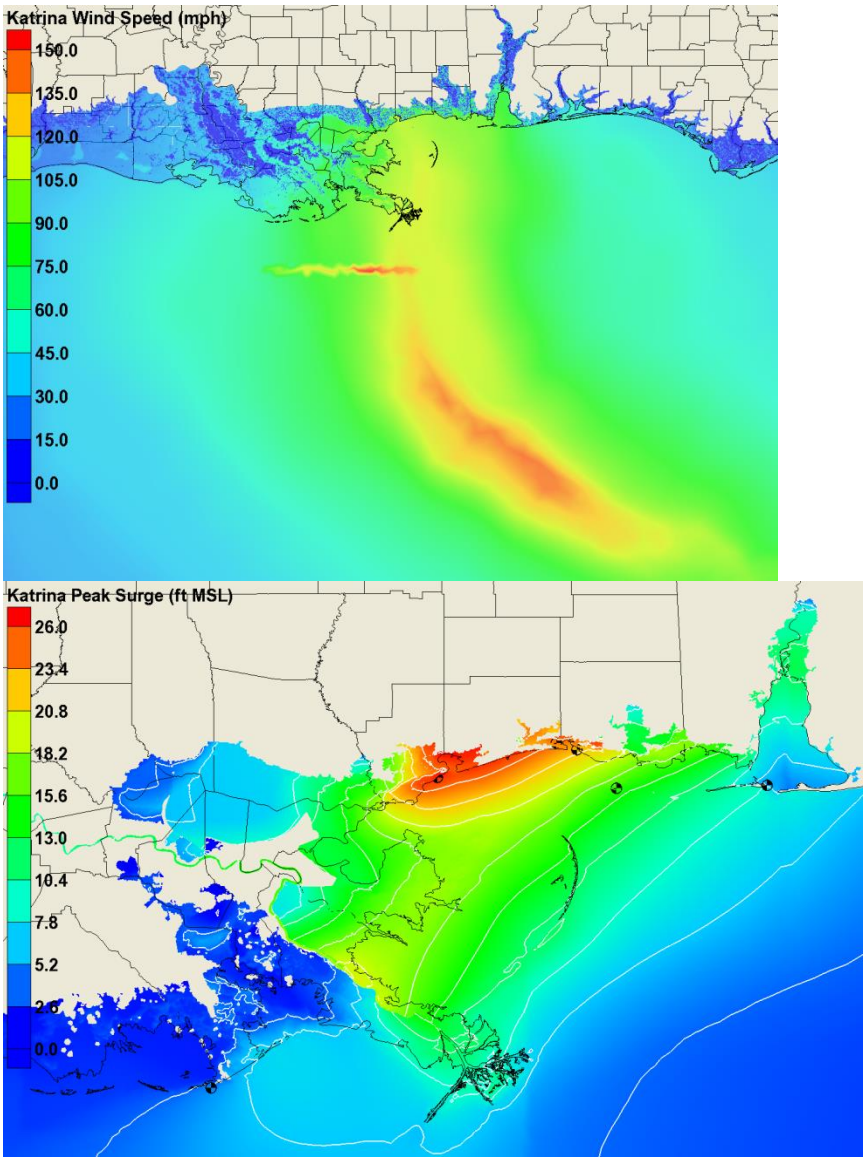

Figure 6-15: Katrina maximum wind speeds (top, mph) and maximum modeled surge (bottom, feet MSL); NOAA gage sites marked by pinwheels (bottom).

6.3.2 *Results and Skill Assessment*

Model skill was generally good with surge rising above the average tidal level the proper amount as visible in the time series plots (Figure 6-18 and Figure 6-19). Four gages west of landfall met the 0.2 meter error metric but a consistent low-bias of around 0.5 feet (probably due to un-modeled steric effects) resulted in an average RMSE greater than the target.

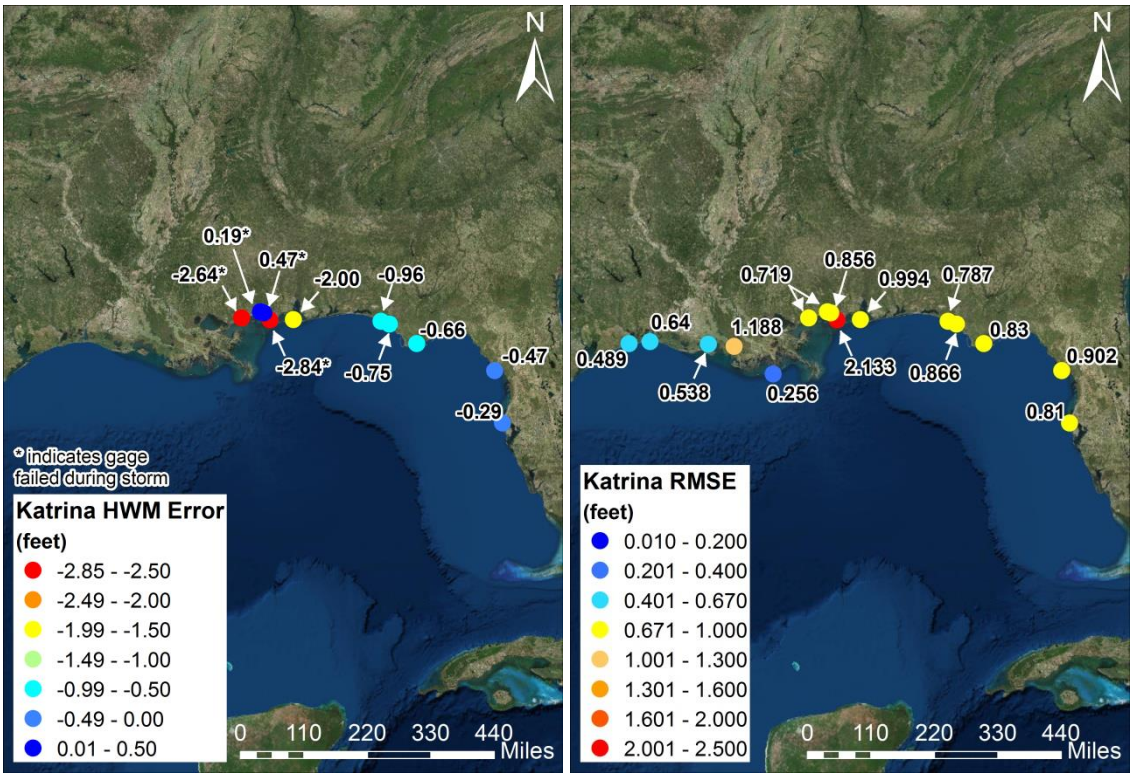

Figure 6-16: Geographic distribution of peak water level error (left) and time series RMSE (right) at NOAA stations. Peak surge errors are only shown for gages with a distinct surge signal.

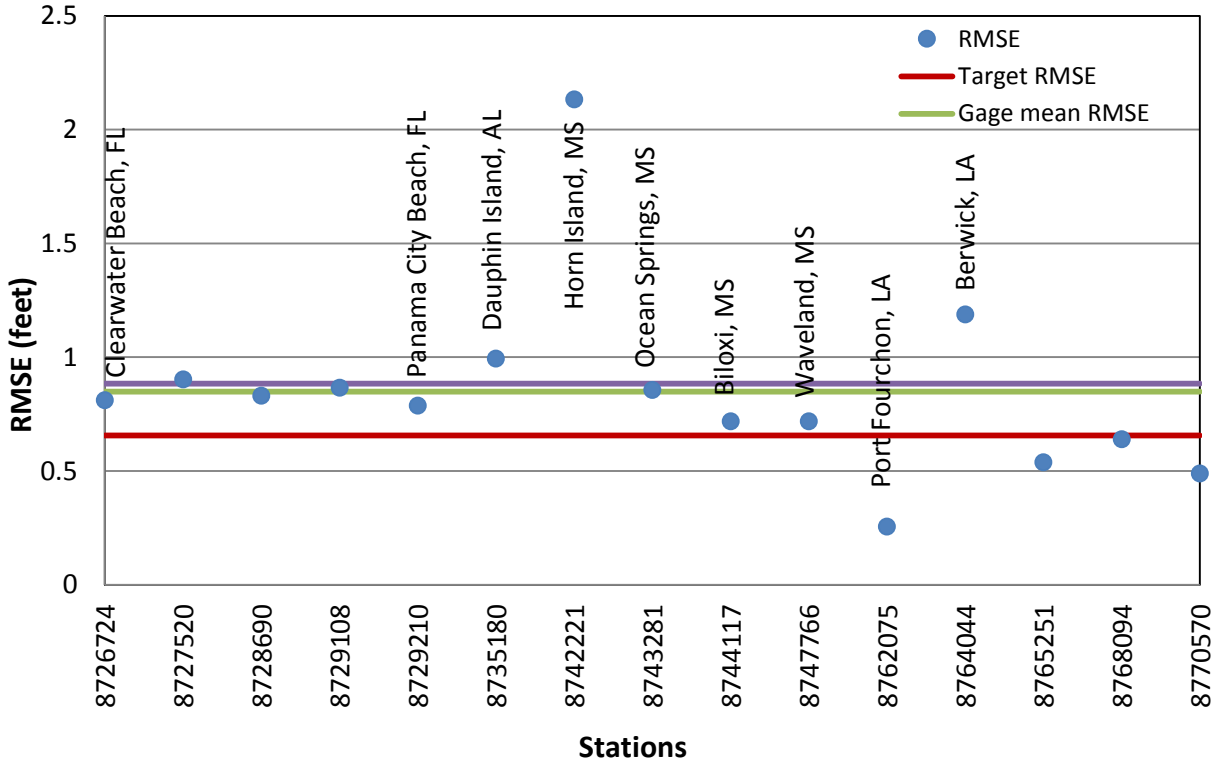

Figure 6-17: Alongshore plot of time series RMSE at NOAA stations; selected stations named for reference; red line indicates target RMSE, green line gives gage mean RMSE, and the purple line is mean RMSE from all storms.

The largest errors in peak surge come from gages that failed during the storm (e.g., Waveland, Miss.; see Figure 6-18), which leads to uncertainty in the final water levels recorded. Model performance was notably lower at the Dauphin Island gage (Figure 6-19), which experienced a sudden surge late in the storm; the cause for the end-of-storm deviation is not understood and not well captured in the simulation.

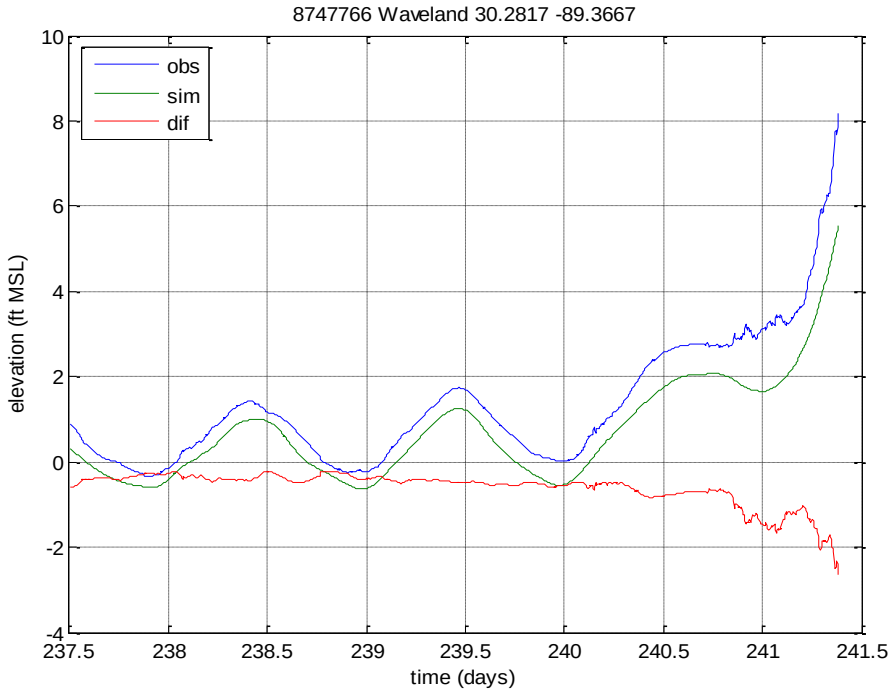

Figure 6-18: Measured and modeled time series at Waveland, Mississippi.

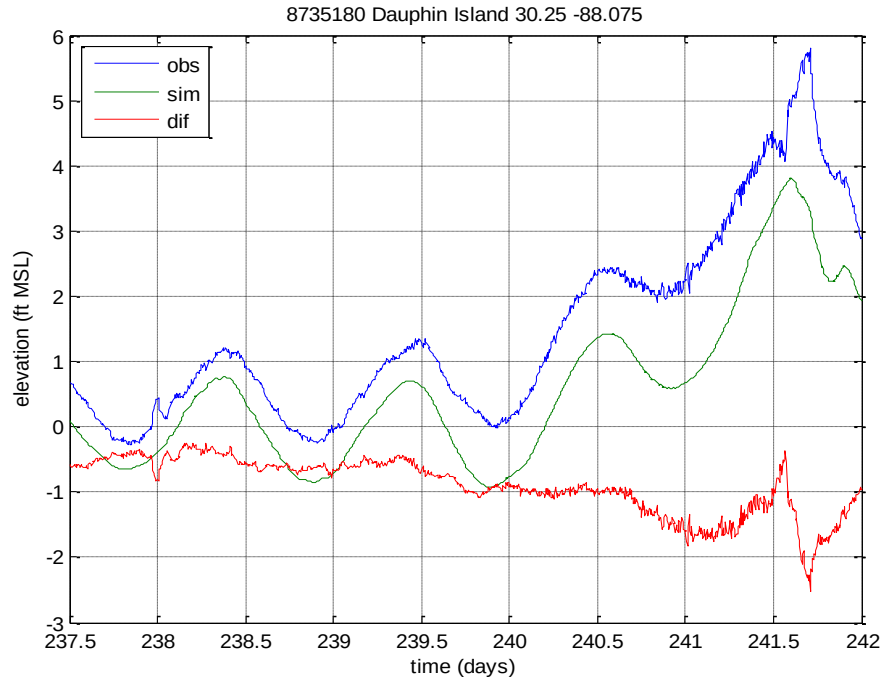

Figure 6-19: Measured and modeled time series at Dauphin Island, Alabama.

Advection changed water levels less than 0.5 feet in most areas. In the mouth of Mobile Bay, in Bay St. Louis, and in other inlets along the Louisiana, Mississippi, and Alabama coast along the storm's northeast quadrant, water levels were lowered by as much as one foot. The largest increase in peak water level occurred in southern Louisiana, where advection increases peak surge by nearly 1 foot in a large area which experienced relatively little surge (2-5 feet) overall. It is unclear why advection was a strong driver in this area, which was just left of the storm's track. The variable nature of the advective response is clearly demonstrated in Figure 6-20.

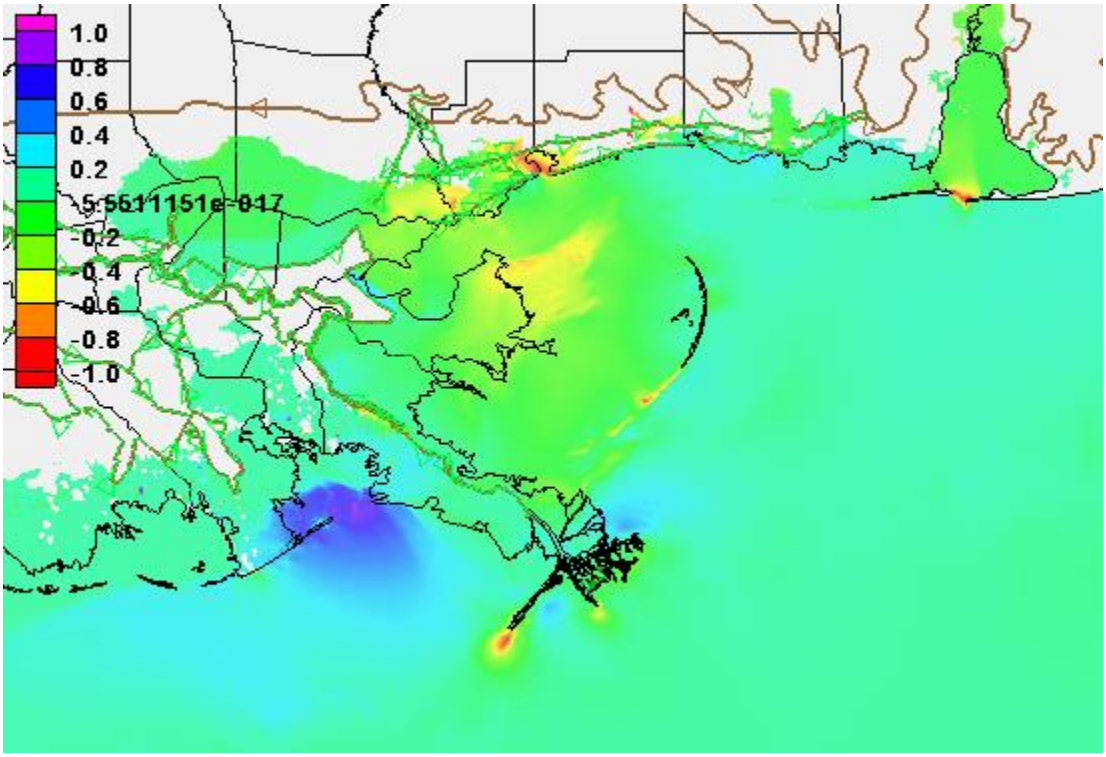

Figure 6-20: Katrina advection-on minus advection-off peak water level (feet).

6.4 **Dennis (2005)**

Hurricane Dennis was a Category 4 hurricane that damaged the Florida Panhandle. Dennis made landfall July 10, 2005 in Pensacola, Florida as a Category 3 hurricane. Storm surge was most prominent in Florida.

Figure 6-21: Storm track of Hurricane Dennis. Dots denote 6-hour intervals and landfall.

6.4.1 ***Model Setup***

The model simulation was 18.5 days long, with a 3.5-day storm run. Meteorological forcing was supplied by OWI wind files derived from multiple FEMA studies (Florida Panhandle and Big Bend), whose datasets were combined into composite wind and pressure fields. The winds were scaled up by a factor of 1.04 for consistency with the other event simulations with the NOMAD mesh; however, the FEMA study scaled the winds by a factor of 1.09. Wind/pressure forcing was supplied at 15-minute intervals. The simulation was executed with advection terms both on and off, and differences were found to be within +/- 0.15 meters (0.5 feet).

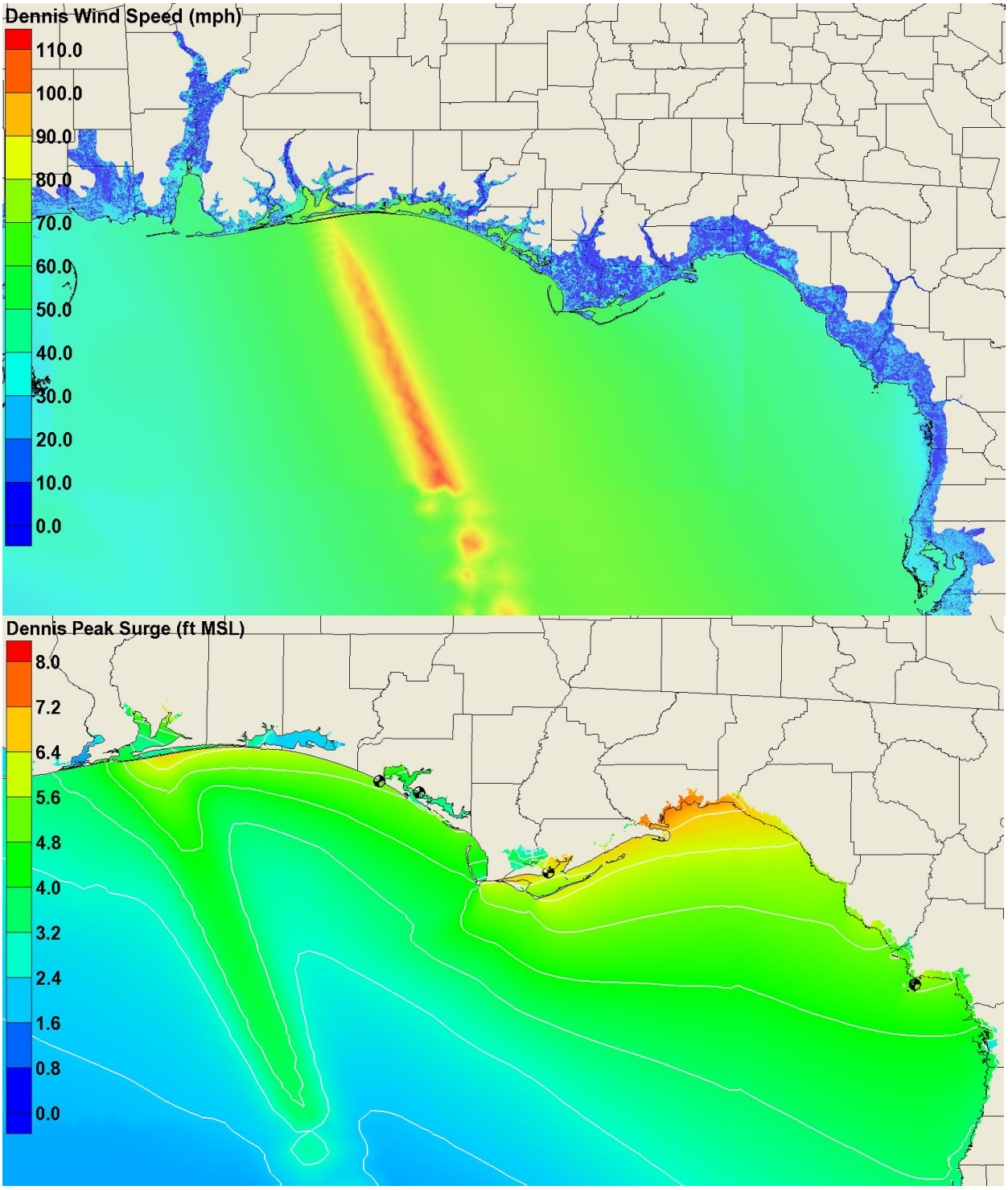

Figure 6-22: Dennis maximum wind speeds (top, mph) and maximum modeled surge (bottom, feet MSL); NOAA gage sites marked by pinwheels (bottom).

6.4.2 *Results and Skill Assessment*

Model skill for Dennis is mixed. The shelf wave that developed from the Tampa area north is captured by the model (Figure 6-25). However, peak surge is low at several gages along the Florida Panhandle. The cause of the under-estimation is unclear. Most of the gages (Apalachicola, Panama City, Pensacola, and

Horn Island) are in sheltered waters or on the back sides of islands so un-modeled wave set-up is not expected to be the cause of low bias. Some gages suffer from consistent tide issues throughout the simulation. For instance, Apalachicola and Panama City (Figure 6-26 and Figure 6-27) both have positive phase errors of 20 to 25 degrees in the M_2 constituent. However, most of the under-estimating of water levels begins around one day before peak surge and is directly associated with the event forcing signal.

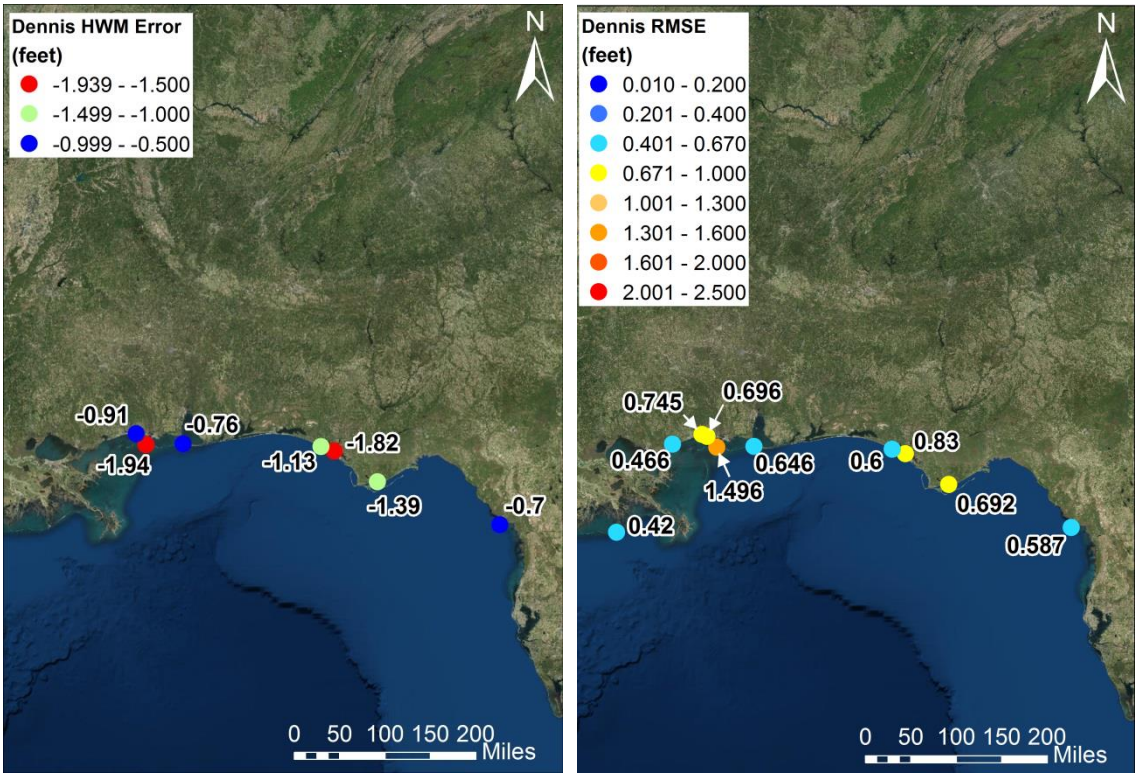

Figure 6-23: Geographic distribution of peak water level error (left) and time series RMSE (right) at NOAA stations. Peak surge errors are only shown for gages with a distinct surge signal.

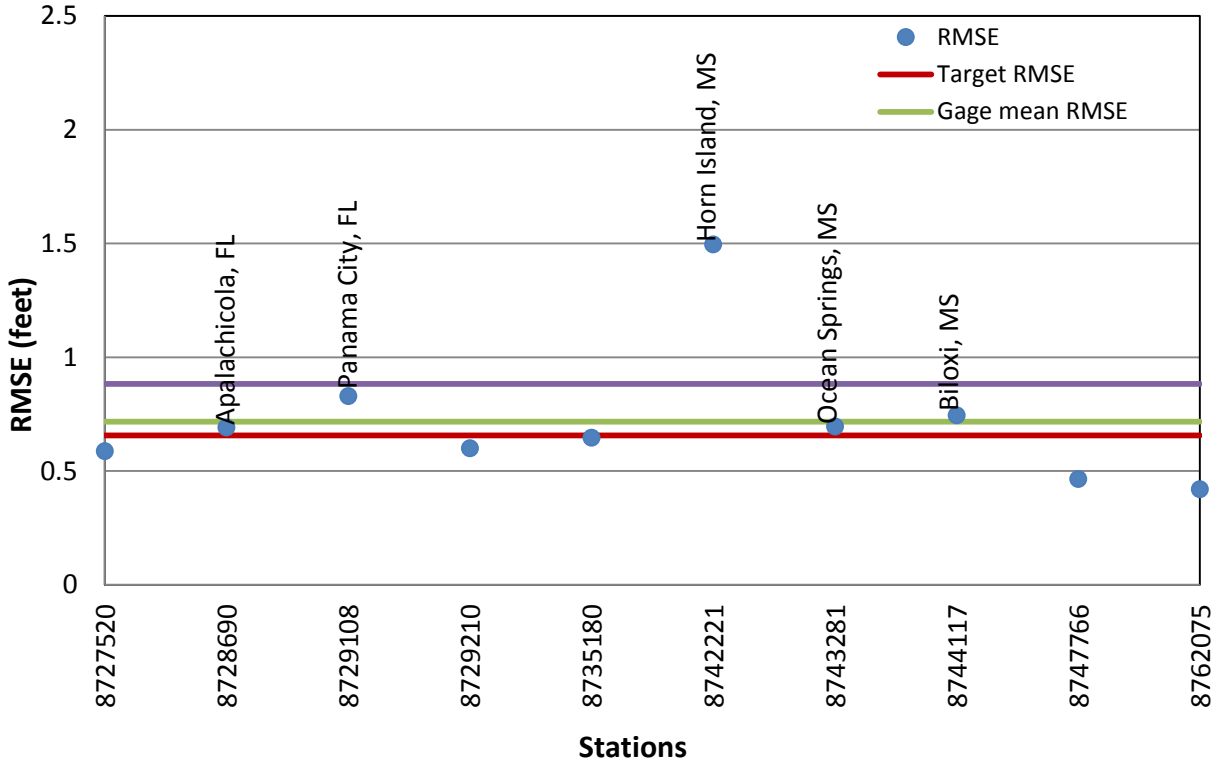

Figure 6-24: Alongshore plot of time series RMSE at NOAA stations; selected stations named for reference, red line indicates target RMSE, green line gives gage mean RMSE, and the purple line is mean RMSE from all storms.

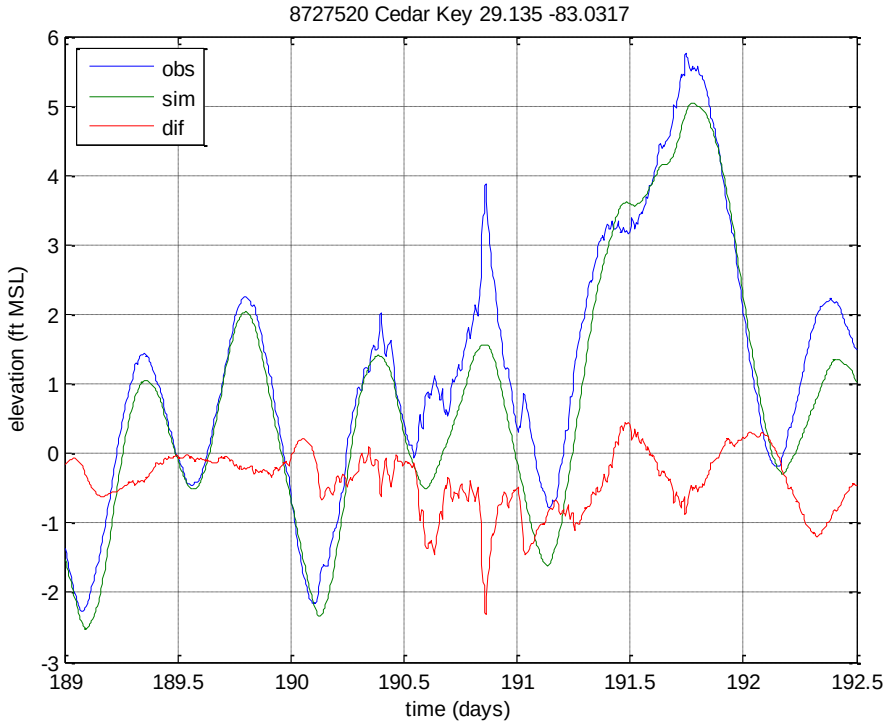

Figure 6-25: Measured and modeled time series at Cedar Key, Florida.

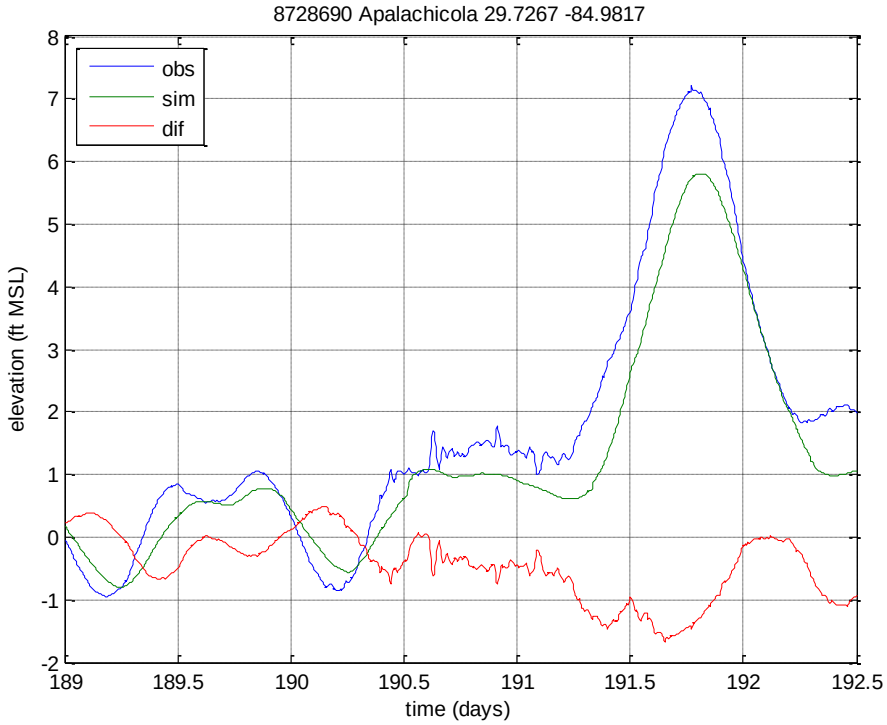

Figure 6-26: Measured and modeled time series at Apalachicola, Florida.

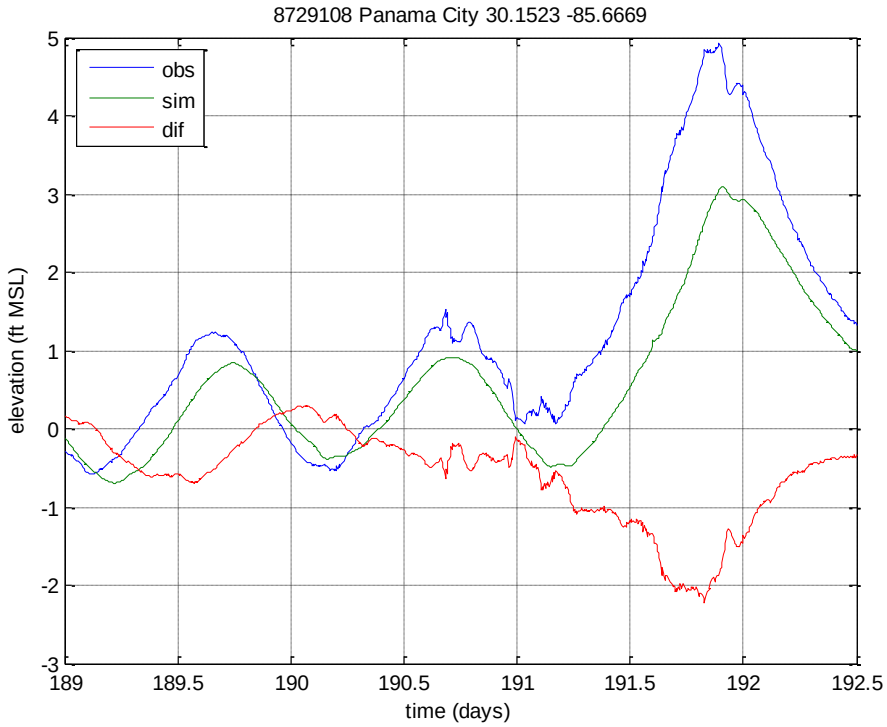

Figure 6-27: Measured and modeled time series at Panama City, Florida.

The FEMA studies that used Dennis as a validation event had similar low biases to the NOMAD results. Testing on the NOMAD mesh with the higher 1.09 wind scaling indicated that model performance was on par with the Franklin-Wakulla-Jefferson Counties, Florida FEMA study, after consideration for the steric effect and the lack of wave setup in the ADCIRC-only NOMAD model.

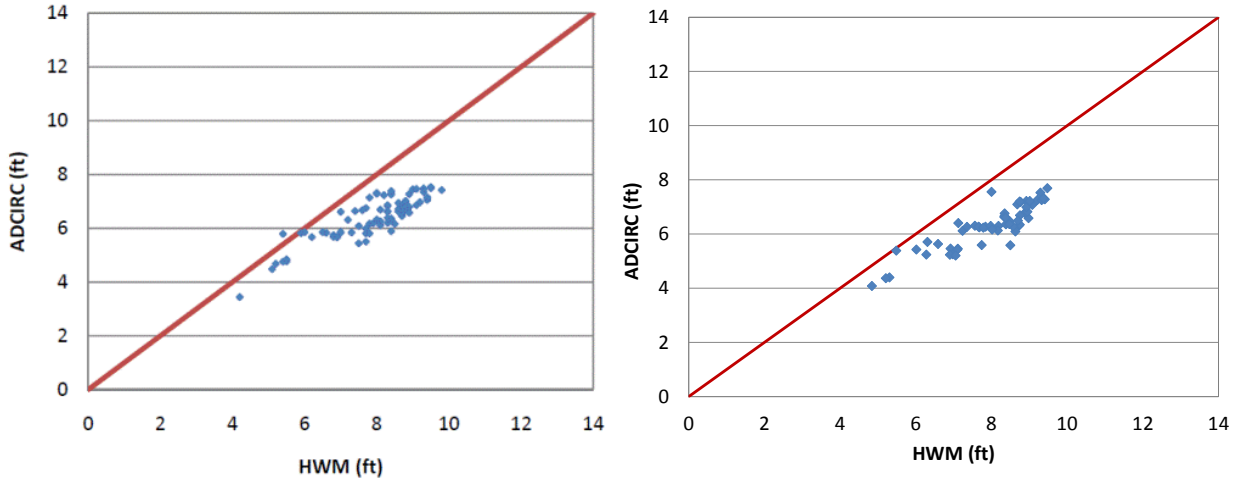

Figure 6-28: Comparison of measured HWMs vs. FEMA study modeled peak water level] (left) and the same HWMs vs. NOMAD modeled peak water levels (right). The NOMAD results shown are from a test run using with 1.09x scaled winds for more direct comparison to the FEMA results.

Advection shows the largest role in the areas immediately east of the landfall location, with a slightly elevated effect along the western coast of the Florida Peninsula, presumably due to the shelf wave generated. However, the effect is generally below 0.4 feet. This is approximately 10% of the surge.

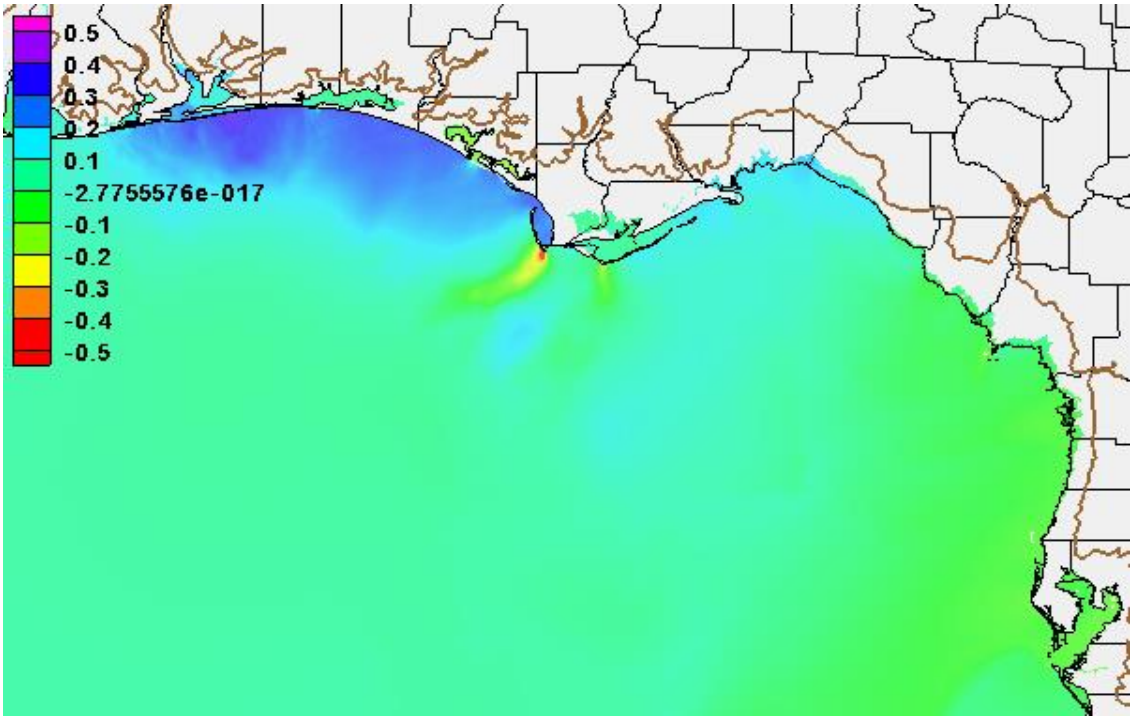

Figure 6-29: Dennis advection-on minus advection-off peak surges (feet).

6.5 **Charley (2004)**

Hurricane Charley was a Category 4 hurricane that damaged southern Florida. Charley made landfall August 13, 2004 near Fort Myers, Florida as a Category 4 hurricane. Storm surge was most prominent in southern Florida.

Figure 6-30: Storm track of Hurricane Charley. Dots denote 6-hour intervals and landfall.

6.5.1 ***Model Setup***

The model simulation was 21 days long, with a six-day storm run. Meteorological forcing was supplied by OWI-formatted wind files from the FEMA Southwest Florida study, and the winds were scaled up by a factor of 1.04, matching the FEMA study scaling. Wind/pressure forcing was supplied at 15-minute intervals. The simulation was executed with advection terms both on and off, and differences were found to be within +/- 0.30 meters (1 foot).

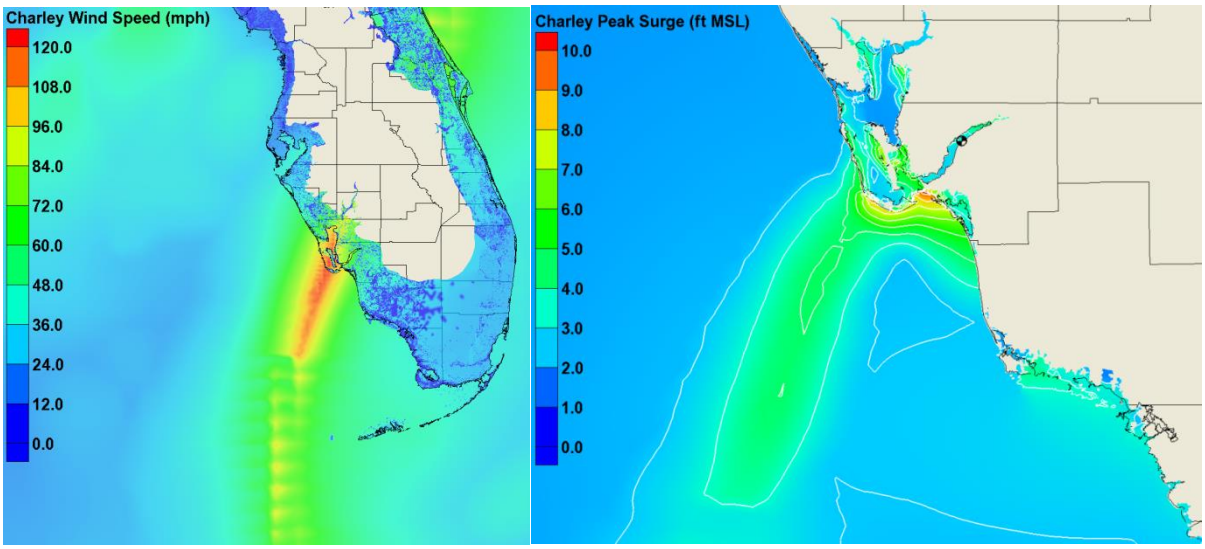

Figure 6-31 Charley maximum wind speeds (left, mph) and maximum modeled surge (right, feet MSL); NOAA gage sites marked by pinwheels (right).

6.5.2 *Results and Skill Assessment*

The spatial extent of Charley's surge was small due to the small size of the storm, resulting in a relatively limited set of gages affected by the storm. The RMSE values (Figure 6-32) are generally good; however, they are largely indicative of tidal performance since very few stations actually recorded a distinct surge signal. The gage at the center of the storm with the most significant recorded surge, Fort Myers, had poor tidal performance (Figure 6-34) contributing to a poor RMSE at that gage. Aerial imagery along the Caloosahatchee River (which holds the Fort Myers gage) indicates fine-scale shoals and channels, which neither the mesh, nor the underlying bathymetric data properly resolve. This implies that manual revision of the bathymetry may improve the model's tidal simulation accuracy.

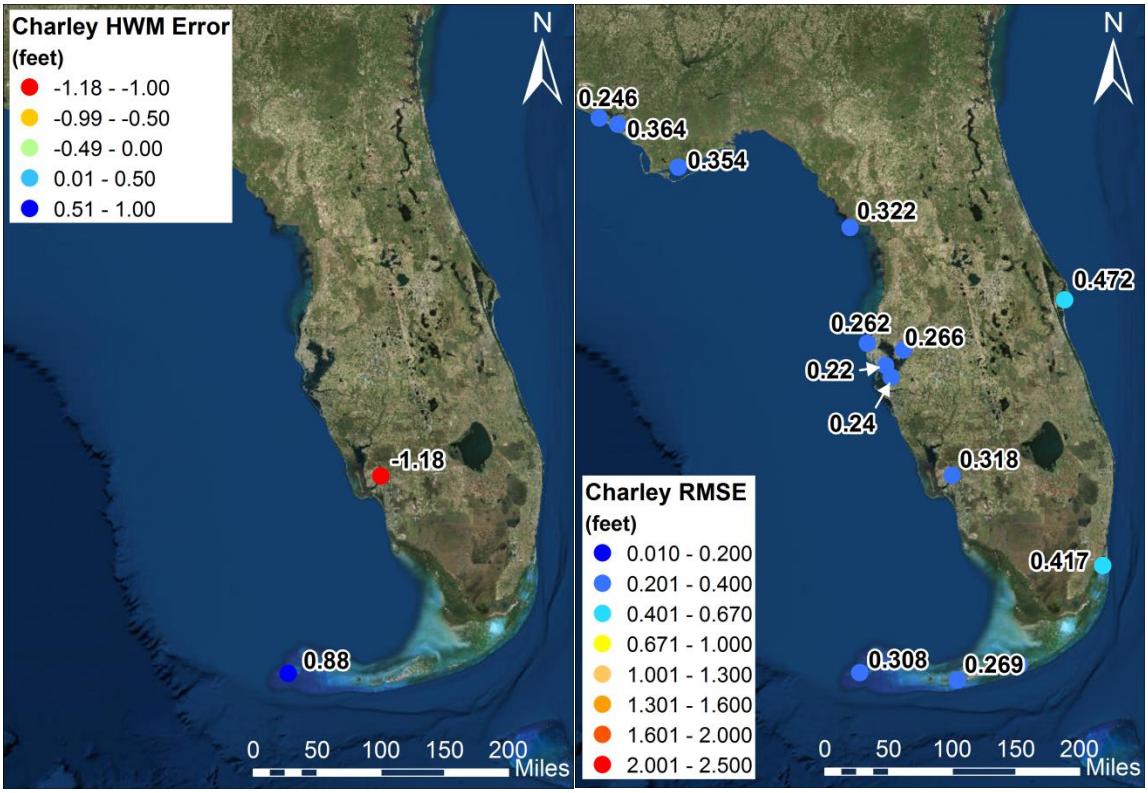

Figure 6-32 Geographic distribution of peak water level error (left) and time series RMSE (right) at NOAA stations. Peak surge errors are only shown for gages with a distinct surge signal.

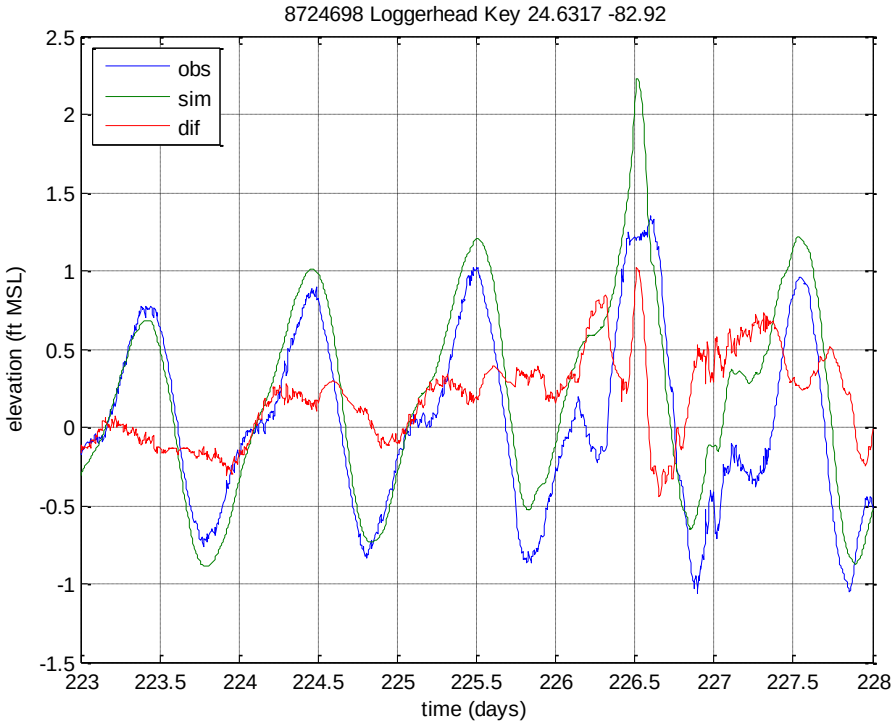

Figure 6-33 Measured and modeled time series at Loggerhead Key, Florida.

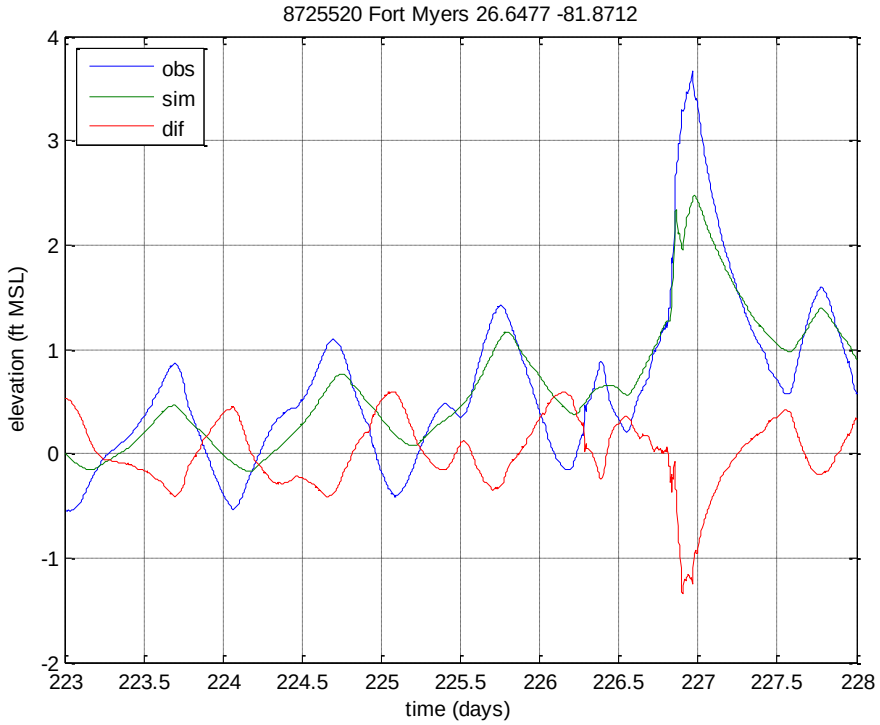

Figure 6-34 Measured and modeled time series at Fort Meyers, Florida.

Because so few NOAA gages captured the surge associated with Charley, the NOMAD simulation results were also compared to a high water mark dataset. These HWMs collected after Charley have proven challenging to work with. Although there is always a high level of uncertainty in post-storm HWM collection, this dataset shows particularly high variability that does not fit with anticipated changes in storm surge due to topographic changes. Three areas, with significant gradients are: 1) Two measured HWMs south of Punta Gorda change 1.7 feet in 640 meters (2100 feet); 2) Around Estero Island (Fort Myers Beach), two HWMs 80 meters (280 feet) apart show a 1.9 foot disagreement in the measured surge; 3) Another pair of points (one on the island, another just behind) show a 4.0 foot difference although they are separate by only 1000 meters (3300 feet). Because of the complexity of the storm, it is difficult to evaluate how much of this is genuine variability and how much is error in the measured HWMs. The rapid spatial variation in the modeled surge, indicates that there is reason to believe at least some of these measurements could be accurate. For completeness, all HWMs that were marked as being from surge in the HWM report were used. HWM elevation and errors are shown in Figure 6-35.

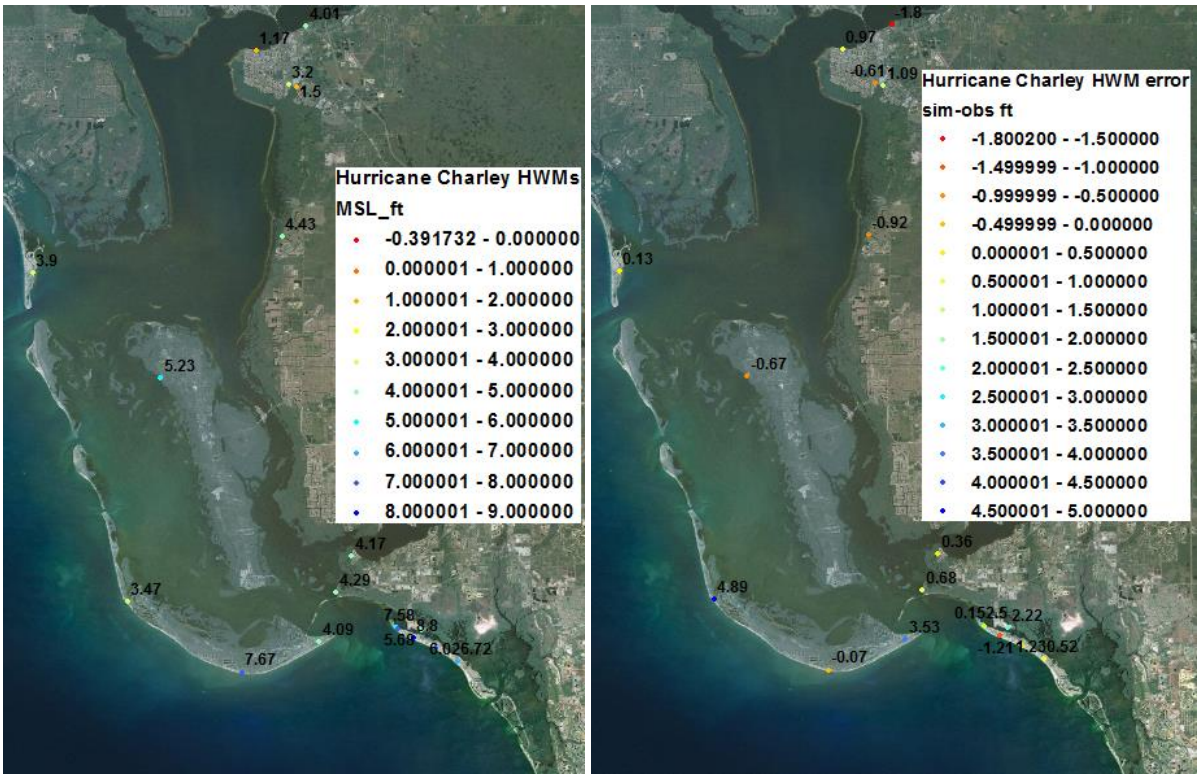

Figure 6-35 Hurricane Charley surveyed post-storm HWMs (left) and HWM error (right).

The fast forward speed of Charley would suggest that advective terms would be significant. Changes in the surge due to advection reaches 1 foot, or about 10% of the local peak surge in much of the surge-affected area as shown in Figure 6-36.

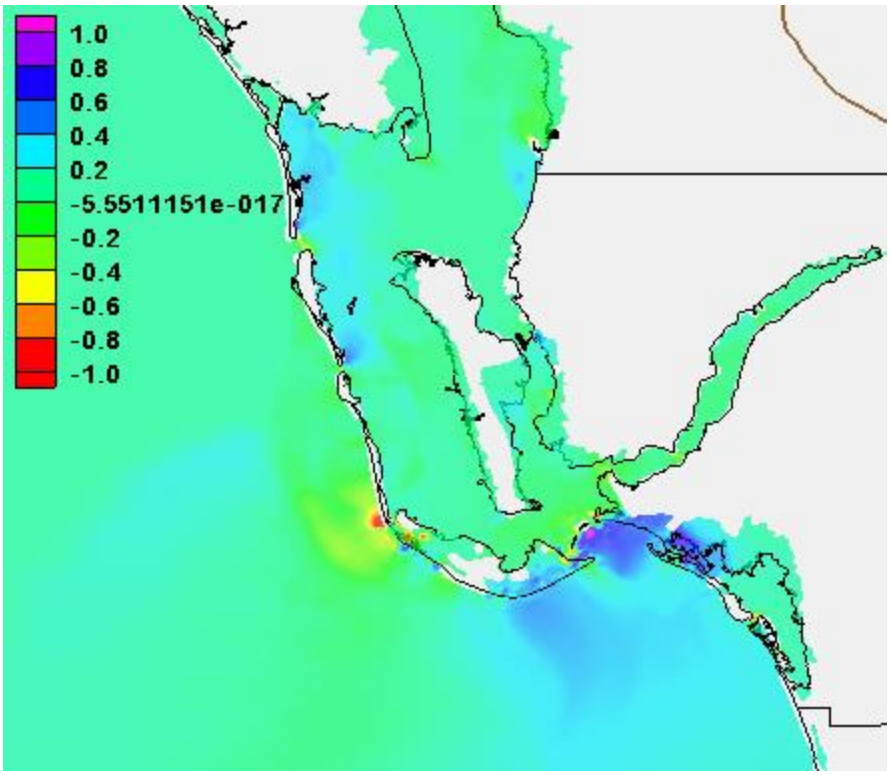

Figure 6-36: Charley advection-on minus advection-off peak surges (feet).

6.6 **Hugo (1989)**

Hurricane Hugo was a Category 5 hurricane that devastated South Carolina. Hugo made landfall September 21, 1989 near Charleston, South Carolina as a Category 4 hurricane. Storm surge was most prominent in South Carolina.

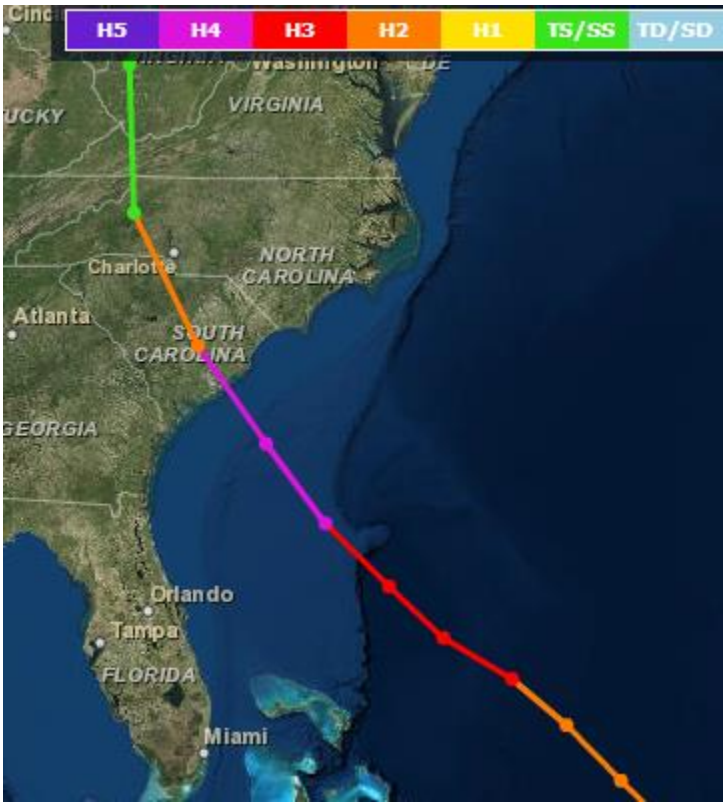

Figure 6-37: Storm track of Hurricane Hugo. Dots denote 6-hour intervals.

6.6.1 ***Model Setup***

The model simulation was 23 days long, with an eight-day storm run. Meteorological forcing was supplied by OWI wind files from the FEMA South Carolina study. The winds were scaled up by a factor of 1.04; however, the FEMA study did not scale the winds. Wind/pressure forcing was supplied at 15-minute intervals. The simulation was executed with advection terms both on and off, however, the advection-on run failed with instabilities on the northern coast of St. Croix around day 18.75 (Sep. 18, 18:00), several hours after Hugo passed directly over the island. Although a shortened 3.5-day advection-on run was completed, results are presented here from the advection off simulations. Differences between the advection-off and shortened advection-on runs were within +/- 0.3 feet except at the immediate mouth of Charleston Harbor as described below.

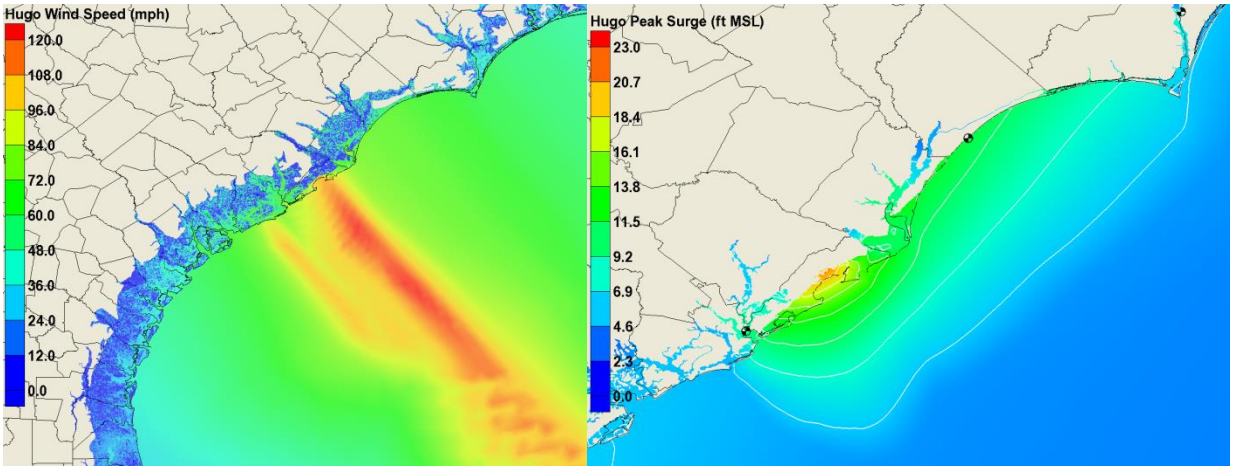

Figure 6-38 Hugo maximum wind speeds (left, mph) and maximum modeled surge (right, feet MSL); NOAA gage sites marked by pinwheels (right).

6.6.2 *Results and Skill Assessment*

There is a limited amount of NOAA gage data for Hugo, in part because the Springmaid Pier gage stopped functioning just over 24 hours before the storm made landfall. Model skill is good at Charleston near the peak surge, though there is significant over-prediction further north at Wilmington as shown in Figure 6-40 and Figure 6-41. Several stations have issues with tide phase, which may affect model performance.

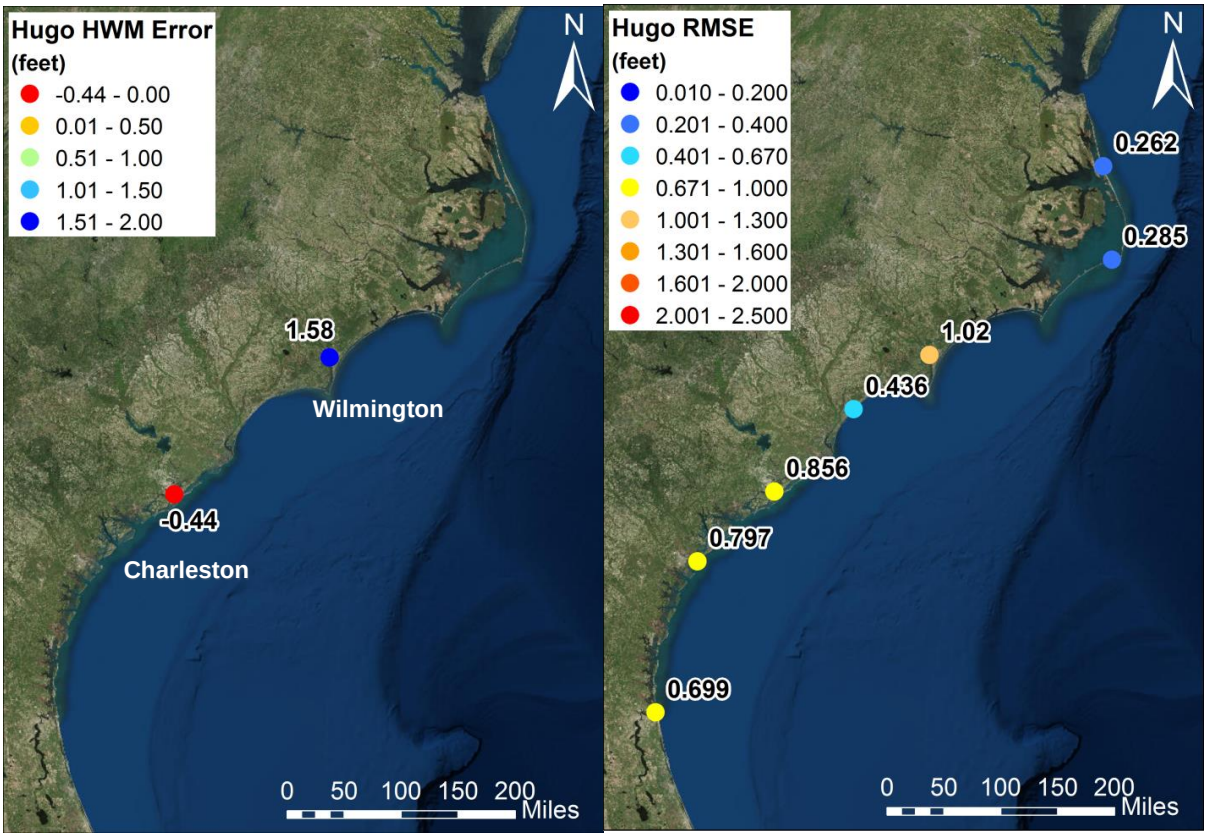

Figure 6-39 Geographic distribution of peak water level error (left) and time series RMSE (right) at NOAA stations. Peak surge errors are only shown for gages with a distinct surge signal.

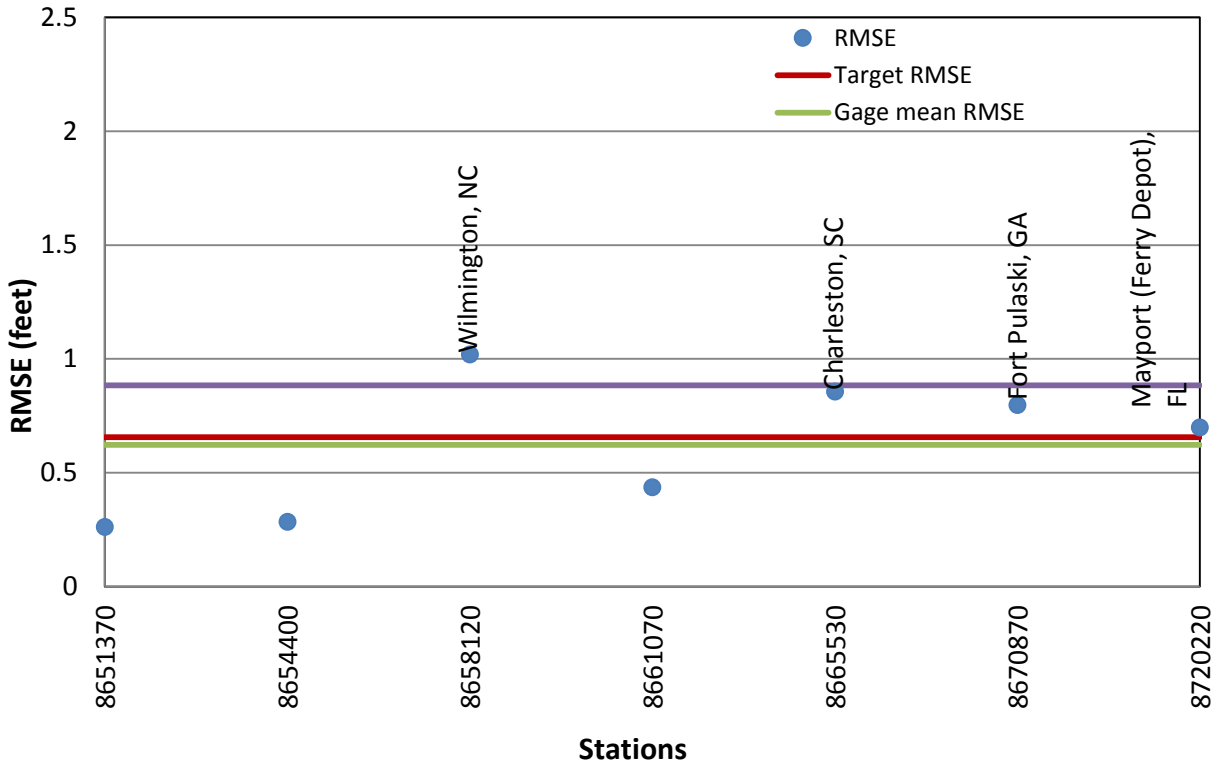

Figure 6-40 Alongshore plot of time series RMSE at NOAA stations; selected stations named for reference; red line indicates target RMSE, green line gives gage mean RMSE, and the purple line is mean RMSE from all storms.

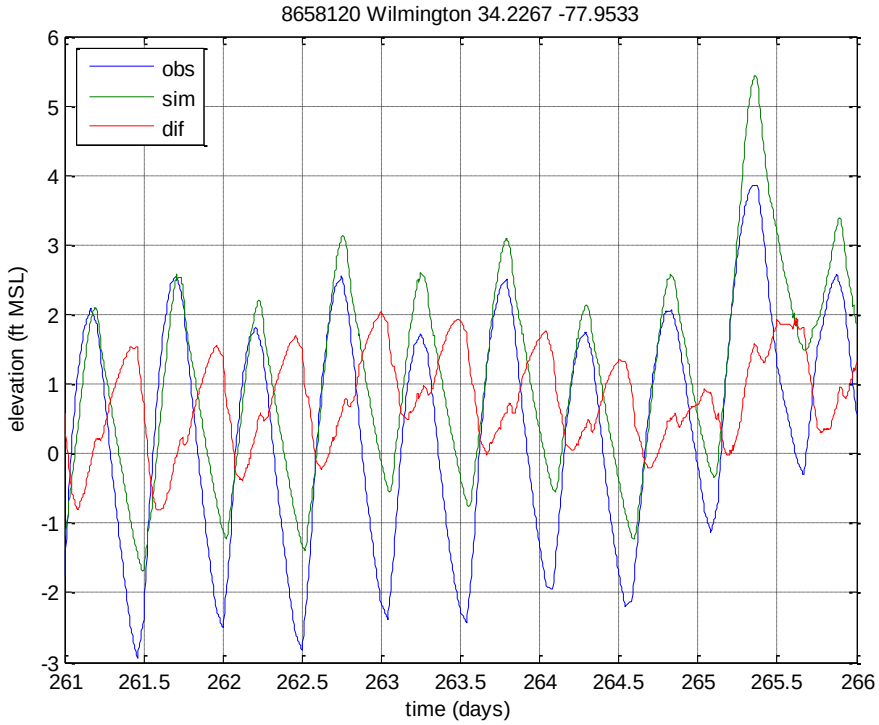

Figure 6-41 Measured and modeled time series at Wilmington, North Carolina.

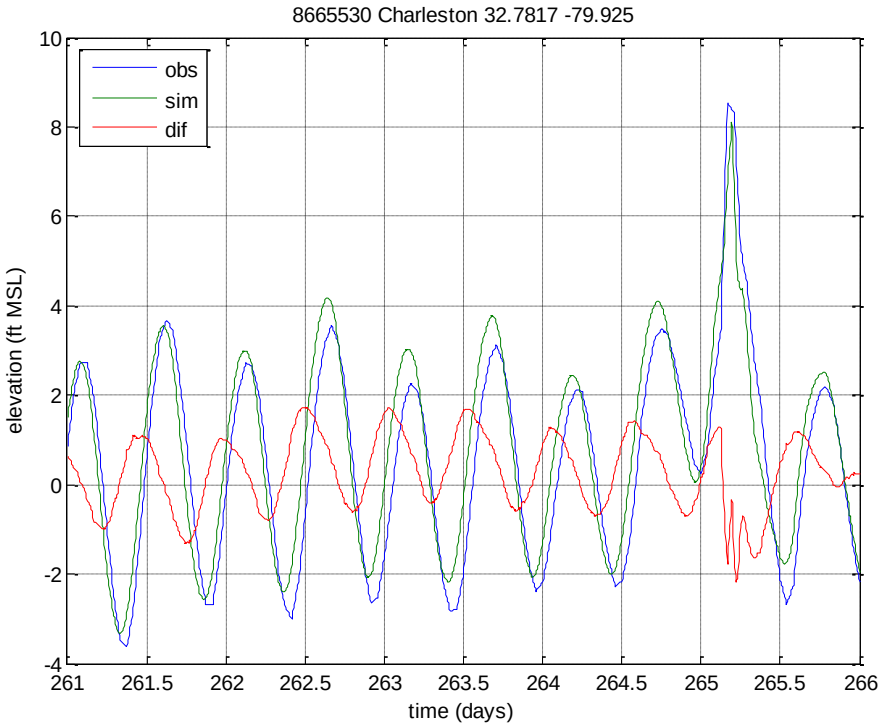

Figure 6-42 Measured and modeled time series at Charleston, South Carolina.

A HWM dataset was collected after Hugo and a subset of these points were used in the FEMA South Carolina study. The same dataset was acquired for this study and compared with the NOMAD simulated water levels as shown in Figure 6-43. The modeled values are on average 0.78 feet lower than the measured HWMs. A high concentration of HWMs around Charleston, where the modeled surge is generally lower than measured, skews the distribution of error. Of the 111 HWMs, all but seven HWMs are within +/- 3 feet. This compares well to the FEMA study, where all but five HWMs were within +/- 1 foot of the FEMA model.

In the NOMAD results, the HWMs show a clear spatial pattern of under-prediction in and around Charleston, over-prediction to the north where the surge peaked, then again under-prediction further north. This indicates a problem with the meteorological forcing, because the spatial pattern is inconsistent with the tide issues experienced. Plotting against the FEMA modeled results (Figure 6-45) show a similar pattern around Sullivan Island in the south, where NOMAD modeled results exceed FEMA's (i.e. are closer to the actual measured HWMs). However, the difference is small, and may be attributable to the scaled-up winds used in the NOMAD simulations or to the absence of advection. Results further south show that advection decreases surges on the southern side of Sullivan's Island. It is also possible that this is caused by the channels' water levels being artificially elevated due to the non-zero mean elevation trend, documented in Appendix D.

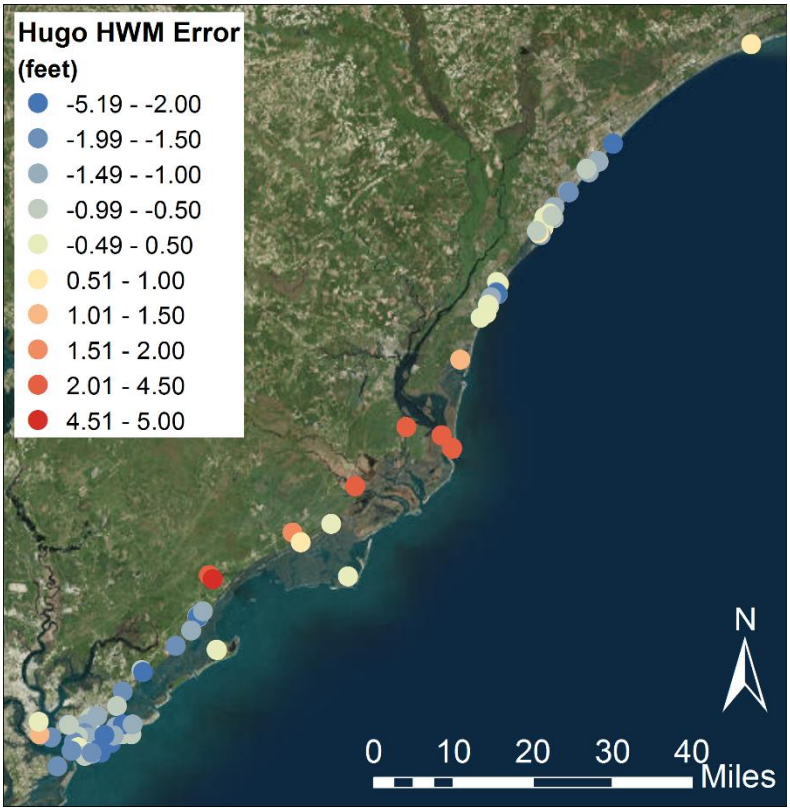

Figure 6-43: Post-storm HWM data error, modeled minus measured.

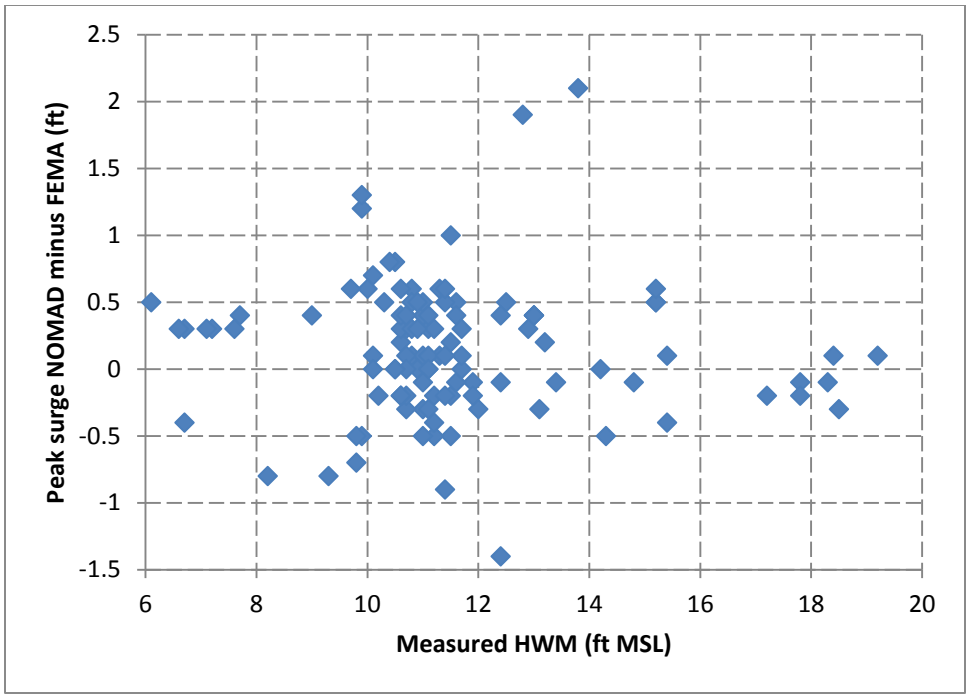

Figure 6-44 Comparison of NOMAD vs. FEMA model skill to measured surge height.

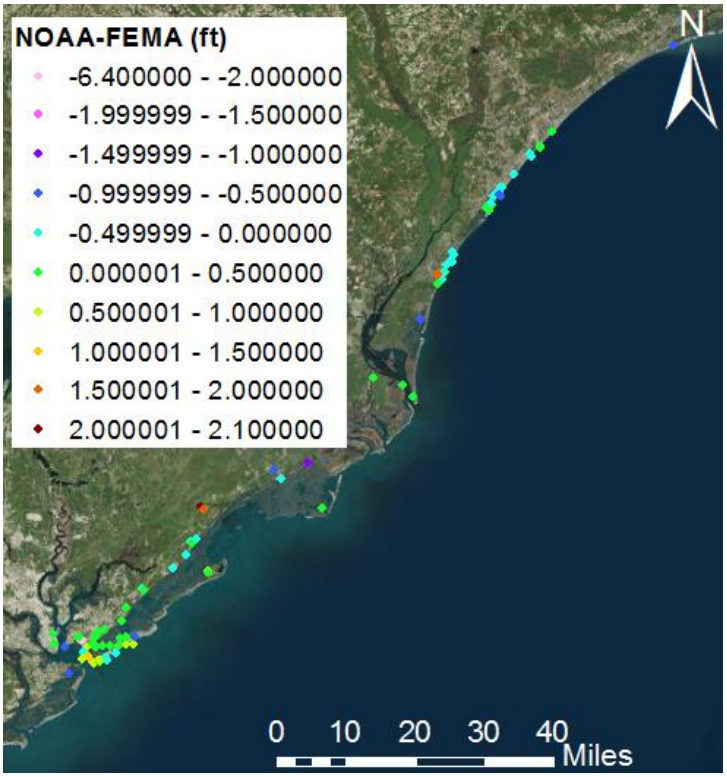

Figure 6-45 Peak water level difference (feet) showing NOMAD modeled minus FEMA modeled values.

Generally, advection did not affect the peak surge by more than about 5%, although a deviation of 1 foot is seen by Sullivan's Island at the mouth of Charleston Harbor. A closer inspection shows that a slight change (~0.5 feet) in the surges between the runs caused a broad dune crest to be wetted in the advection-off run, dramatically altered the geometry of the wetted domain, which likely contributed to the difference.

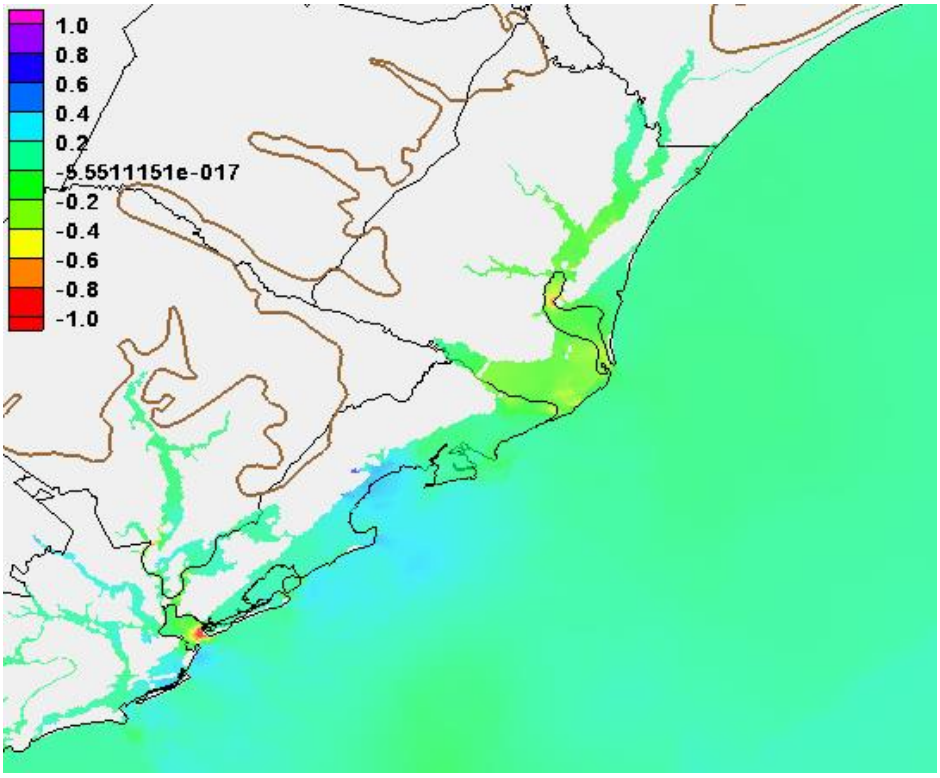

Figure 6-46: Hugo advection-on minus advection-off peak surges (feet).

6.7 **Floyd (1999)**

Hurricane Floyd was a Category 4 hurricane that brought significant storm surge primarily to North Carolina. Floyd made landfall near Cape Fear, North Carolina September 16, 1999 as a Category 2 hurricane. In addition to significant surge, Floyd and associated precipitation caused record flooding in numerous coastal river systems of North Carolina.

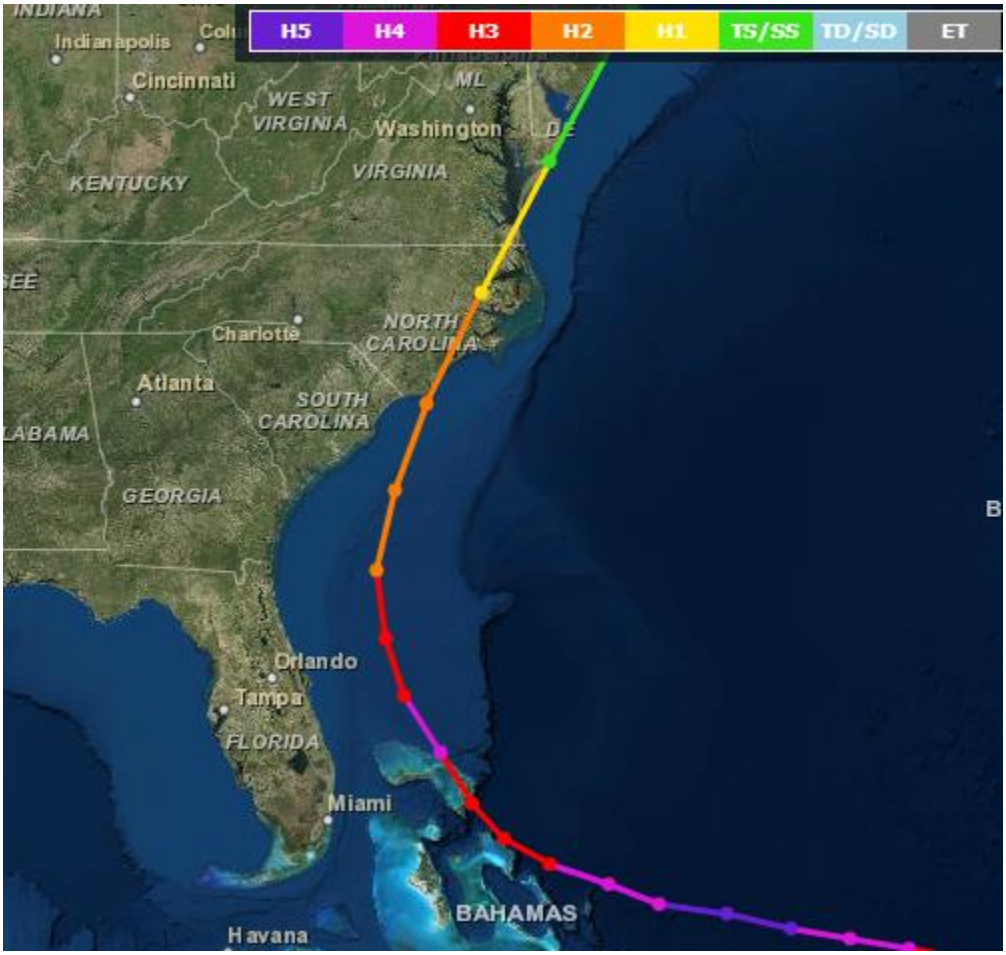

Figure 6-47: Storm track of Hurricane Floyd. Dots denote 6-hour intervals.

6.7.1 ***Model Setup***

FEMA-sourced OWI meteorology was not available for the Floyd simulations. The AOML archived H*Wind was first tested but yielded low-biased surges and overall water levels prompting an examination of other forcing options. The ADCIRC internal vortex model parameterized with the NHC best track data (best track) was the only practical alternative due to the relatively early date of the event. Unfortunately, the NHC best track estimate terminated early and produced a wind field that did not progress far enough up the coast and did not capture the peak at northeastern locations as seen in Figure 6-48.

H*Wind peak velocities were more intense than the best track velocities, especially near the landfall coast and ocean response to H*Wind is generally greater than the best track simulation. However, Figure 6-48 shows that the H*Wind data were inconsistent through time, and this may have accounted for some of the

reduced surge. As with all H*Wind real-time analyses, the wind and pressure forcing for Floyd is irregularly spaced at roughly three to six hour intervals. However, due to the truncated duration of the best track data, the H*Wind results were used in the tabulation of overall model performance reported here and in Section 7.

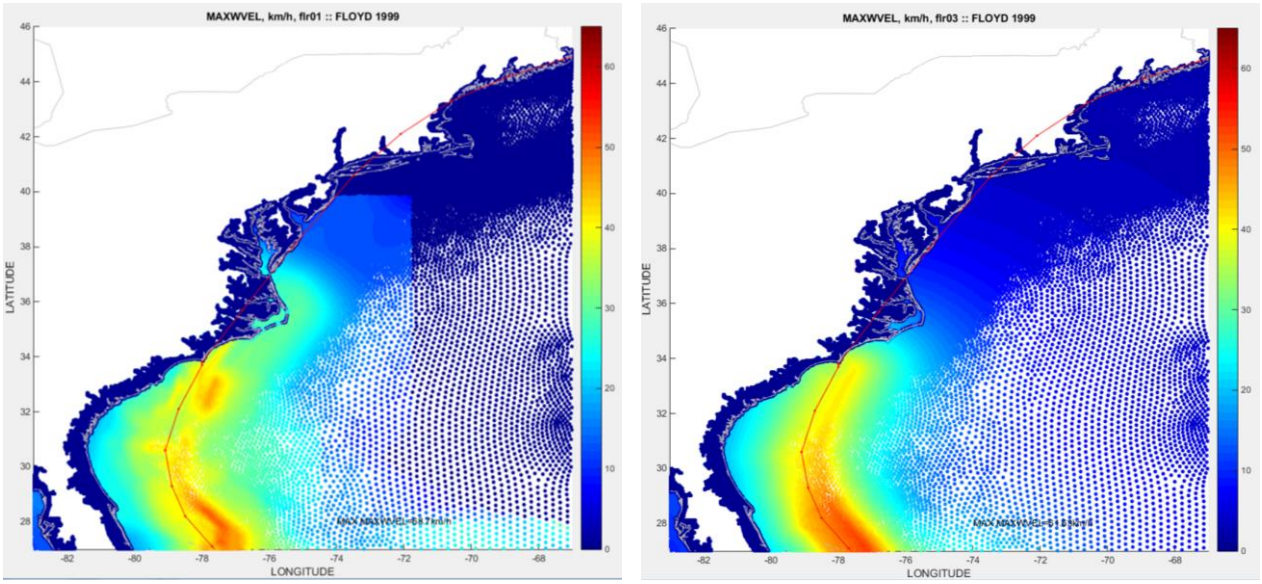

Figure 6-48: Floyd H*Wind and Best track maximum wind speed (left and right, respectively, kilometers per hour)

For the H*Wind forcing, both advection-on and advection-off simulations were executed. Maximum water level is shown in Figure 6-49 for the advection-on H*Wind simulation. Differences between advection-on and advection-off simulations were minimal, less than +/- 0.5 feet, as shown in Figure 6-50. Each model simulation was 19.5 days long, with 4.5 days of event forcing.

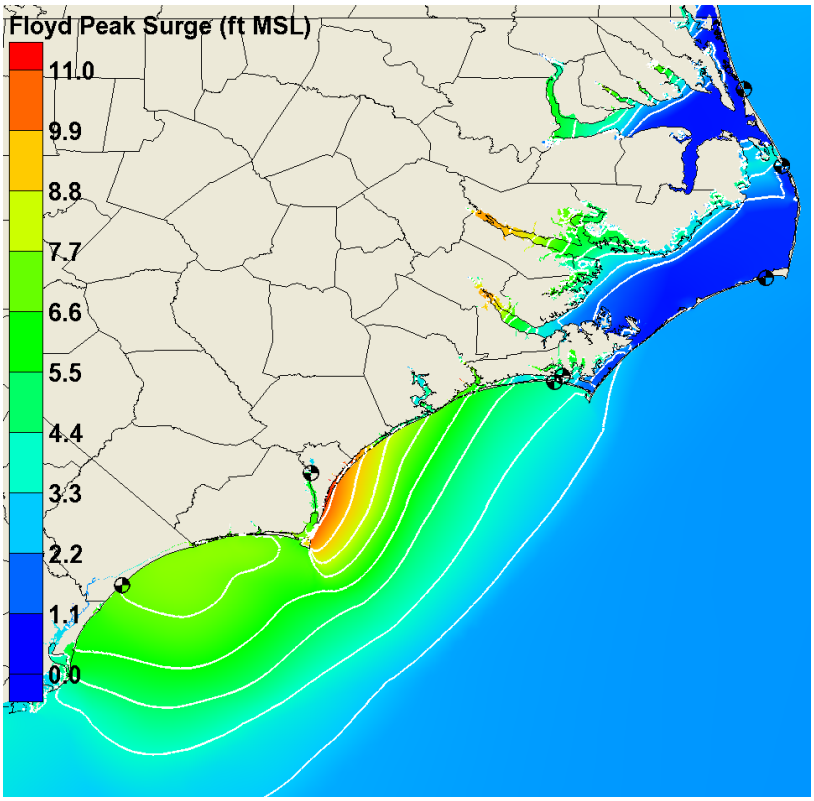

Figure 6-49: H*Wind maximum modeled surge (bottom left and bottom right, respectively, meters MSL)

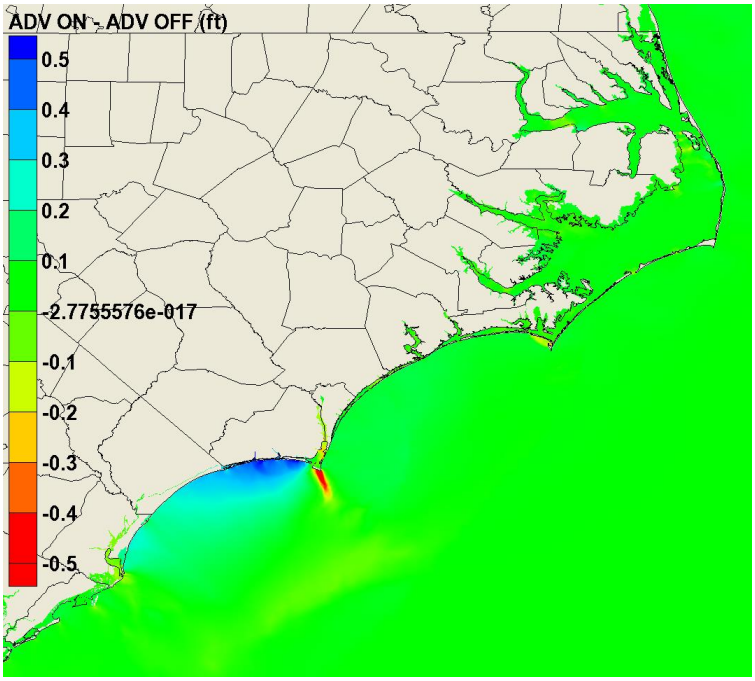

Figure 6-50: Differences between advection-on and advection-off simulations using the H*Wind forcing data for Floyd.

6.7.2 *Results and Skill Assessment*

Some of the difficulty with the H*Wind product results from derivation as a stochastic gust wind product and how ADCIRC handles this type of product. For gust wind forcings, ADCIRC uses a factor of approximately 0.89 to scale the gusts down, but the appropriateness of this exact value is unknown and other factors have been suggested (Fleming and Jelley 2014; Powell 2012) leading to an uncertain bias in the wind forcing. The low bias in sites further from the storm may also be due to an insufficient representation of the outer wind field in H*Wind, which is more focused on the storm's core. No direct meteorological data review was conducted to examine this hypothesis. High bias for some gages closer to the storm doesn't have a clear cause, except potential wind error. Poor results for Floyd are consistent with H*Wind tests for Sandy and Ike using H*Wind fields making the outcomes with Floyd generally unsurprising. NOAA peak water level error and gage RMSE is shown for the H*Wind advection-on simulation in Figure 6-51. The relatively low RMSE of gages beyond North Carolina (i.e., to the north) is only indicative of very small or non-existent surge signal in those gage time series.

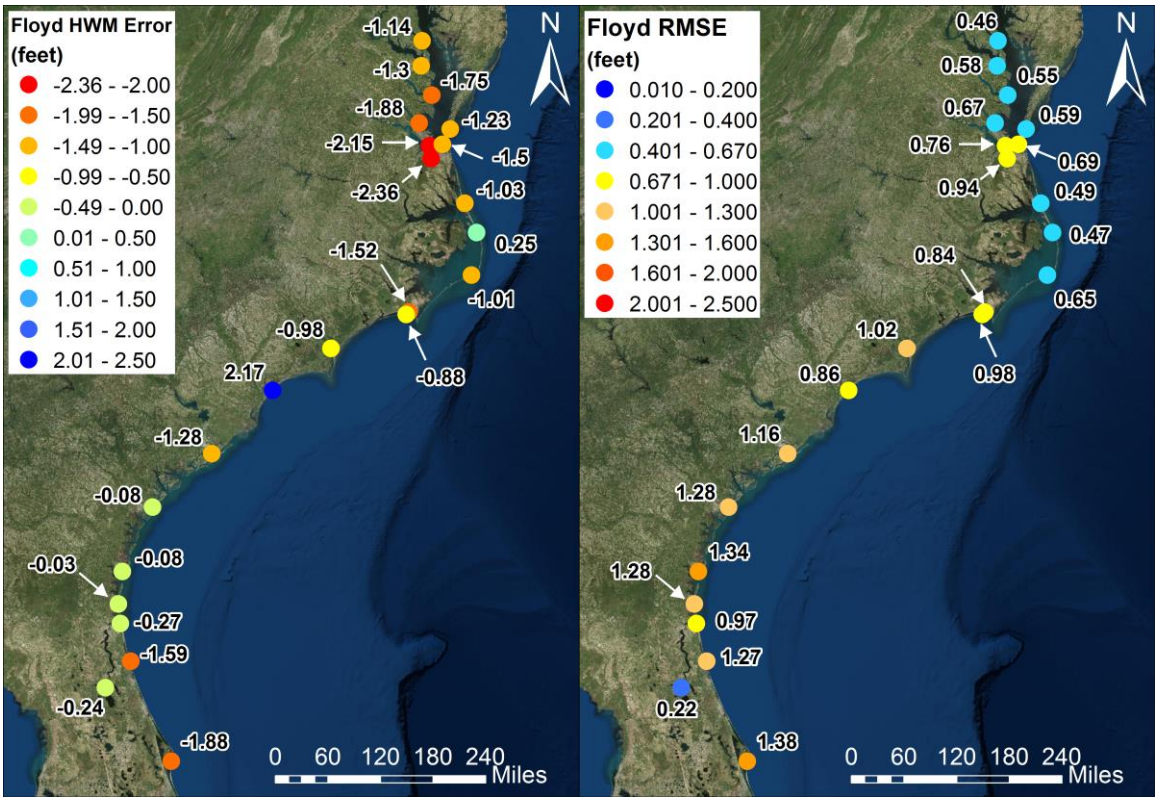

Figure 6-51: Geographic distribution of peak water level error (left) and time series RMSE (right) at NOAA stations. Peak surge errors are only shown for gages with a distinct surge signal.

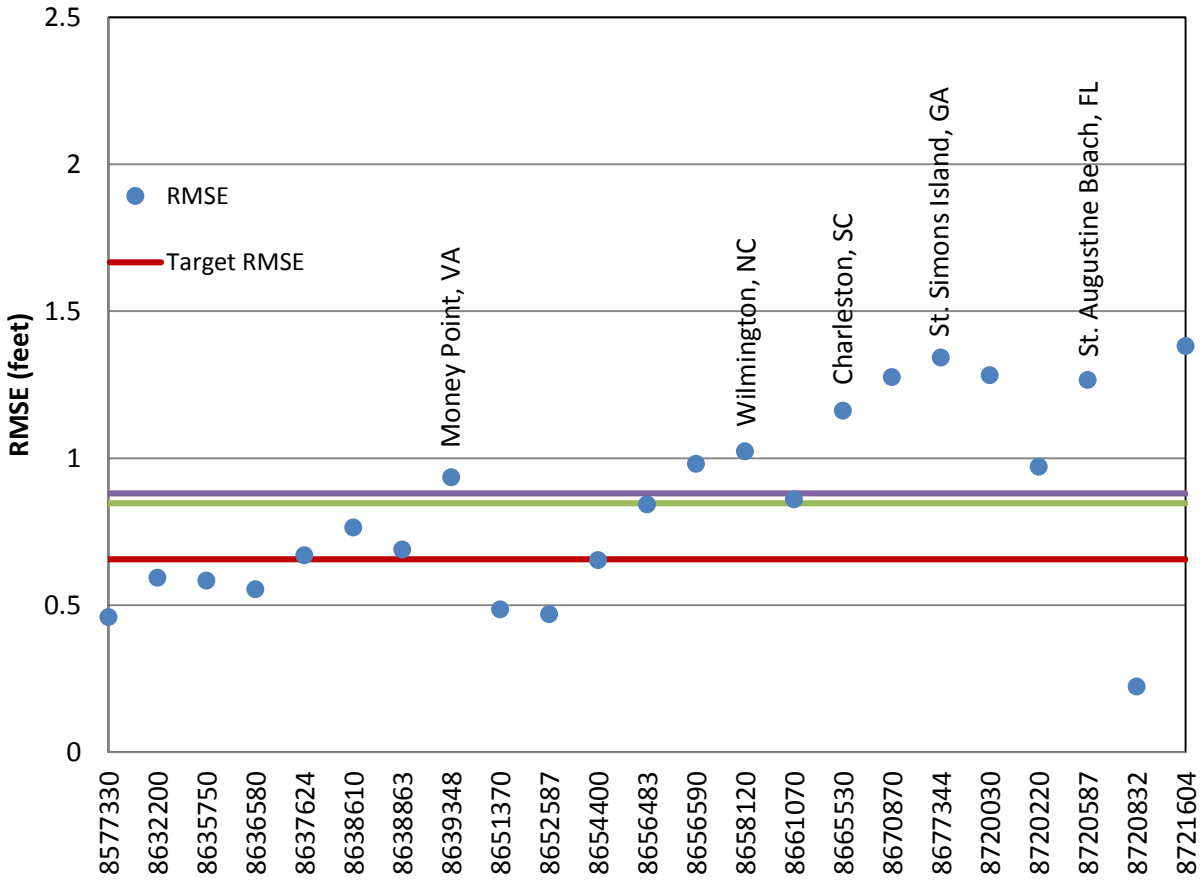

Figure 6-52: Alongshore plot of time series RMSE at NOAA stations; selected stations named for reference; red line indicates target RMSE, green line gives gage mean RMSE, and the purple line is mean RMSE from all storms.

From north to south, the gage time series plotted in Figure 6-53 – Figure 6-58 give clear indication of the relative performance of the model and highlight the deficiencies in the meteorological data. For each of the plots, the best track simulation shows almost no surge signal except in the southern-most gages, Springmaid Pier, SC and St Simons Island, GA. At the Money Point, VA. gage, the H*Wind simulation also shows the complete lack of simulated surge response; however, at the Cape Hatteras, NC gage in the central Outer Banks, a minimal response was detected.

At Atlantic Beach and Wilmington, NC, closer to landfall and to the core of the Hurricane , the H*Wind simulations produce a strong surge response but miss the building water levels preceding landfall. The over-strong central wind field and the under-considered outer wind field could explain the underpredicted buildup with a peak which makes up for the underprediction. Results at Springmaid Pier, SC show over-predicted surge, possibly relating to the strong central wind field of H*Wind. Further south at St. Simons Island, GA, the under-prediction is likely caused by insufficient characterization of the outer wind field.

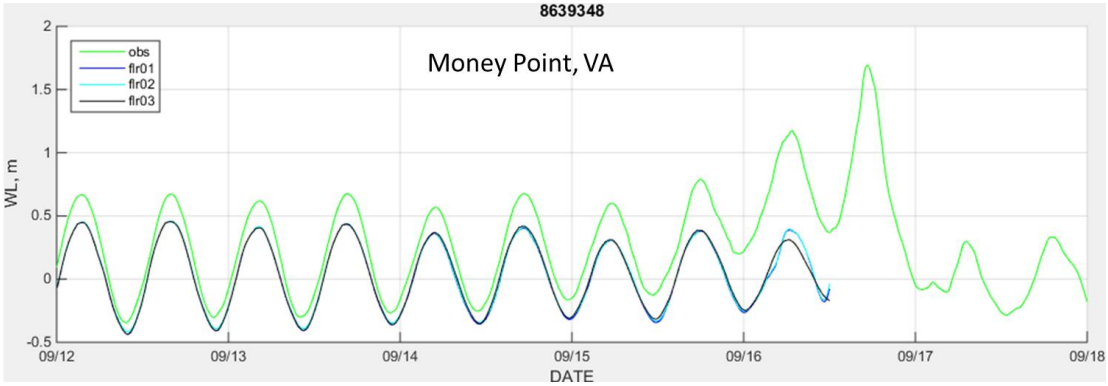

Figure 6-53: Observed and simulated water levels during Floyd at Money Point, VA. Green is observed (obs); dark blue is advection-off H*Wind (flr01); light blue is advection-on H*Wind (flr02); black is best track (flr03).

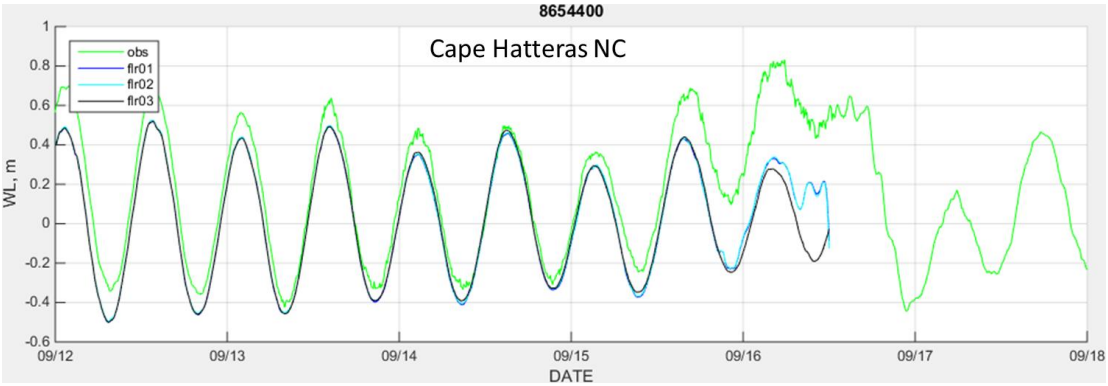

Figure 6-54: Observed and simulated water levels during Floyd at Cape Hatteras, NC. Green is observed (obs); dark blue is advection-off H*Wind (flr01); light blue is advection-on H*Wind (flr02); black is best track (flr03).

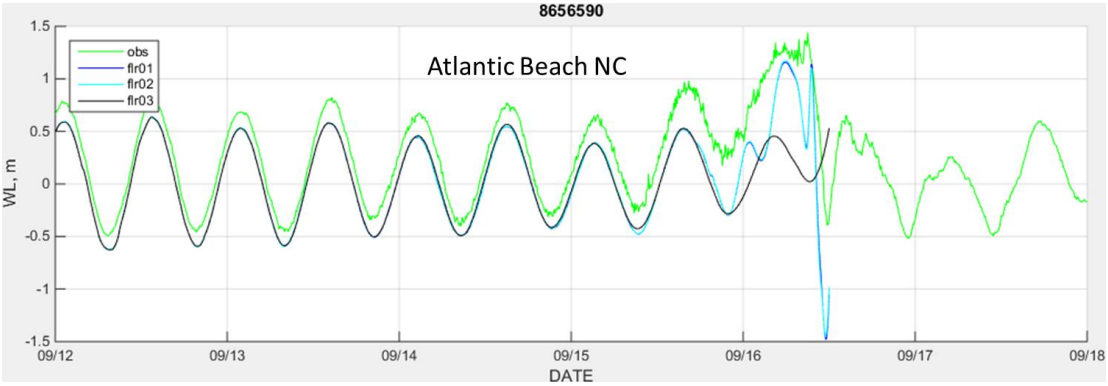

Figure 6-55: Observed and simulated water levels during Floyd at Atlantic Beach, NC. Green is observed (obs); dark blue is advection-off H*Wind (flr01); light blue is advection-on H*Wind (flr02); black is best track (flr03).

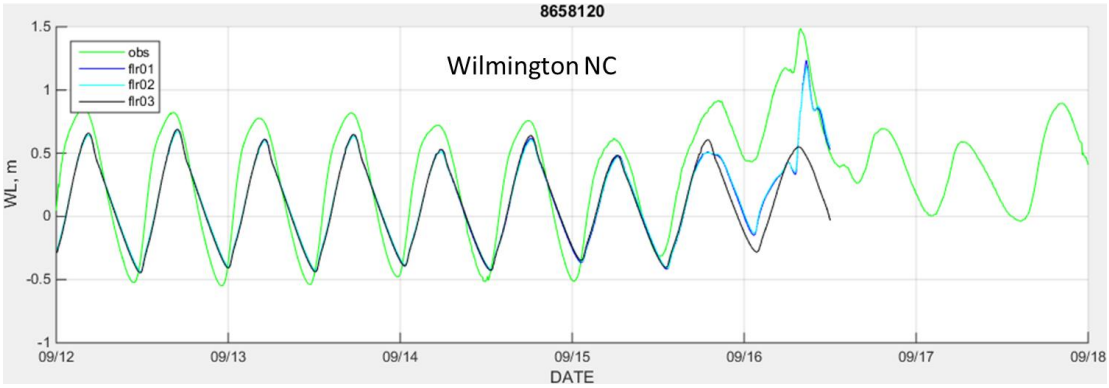

Figure 6-56: Observed and simulated water levels during Floyd at Wilmington, NC. Green is observed (obs); dark blue is advection-off H*Wind (flr01); light blue is advection-on H*Wind (flr02); black is best track (flr03).

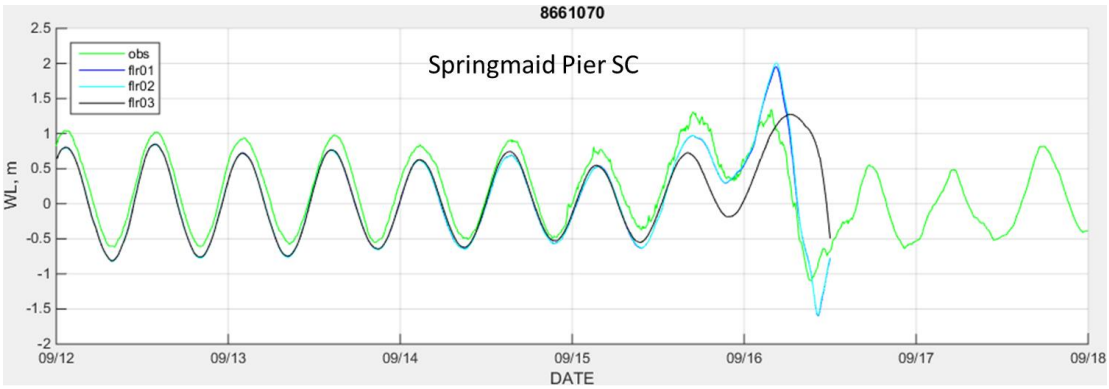

Figure 6-57: Observed and simulated water levels during Floyd at Springmaid Pier, SC. Green is observed (obs); dark blue is advection-off H*Wind (flr01); light blue is advection-on H*Wind (flr02); black is best track (flr03).

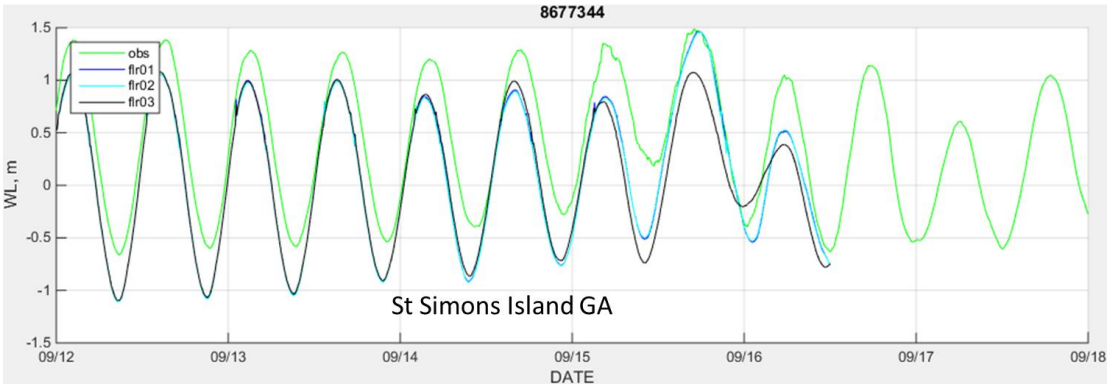

Figure 6-58: Observed and simulated water levels during Floyd at St. Simons Island, GA. Green is observed (obs); dark blue is advection-off H*Wind (flr01); light blue is advection-on H*Wind (flr02); black is best track (flr03).

6.8 **Isabel (2003)**

Hurricane Isabel was a Category 5 hurricane that caused major damage in the coastal states of North Carolina through New York. Isabel made landfall September 18, 2003 in the Outer Banks of North Carolina as a Category 2 hurricane. Storm surge was most prominent in North Carolina, Virginia, Maryland, and Delaware.

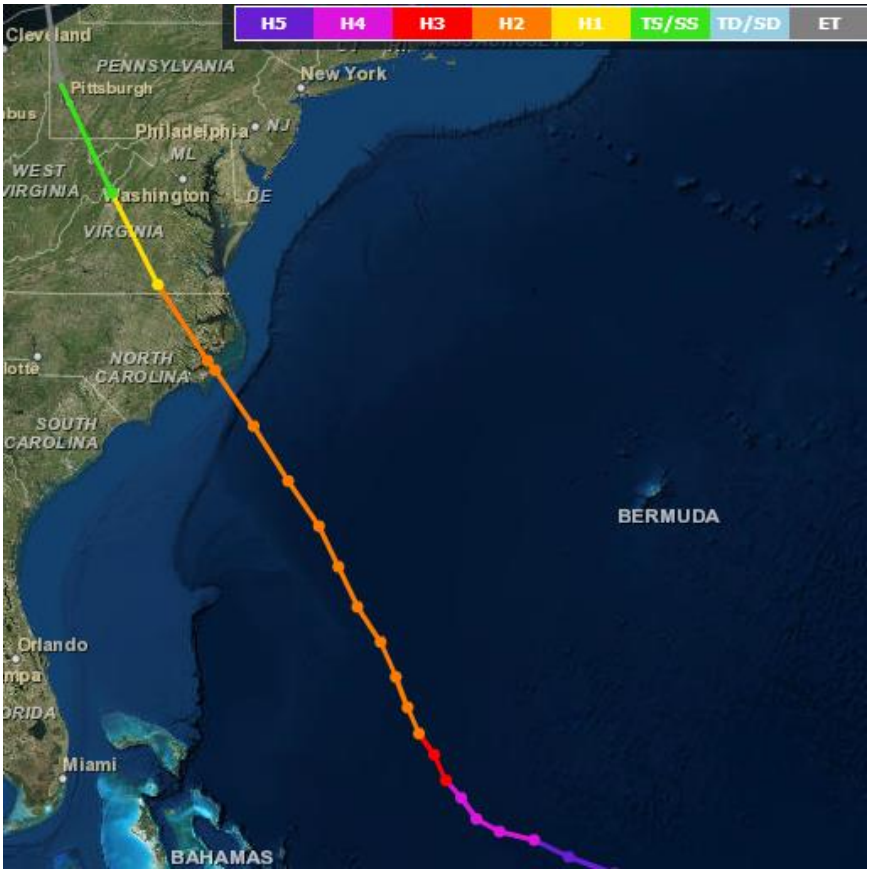

Figure 6-59: Storm track of Hurricane Isabel. Dots denote 6-hour intervals and landfall.

6.8.1 ***Model Setup***

The model simulation was 23 days long, with an eight-day storm run. Meteorological forcing was supplied by OWI-formatted wind files from the FEMA Region III study, and the winds were scaled up by a factor of 1.04, however it is not clear what wind scaling factor was used in the FEMA study. Wind and pressure forcing was supplied at 15-minute intervals. Figure 6-60 illustrates the modeled peak surge from Hurricane Isabel. The largest surge values were predicted in upstream areas of the Chowan River, James River, Chickahominy River, and Potomac River. The Isabel simulation was executed with advection terms both on and off, and differences were under an inch.

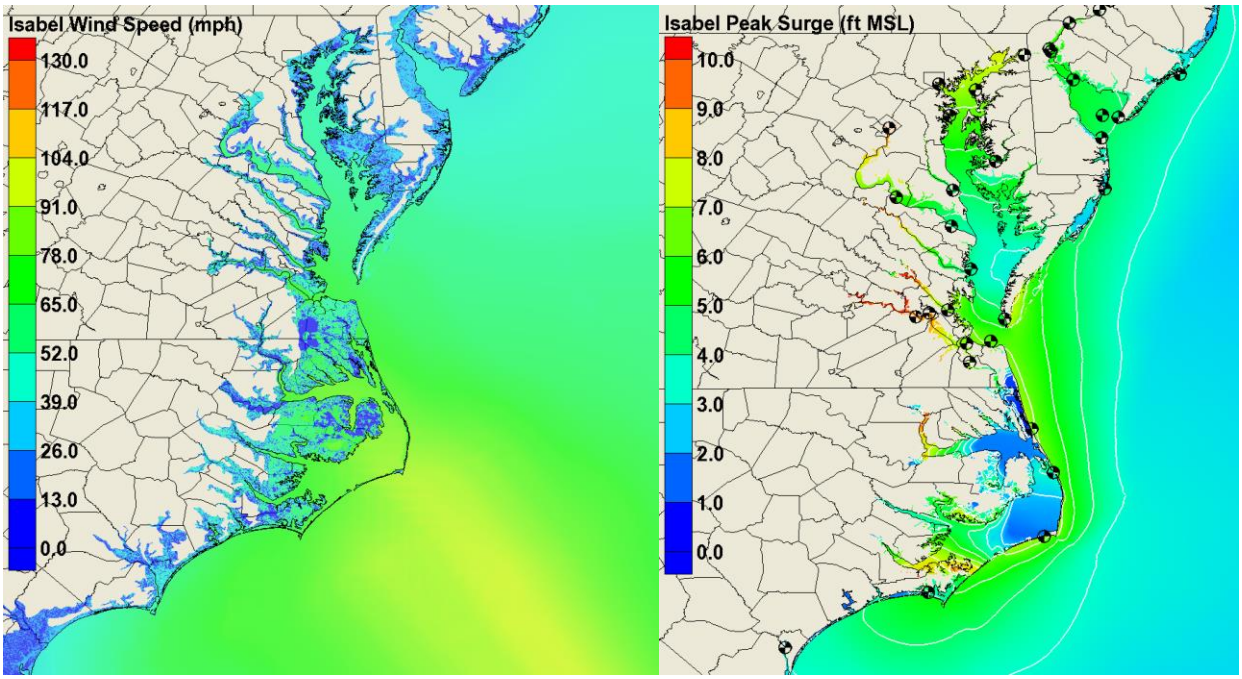

Figure 6-60: Isabel maximum wind speeds (left) and maximum modeled surge (left); NOAA gage sites marked by pinwheels (right).

6.8.2 *Results and Skill Assessment*

Comparisons of peak water levels and RMSE indicate model performance was good overall. Figure 6-61 illustrates the peak water level error at NOAA gages during Hurricane Isabel; the error was calculated as modeled peak minus measured peak (error = modeled – measured). For gages that failed during the storm, the maximum value for the portion of the time series available while the gage was functional was used for comparison. Gages represented in the geographic RMSE figure that did not show evidence of a surge signal in the time series are omitted from Figure 6-61.

Of the 38 gages evaluated, 31 produced an RMSE less than the 0.66 feet (0.2 meter) target value, as illustrated in Figure 6-61 and Figure 6-62. The remaining eight gages had RMSE values less than 1 foot. The largest discrepancies between observed and measured data typically occurred at upstream gages including Washington, DC and Newbold, Pennsylvania.

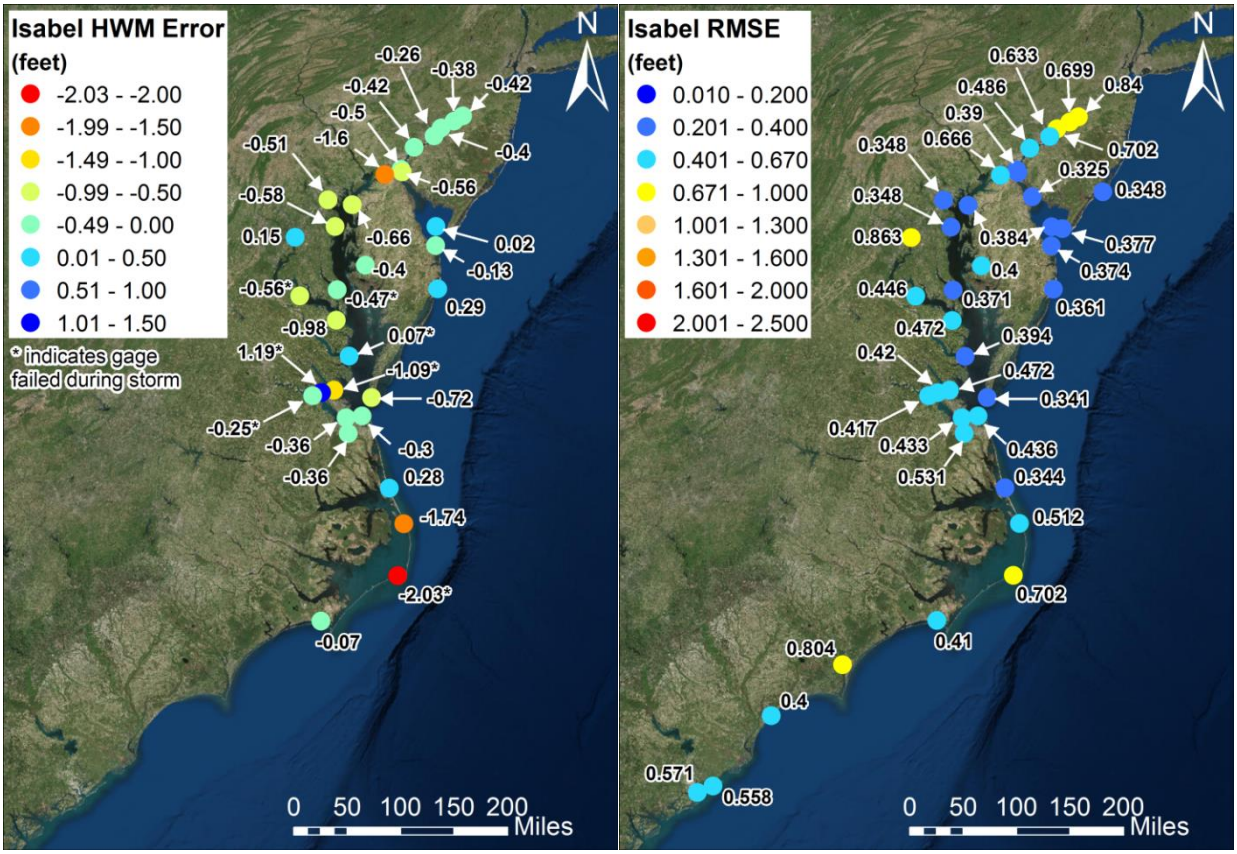

Figure 6-61: Geographic distribution of peak water level error (left) and time series RMSE (right) at NOAA stations. Peak surge errors are shown only for gages with a distinct surge signal.

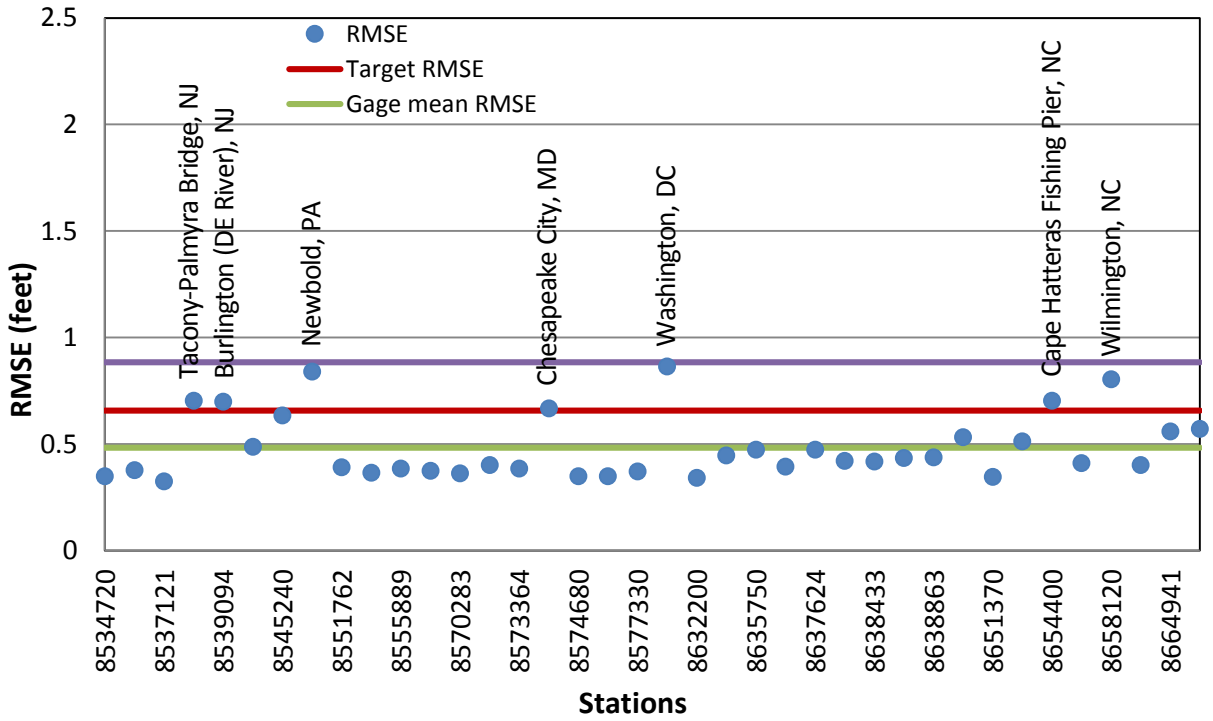

Figure 6-62: Alongshore plot of time series RMSE at NOAA stations; selected stations named for reference; red line indicates target RMSE, green line gives gage mean RMSE, and the purple line is mean RMSE from all storms.

Time series for these gages are provided in Figure 6-63 and Figure 6-64. The Washington, DC gage shows disagreement in both the tidal phase and amplitude, but captures the peak surge within 0.5 feet. The Newbold, Pennsylvania gage demonstrates stronger agreement in the tidal phasing, but under predicts the amplitude of the tide throughout the time series. At both gages, the local waterway is under-represented by a two-node channel and riverine inflow is not included. These simplifications could affect the model performance.

At the Oregon Inlet Marina gage, the surge was driven by winds across Pamlico Sound, however the surge is not well-captured in the model (Figure 6-65). The exaggerated set-down in water levels at the gage before the surge also indicates issues with the model's ability to represent circulation within the sound. The gage at Cape Hatteras Fishing Pier was not well represented, as evidenced by both Figure 6-61 and Figure 6-66. The gage failed during the peak surge, but the model under predicts the maximum observation by just over 2 feet. The time series shows that model performance degrades as the storm surge reaches the area, producing consistently low values. The magnitude of the discrepancy is potentially exaggerated by missing the peak surge in the measured data. Due to its location on the open coast, some of the discrepancy could also be accounted for by exclusion of wave setup in the ADCIRC simulation.

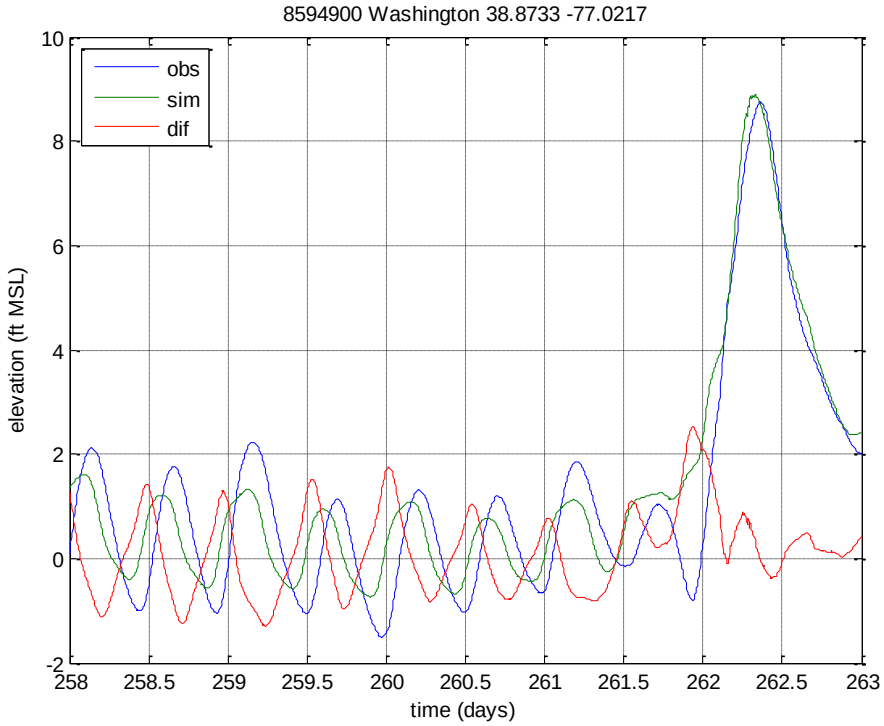

Figure 6-63: Measured and modeled time series at Washington, DC.

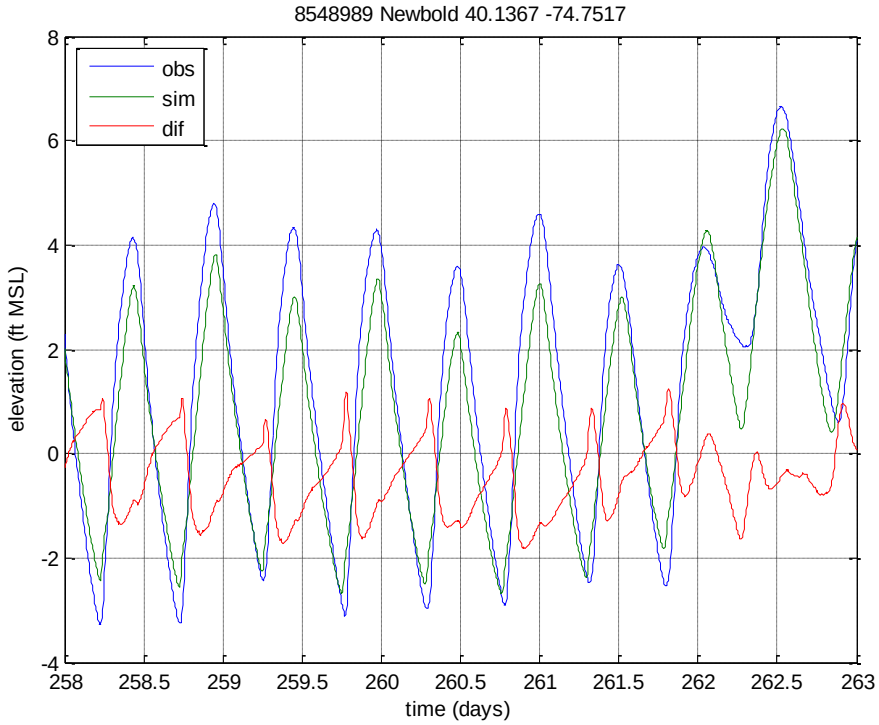

Figure 6-64: Measured and modeled time series at Newbold, Pennsylvania.

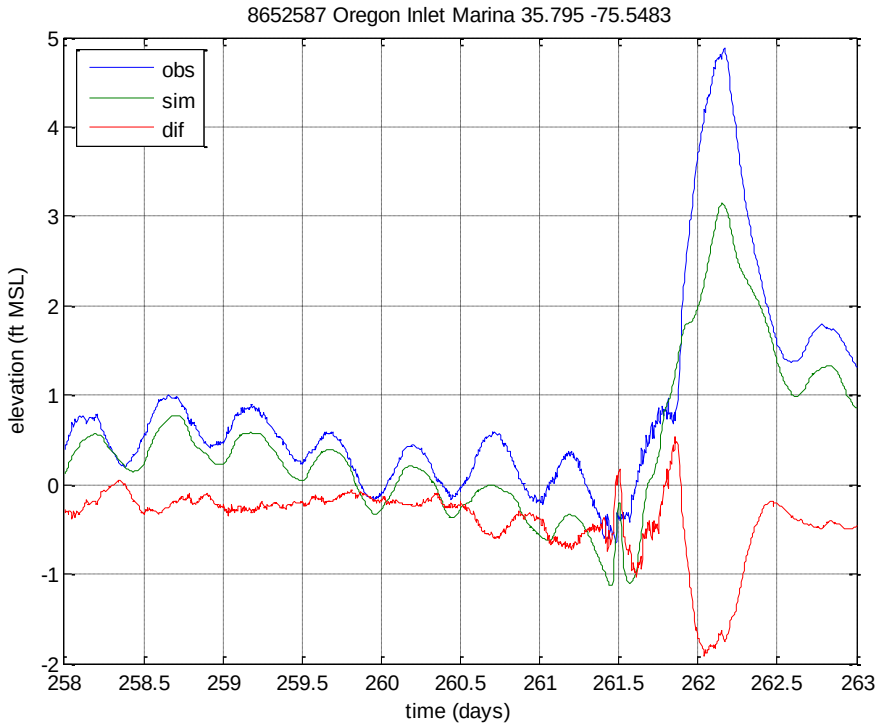

Figure 6-65 Measured and modeled time series at Oregon Inlet Marina, North Carolina.

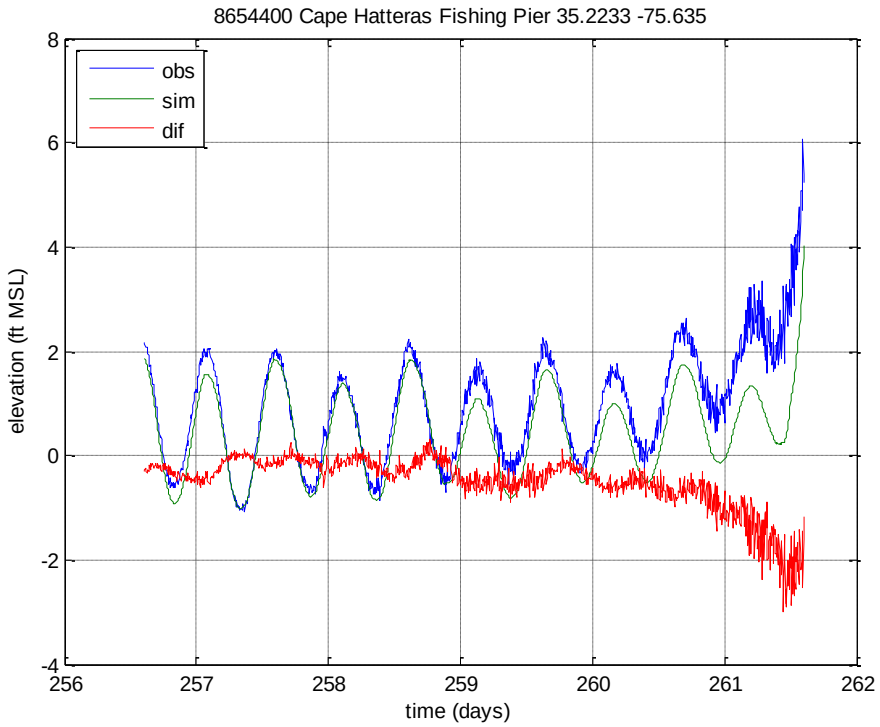

Figure 6-66: Measured and modeled time series at Cape Hatteras Fishing Pier, North Carolina.

6.9 **Sandy (2012)**

Hurricane/Post-Tropical Cyclone Sandy was a Category 3 hurricane that devastated New Jersey and New York. Sandy made landfall October 29, 2012 near Atlantic City, New Jersey as a post-tropical cyclone with wind speeds of a Category 1 hurricane. Storm surge was most prominent in New Jersey and New York.

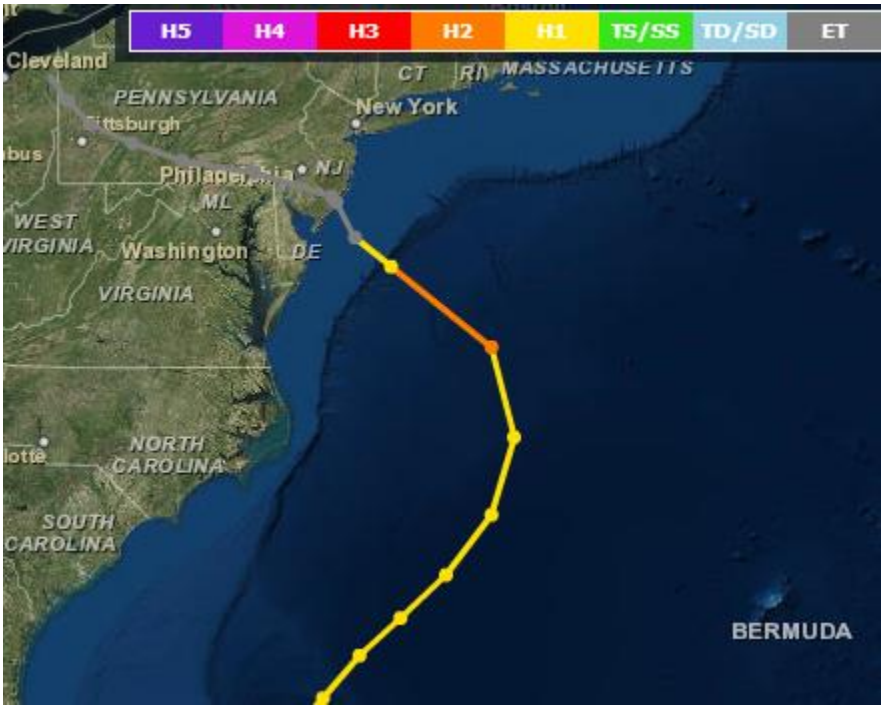

Figure 6-67: Storm track of Hurricane Sandy. Dots denote 6-hour intervals, extratropical transition, and landfall.

6.9.1 ***Model Setup***

The model simulation was 19.25 days long, with a 4.25-day storm run. Meteorological forcing was supplied by unscaled HWRF model output. Wind/pressure forcing was supplied from HWRF at 15-minute intervals. The simulation was executed with advection terms both on and off, and differences were found to be within +/- 0.06 meters (0.2 feet).

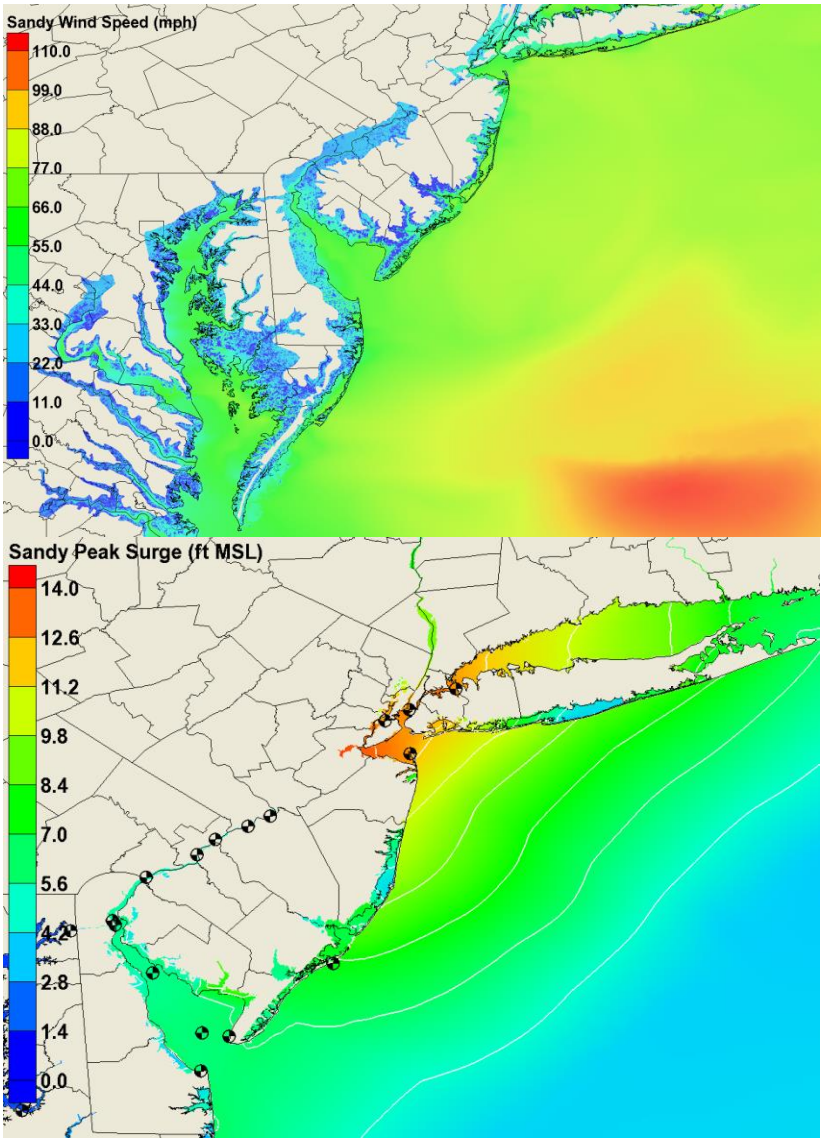

Figure 6-68 Sandy maximum wind speeds (top, mph) and maximum modeled surge (bottom, feet MSL); NOAA gage sites marked by pinwheels (bottom).

6.9.2 *Results and Skill Assessment*

Model skill was generally good, with most of the error (especially in the RMSE results) coming from a mean low bias in modeled data that exceeded 0.7 feet from Atlantic City and further south, presumably due to the absence of the steric effect. In spite of this, several of the gages (Atlantic City Figure 6-77, The Battery Figure 6-74, Bergen Point Figure 6-75) show good agreement at peak surge, indicating that the wind forcing may be slightly too strong if the steric effect were included. The Sandy Hook gage (Figure 6-76) failed prior to arrival of the peak surge. Water levels in Delaware Bay (Figure 6-78) are under-estimated largely due to the mean water level difference, which nears 1 foot. All coastal gages from Lewes, Delaware and Cape May, New Jersey, north to The Battery, New York show appreciable water level increase while winds are still shore-parallel. Given the shape of the region, the immense size of Sandy, and the direction of the winds, this may indicate Ekman setup preceding the primary surge.

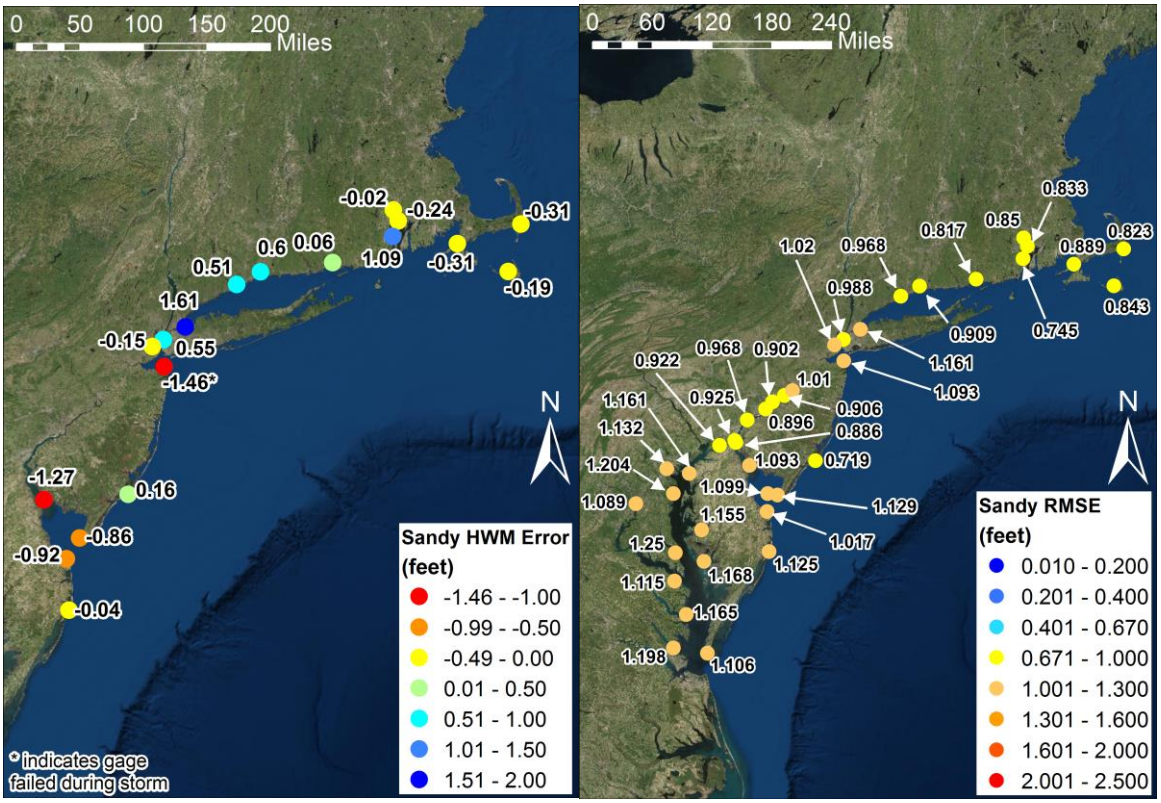

Figure 6-69 Geographic distribution of peak water level error (left) and time series RMSE (right) at NOAA stations. HWM errors are limited to gages with a distinct surge signal

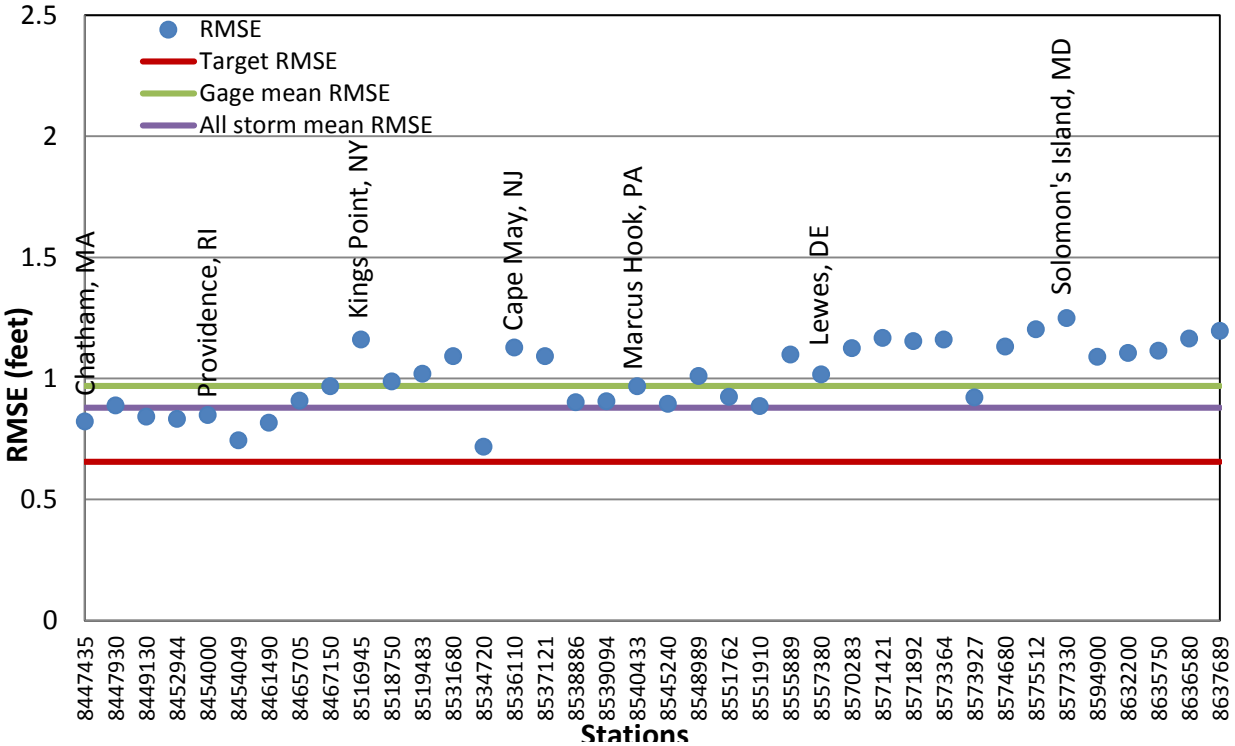

Figure 6-70 Alongshore plot of time series RMSE at NOAA stations; selected stations named for reference; red line indicates target RMSE, green line gives gage mean RMSE, and the purple line is mean RMSE from all storms.

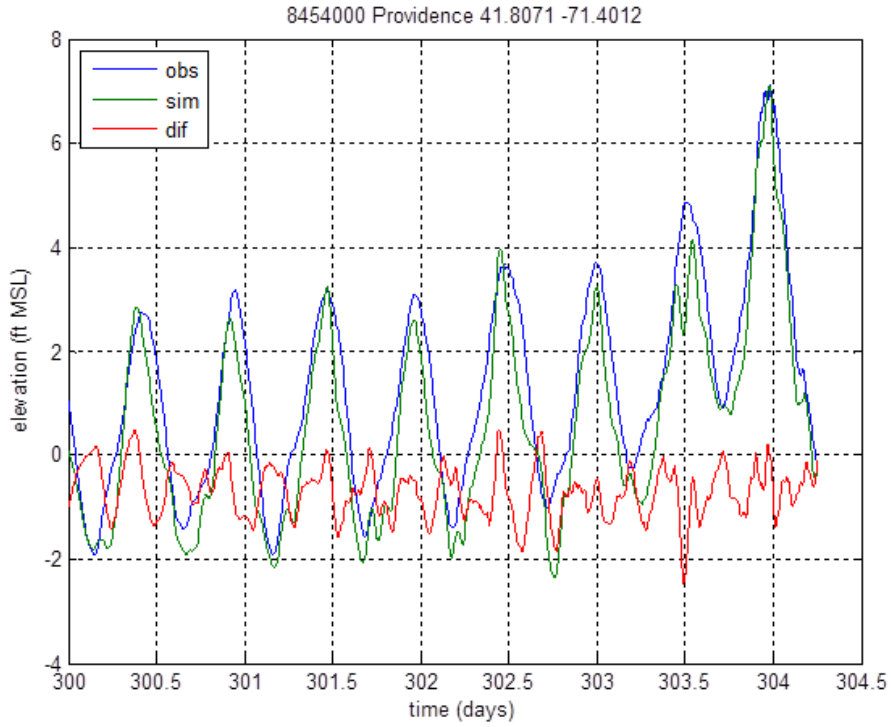

Figure 6-71: Measured and modeled time series at Providence, Rhode Island.

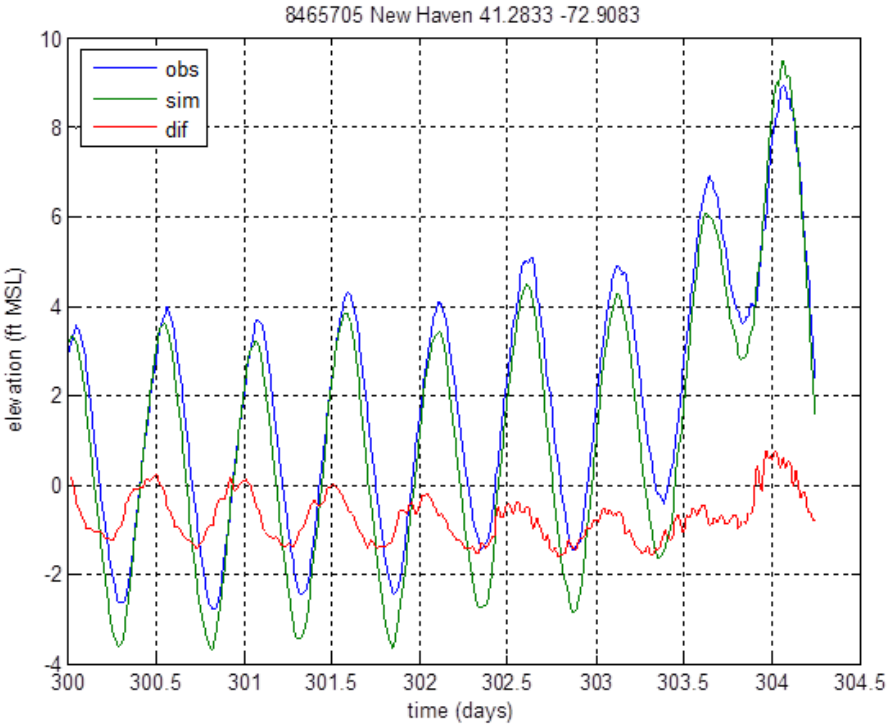

Figure 6-72: Measured and modeled time series at New Haven, Connecticut.

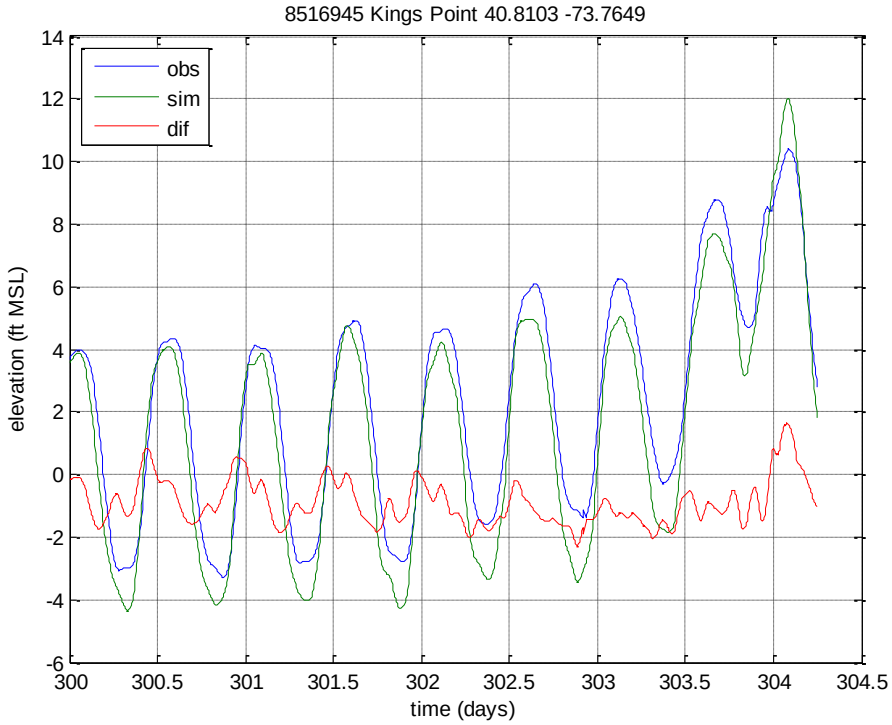

Figure 6-73 Measured and modeled time series at Kings Point, New York.

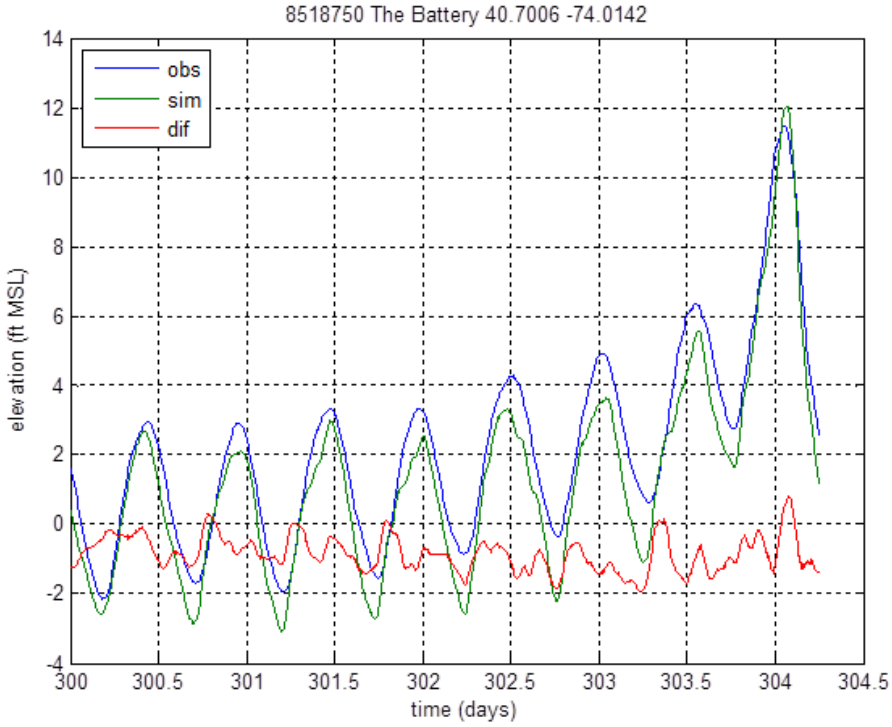

Figure 6-74: Measured and modeled time series at The Battery, New York.

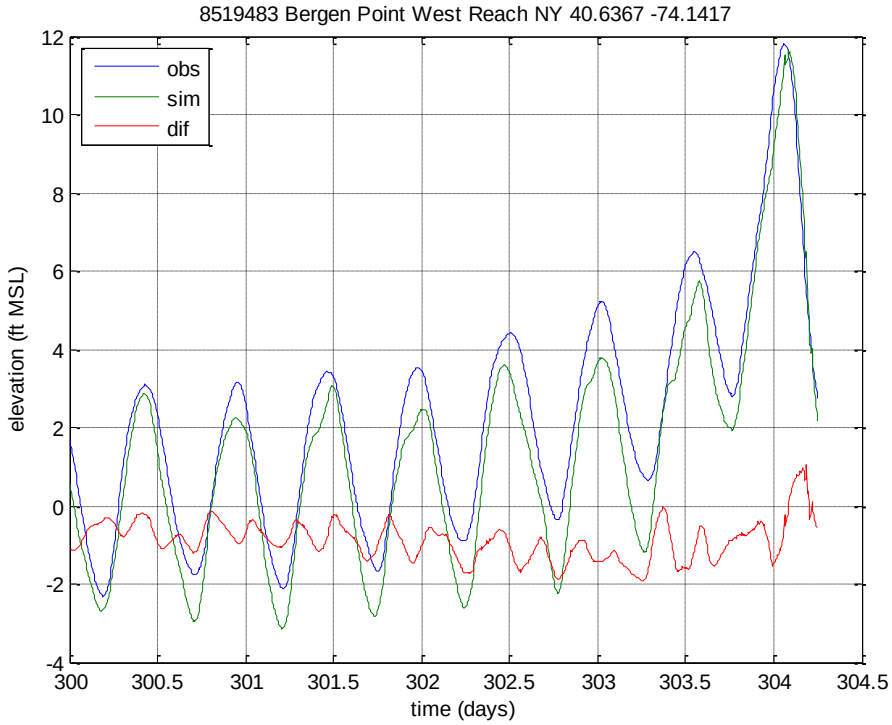

Figure 6-75: Measured and modeled time series at Bergen Point, New York.

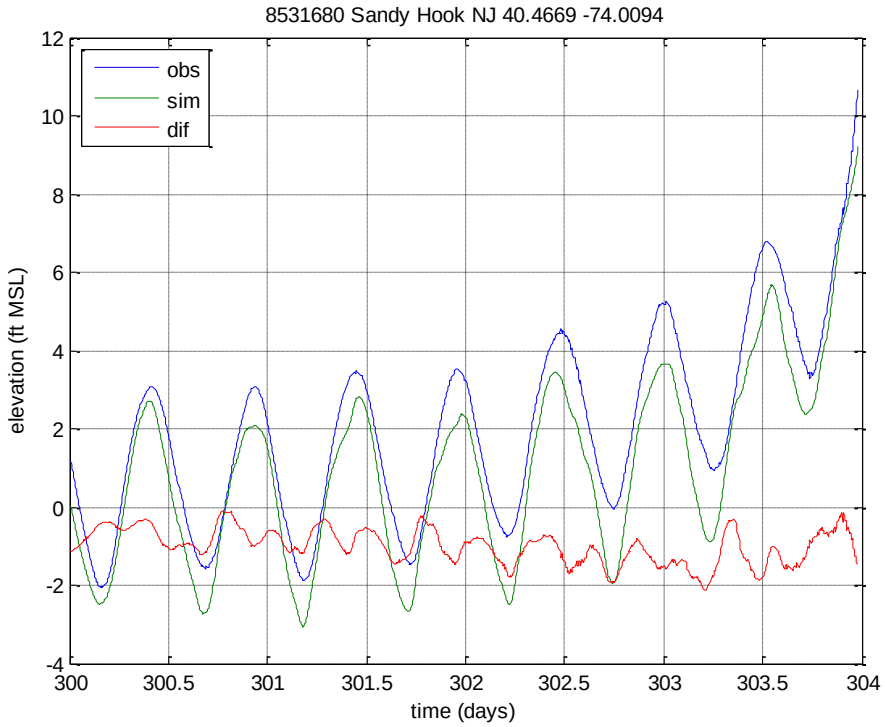

Figure 6-76: Measured and modeled time series at Sandy Hook, New Jersey.

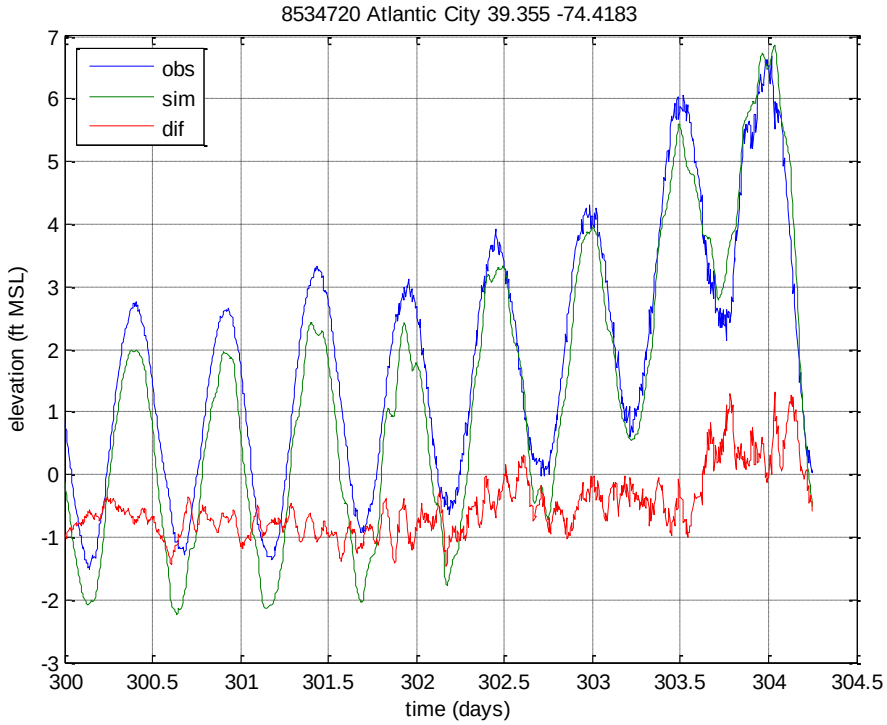

Figure 6-77 Measured and modeled time series at Atlantic City, New Jersey.

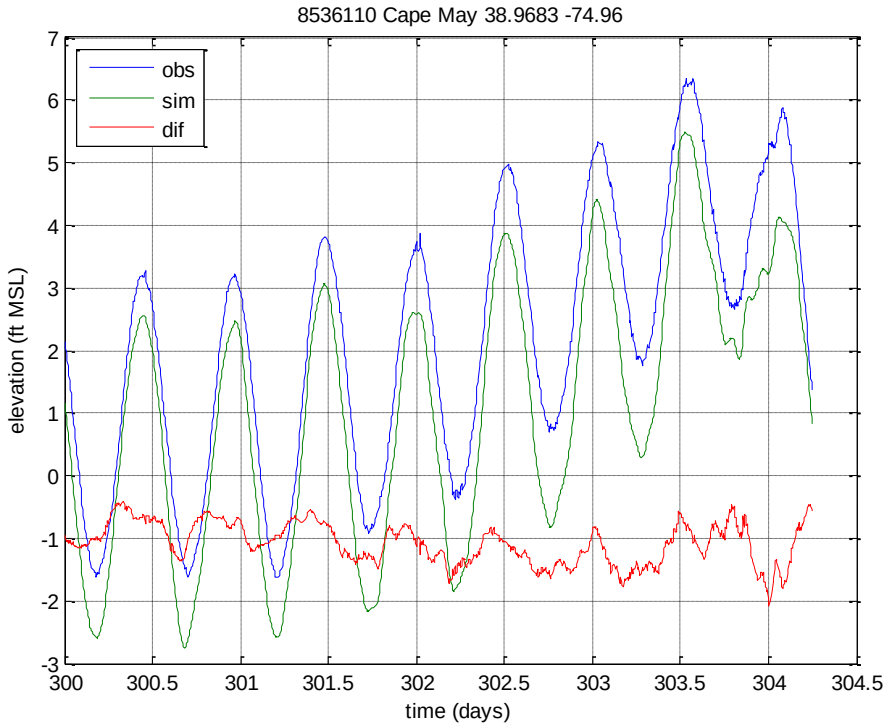

Figure 6-78 Measured and modeled time series at Cape May, New Jersey.

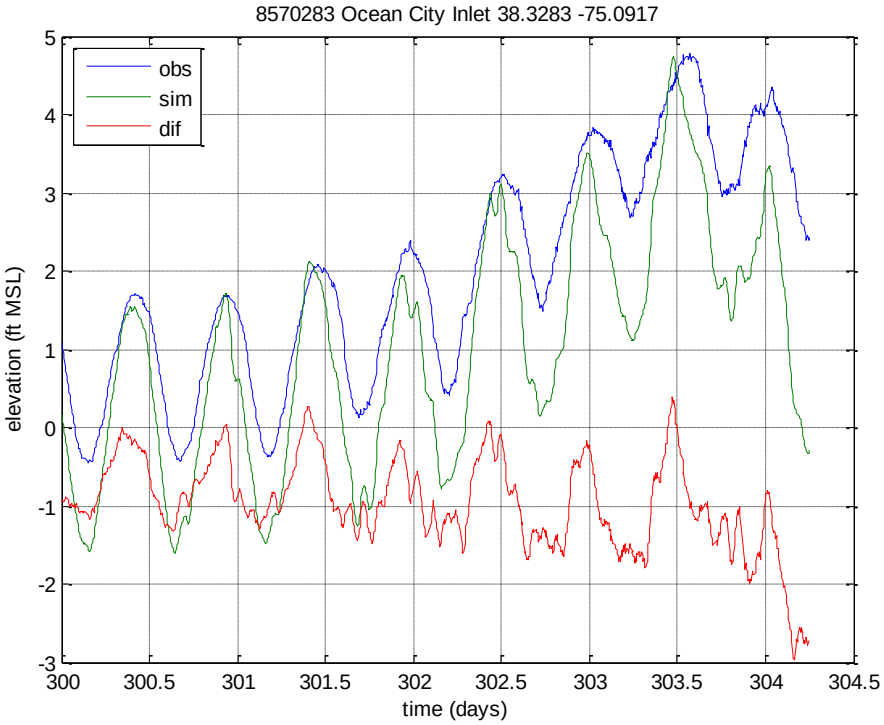

Figure 6-79 Measured and modeled time series at Ocean City, Maryland.

Initial simulations performed with H*Wind data showed very poor performance, with most of the modeled results being below the observations, many by more than 3 feet.

6.10 Long Island Express (1938)

The 1938 Long Island Express (also known as the Great New England Hurricane) was a Category 5 hurricane that damaged much of New York and southern New England. The storm made landfall September 21, 1938 in central Long Island as a Category 3 hurricane. Storm surge was most prominent in New Jersey, New York, Connecticut, Rhode Island, and Massachusetts.

Figure 6-80: Storm track of the Long Island Express. Dots denote 6-hour intervals and landfall.

6.10.1 *Model Setup*

The model simulation was 16.25 days long, with a 1.25-day storm run. The short duration is due to the storm's exceptional forward speed, at times as great as 50 mph. The meteorological forcing begins with the storm east of Florida. Meteorological forcing was supplied by OWI wind files from the FEMA Region II New York - New Jersey study, and the winds were scaled up by a factor of 1.04, consistent with the scaling used in the FEMA study. Wind and pressure forcing was supplied at 15-minute intervals. Figure 6-81 illustrates the modeled peak surge from the Long Island Express. Simulation of the storm predicted the highest surge values occur at the confluence of the East River and Long Island Sound in New York and in upstream reaches of Buzzards Bay and Narragansett Bay.

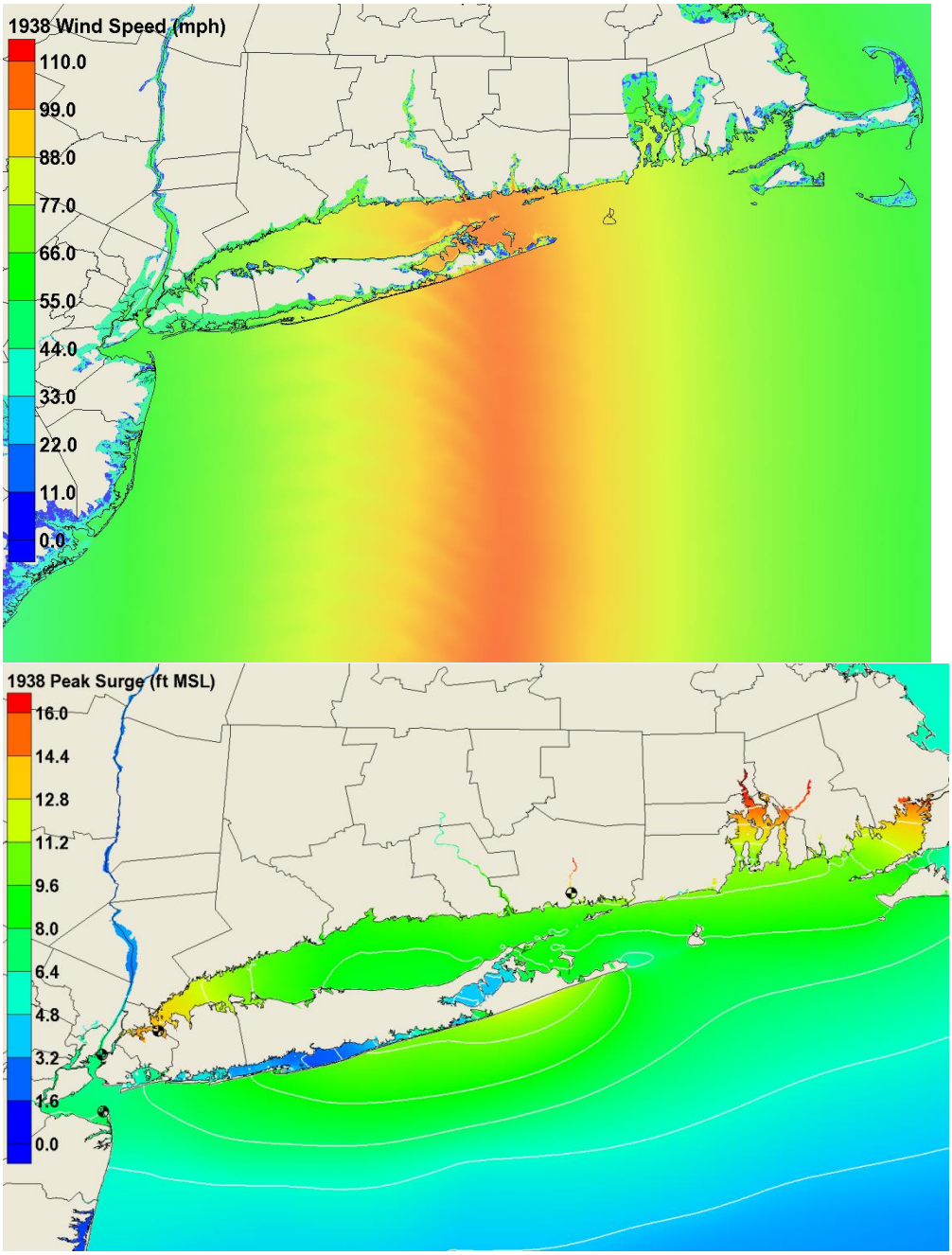

Figure 6-81 Long Island Express maximum wind speeds (top, mph) and maximum modeled surge (bottom, feet MSL; NOAA gage sites marked by pinwheels (bottom).

6.10.2 *Results and Skill Assessment*

Model skill for the Long Island Express was generally good. Peak water level error at NOAA gages is provided in Figure 6-82 and for additional post-storm surveyed HWMs in Figure 6-83. Approximately two thirds of the HWMs demonstrate the modeled results are within 1 foot of the measured elevations and show just a slight high bias. A few HWMs in Figure 6-83 show a very large discrepancy between modeled and measured data (up to 10 feet). These instances could result from inaccuracies in the collected high water mark data, but are also likely attributable to historical differences in topography not represented in the mesh. The south side of central and eastern Long Island, where the largest differences

occur, has several inlets that have opened and closed over time. A storm of this strength is also very capable of having made a cut of its own.

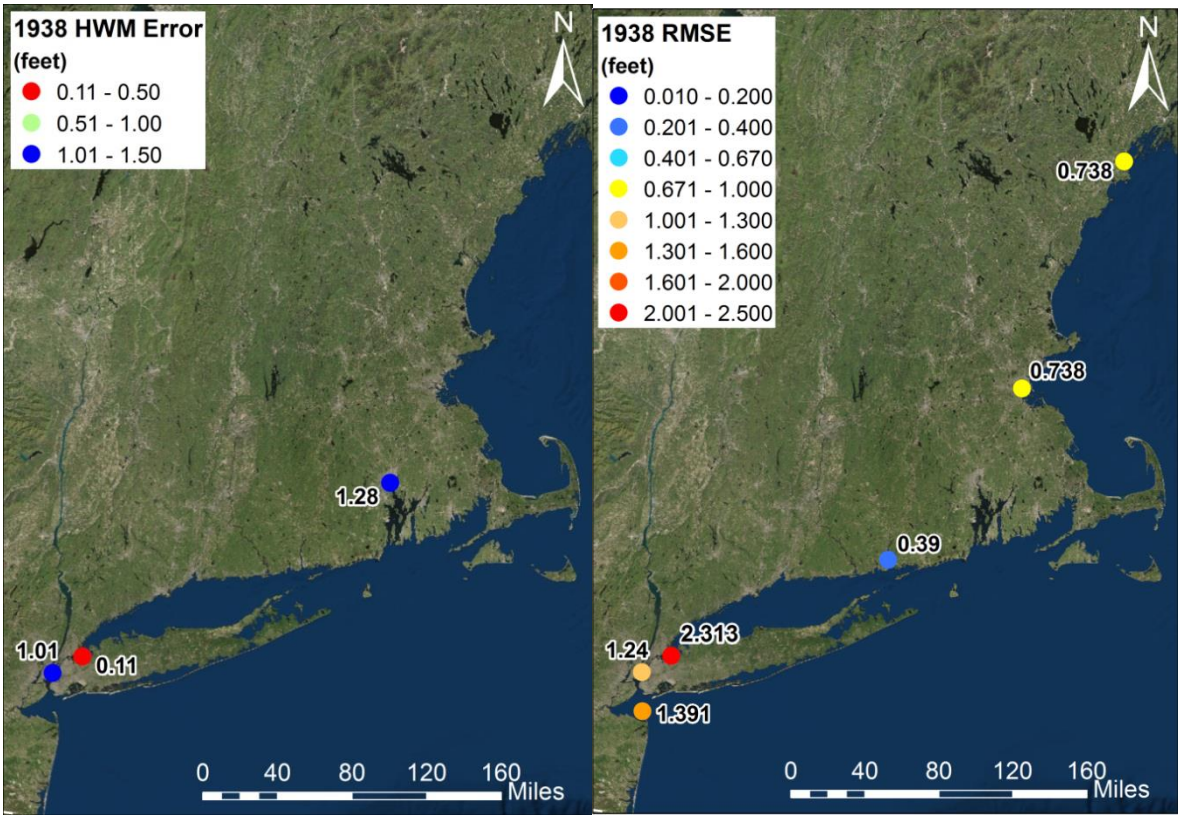

Figure 6-82 Geographic distribution of peak water level error (left) and time series RMSE (right) at NOAA stations. HWM errors are limited to gages with a distinct surge signal.

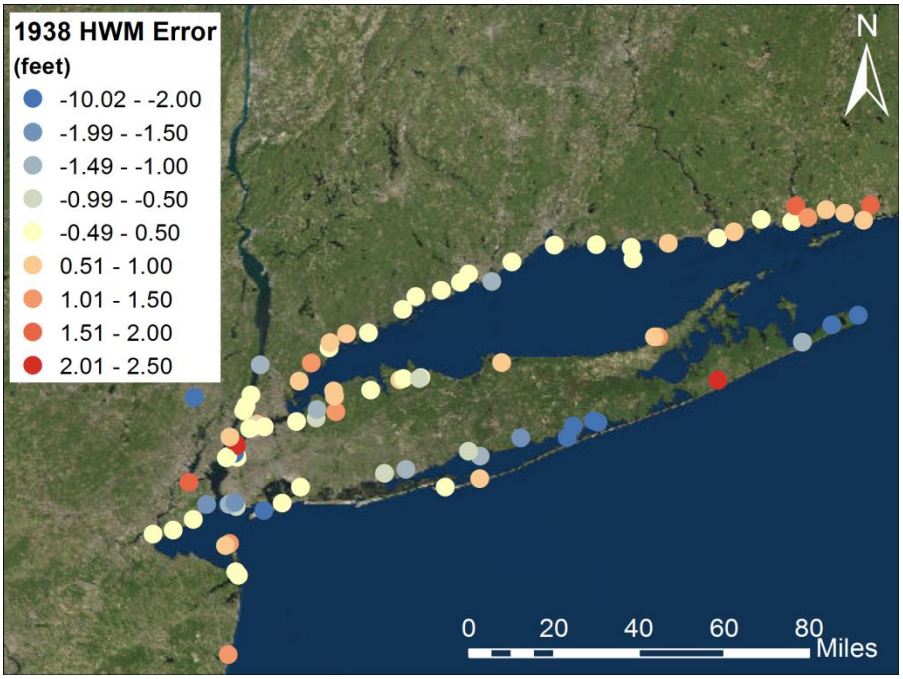

Figure 6-83: Geographic distribution of peak water level error from additional high water marks.

The RMSE data presented in Figure 6-82 and Figure 6-84 suggest weaker model performance than the peak water level error. However, some of the discrepancy can be accounted for by the temporal resolution of the measured data. Available measured time series data is limited and was recorded at 60 minute intervals, as illustrated in Figure 6-86 and Figure 6-85. The model captures the tide data adequately prior to the storm, with a slight over prediction of the amplitude. However, as the storm approaches, the coarseness of the measured data appears to skip over some the peaks within the time series. This is especially apparent around day 265.1 in Figure 6-85 and day 264.8 in Figure 6-86.

The 1938 storm's small positive bias, is inconsistent with nearly all other storms simulated on the NOMAD mesh. Because of the significant amount of time which has passed since this storm occurred, there may be additional long-term factors such as topographic changes, shoreline modifications (both natural and man-made), and relative sea level rise, all affecting the interpretation and comparison of the gage water levels and high water mark data with the NOMAD model results. For instance, the long-term relative sea level rise trends at The Battery and at Sandy Hook are 2.8 and 4.1 millimeters per year[11], respectively, allowing for 0.5-0.7 feet of relative rise since the 1938 storm occurred.

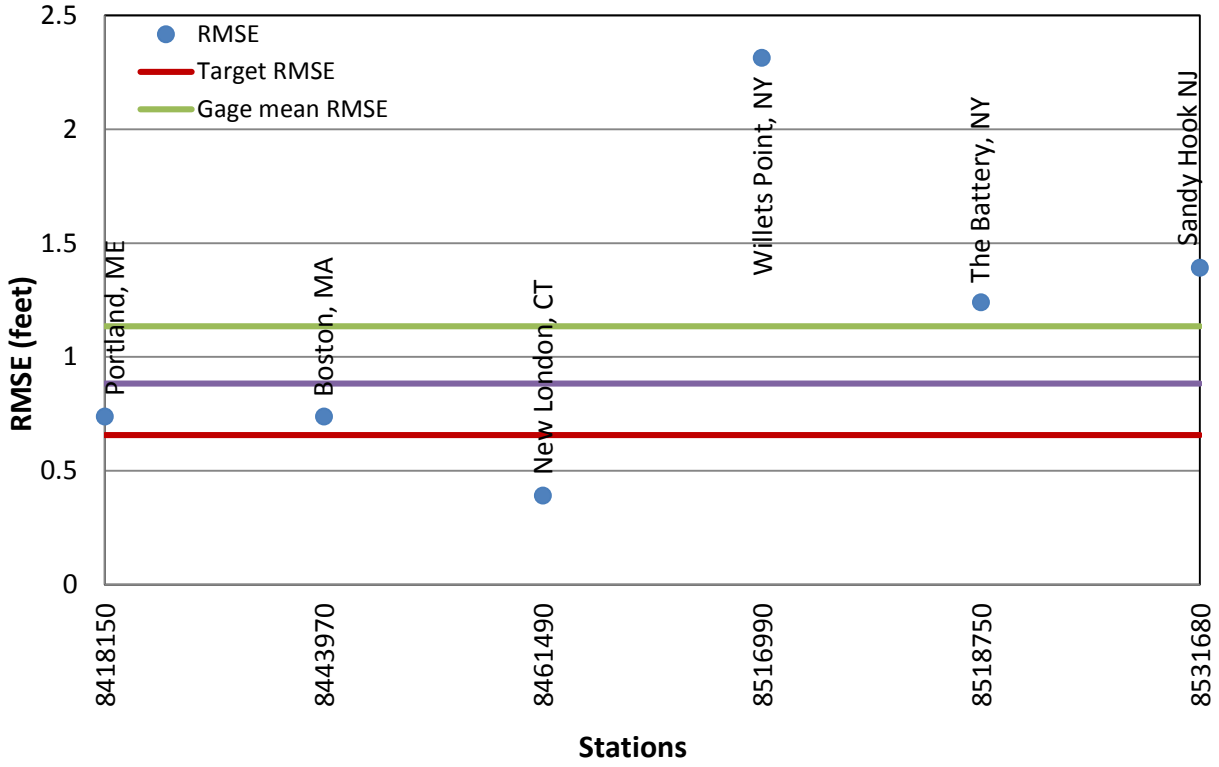

Figure 6-84 Alongshore plot of time series RMSE at NOAA stations; selected stations named for reference; red line indicates target RMSE, green line gives gage mean RMSE, and the purple line is mean RMSE from all storms.

[11] Sea level trends obtained from http://tidesandcurrents.noaa.gov/sltrends/sltrends_station.shtml?stnid=8518750 http://tidesandcurrents.noaa.gov/sltrends/sltrends_station.shtml?stnid=8531680

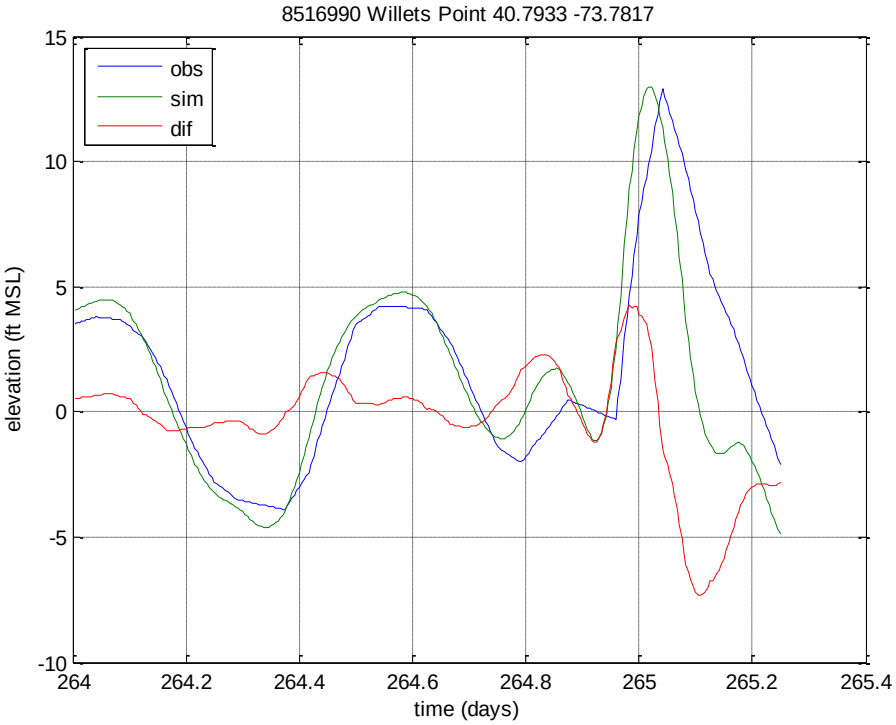

Figure 6-85 Measured and modeled time series at Willets Point, New York.

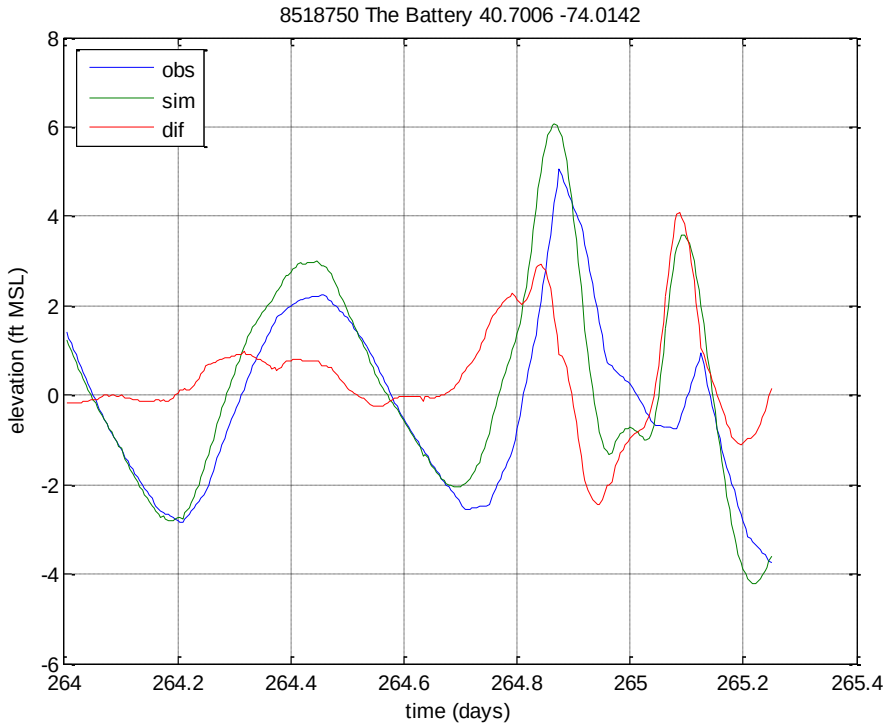

Figure 6-86 Measured and modeled time series at The Battery, New York.

The Long Island Express simulation was executed with advection terms both on and off, and differences range dramatically across the storm affected area. In the areas with highest surge (i.e. Long Island Sound, Buzzards Bay, and Narragansett Bay), the advection-on simulation produced surge elevations between 1 and 4 feet higher than its advection off counterpart. However, inclusion of advection terms resulted in a reduction of up to 1 foot in storm surge in the Raritan Bay through the Hudson River and in Cape Cod Bay. These differences between advection-on and advection-off results are depicted in Figure 6-87.

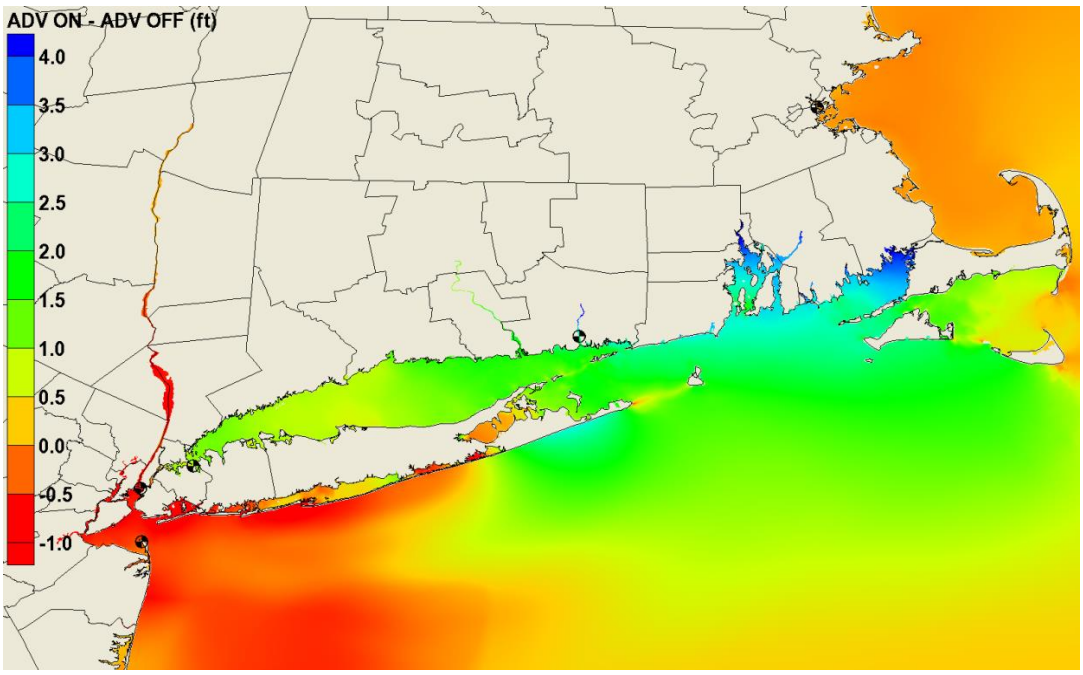

Figure 6-87: Long Island Express advection-on minus advection-off peak surges (feet).

6.11 **Perfect Storm (1991)**

The 1991 Perfect Storm (also known as the Halloween Storm) was an extratropical storm that caused devastation for much of the Northeast United States. The storm swept southward offshore of New England on October 31, 1991 as an extratropical system, then circled back northward as a tropical storm and eventually as a Category 1 hurricane. Damages and storm surge were most significant in New England states including Massachusetts, Maine, and New Hampshire.

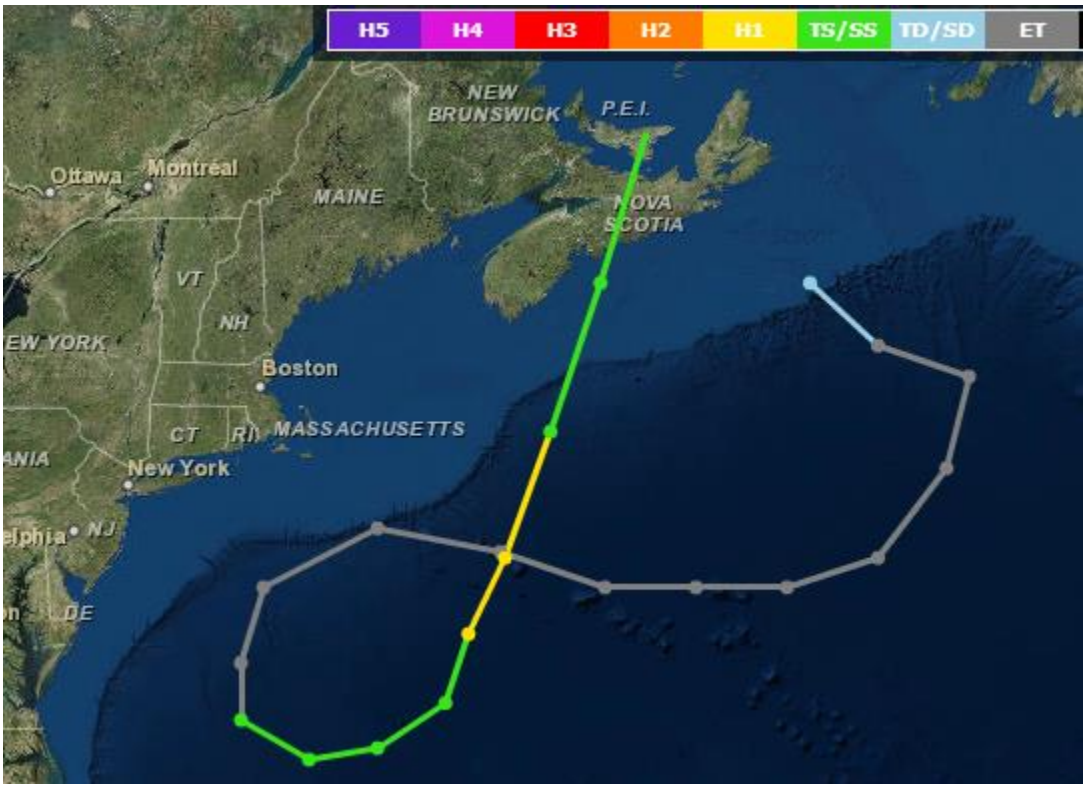

Figure 6-88: Storm track of the Perfect Storm. Dots denote 6-hour intervals.

6.11.1 ***Model Setup***

The model simulation was 23 days long, with an eight-day storm run. Meteorological forcing was supplied by OWI wind files from the FEMA Region II New York- New Jersey study, and the winds were scaled up by a factor of 1.04; this value is consistent with what was used in the FEMA study. Wind and pressure forcing was supplied at 15-minute intervals. Figure 6-89 illustrates the modeled maximum wind speed and the modeled peak surge from the Perfect Storm simulation. The largest surge values were predicted at the confluence of the East River and Long Island Sound in New York and in Cape Cod Bay. The Perfect Storm simulation was executed successfully with advection terms off only; advection-on simulations failed due to instability issues.

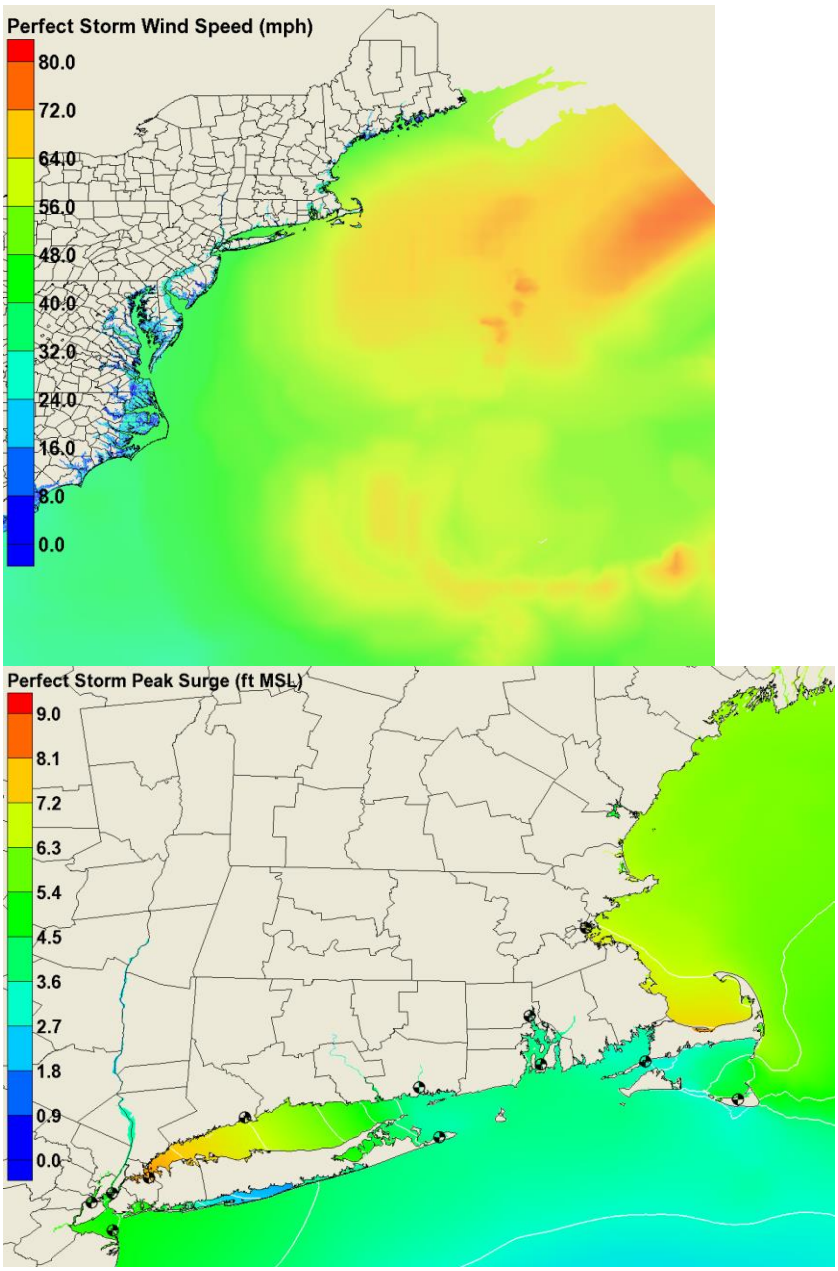

Figure 6-89: Perfect Storm maximum wind speeds (top, mph) and maximum modeled surge (bottom, feet MSL); NOAA gage sites marked by pinwheels (bottom).

6.11.2 *Results and Skill Assessment*

Comparisons of peak water level errors and RMSE indicate simulation of the Perfect Storm typically under predicted storm surge in comparison to observed data. Figure 6-90 illustrates the peak water level error at NOAA gages during the Perfect Storm; the error was calculated as modeled peak minus measured peak (error = modeled – measured). Gages represented in the geographic RMSE figure that did not show evidence of a surge signal in the time series were removed from the HWM error plot.

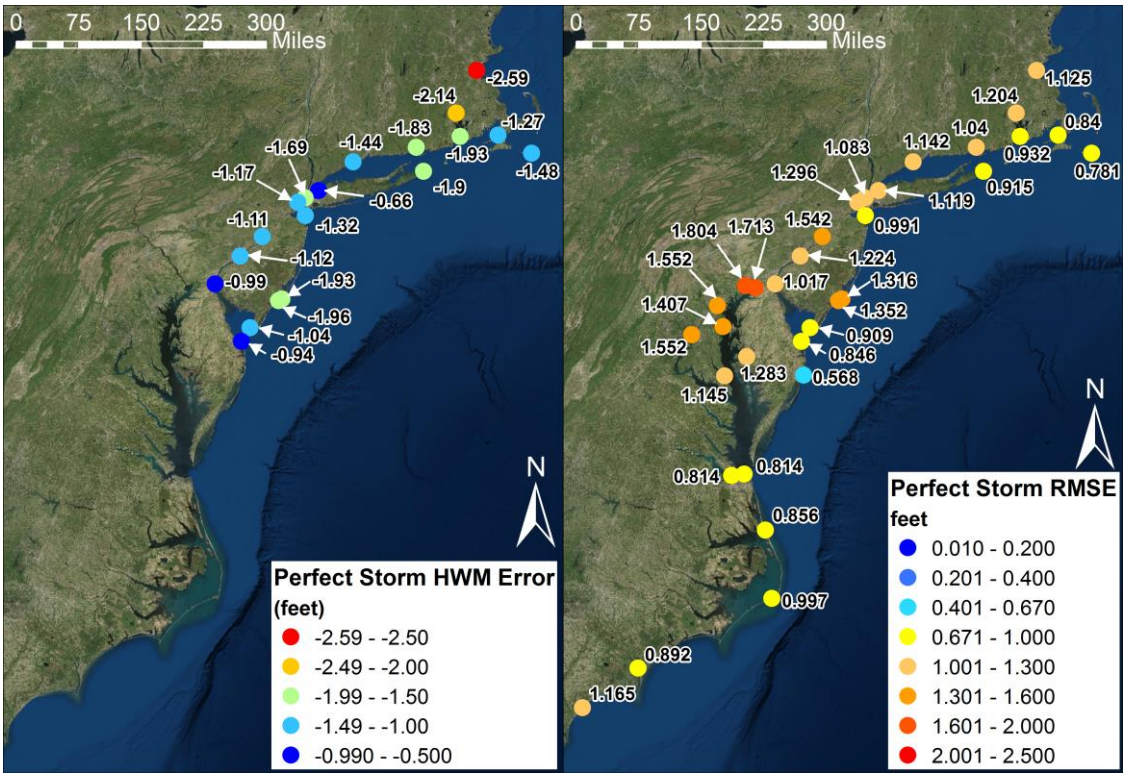

Figure 6-90: Geographic distribution of peak water level error (left) and time series RMSE (right) at NOAA stations. HWM errors are limited to gages with a distinct surge signal

Peak water level errors in Figure 6-90 demonstrate a consistent low-bias across the entire storm-affected area with under prediction ranging from 2.6 feet to 0.7 feet. The poor performance is also reflected in the RMSE data displayed in Figure 6-90 and Figure 6-91. With the exception of one gage at the Ocean City, Maryland Fishing Pier, no gages met the target RMSE value of 0.66 feet (0.2 meters). Sample time series provided in Figure 6-92 and Figure 6-93 show the modeled water surface is considerably lower than measured records.

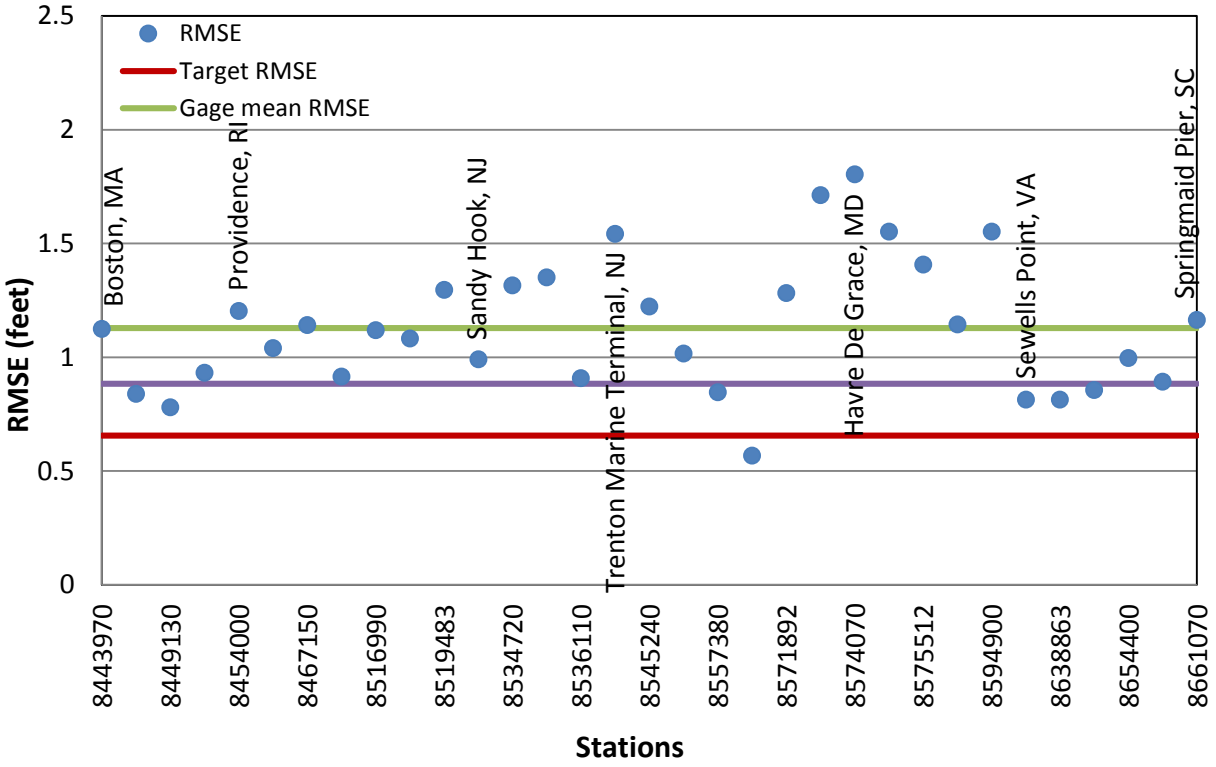

Figure 6-91: Alongshore plot of time series RMSE at NOAA stations; selected stations named for reference; red line indicates target RMSE, green line gives gage mean RMSE, and the purple line is mean RMSE from all storms.

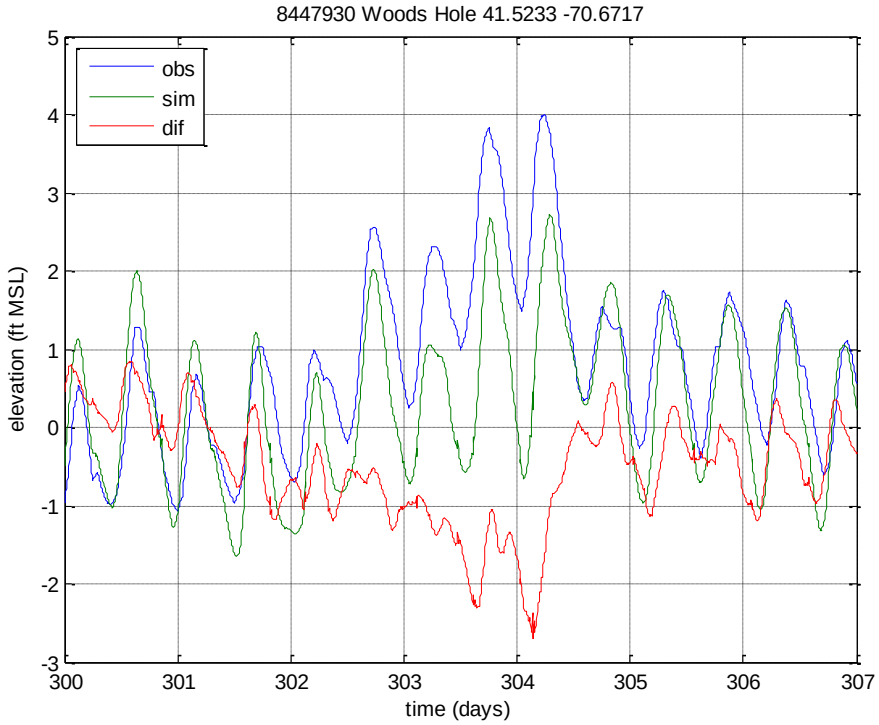

Figure 6-92: Measured and modeled time series at Woods Hole, Massachusetts.

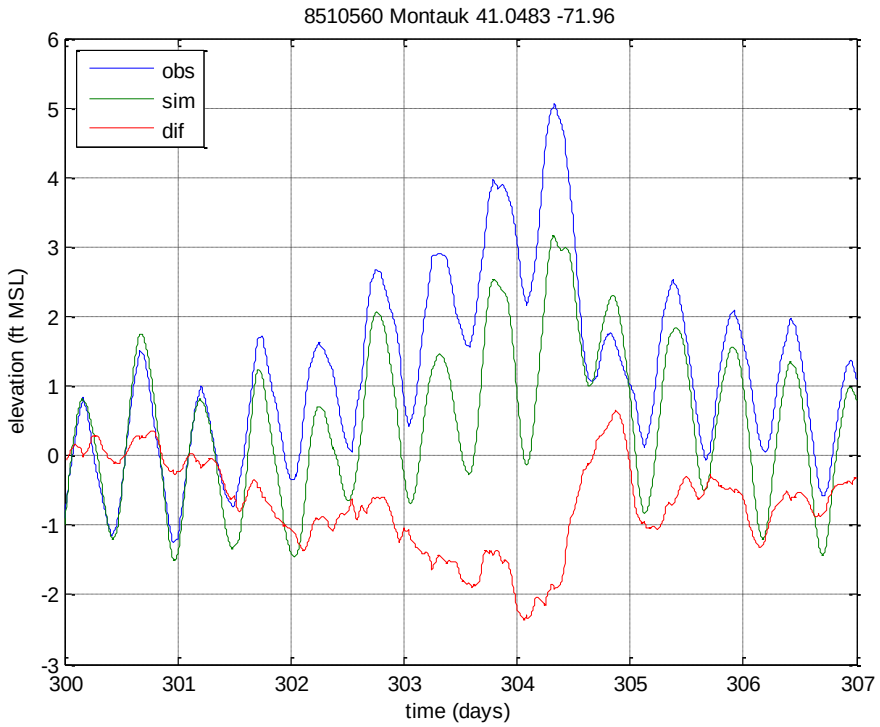

Figure 6-93: Measured and modeled time series at Montauk, New York.

The poor performance observed in the Perfect Storm simulation is similarly reflected in modeled data from the FEMA Region II study. Table 6-2 and Figure 6-94 demonstrate the NOMAD predicted peak surge values are within 0.3 to 0.4 feet of the FEMA Region II study. The similarity in the under-prediction could mean that the wind and pressure forcing does not adequately represent the storm event.

Table 6-2: Comparison of HWM Error.

Gage	Location	HWM Error (NOMAD)	HWM Error (FEMA)
		(feet)	(feet)
8510560	Montauk, N.Y.	-1.9	-1.5
8518750	The Battery, N.Y.	-1.7	-1.4
8519483	Bergen Point West Reach, N.Y.	-1.2	-0.9
8531680	Sandy Hook, N.J.	-1.3	-1.0
8534720	Atlantic City, N.J.	-1.9	-1.7

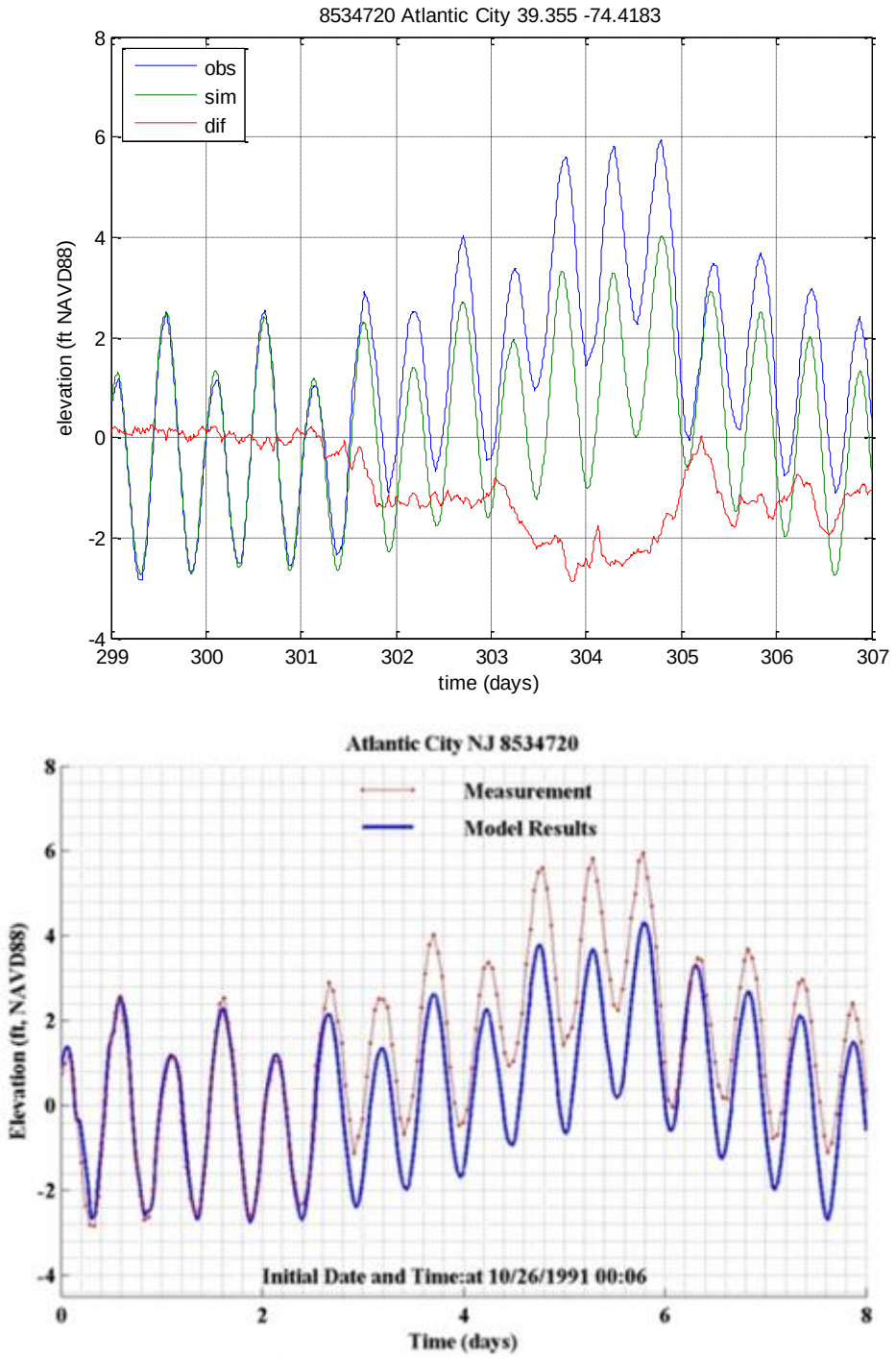

Figure 6-94 Comparison of NOMAD (top) to FEMA (bottom) time series at Atlantic City, New Jersey.

7. RESULTS FOR ALL HINDCAST EVENTS

The target RMSE for time series comparison was 0.2 meters (0.66 feet) and overall, the mean RMSE for all stations evaluated using the skill assessment software was 0.27 meters (0.89 feet). Additional summary statistics are given in Table 7-1. The RMSE ranged from approximately 0.1 to 0.7 meters (0.3 to 2.3 feet) for all functioning gages. Several failed gages reported slightly lower RMSE values. Low-biased mean water elevations account for a large portion of RMSE in several of the storms and make it difficult for most of the gages to meet the 0.2 meters RMSE target. Ike stands out with exceptionally poor performance on all metrics due to an inadequate representation of the forerunner surge that characterized that storm. The 1991 Perfect Storm also has very poor error metrics, however these are largely consistent with the results from the Region II FEMA study, which used the same meteorological forcing. The overall consistency of the NOMAD results with those of that study's much higher-resolution mesh indicate that the issue is likely with the meteorological inputs and cannot be resolved here. The significant RMSEs during Sandy are largely driven by very high mean water levels at most gages, which are presumably from steric and other effects that were not modeled but which could be accounted for with a simple mean correction.

Peak water levels also generally suffer from a low bias. Like the gage time series RMSE, the peak water level bias can be at least partially attributed to seasonal water level fluctuations that are not modeled, since most storms occur in the summer when the water level is highest. It can also be partially attributed to the lack of wave setup, which may increase peak water levels 5-20%, especially at the open coast. One notable exception is the 1938 Long Island Express, whose means show a positive bias and whose peaks are slightly overestimated on average. It is difficult to evaluate data from such an old storm. Among the long-term factors that may affect the interpretation of the bias in the validation data is the general increase in relative sea level throughout the northeast since 1938. The magnitude of the relative sea level increase is on the order of the positive bias and, depending on how datums were used to document the high water marks and gage water levels, may account for at least a portion of the bias.

Table 7-1: Summary error statistics for all simulations.

Summary Statistic	Value
Mean RMSE (feet)	0.89
Mean gage peak water level error (feet)	-0.94
Mean absolute gage peak water level error (feet)	1.1
Mean all-HWM (gages and HWM data) and error (feet)	-0.8
Mean abs all-HWM (gages and HWM data)error (feet)	1.2

Although select gages experience issues with tidal phasing and amplitude, tidal errors are generally much smaller than other sources of error. However, improvements to tidal performance may be important in improving overall model performance, especially in areas where advection concerns dominate.

Figure 7-1 and Figure 7-2 show the RMSE and mean difference for gages evaluated for each storm. As noted in the previous section, the 1991 Perfect Storm and Hugo results are reported from simulations without advection while the remaining simulations apply advection. Figure 7-3 and Figure 7-4 show the

same data in a pseudo-geographic distribution ordered by NOAA gage number proceeding from Texas gages numbered 87xxxxx to the Maine gages numbered 84xxxxx. No obvious spatial patterns are visible in the geographic distribution of error but the data are very limited. While there is overlap in the sets of gages analyzed for each storm, the areas severely impacted by each storm rarely overlap.

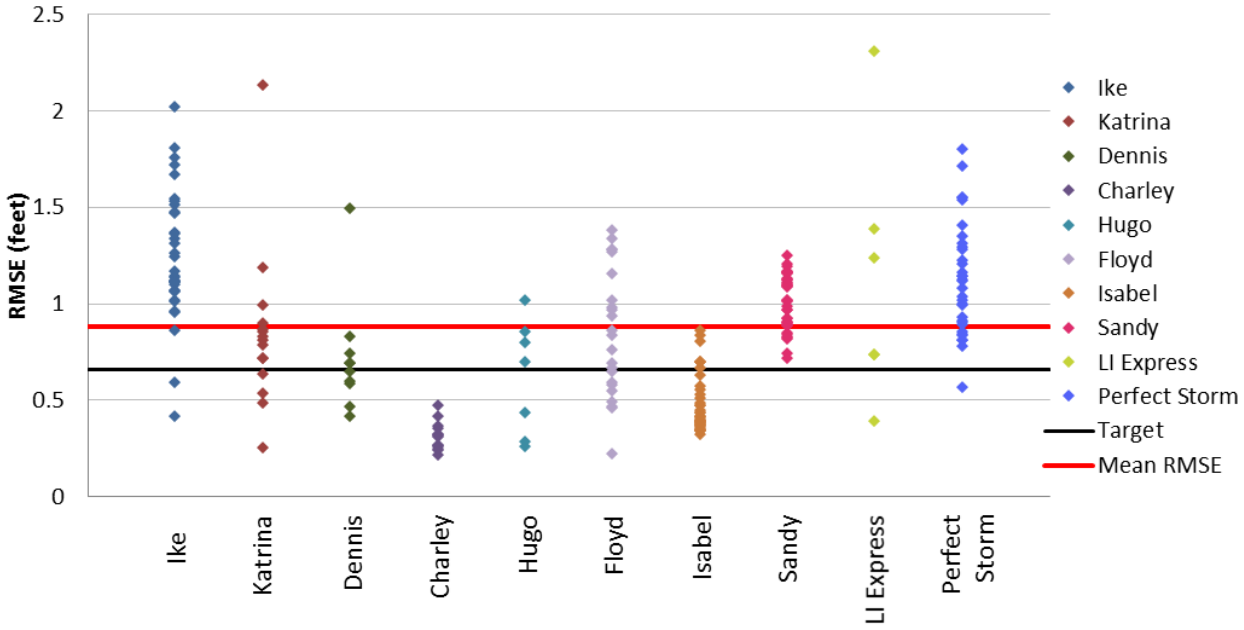

Figure 7-1: NOAA gage time series RMSE for all storms.

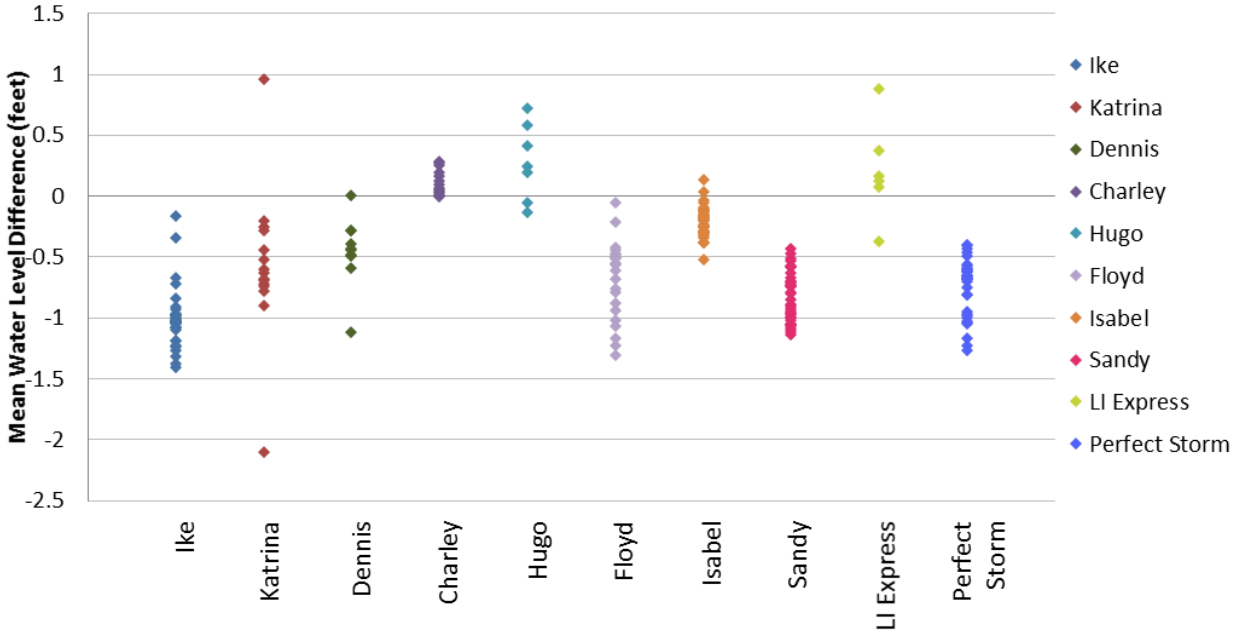

Figure 7-2: NOAA gage mean water level difference for all storms.

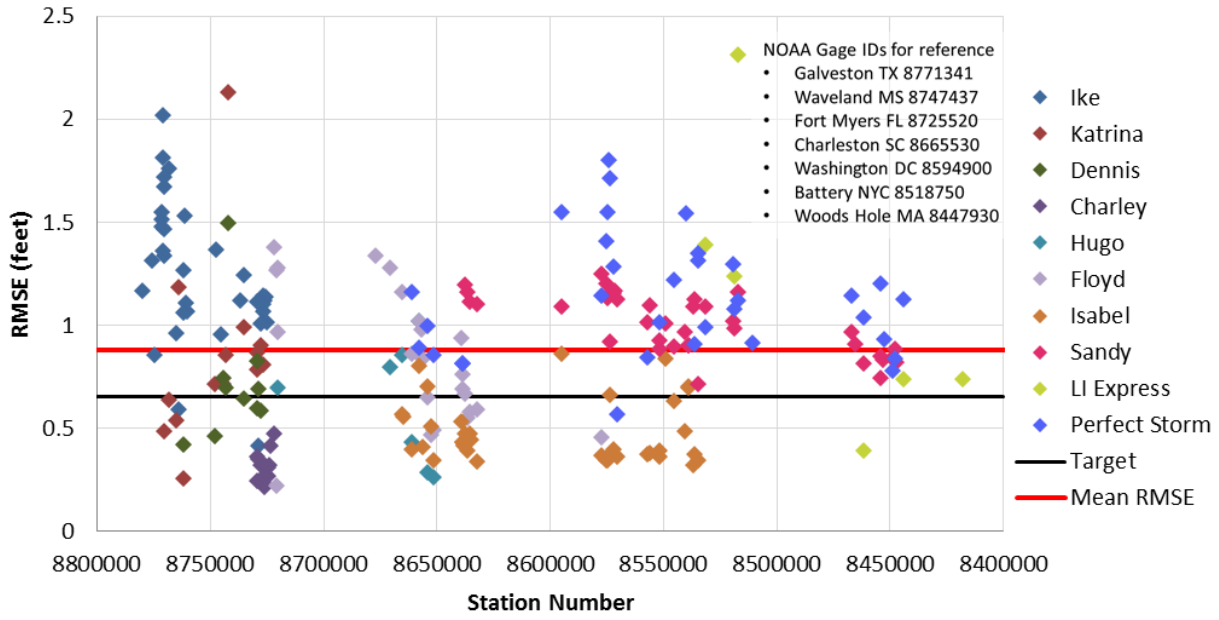

Figure 7-3: Along-shore NOAA gage time series RMSE for all storms.

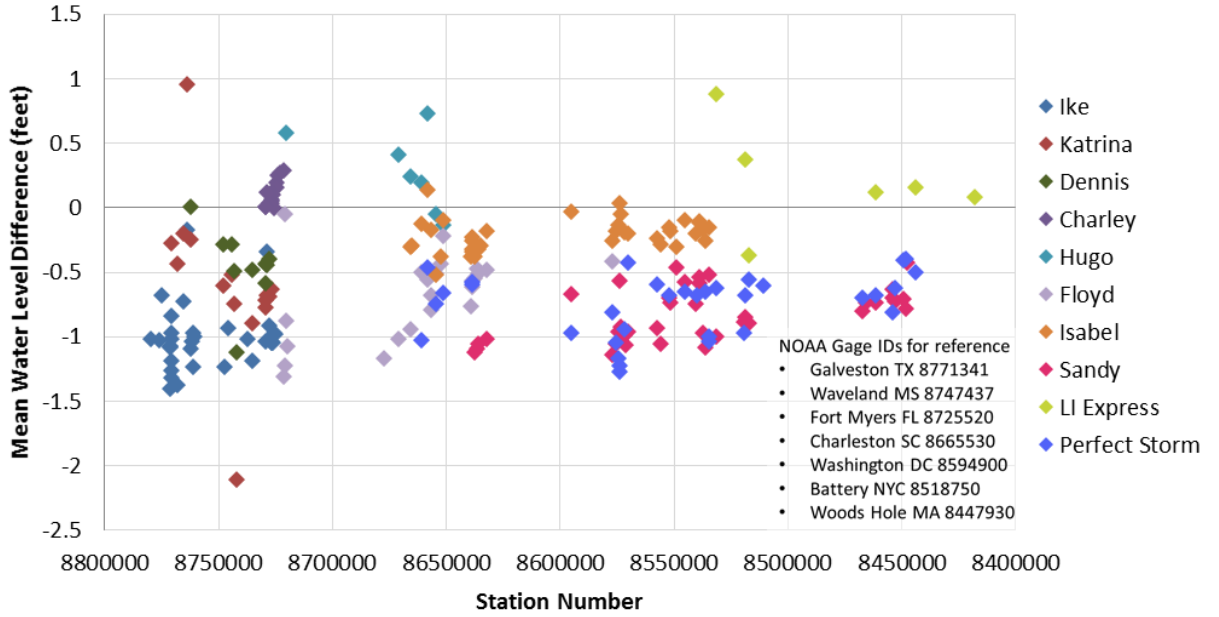

Figure 7-4: Along-shore NOAA gage time series mean difference for all storms.

Peak water levels at NOAA gages and at surveyed HWMs are presented together in Figure 7-5 and Figure 7-6. Of the NOAA gage peak water levels, 90% are within +/-2 feet. As with the simulated time series, there is a low bias overall, similarly affected by the persistent low bias of the mean but also from the lack of wave setup along open coasts. The mean difference in peak water level is -1.1 feet and the mean absolute error is 1.2 feet. These summary values are heavily influenced by large deviations for Ike and the Perfect Storm. Dennis shows some low bias, as well, though not as strong.

Considering all peak water levels, both at NOAA gages and from surveyed HWMs, 90% are within +/-2.5 feet and have (like all the other skill metrics) a low bias overall. For all peaks and HWMs, the mean difference is -0.80 feet and the mean absolute error is 1.3 feet. A combined correlation plot of all peaks and HWMs is shown in Figure 7-7.

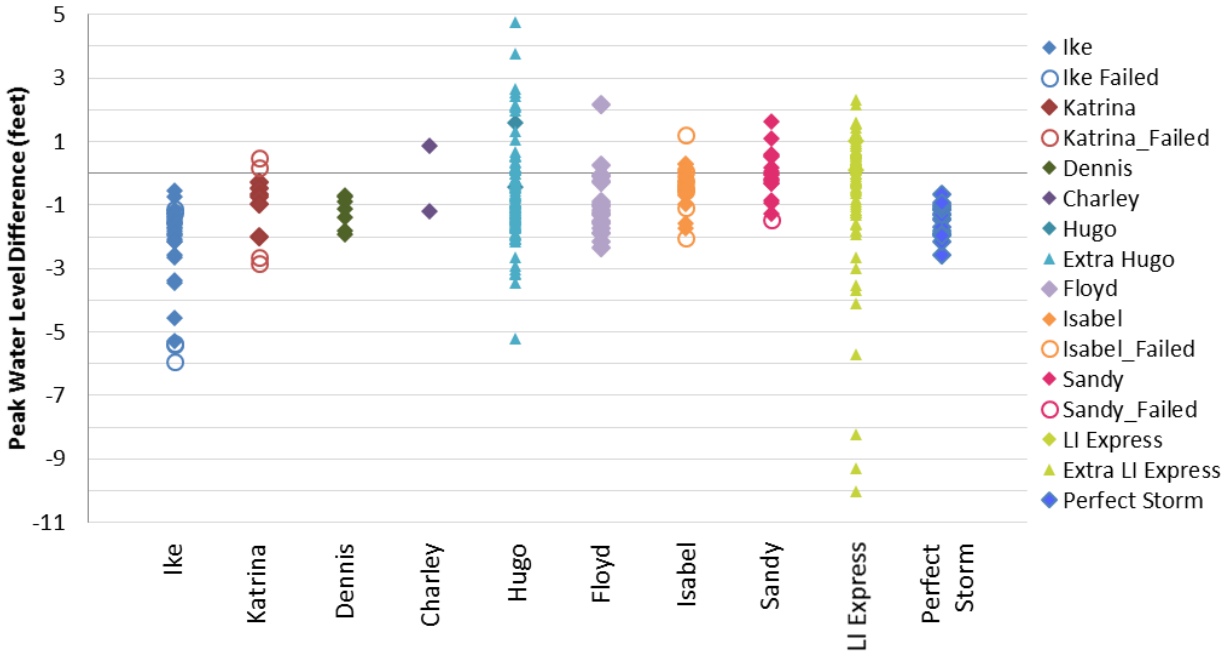

Figure 7-5 Peak water level error and surveyed HWM error for all storms. Data points labeled 'extra' are surveyed HWM datasets for the corresponding events

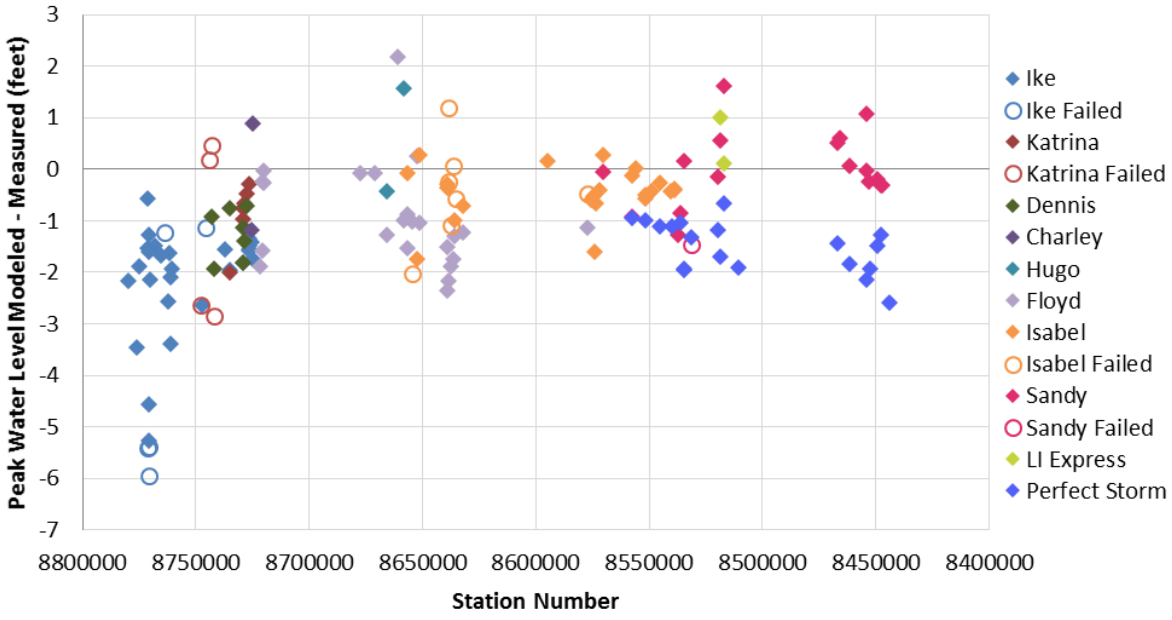

Figure 7-6: Along-shore NOAA gage peak water level error.

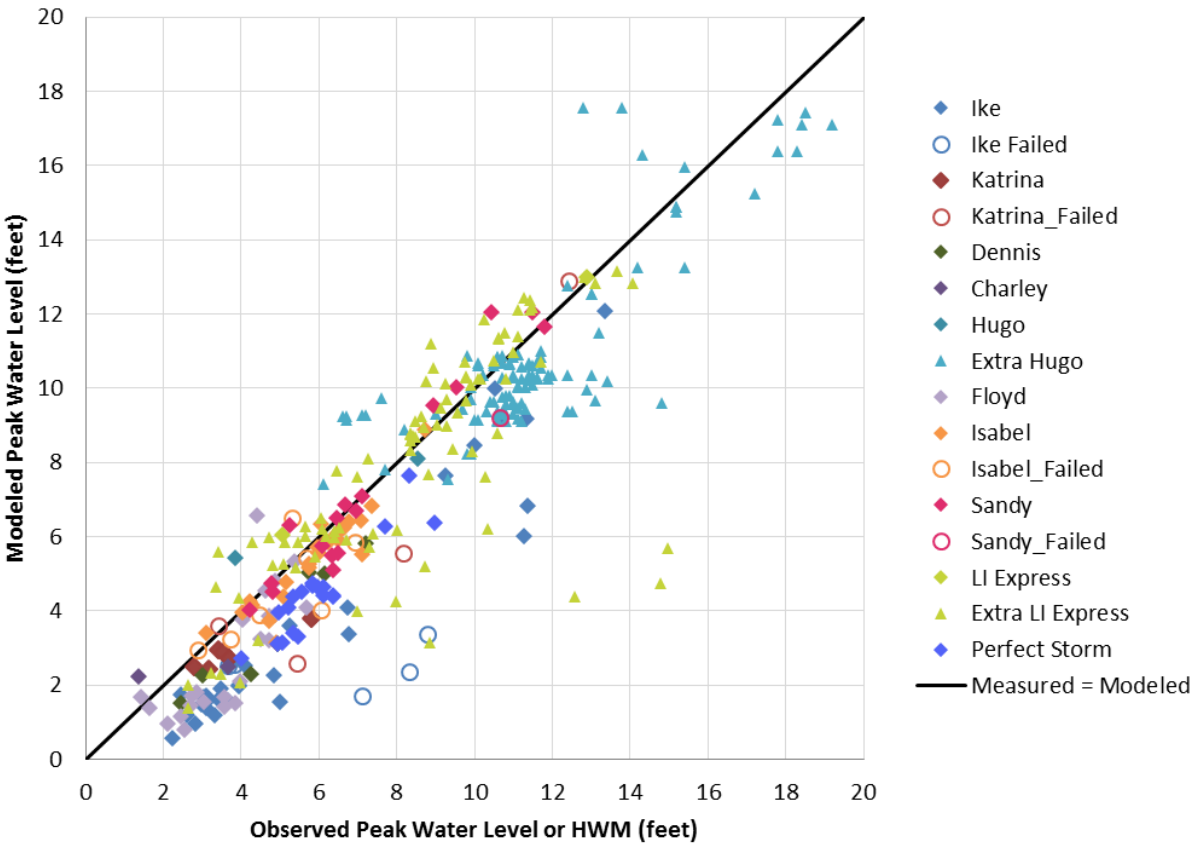

Figure 7-7: Peak water level and surveyed HWM comparison for all storms. Data points labeled 'extra' are surveyed HWM datasets for the corresponding events.

Figure 7-8 shows the sorted RMSE and Figure 7-9 shows sorted peak water level difference for all gages. The curves shows that over 90% of RMSE values are less than 1.5 feet and most are less than 1 foot. The highest RMSEs are from a low-quality dataset for the 1938 storm and Ike, whose forerunner surge was not properly represented by the model. Within the sorted peak differences (Figure 7-9), the low bias is evident with the majority of points on the curve less than zero.

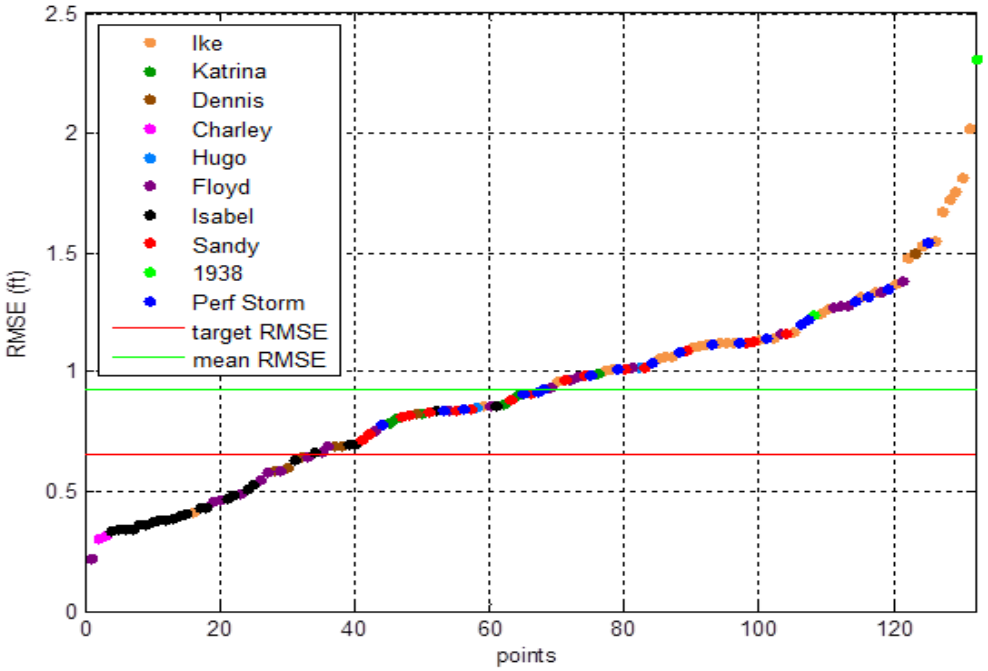

Figure 7-8 Sorted RMSEs from all NOAA gages (excluding gages which failed during the event) across all validation storm simulations. Gages used in multiple storms have multiple points.

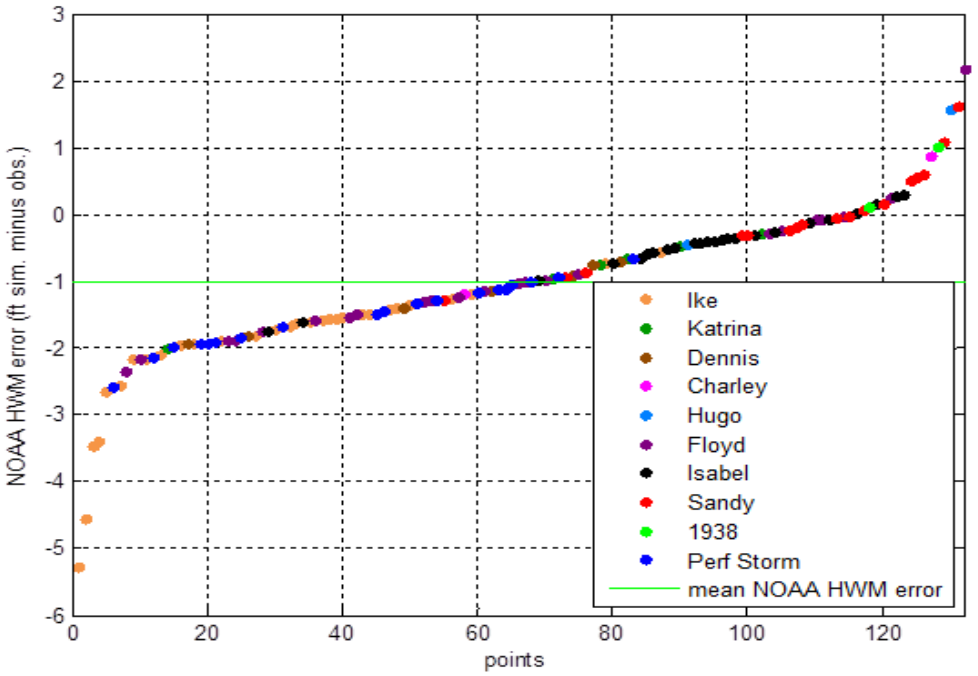

Figure 7-9 Sorted HWM errors from all NOAA gages (excluding gages which failed during the event) across all validation storm simulations. Gages used in multiple storms have multiple points.

8. CONCLUSIONS AND RECOMMENDED NEXT STEPS

The NOMAD mesh and model setup have been put through tidal validation and storm validation, using a suite of 10 test storms. The model was able to meet the 0.2 RMSE metric for most NOAA stations during tidal simulation. However, model accuracy was not sufficient in the Gulf of Maine without including advection terms, which was not possible because the model could not run stably with advection on.

For all but a few of the event simulations, the model has difficulty meeting the 0.2 meter RMSE error metric due to various issues. The principal problems appear to be a lack of mean water level adjustments and wave setup effects. The water level offsets are visible in several time series and are due to longer time-scale changes in water levels, such as seasonal steric and inter-annual variations. The wave setup effects are expected (at least along open coast lines) during storms; however, definitively attributing water level errors to them is difficult. Generally, areas that are exposed to the open ocean, have long fetches, and steeper shorelines will result in higher wave setup.

The testing with a variety of meteorological data sources has clearly demonstrated the wide differences in water levels that can result from uncertainty and error in meteorological forcing. Further validation work should be careful to apply consistent winds and to consider any potential systematic differences between the meteorological data used for validation and that used operationally.

Hurricane Ike suffers from a systematic low bias due to an inability to properly represent the forerunner surge evident in measured data. Other modeling studies have successfully represented the forerunner surge by altering the bottom friction across the Louisiana-Texas shelf as discussed in Section 6.2. The justification for the change is the fine grain mud that typifies the shelf sediments. These studies have also increased the wind forcing scaling factor, and our modeling results show that this increase in wind strength drastically changes results. To properly model this storm, testing would be needed to evaluate how to best-emulate the long wave forerunner surge. Modulating bottom friction values along the shelves of the entire US coastline using available data, e.g., the usSEABED data (Buczkowski et al. 2006), may be of value. If bottom friction is modified, care should be taken to run other storms in the same region (possibly Rita, but preferably another storm with a smaller radius) and validate that any changes made to improve performance during Ike are applicable to other major events in the area. The low bias present in all gages across the Gulf during the Ike simulations is partially due to mean water level differences. But the difference in peak surges should be evaluated to see whether, for instance, a significant long-period signal is present and affecting results, or if broader bottom friction modifications are warranted, or if the far-field winds are just not well-represented. Water level data from University of Notre Dame[12] and the Texas Coastal Ocean Observation Network (TCOON)[13] would also prove useful for verification, as most of the NOAA gages failed during the storm.

[12] Andrew Kennedy at University of Notre Dame has investigated the cause of the forerunner surge in Kennedy et al. (2011).

[13] Further background information regarding TCOON, a research institute of the Texas A&M University Corpus Christi funded by a consortium of several state and federal entities, may be found here: http://www.cbi.tamucc.edu/TCOON/. Data is provided on-line at http://www.tcoon.org/.

The model is unable to run with advection on for long periods without becoming unstable—fatal instabilities were seen to form between 3 – 15 weeks after simulation cold start. The instabilities typically become apparent near the offshore boundary (far from the US coastline), either in the southeast corner of the mesh or around the same latitude as Bermuda. Due to the short length of the hindcast simulations, nine out of ten were successfully executed in advection-on mode without these instabilities forming; the 1991 Perfect Storm was the only exception[14]. Lack of accounting for advection was found to significantly reduce accuracy of simulated tides in the Gulf of Maine, and to a lesser degree in Long Island Sound and the South Atlantic Bight. Advection was also found to affect surge differently for different storms. In most cases, it changed peak surge by less than 0.5 feet and less than 5% of the surge. Hugo, Katrina, and Ike had isolated areas where the difference in peak water level between advection and non-advection simulations reached 1 foot. Hurricanes Dennis and Charley showed advection effects reaching 10% or more of the total surge.

The 1938 Long Island Express is the outstanding exception, with advection causing widespread and drastic changes to the peak surge, with a maximum increase in surge of 4.8 feet in Providence, RI. Simulating the 1938 event with advection terms included increased the peak surge by 4 feet (25% to 30%) in two areas and by over 2 feet for most of the southern New England coastline and parts of Long Island. It also caused a decrease in peak surge of up to 1 foot in several areas in New York and New Jersey. The spatial extent of the changes also differentiates this event: peak surge increased by at least 2 feet across 100 km of the CT-RI-MA coastline and extended 40 km offshore; peak surge increased by at least 1 foot across 200 km of the NY-CT-RI-MA coastline and extended 70 km offshore. Other examples of the changes induced by advection include a 6-km stretch of Long Island's southeast coast where the difference between advection-on and advection-off peak surges changes from +2.0 to -0.5 ft, and a change in peak surge of at least 25% for all of RI's Atlantic coast. A common thread between the storms most affected by advection is that they were all relatively fast moving, with the 1938 storm being by far the fastest of any storm modeled at 40 to 50 mph. Also significant is that the 1938 storm impacted the coastline where advection had the strongest effect on tidal performance of the model.

The advection issue is challenging both because modeling demonstrates how difficult it is to predict whether it is important and because identifying the cause(s) of the pervasive instabilities seen during longer simulations has proven elusive. The instabilities in the deep ocean east of Bermuda are often present (though small) for weeks, from an early stage in the simulation. Logically, there should not be a reason for the instability to form locally; the boundary forcing is smooth and the bathymetry is several thousand meters deep. Testing of a highly smoothed mesh in this area failed to reduce the tendency toward instability. This indicates that the instabilities may begin elsewhere, and become trapped along the forced boundary. Creating a half-speed (and perhaps quarter-speed) version of the 1938 storm and running it with and without advection could provide evidence of whether the forward speed is the root cause of advection's major role.[15] Next, testing the advection state nodal attribute to observe whether disabling advection in the deep ocean can prevent the instabilities (without affecting tidal accuracy) could

[14] As previously noted, the advection-on simulation for Hugo also failed, however, the instabilities were the result of strong, local wind forcing in the Antilles rather than the long-run instabilities observed discussed in this paragraph. Hot-starting the Hugo simulation with the cyclone beyond the Antilles allowed the advection-on simulation to run to completion.

[15] Note that changing forward speed does not affect the magnitude nor direction of wind stress to the model.

be carried out. If this cannot resolve the instability, spatially variable eddy viscosity is another potential solution. However, it is most likely that it is necessary to manually identify the areas that are becoming unstable and attempt to fix them by adjusting the grid.

Creation of mass in the model domain has been shown (see Appendix D) to be a pervasive issue endemic to ADCIRC's wetting and drying algorithm that cannot be readily resolved and which may affect model accuracy in some areas. Relatively few major storms have hit the areas most affected by this artificial phenomenon, i.e., the extensive tidal marshes of South Carolina, Georgia, and North Florida. Hugo was the closest modeled storm to these areas. Results behind Sullivan's island near Charleston, South Carolina during Hugo seem to indicate water levels were abnormally higher than those found in the FEMA South Carolina study in this area, which could be attributed to this issue. However, the differences between the studies (e.g., FEMA used ADCIRC+SWAN, steric corrections were not applied for NOMAD simulations, mesh resolutions are significantly different, wind scaling is not treated equally, etc.) makes a root-cause analysis very difficult. It is not clear whether this might significantly affects model results, however given that it can substantially increase water elevations, it is possible. The added mass could boost surges, yet the presence of water higher than the incoming surge might also induce a reversal of flow that could retard or even reduce the peak surge. Testing with a hypothetical storm while varying the local ground elevation to try to prevent the artificial water retention is one option for studying this issue. However, since the topography would be changed, some differences in results should be expected.

NOMAD model results within Pamlico Sound from Floyd and Isabel should be inspected closely to evaluate model performance. The only gage data available during Isabel (Oregon Inlet Marina) indicated this area might have some accuracy issues, and CSDL's modeling experience in this area should help in analyses.

A review of differences between EC2012 and EC2001 bathymetry shows that several areas outside of the immediate US coastline have had significant changes. The most notable instances were in the Gulf of Maine (especially near the Bay of Fundy) and at Lake Maracaibo in Venezuela. Based on these differences, a recommended improvement for the NOMAD mesh is a general bathymetric elevation update using a current version of the East Coast tidal database grid (e.g., EC2012) for areas beyond 50 to150 kilometers from the coast.

The poor model skill for the 1991 Perfect Storm was similar to that seen in the FEMA Region II study meaning that improving model skill using the FEMA wind fields may not be possible. Since this is the only full extratropical event and the only event to impact north of Cape Cod, this limits the conclusions that the validation study can make about extratropical storms and about any geographies in the northern-most US East Coast. Additional validation of other extratropical storms in the region (and throughout the model domain) would be beneficial, especially for future extratropical implementations. Gathering additional meteorological data for these additional storms would be a valuable next step.

The combination of hurricane Charley's unique characteristics as a small, fast moving event and the presence of low barrier islands in the area of landfall together challenge multiple aspects of the modelling system such as mesh resolution, meteorological resolution, model physics and numerics. This means that issues such as phase lag in the surge signal can lead to large errors in the amplitude. Mesh resolution may

also play a role, as smaller topographic features are lost and slopes distorted. Narrowly overtopped barrier islands may not be well-modeled because ADCIRC does not simulate super-critical flow, which has an uncertain effect on the overall water level prediction. Lastly, Charley was modeled with five-minute meteorological data instead of the normal 15-minute data, yet aliasing is still evident in the wind and pressure field results from the spatial resolution.

The SURA-IOOS Ultralite mesh used for Louisiana, Mississippi, and a small portion of Texas provided a very efficient method for incorporating a characterization of the complex levee and river systems throughout that region into the NOMAD mesh. However, this mesh is less resolved in many areas than the rest of the NOMAD mesh and overland features such as roadway embankments are frequently omitted, causing changes to surge extent and shape that may be misleading. Improvement of this section of the mesh is encouraged due to these deficiencies and the tendency of this area to be struck by major storms.

The South Carolina-Georgia area relied on lower-quality topography, as lidar was generally un-available. This, and the exceptional complexity of the tidal creeks throughout the region, made high-quality meshing difficult. Blanton et al. (2002) demonstrated that accurate modeling of tides in the region was difficult to achieve without representing these finer scale features. Acquisition and incorporation of lidar-based topobathymetry and development of higher resolution representation of the tidal creeks would be expected to improved model representation of water levels in this area.

All simulations reported for this study were carried out using the implicit mode of ADCIRC's time stepping algorithm. Preliminary tests of both lumped explicit mode showed that it reduced run time to little as 60% of the implicit run times. However, the explicit mode was more prone to instabilities and oscillations in the solution. Additional runs are recommended to verify the stability of the lumped explicit mode before considering it operationally with HSSOFS.

9. **ACKNOWLEDGMENTS**

This project was funded under Public Law 113-2, Sandy Supplemental.

We acknowledge the contributions from FEMA Headquarters, FEMA Regions II, III, IV, and VI, and the U.S. Army Corps of Engineers, particularly Larry Voice, Christina Lindemer, Tucker Mahoney, Robin Danforth, and Jay Ratcliff, for providing access to wind forcing data and various datasets used for verification.

Staff from the Center for Operational Oceanographic Products and Services (CO-OPS) provided key assistance with the NOS skill assessment software.

Chris Szpilka provided access to the EC2012 mesh and all members of the ADCIRC community contributed significantly to discussions related to development and execution of the HSSOFS model.

10. **REFERENCES**

Blanton, J. O., Lin, G., and Elston, S. A. (2002). "Tidal current asymmetry in shallow estuaries and tidal creeks." *Continental Shelf Research*, Proceedings from the Tenth Biennial Conference on the Physics of Estuaries and Coastal Seas, 22(11–13), 1731–1743.

Buczkowski, B. J., Reid, J. A., Jenkins, C. J., Reid, J. M., Williams, S. J., and Flocks, J. G. (2006). *usSEABED: Gulf of Mexico and Caribbean (Puerto Rico and U.S. Virgin Islands) offshore surficial sediment data release*. Data Series, USGS Numbered Series, U.S. Geological Survey, Reston, VA, 50.

Dietrich, J. C., Kolar, R. L., and Luettich, R. A., Jr. (2004). "Assessment of ADCIRC's wetting and drying algorithm." *Developments in Water Science*, Computational Methods in Water Resources: Volume 2 Proceedings of the XVth International Conference on Computational Methods in Water Resources, C. T. M. and G. F. Pinder, ed., Elsevier, 1767–1778.

Dietrich, J. C., Kolar, R. L., and Westerink, J. J. (2005). "Refinements in Continuous Galerkin Wetting and Drying Algorithms." *Estuarine and Coastal Modeling*, American Society of Civil Engineers, 637–656.

Egbert, G. D., and Erofeeva, S. Y. (2002). "Efficient Inverse Modeling of Barotropic Ocean Tides." *Journal of Atmospheric and Oceanic Technology*, 19(2), 183–204.

FEMA. (2014). "Multi-hazard Loss Estimation Methodology: Hurricane Model. Hazus(r)-MH MR5 Technical Manual." Department of Homeland Security, Federal Emergency Management Agency, Mitigation Division, Washington D.C.

Fleming, J. G., and Jelley, B. (2014). "Best practices with H*Wind and ADCIRC." (Email Communication)

Funakoshi, Y., Feyen, J. C., Aikman III, F., van der Westhuysen, A., and Tolman, H. (2013). *The Extratropical Surge and Tide Operational Forecast System (ESTOFS) Atlantic Implementation and Skill Assessment*. NOAA Technical Report NOS CS 32, 147 pp.

Gonzalez-Lopez, J. (2014). "Tides and Resonant Features in the Caribbean Sea and Gulf of Mexico." 2014 ADCIRC Workshop. Infinity Science Center, Mississippi, USA.

Hess, K. W., Gross, T. F., Schmalz, R. A., Kelley, J. G. W., Aikman III, F., Wei, E., and Vincent, M. S. (2003). *NOS standards for evaluating operational nowcast and forecast hydrodynamic model systems*. U.S. Dept. of Commerce, National Oceanic and Atmospheric Administration, National Ocean Service, Office of Coast Survey, Coast Survey Development Laboratory, [Silver Spring, Md.].

Hess, K. W., Schmalz, R., Zervas, C., and Collier, W. (2004). *Tidal Constituent And Residual Interpolation (TCARI) a new method for the tidal correction of bathymetric data*. U.S. Dept. of Commerce, National Oceanic and Atmospheric Administration, National Ocean Service, Office of Coast Survey, Coast Survey Development Laboratory, [Silver Spring, Md.].

Kennedy, A. B., Gravois, U., Zachry, B. C., Westerink, J. J., Hope, M. E., Dietrich, J. C., Powell, M. D., Cox, A. T., Luettich, R. A., Jr., and Dean, R. G. (2011). "Origin of the Hurricane Ike forerunner surge." *Geophysical Research Letters*, 38(8), L08608.

Luettich, R. A., Jr., and Westerink, J. J. (2004). *Formulation and numerical implementation of the 2D/3D ADCIRC finite element model version 44. XX*. Texas Water Development Board, Morehead City, N.C.

Luettich, R. A., Jr., Westerink, J. J., and Scheffner, N. W. (1992). *ADCIRC: An Advanced Three-Dimensional Circulation Model for Shelves, Coasts, and Estuaries. Report 1. Theory and Methodology of ADCIRC-2DDI and ADCIRC-3DL*. DTIC Document.

Powell, M. D. (2012). "Note on using H*Wind fields for storm surge and wave modeling." <http://www.hwind.co/legacy_data/readme.html> (Mar. 30, 2015).

Vickery, P., Lin, J., Skerlj, P., Twisdale, L., and Huang, K. (2006). "HAZUS-MH Hurricane Model Methodology. I: Hurricane Hazard, Terrain, and Wind Load Modeling." *Natural Hazards Review*, 7(2), 82–93.

Zhang, A., Hess, K. W., and Aikman III, F. (2010). "User-based skill assessment techniques for operational hydrodynamic forecast systems." *Journal of Operational Oceanography*, 3(2), 11–24.

Zhang, A., Hess, K. W., Wei, E., and Myers, E. (2006). *Implementation of Model Skill Assessment Software for Water Level and Current in Tidal Regions*. NOAA Technical Report NOS CS 24, 61 pp.

11. **APPENDIX A – MODEL DOMAIN DEVELOPMENT**

In preparation of the mesh development for the Atlantic and Gulf of Mexico storm surge study, the Riverside/AECOM technical team prepared a mesh boundary for the Advanced Circulation (ADCIRC) storm surge model. Based on comments from NOAA Coast Survey Development Laboratory (CSDL) the boundary was been revised from the preliminary mesh boundary (submitted to CSDL on November 19, 2013) to extend farther inland to include major population centers. Various additional small adjustments to the interior boundary line were made during the development of the mesh. The final mesh outline highlighting deviations from the preliminary mesh are shown in Figure 11-1.

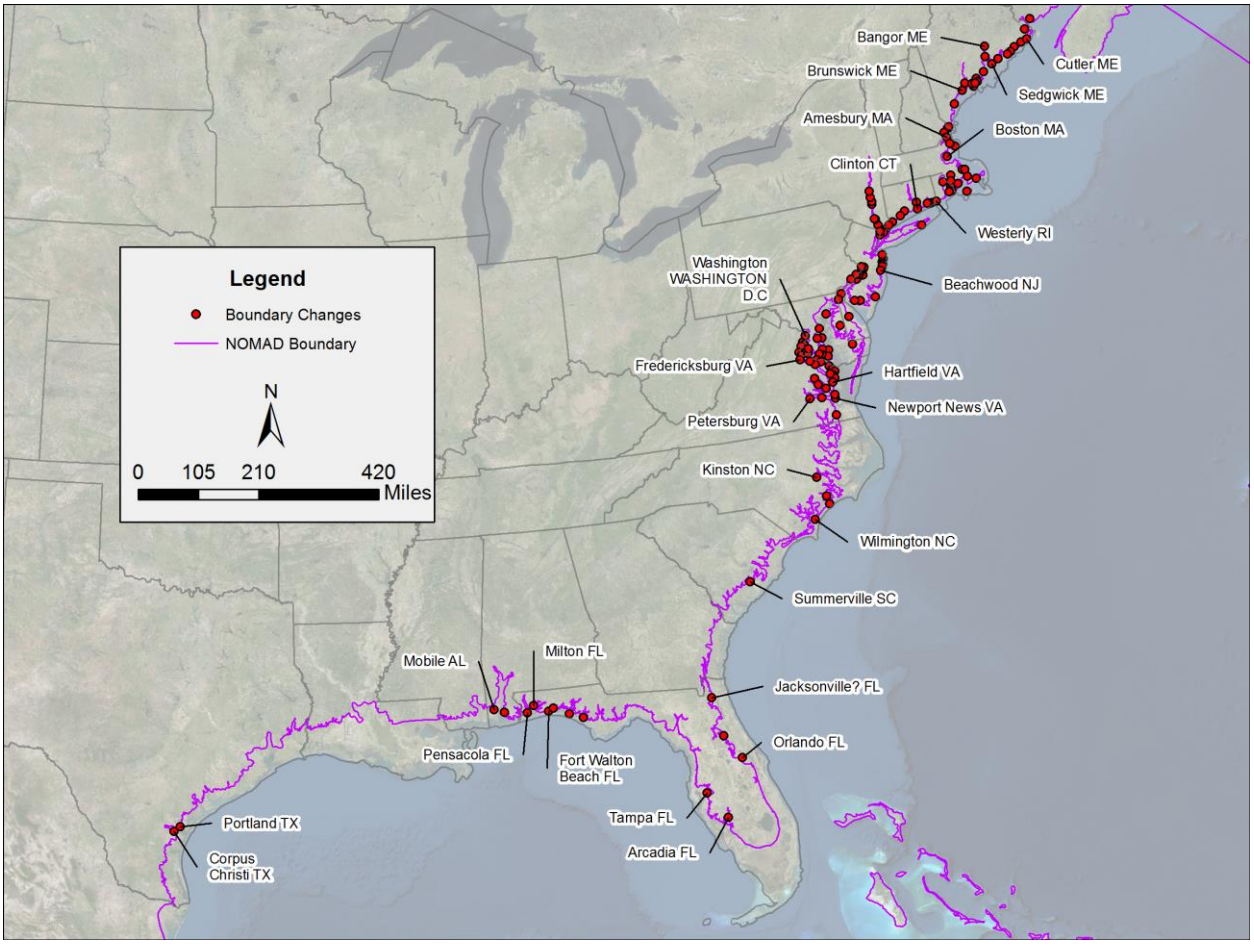

Figure 11-1: Final NOMAD Mesh boundary and locations where modifications were made from preliminary versions.

11.1 ADCIRC Mesh Boundary Data Sources

The following table gives data sources that were reviewed to develop the boundary under the stipulated guidelines. To develop an inland boundary for the ADCIRC mesh with an overland resolution along the entire US Atlantic and Gulf coasts, the project team began by reviewing the following data:

Dataset	Source
10-meter, 7-meter, and 5-meter contours derived from U.S. Geological Survey (USGS) National Elevation Dataset	National Elevation Dataset accessed November 2013, http://ned.usgs.gov/
ec2012_v1b_chk_021513_fixed.grd ADCIRC mesh (henceforth, "EC2012 Mesh")	Mesh provided by Jesse Feyen, CSDL, November 2013
GM_LA_TX_v3_chk.grd ADCIRC mesh from SURA-IOOS Round 1 testbed project (henceforth, "Gulf Mesh")	Mesh provided by Jesse Feyen, CSDL, November 2013
Recent "major" storm landfall locations	Blake, Eric. S., Landsea, Christopher W., Gibney, Ethan J. "The Deadliest, Costliest, and Most Intense United States Tropical Cyclones from 1851 to 2010 (and Other Frequently Requested Hurricane Facts)" NOAA Technical Memorandum NWS NHC-6. August 2011, http://www.nhc.noaa.gov/pdf/nws-nhc-6.pdf; See also, Gray, William, "United States Landfalling Hurricane Probability Project." Accessed November 2013, http://www.e-transit.org/hurricane/regions_map.bmp; and National Oceanic and Atmospheric Administration Historical Hurricane Tracks accessed November 2013, http://www.csc.noaa.gov/hurricanes/index.html.
NWS riverine planned and active unsteady Hydrologic Engineering Centers River Analysis System (HEC-RAS) model domains	A Report on NWS River Hydraulic Modeling for Both Inland and Coastal Applications accessed December 2013, http://www.nws.noaa.gov/oh/hrl/hsmb/hydraulics/documents/fldwav_to_hecras/HEC-RAS_and_REO_gate_distribute2.pdf.
NWS forecast points and NOAA Center for Operational Oceanographic Products and Services (CO-OPS) tidal observation stations	CO-OPS Active Water Level and Meteorological stations accessed November 2013, http://tidesandcurrents.noaa.gov/googleearth.html.
FEMA 0.2%-annual-chance flood elevations (i.e., 500-year) data	FEMA Map Service Center National Flood Hazard Layer. Accessed November 2013, https://msc.fema.gov/
U.S. Census population data	ESRI StreetMaps 9.3 2007 U.S. Census data (http://downloads2.esri.com/support/whitepapers/ao_/ESRIData&Maps9.3.pdf)

Based on those data, the proposed mesh boundary was developed following these general guidelines:

- At most locations, the mesh extends inland to a smoothed version of the 10-meter topographic contour.
- In some areas with major population centers, the mesh was extended inland beyond the 10-meter topographic contour to include the entire developed area in the final mesh.
- Except for significant rivers to be considered for coupled modeling, the boundary extends into coastal river inlets only to the point where the channel width decreases below approximately 1,500 meters.
- In some areas where the 10-meter contour was significantly inland of the FEMA 0.2-percent-annual-chance coastal flood elevation, the amount of modeled inland area was reduced.
- The SURA-IOOS mesh for portions of Texas, Louisiana, and Mississippi provided the mesh boundary in those areas.
- Portions of the Everglades, though well below the 10-meter contour, were specifically excluded from the mesh because of low population, complex flow dynamics, and the presence of levees.
- Non-US overland areas are excluded from the mesh. Coastal boundaries outside of the United States are from the EC2012 Mesh boundary.
- All of the ESTOFS-modeled area is included in the new mesh.

11.2 ADCIRC Mesh Boundary Development and Modification

For the areas outside the United States, the project team used the EC2012 Mesh coastal boundary (including Caribbean island boundaries) shown in Figure 11-2. The EC2012 mesh also provided the open ocean boundary.

Figure 11-2: EC2012 Mesh boundary outside the United States (green).

The team reviewed the Gulf Mesh and found the resolution matched the specifications from CSDL (i.e., 250 to 500 meter minimum resolution and extension to the 10 meter contour) for the coastal area considered. The Gulf Mesh includes an extensive interior levee system that would be time-consuming to replicate, so the project team proposes incorporating sections of this mesh into the final mesh for this project. As such, the boundary from the Gulf Mesh was used in the development of the final mesh boundary for Louisiana and Mississippi. The Gulf Mesh boundary generally follows the 10 meter contour; however, in western Louisiana the mesh generally extends beyond the 10 meter contour to provide a smoother boundary. This area is shown in Figure 11-3.

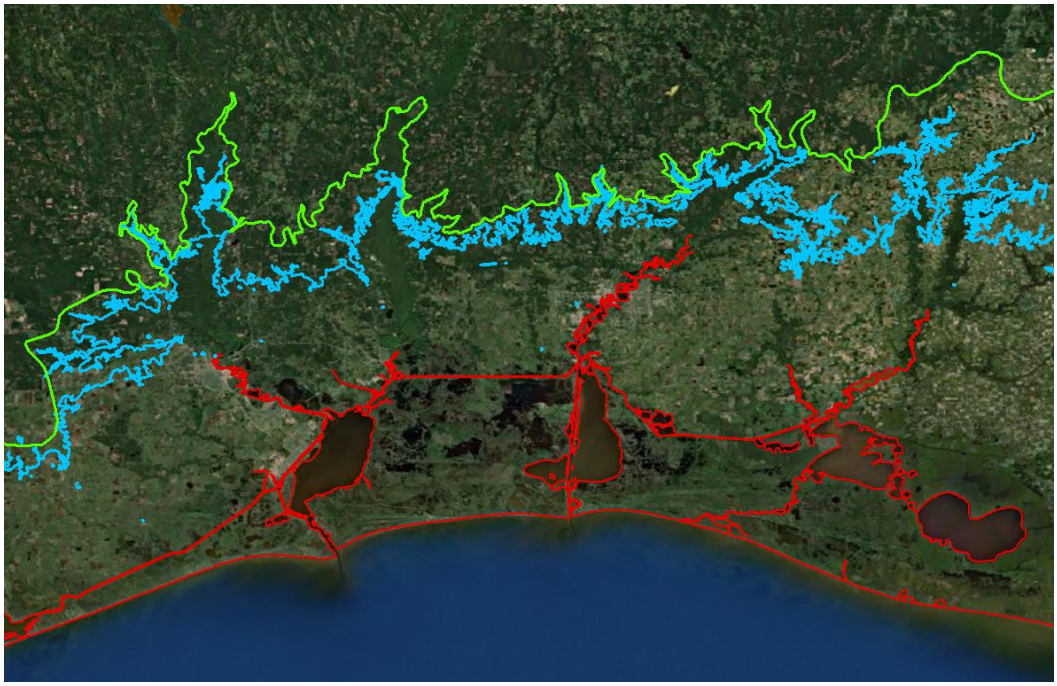

Figure 11-3: Final mesh boundary (green), approximate 10 meter (blue), and EC2012 Mesh shoreline (red) in western Louisiana.

Outside of Louisiana and Mississippi the team began to build the final mesh boundary by extracting the 10 meter contour from the USGS NED and eliminating extraneous lines to create a single, continuous 10 meter contour. This contour was smoothed and simplified using ArcGIS 10 toolsets.

The next step in the boundary development process was to compare the proposed model boundary to additional data sources to determine where it could be revised to a lower contour line to decrease the overall mesh size while maintaining the mesh's ability to capture all major surge events. The team reviewed the NWS lists of recent major hurricane landfall locations and reviewed hurricane track data through the Coastal Service Center's (CSC's) Historical Hurricane Tracks Web viewer.[16] The CSC's Web viewer displays the number of strikes per county from 1900 to the present. Areas with fewer landfalling hurricanes are shown in Figure 11-4 in the lightest pink. These areas are the Big Bend region on the Gulf coast of Florida (between Wakulla County, Florida in the north to Citrus County, Florida in the south), along the Atlantic coast in Georgia, in the Chesapeake Bay region, and along the Atlantic coast in Maine.

[16] http://www.csc.noaa.gov/hurricanes/index.html. Accessed November 19, 2013

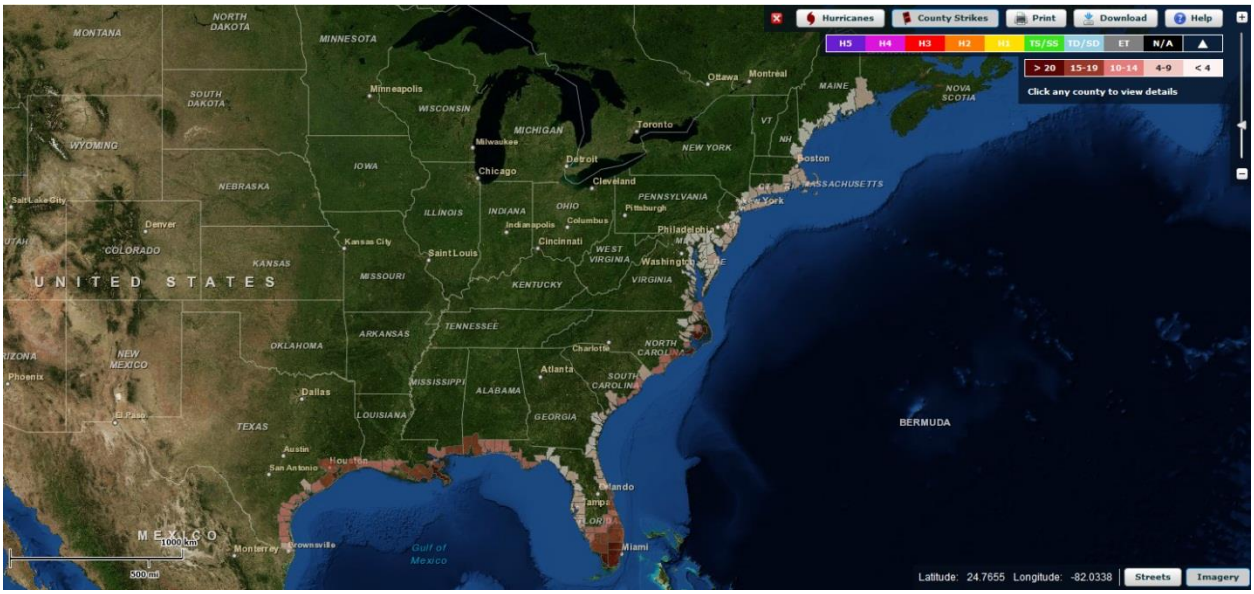

Figure 11-4: Number of hurricane strikes per county from NOAA CSC Historical Hurricane Tracks Web site for the US shoreline along the Gulf of Mexico and Atlantic Ocean.

In the Big Bend, Florida area, the population density is low and the FEMA 0.2%-annual-chance coastal flood elevations are between 4.5 and 6.5 meters. Although this area has a coarser resolution than other areas in the mesh as there is a lower hurricane risk and a low population the 10 meter contour was still used as the boundary. This area is shown in Figure 11-5.

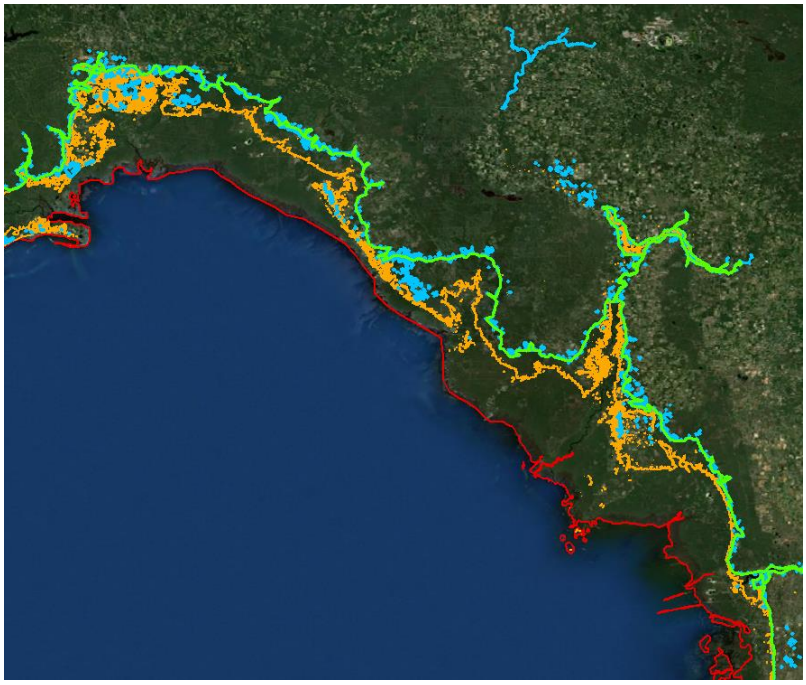

Figure 11-5: Final mesh boundary (green), approximate 10 meter contour (blue), approximate 7 meter contour (orange), and EC2012 Mesh shoreline (red) in Big Bend, Florida region.

In Georgia, the FEMA 0.2-percent-annual-chance coastal flood elevations are between 4 and 5 meters. The 6 meter and 7 meter contours extend inland to nearly the point of the 10 meter contour, so the 10 meter contour was followed closely in this area. This area is shown in Figure 11-6.

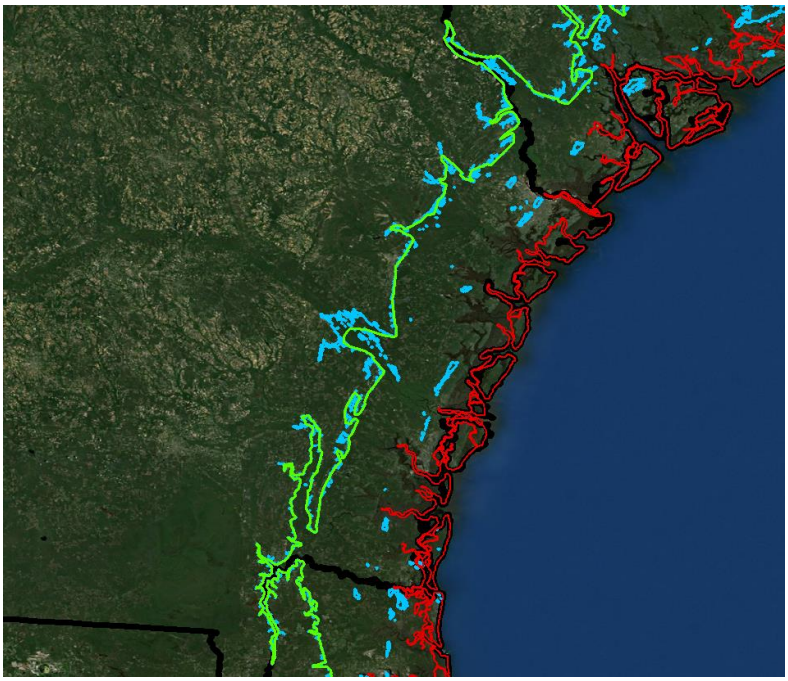

Figure 11-6: Final mesh boundary (green), approximate 10 meter contour (blue), EC2012 Mesh shoreline (red), and State boundaries (black) along the Georgia coast.

Because of Hurricane Isabel and a strategic interest in the Washington, D.C. region, the boundary was extended to the 10 meter contour, and along the Potomac River it was smoothed to include some areas above this contour, as shown in Figure 11-7. In other areas throughout the Chesapeake Bay region, because of the lower 0.2-percent-annual-chance flood elevations (between about 1.25 and 3.5 meters), smaller channels were trimmed or eliminated for a smoother boundary line.

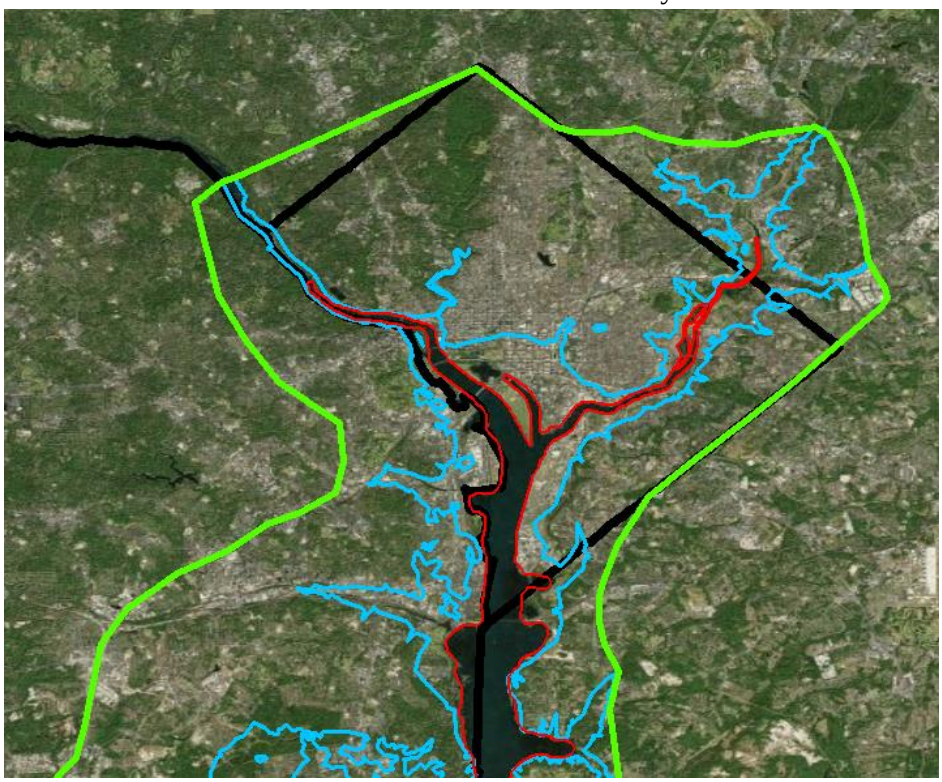

Figure 11-7: Final mesh boundary (green), approximate 10 meter contour (blue), EC2012 mesh shoreline (red), and State boundaries (black) in Washington, D.C. area.

Based on comments on the preliminary mesh boundary, the final boundary was extended farther inland in some locations to include more high-density population areas. In Figure 11-8, the preliminary mesh boundary is shown as a dark black line, and the revised, final mesh boundary is in green. Population data is displayed with high-density areas shown in orange and red. This demonstrates how the final boundary was revised from the preliminary boundary to include high-population areas inside the mesh boundary.

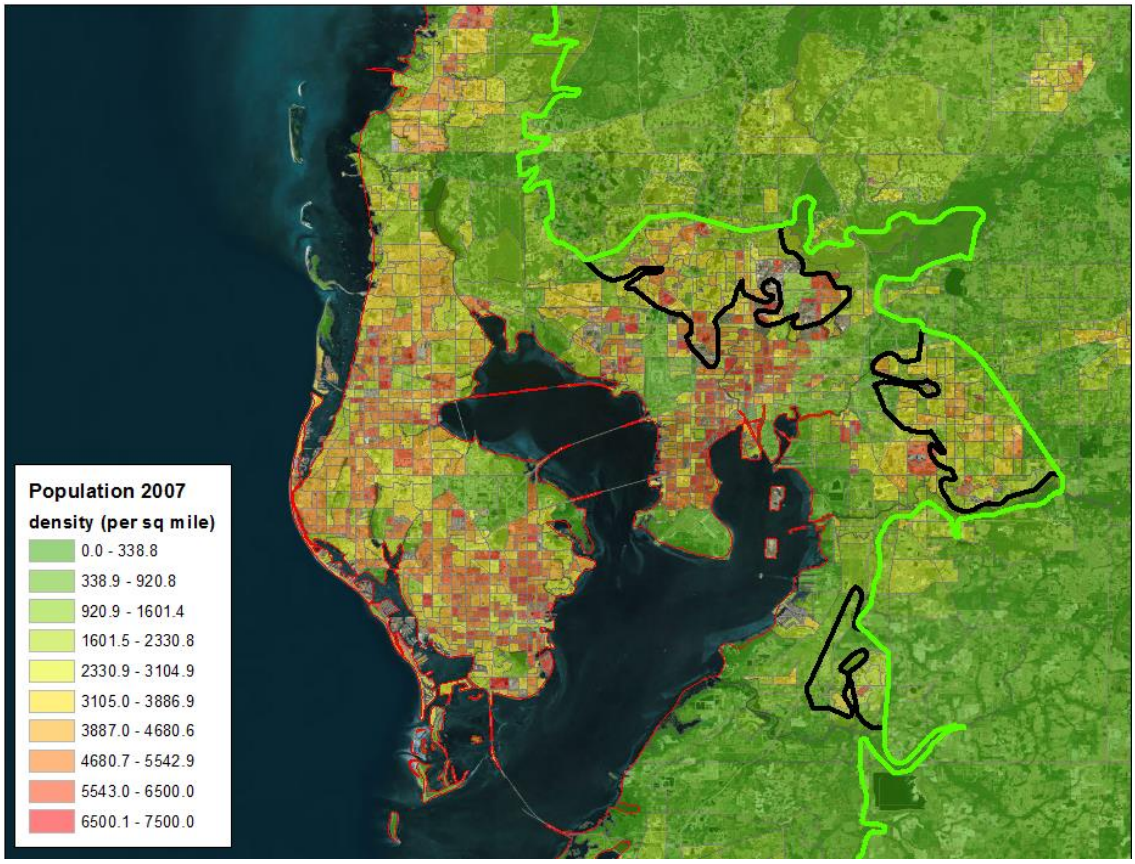

Figure 11-8: Final mesh boundary (green), preliminary mesh boundary (black), and population density around Tampa Bay, Florida.

Along the Maine coastline, the terrain is steep, and the 10 meter contour is relatively close to the shoreline. The boundary was maintained close to the 10 meter contour with some smoothing. A zoomed view of the Maine/New Hampshire border is shown in Figure 11-9.

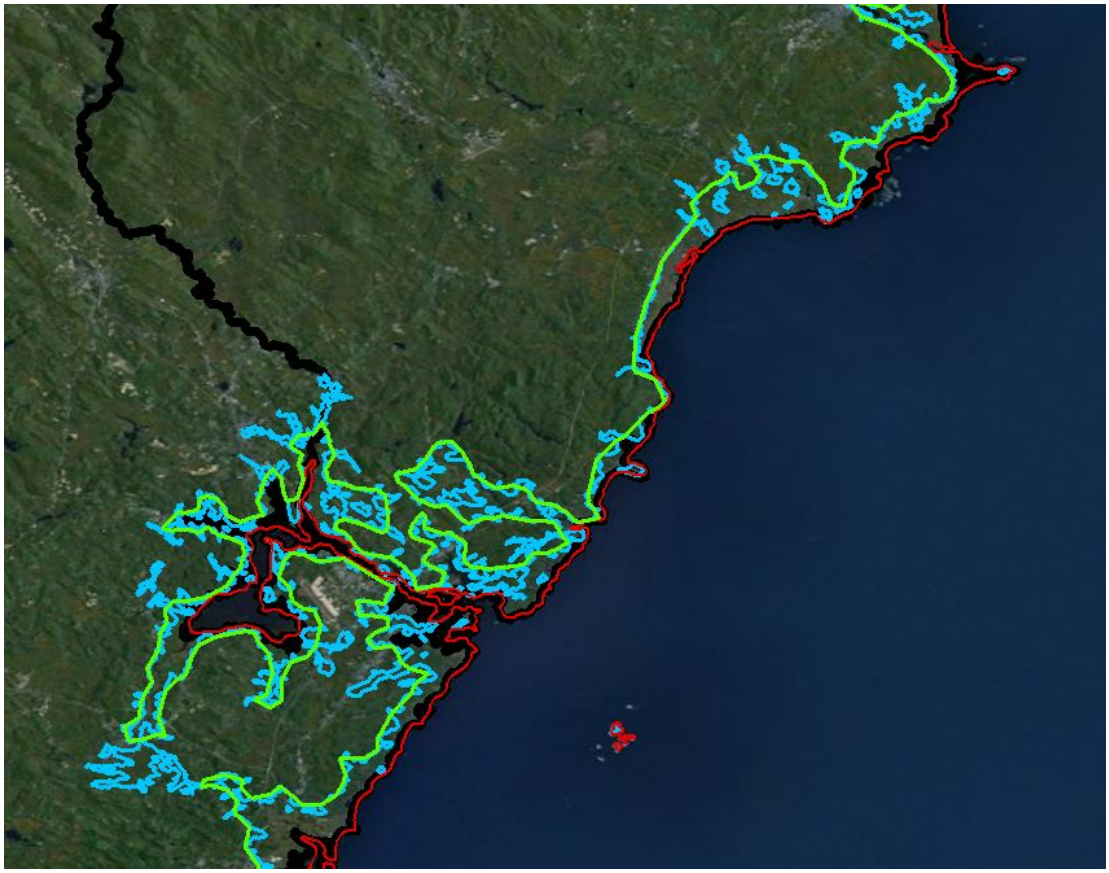

Figure 11-9: Final mesh boundary (green), approximate 10 meter contour (blue), EC2012 mesh shoreline (red), and State boundaries (black) at Maine/New Hampshire border.

Although southern Florida is a relatively hurricane-prone region, the mesh was revised to follow more closely to the 7 meter contour. This contour line is generally more than 50 kilometers inland from the shoreline, and following this line eliminated Lake Okeechobee from the final mesh. This area is shown in Figure 11-10.

Figure 11-10: Final mesh boundary (green), approximate 10 meter contour (blue), EC2012 mesh shoreline(red) in southern Florida.

11.3 **Connections with River Models**

During boundary development, the team reviewed the following areas along the Atlantic and Gulf coasts where NWS is working on developing riverine HEC-RAS models:

- Colorado River, Texas
- Houston Rivers, Texas
- Vermilion River, Louisiana
- Atchafalaya River, Louisiana
- Pascagoula River, Mississippi
- Southern Mississippi River, Louisiana
- Pearl River, Louisiana and Mississippi
- St. John's River, Florida
- Waccamaw River, South Carolina
- Tar River, North Carolina
- Potomac River, Maryland
- Hudson River, New York
- Connecticut River, Connecticut
- Kennebec River, Maine

Figure 11-11 gives the relative geographic location of these Rivers along with an indication of whether the implementation is already complete or underway, or only planned.

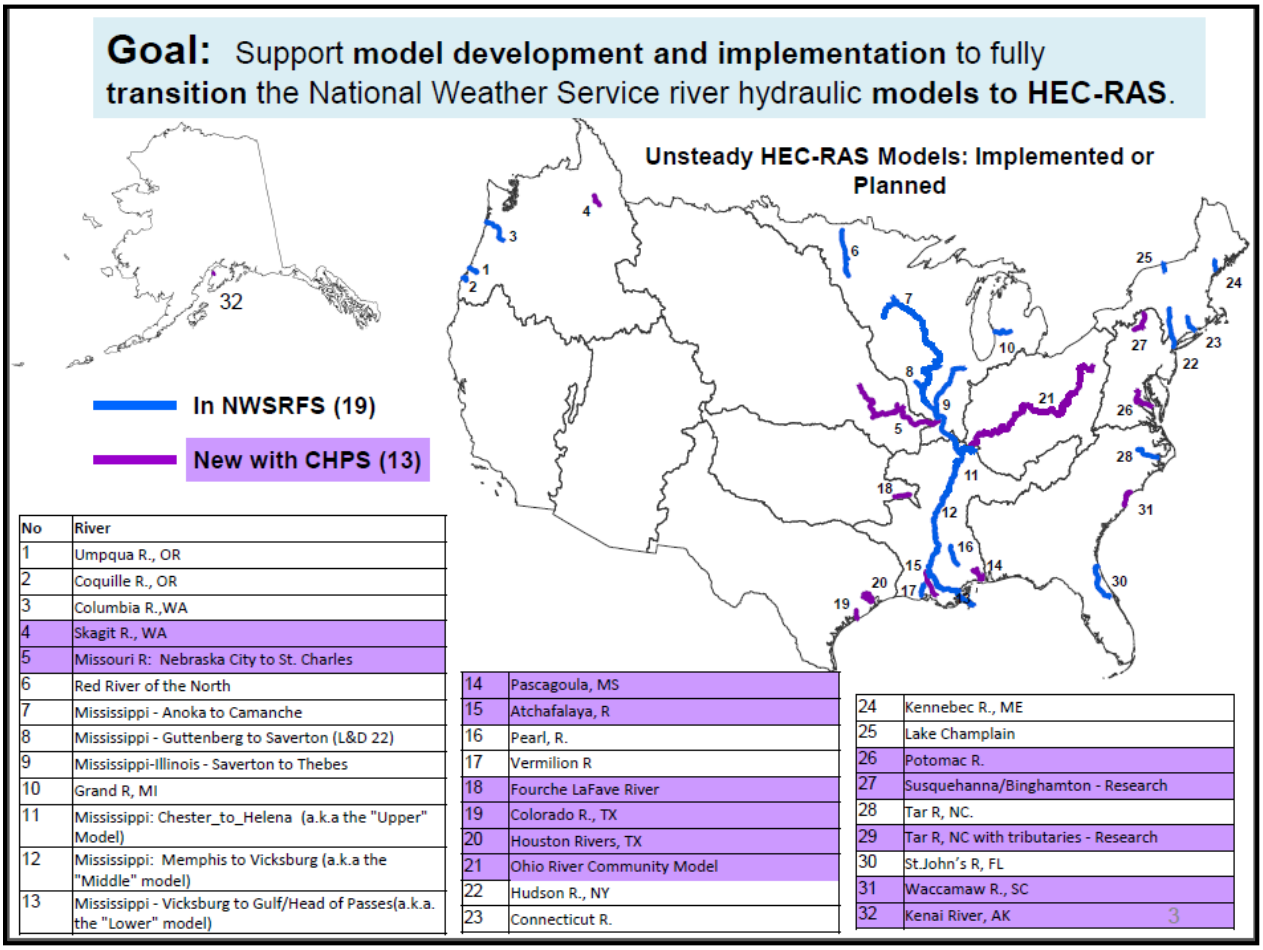

No	River
1	Umpqua R., OR
2	Coquille R., OR
3	Columbia R.,WA
4	Skagit R., WA
5	Missouri R: Nebraska City to St. Charles
6	Red River of the North
7	Mississippi - Anoka to Camanche
8	Mississippi - Guttenberg to Saverton (L&D 22)
9	Mississippi-Illinois - Saverton to Thebes
10	Grand R, MI
11	Mississippi: Chester_to_Helena (a.k.a the "Upper" Model)
12	Mississippi: Memphis to Vicksburg (a.k.a the "Middle" model)
13	Mississippi - Vicksburg to Gulf/Head of Passes(a.k.a. the "Lower" model)

14	Pascagoula, MS
15	Atchafalaya, R
16	Pearl, R.
17	Vermilion R
18	Fourche LaFave River
19	Colorado R., TX
20	Houston Rivers, TX
21	Ohio River Community Model
22	Hudson R., NY
23	Connecticut R.

24	Kennebec R., ME
25	Lake Champlain
26	Potomac R.
27	Susquehanna/Binghamton - Research
28	Tar R, NC.
29	Tar R, NC with tributaries - Research
30	St.John's R, FL
31	Waccamaw R., SC
32	Kenai River, AK

Figure 11-11: OHD graphic giving ongoing and upcoming hydraulic model implementations in the River Forecast Centers, ca. 2012.

Based on river widths and locations of NWS forecast points compared to the 10 meter contour we specifically resolved eight channels in the ADCIRC mesh for possible riverine/coastal model coupling as shown in the following figures and notes.

- The **Atchafalaya River** is currently included in the Gulf Mesh, and 5 forecast points can be captured up to the inland extent of the mesh where the river is still over 400 meters wide.

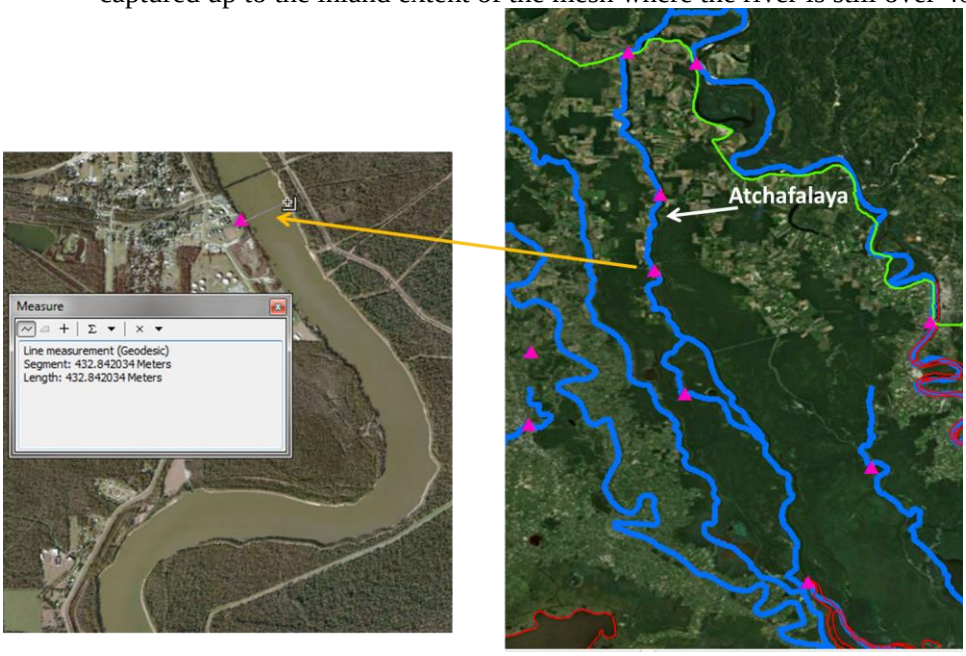

Figure 11-12: Left, aerial image showing width of Atchafalaya River at NWS forecast point contained in resolved portion of channel. Right, context of aerial image showing: green, proposed model boundary; blue, stream centerline; red = EC2012 mesh boundary (i.e. shoreline); pink triangles; NWS forecast points.

- The **Mississippi River** has 4 forecast points that can be captured up to Baton Rouge, Louisiana (the inland extent of the mesh), where the river is still wide and fully resolved in the Gulf Mesh.

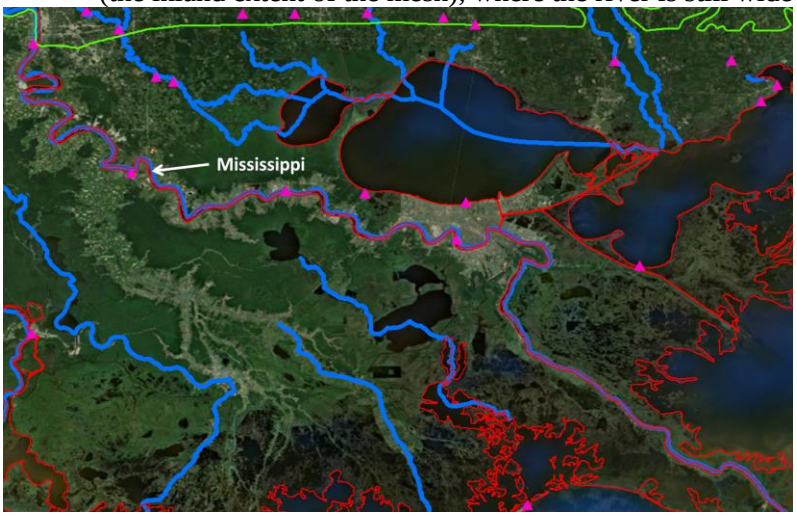

Figure 11-13: Aerial image showing, for the region of the southern Mississippi River: green, proposed model boundary; blue, stream centerline; red = EC2012 mesh boundary (i.e. shoreline); pink triangles; NWS forecast points. Channel is resolved is mesh where outlined in magenta.

- The **St. John's River** includes 2 forecast points near the mouth that can be resolved and 1 additional gage upstream where the river is around 200 m wide and may be able to be resolved in the mesh.

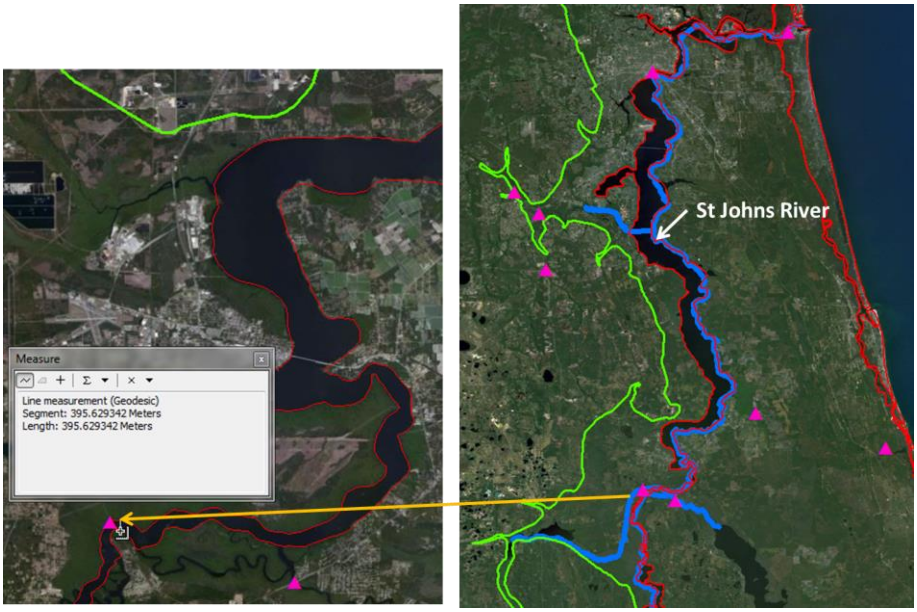

Figure 11-14: Left, aerial image showing width of St Johns River at NWS forecast point contained in resolved portion of channel. Right, context of aerial image showing: green, proposed model boundary; blue, stream centerline; red = EC2012 mesh boundary (i.e. shoreline); pink triangles; NWS forecast points.

- The **Waccamaw River, South Carolina** includes 2 forecast points where the river is around 250 meters wide and several additional gages farther upstream where the river is less than 200 meters wide.

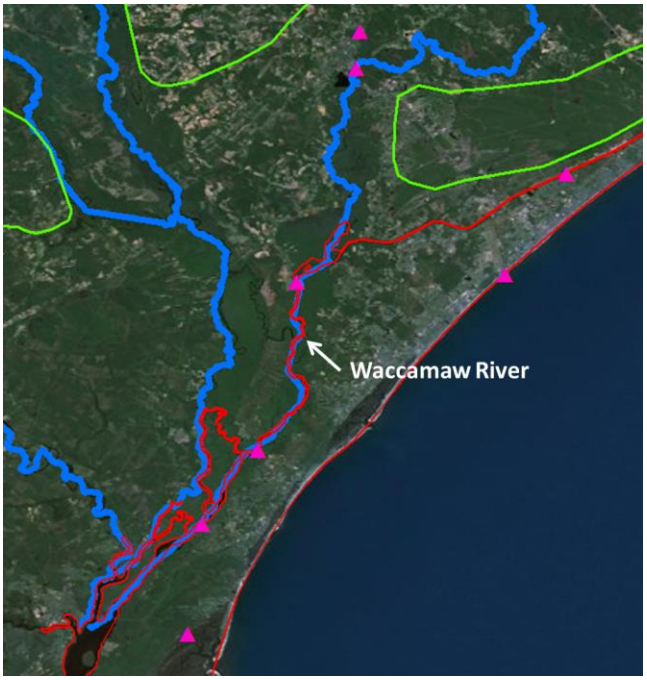

Figure 11-15: Aerial image showing, for the region of the Waccamaw River: green, proposed model boundary; blue, stream centerline; red = EC2012 mesh boundary (i.e. shoreline); pink triangles; NWS forecast points.

- The **Tar River** includes 1 forecast point where the river is around 350 meters wide. This gage is approximately 55 kilometers upstream from the confluence with Pamlico Sound, so the coastal results should be available relatively far up this river.

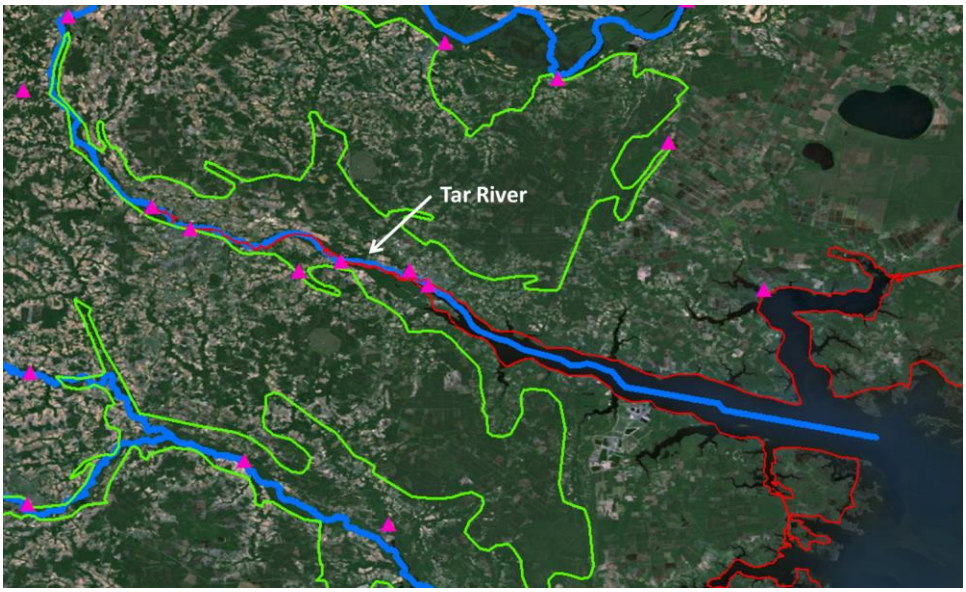

Figure 11-16: Aerial image showing, for the region of the Tar River: green, proposed model boundary; blue, stream centerline; red = EC2012 mesh boundary (i.e. shoreline); pink triangles; NWS forecast points.

- The **Potomac River** includes 2 forecast points where the river is more than 500 meters wide.

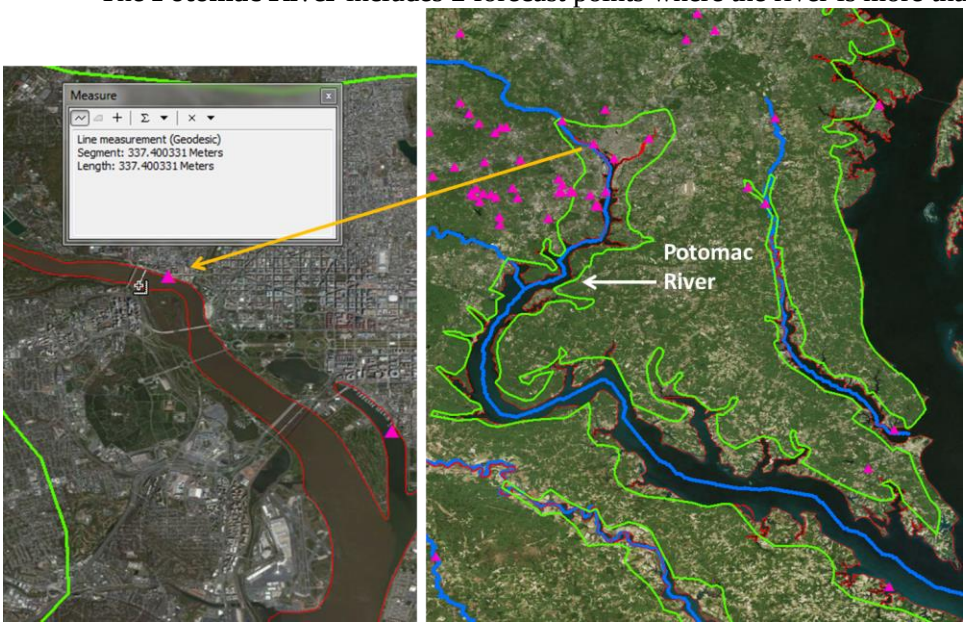

Figure 11-17: Left, aerial image showing width of Potomac River at NWS forecast point contained in resolved portion of channel. Right, context of aerial image showing: green, proposed model boundary; blue, stream centerline; red = EC2012 mesh boundary (i.e. shoreline); pink triangles; NWS forecast points.

- The **Hudson River**, in addition to forecast points in the Hudson Bay area, includes 1 forecast point at Poughkeepsie where the river is more than 1,000 meters wide and several additional gages farther upstream where the river is around 200 meters wide.

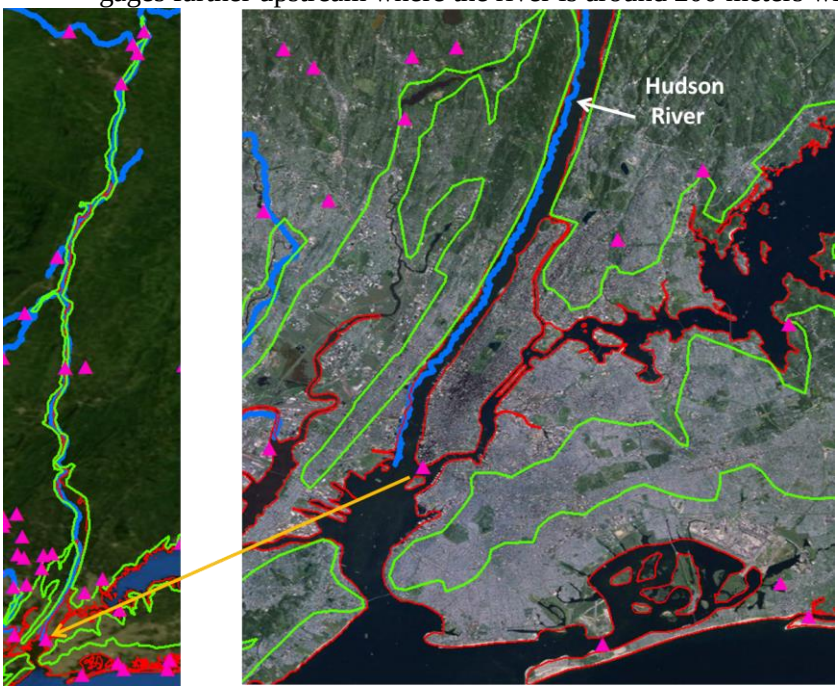

Figure 11-18: Left, aerial image of Hudson River from mouth to confluence with Mohawk River above Troy, New York. Right, zoomed in image showing Hudson River in context of the southern portion of Long Island sound, East River, and New York Harbor. In both graphics the following are shown: green, proposed model boundary; blue, stream centerline; red = EC2012 mesh boundary (i.e. shoreline); pink triangles; NWS forecast points.

- The **Connecticut River** includes 2 forecast points where the river is approximately 350 meters wide.

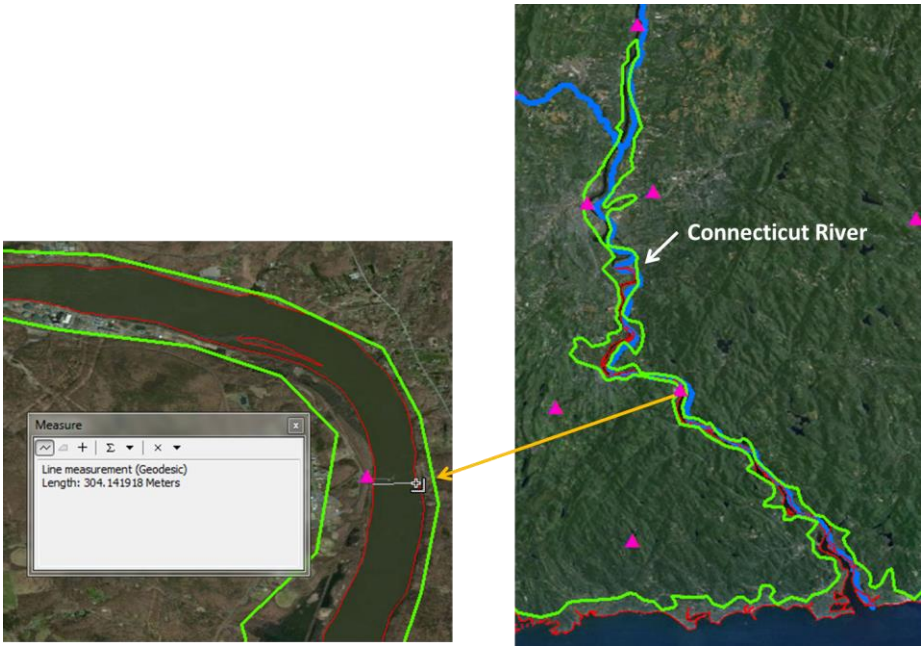

Figure 11-19: Left, aerial image showing width of Connecticut River at NWS forecast point contained in resolved portion of channel. Right, context of aerial image showing: green, proposed model boundary; blue, stream centerline; red = EC2012 mesh boundary (i.e. shoreline); pink triangles; NWS forecast points.

Six other rivers were considered but excluded, including:

- The **Colorado River in Texas** which is only about 300 feet wide at the downstream-most gaging point.

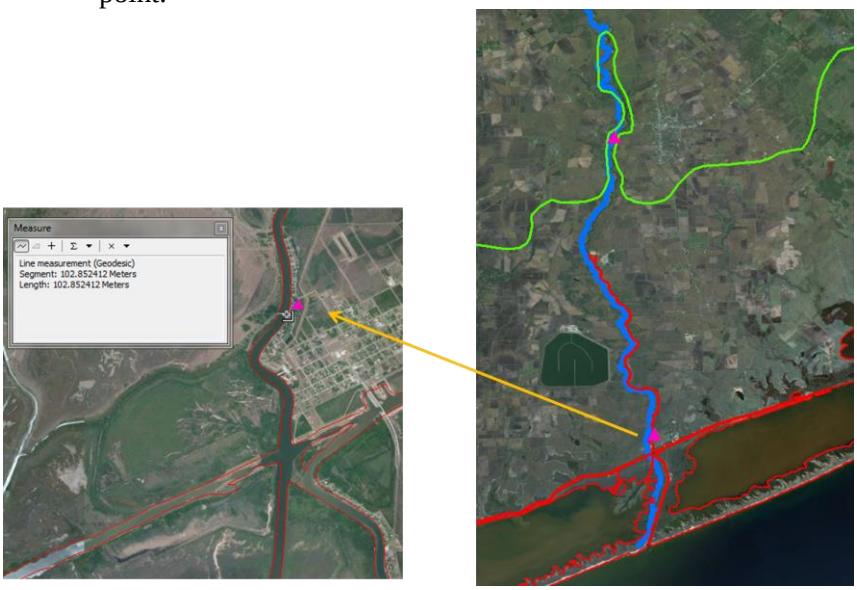

- The **Houston Rivers (referring to tributaries to the Trinity and Galveston Bays in Texas, including San Jacinto River and Buffalo Bayou)** are all narrow and channelized, in some place only 10 – 15 feet wide.

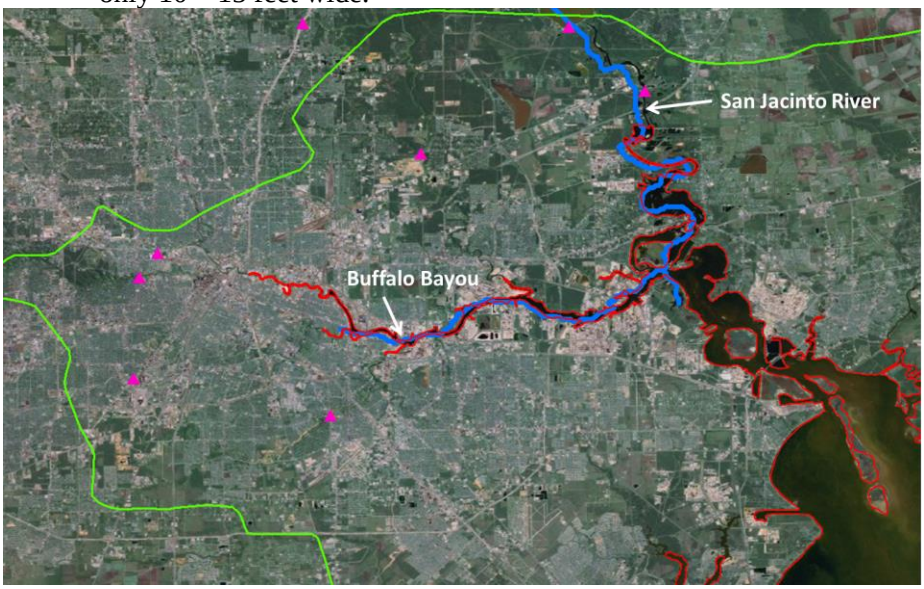

- The **Vermillion River** is within the mesh boundary but the channel is not resolved because the river is only approximately 100 feet wide at the downstream-most NWS forecast point.

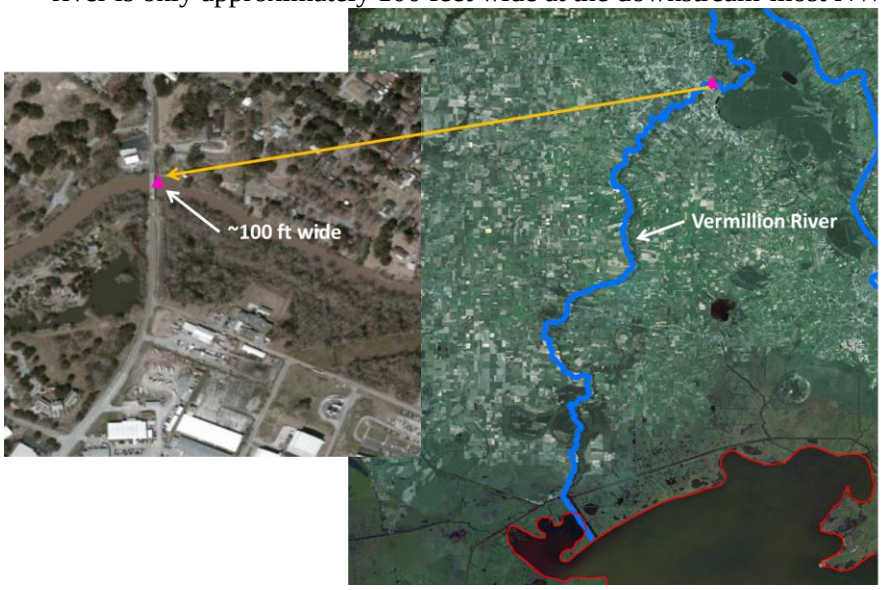

- The **Pearl River, in Louisiana and Mississippi** is only approximately 300 feet wide at the NWS forecast point and is not resolved in the SURA-IOOS gulf mesh used for that area.

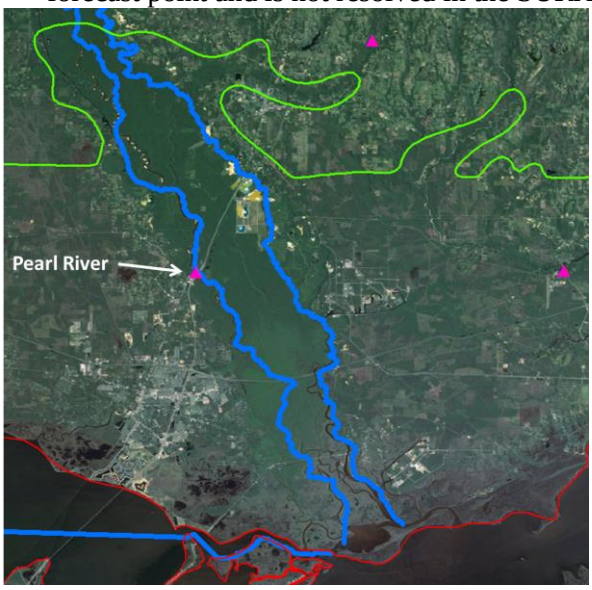

- The **Pascagoula River** is also only approximately 300 feet wide at the NWS forecast point and is not resolved in the SURA-IOOS gulf mesh used for that area. The NWS gage at the mouth of the distributary system on the coast is included in the mesh.

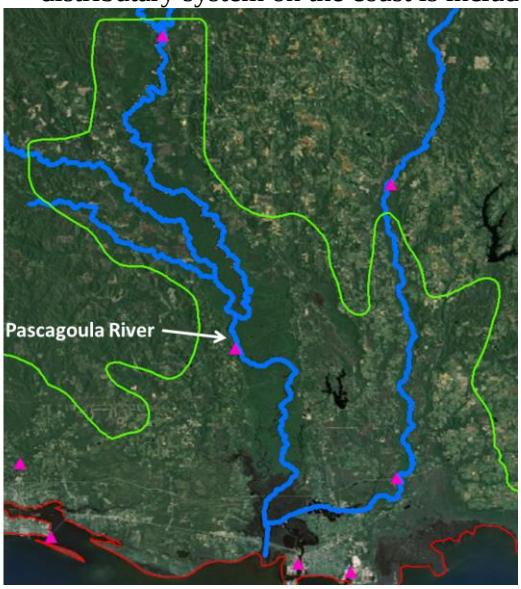

- The **Kennebec River** is only approximately 400 feet wide at the downstream-most NWS forecast point.

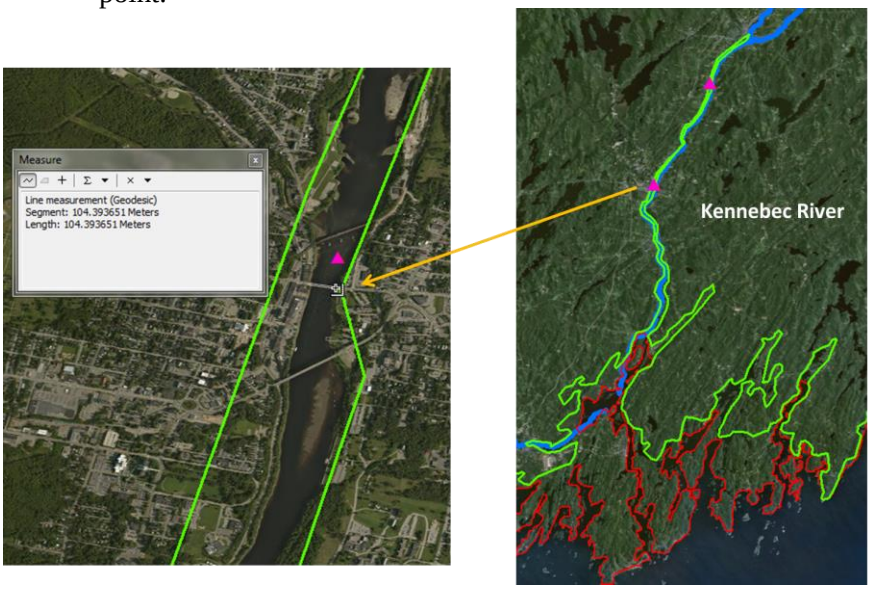

12. APPENDIX B – DEVELOPMENT OF TOPO-BATHY DATA AND OF MESH

Attention to mesh quality is essential to produce a mesh that not only accurately represents the terrain and bathymetry, but also produces stable and consistent results when run with the Advanced Circulation (ADCIRC) model. The ADCIRC model runs on a triangulated mesh that can have varying element sizes. Each node has an associated elevation, and additional spatial parameters can be associated with each node. Although there are software toolkits to help develop ADCIRC meshes, there is still a considerable amount of manual input. For an area as large as this project's domain of the Atlantic and Gulf of Mexico, the mesh is usually built in sections and often by different team members, so a guiding meshing methodology is necessary to maintain a consistent mesh throughout the study domain.

This appendix describes the underlying elevation data sources and the meshing methodology used to produce an ADCIRC mesh for this project – the NOAA Coastal Survey Development Laboratory's (CSDL's) operational storm surge model. For this report, this mesh will be referred to as the NOAA Operational Model with ADCIRC (NOMAD)[17]. For this project, the goal was to develop a mesh with less than 2,000,000 nodes with an average spacing around 400 to 500 meters in the nearshore and onshore areas and a minimum spacing around 200 meters. These parameters should allow for reasonable run times on the NOAA high performance computing resources. The methodology discussed in this appendix outlines the guidance regarding mesh size, flow path, and flow barrier design in the mesh.

12.1 Data Sources

Two primary data sources provided the majority of mesh node elevations: the USGS 1/3 arc-second (nominally 10 meter) National Elevation Dataset (NED) digital elevation model (DEM) supplied overland topography and the NOAA EastCoast2012 (EC2012) tidal constituent database mesh nodes constituted the primary bathymetry data source. In addition to these primary sources for mesh node elevations, several further sources provided more specific definition of flow obstructions and prominent flow paths. Features identified in these high resolution datasets were used to condition node elevations extracted from the continuous topobathy coverage during mesh generation. Summary explanations of the various elevation and bathymetry datasets are provided in Table 12-1. In addition to the data sources listed in the table, the study team examined data extracted from the National Levee Database to confirm that these major flow barriers had been captured. No elevation data was used from this source. This source was solely used to confirm the location of levees in the study area.

[17] NOMAD was used to refer to early versions of the HSSOFS mesh.

Table 12-1: Sources of topo-bathymetric data for development of the HSSOFS mesh node elevations.

Data	*Description*	*Purpose*	*Source*	*Processing*
NED 1/3 arc-second	Continuous coverage of CONUS at 1/3 arc-second resolution (nominally 10 meters) incorporating wherever available the highest resolution source elevation information. Data are provided referenced to NAVD 88.	Primary source for topographic (over land) elevations.	USGS	1x1 degree tiles mosaicked; shoreline masked to remove data over ocean; clipped within 60 mile inland buffer.
EC2012 Mesh	2012-2013 updated to ADCIRC model for verifying tidal datums, Node spacing varies down to approximately 20 meters.	Primary source for bathymetric data definition and specific flow channel delineation.	NOAA CSDL	Mesh elevations shifted to NAVD88 with VDatum; converted to grid via TIN/terrain interpolation; clipped to remove interpolated landward elevations; merged with 1/3 arc-second NED.
NED 1/9 arc-second	Discontinuous, as-available coverage at 1/9 arc-second resolution (nominally 3 meters) based on lidar or other recent high-vertical-accuracy sources. Coverage is continuously expanding as new data sources become available.	Refinement of specific fine-detail flow obstructions and flow channel definition.	USGS	One-quarter degree tiles mosaicked for 11 discrete lengths of US coastline.
Coast Services Center lidar	Standardized collection of lidar point clouds sourced from various agencies and provided on CSC clearing house.	Replaced inaccurate portions of 1/3 arc-second NED in SC and GA and provided additional fine-detail channels and obstructions for portions of MA; NY; and VA.	NOAA CSC	Decompressed from LAZ to LAS; combined into GIS-compatible LASD datasets; filtered for ground-only points; interpolated to 1/9 arc-second mesh via TIN/terrain.
South Carolina county DEMs	AECOM in-house datasets made available for this project. 50 feet (~15 meter or ½ arc-second) cell resolution in Charleston, Berkeley, and Georgetown counties; and 15 feet (~4.5 meter or ~1/6 arc-second) cell resolution in Horry and Beaufort counties.	Replaced anomalous 1/3 arc-second data for SC coast and provided some detail for channels and obstructions.	AECOM	Resampled from native resolution to 1/3 and 1/9 arc-second; merged with CSC lidar for SC.
SURA-IOOS ultralite mesh	ADCIRC mesh from SURA-IOOS Round 1 testbed project	Topography, bathymetry, and general mesh definition for Louisiana, and portions of Texas and Mississippi.	SURA-IOOS/ CSDL	Extended northward in portions of Coastal Louisiana; otherwise, used as-is.

The USGS 1/3 arc-second data were obtained in 1x1 degree tiles for the area of interest via bulk download. The NOAA EC2012 mesh node elevations were interpolated to 1/3 arc-second grid aligned with the USGS data. Both collections (the USGS tiles and the NOAA-derived bathymetry grid) were then merged into a seamless full coastline 1/3 arc-second merged dataset. The EC2012 mesh node elevations were converted from MSL to NAVD88 in order to combine them with the topographic data from the USGS. Additional detail regarding the process used to obtain conversion values between MSL and NAVD88 datums is provided in section 12.2.

To cleanly define the shoreline and limit of topographic vs. bathymetric data, all DEM datasets were either masked or clipped using a polygon developed from the concave hull of the EC2012 points.

The 1/9 arc second USGS NED provides coverage for nearly all of the Gulf Coast, Florida, North Carolina, the Delmarva Peninsula, and most of New England. These data were obtained as a bulk download from the USGS and combined into twelve segments, conveniently sized for display and delivery.

An inventory of gaps in the 1/9 arc-second coverage was compared to a catalog of potential lidar sources within the model boundary. Potential lidar sources were examined in the catalog of the NOAA Coastal Services Center (CSC). Four lidar point clouds were obtained: Boston area, Massachusetts; Long Island New York City and the Hudson riverbank, New York; Norfolk and Virginia Beach, Virginia; and portions

of coastal South Carolina in Colleton and Jasper counties as well as Chatham County in Georgia. Each dataset was converted to a GIS terrain dataset then interpolated to a high-resolution raster at the same resolution as the 1/9 arc-second NED data. The lidar point clouds were provided by the CSC as classified LAZ (compressed LAS) datasets. Only ground points were included in any analysis and derived grids were masked to prevent interpolation of ground elevations across open water.

Figure 12-1 shows the relative extents of the NED and lidar-based elevation datasets with Figure 12-2 giving more detail specifically for the CSC lidar dataset extents.

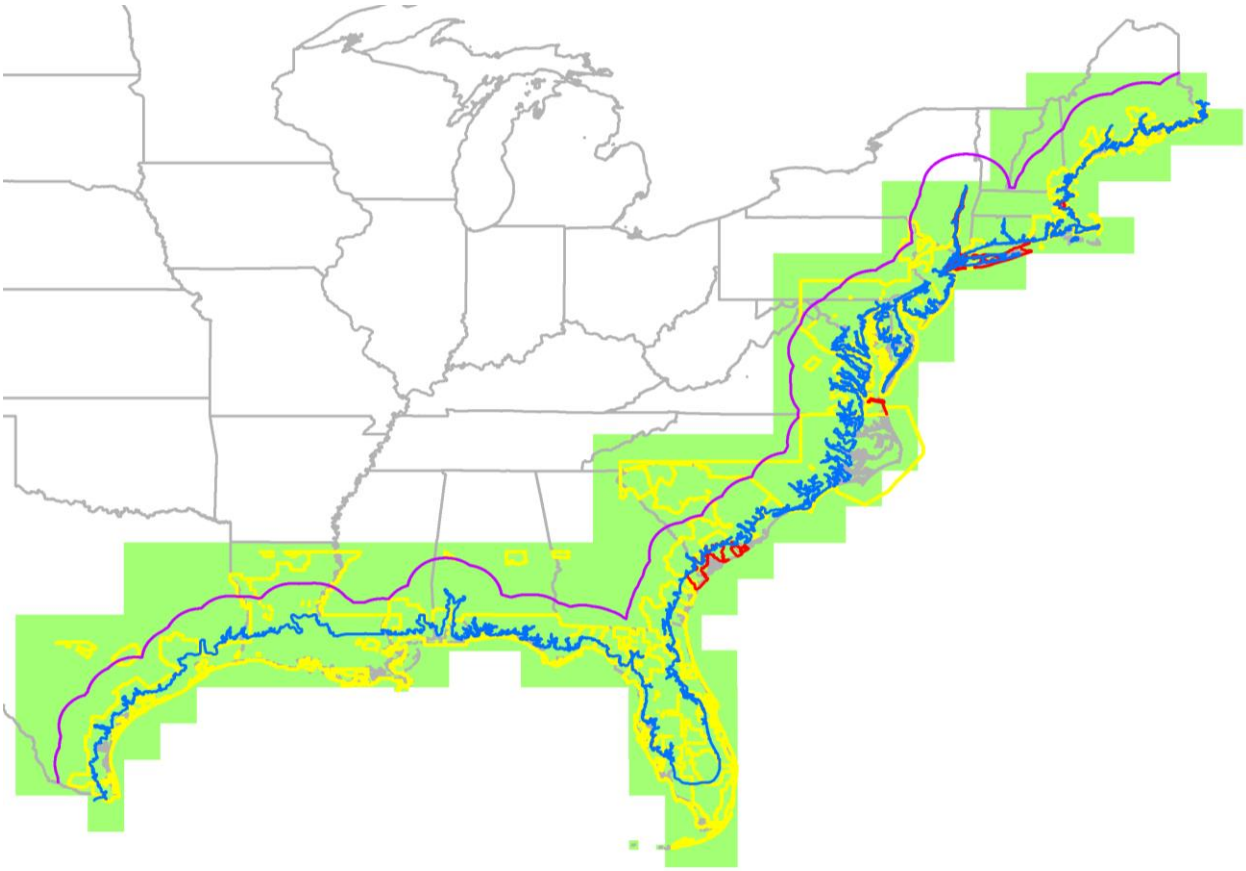

Figure 12-1: Relative extents of data sources for land elevations. Green shading indicates 1/3 arc-second coverage (areas over ocean give only a value of zero). The yellow boundary indicates 1/9 arc-second NED extents. Red outlines show areas of CSC lidar datasets. The purple and blue lines indicate, respectively: the 60-mile inland buffer used to truncate the 1/3 arc second continuous topo-bathy dataset delivered to NOAA; and the model inland boundary approximately following the 10-meter elevation contour.

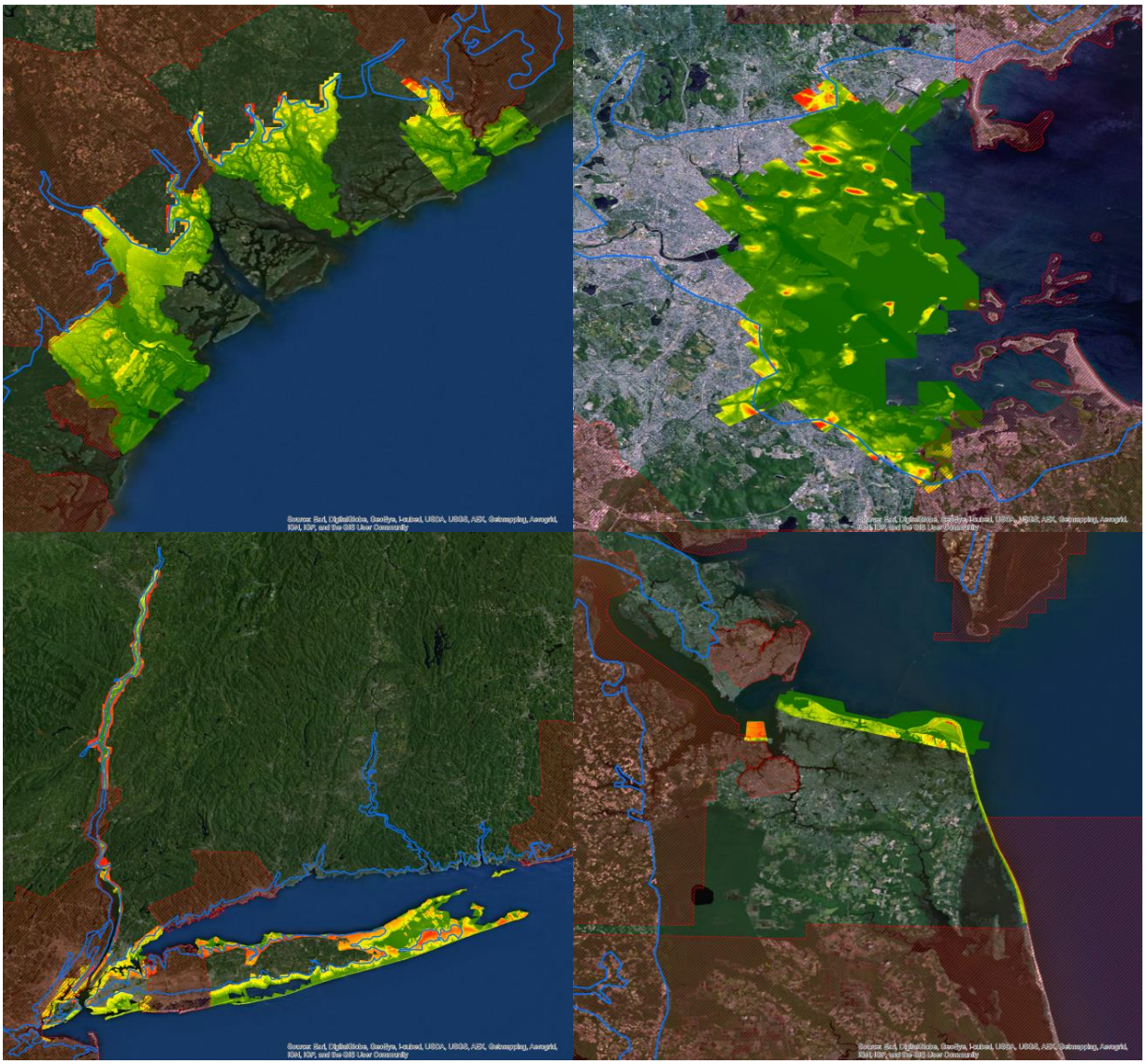

Figure 12-2: Gridded elevation data derived from NOAA Coastal Services Center lidar datasets. lidar were obtained to fill gaps in coverage of high-resolution 1/9 arc-second NED from USGS. Lidar elevations are shaded green to red and are shown with the extent of 1/9 arc-second NED coverage hatched in red. The blue line in each figure indicates the approximate boundary of the model mesh, usually at the 10-meter elevation contour. Areas shown are (clockwise from top-left): Coastal South Carolina; Boston, Massachusetts; Virginia Beach, Virginia; and New York City, Long Island, and Hudson River, New York. Lidar extents shown are full datasets as obtained from CSC.

Along the South Carolina coast, a number of significant anomalies were present in the 1/3 arc-second NED representation of the topography, and other potential public data sources are also quite limited. For these areas, several gridded elevation datasets from in-house archives were used to improve topographic elevation estimates for five South Carolina counties:

- 50 foot (~15 meter or ½ arc-second) cell resolution in Charleston, Berkeley, and Georgetown counties; and
- 15 foot (~4.5 meter or ~1/6 arc-second) cell resolution in Horry and Beaufort counties.

These data, together with the lidar for Colleton and Jasper counties in South Carolina and Chatham County in Georgia, filled in the most significant gap in elevation data for the East Coast. Figure 12-3 shows the extent of the AECOM-provided datasets alongside the CSC lidar.

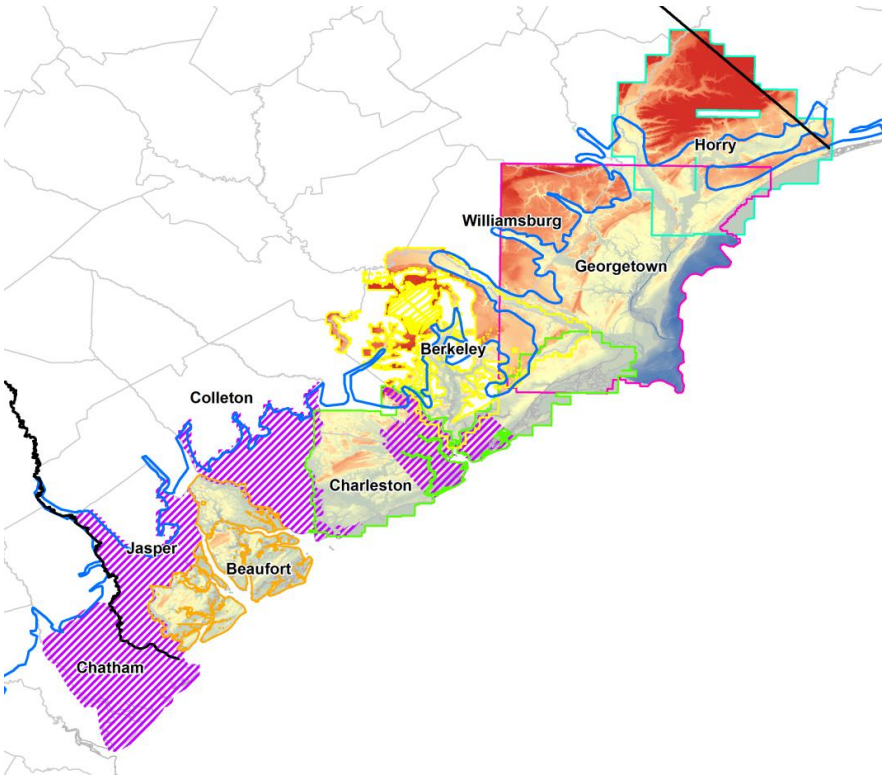

Figure 12-3: AECOM-provided elevations datasets for five counties in coastal South Carolina. Extents of CSC lidar are hatched in purple.

Elevations for coastal Louisiana and portions of Texas and Mississippi were derived from a mesh obtained from the Southeastern Universities Research Association - Integrated Ocean Observing System (SURA-IOOS) Round 1 Test Bed project as explained in Section 12.4.

12.2 **Datum Conversion**

As previously noted, the EC2012 mesh node elevations are the primary source for bathymetric data for building the storm surge modeling mesh. It was necessary to convert the node elevations from MSL to NAVD88 in order to combine them with the topographic data from the USGS. Normally, a translation of this type would be performed using the NOS-provided tool, VDatum. However, the VDatum application provided on the NOS website (http://vdatum.noaa.gov/) uses a translation grid with several key areas missing, including Pamlico Sound and the Indian River inlet.

CSDL provided code and an updated bathymetric translation grid which was extremely efficient for converting the large point datasets represented by the mesh nodes. The CSDL grid extends beyond the publically available VDatum grid and uses the TCARI (Hess et al. 2004) interpolation technique to allow extrapolation of the datum conversion field. The conversion is identical to the VDatum grid conversion where they overlap. Using the CSDL code, a complete set of MSL-to-NAVD88 conversion values was

generated for the entire near-shore bathymetric dataset from the EC2012 grid nodes. Figure 12-4 shows the extent of the EC2012 mesh nodes as well as the extent of the extended VDatum conversion grid.

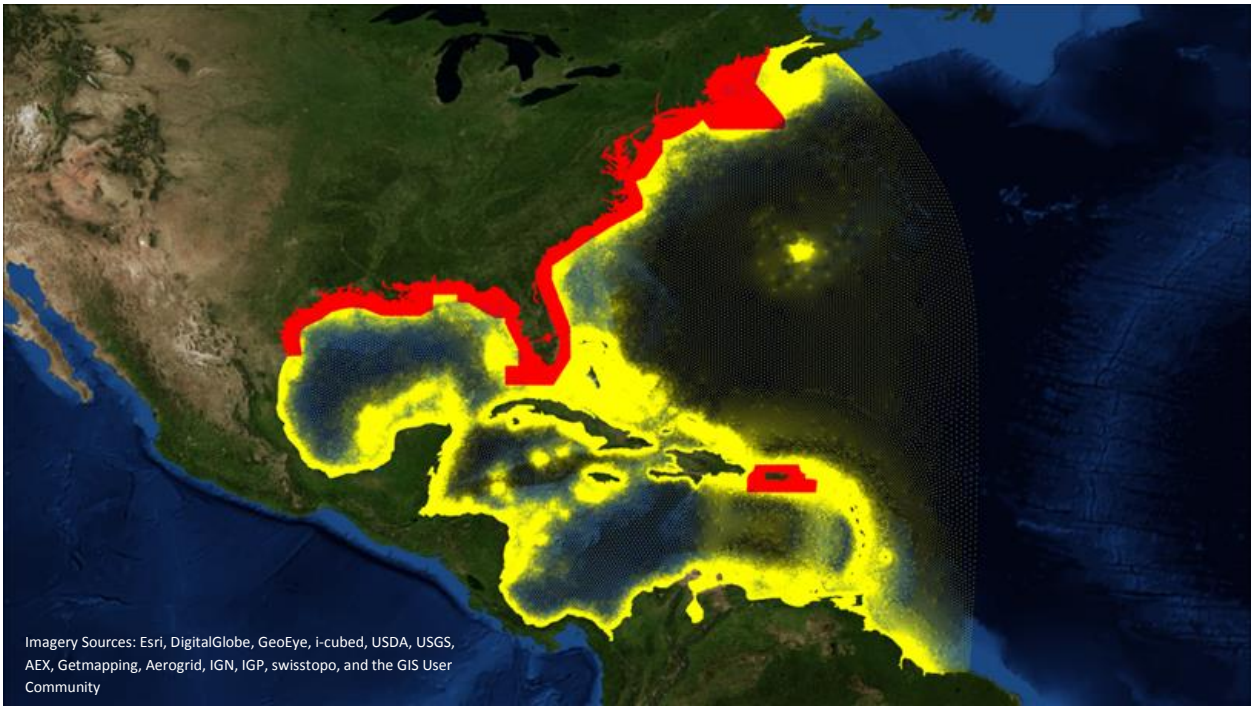

Figure 12-4: EC2012 mesh nodes in yellow and red. Red mesh nodes are those within the extent of the extended VDatum conversion grid.

A similar process was applied to convert the combined storm surge modeling mesh nodes back to MSL for use in modeling. When simulation results have been obtained, these conversion values will be applied as needed to compare to verification datasets in either MSL or NAVD88.

The CSC lidar data provided were referenced to NAVD88. However, the metadata provided with the lidar is confusing. A key confirmation of the datum is found in the download readme[18]:

> "The data are all in geographic coordinates using the North American Datum of 1983 (NAD83). The version of the NAD83 datum may vary slightly, but all are one of the updated realizations such as the High Accuracy Reference Network (HARN), Continuously Operating Reference System of 1996 (CORS96), or National Spatial Reference System of 2007 (NSRS2007), and not the original NAD83(86). ***This may not be evident in the metadata***. Vertical units are meters and all have been converted from NAD83 ellipsoid heights to orthometric North American Vertical Datum (NAVD) of 1988 heights using GEOID12a." (emphasis added)

[18] Download readme available here: http://www.csc.noaa.gov/htdata/lidar1_z/geoid12a/data/117/0README.html

12.3 **Meshing Methodology**

Striking a balance between minimizing the total node count to keep the computation time to a minimum and accurately representing the elevation features is a goal of all ADCIRC mesh developers. For this study, the mesh development team aimed to capture the area of the US coast from Maine through Texas with an average node spacing of 400 to 500 meters and a minimum node spacing of 200 meters. The mesh was extended overland to the 10 meter contour with some further inland extensions around densely populated areas. An initial inland boundary ArcGIS shapefile was delivered to NOAA on November 19, 2013. A final boundary will be delivered with the final mesh.

12.4 **Base Meshes**

Several meshes were provided to the project team by CSDL for review and use in this project. The EC2012 and the Extended EastCoast2001 (ExEC2001) meshes both cover the same area but include only bathymetry. The EC2012 mesh has more than two million nodes while the ExEc2001 mesh has approximately 258,000 nodes. Aiming towards a *total* mesh size of two million nodes, representing both bathymetry and overland areas, the ExEC2001 mesh was used as a base mesh and is shown in Figure 12-5.

A Gulf Coast-focused mesh developed for the Southeastern Universities Research Association - Integrated Ocean Observing System (SURA-IOOS) Coastal Ocean Modeling Round 1 Test Bed project (GM_LA_TX_v3_chk.grd) that was used for storm surge studies centered in Louisiana was provided, as well. The node and element configuration from the on-shore and near-shore areas in Louisiana and Mississippi were taken from this mesh and used in the NOMAD mesh for this project. Generally, the GM_LA_TX mesh had a less dense node spacing than what was developed from scratch for other areas on the Gulf and Atlantic coasts. Figure 12-6 shows the variation in node spacing at the Louisiana/Texas border.

To make sure high enough elevations were used at the inland boundary, a slight change was made to the SURA-IOOS mesh area just north of Lake Pontchartrain. The mesh was extended about 2,000 meters inland to reach the 10 meter contour. This area is highlighted in Figure 12-7 and Figure 12-8

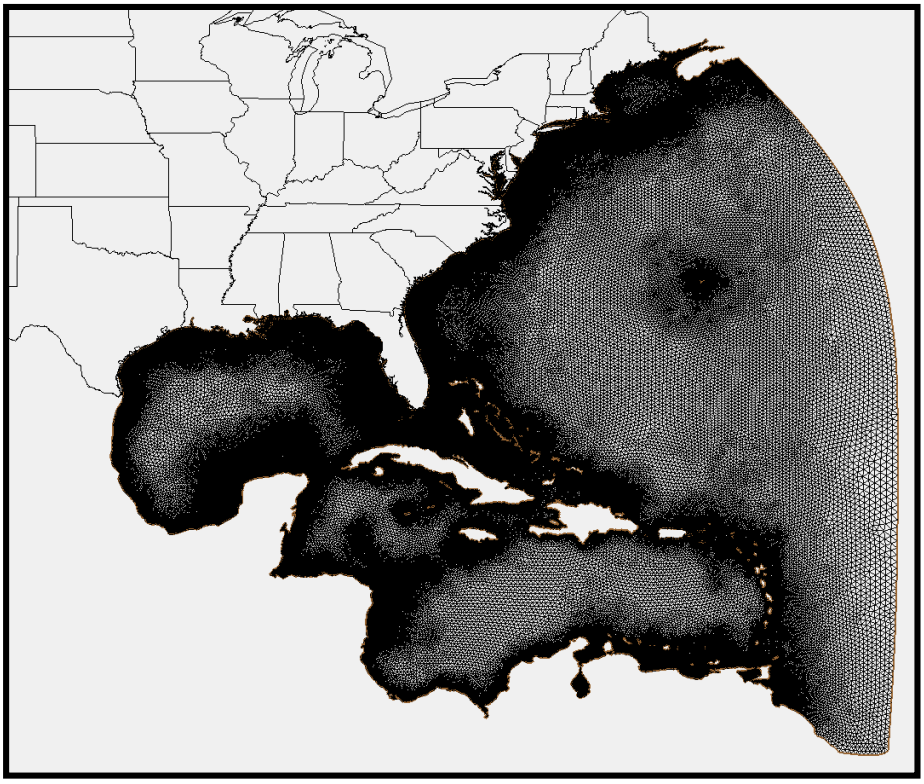

Figure 12-5. Extended EastCoast2001 ADCIRC mesh.

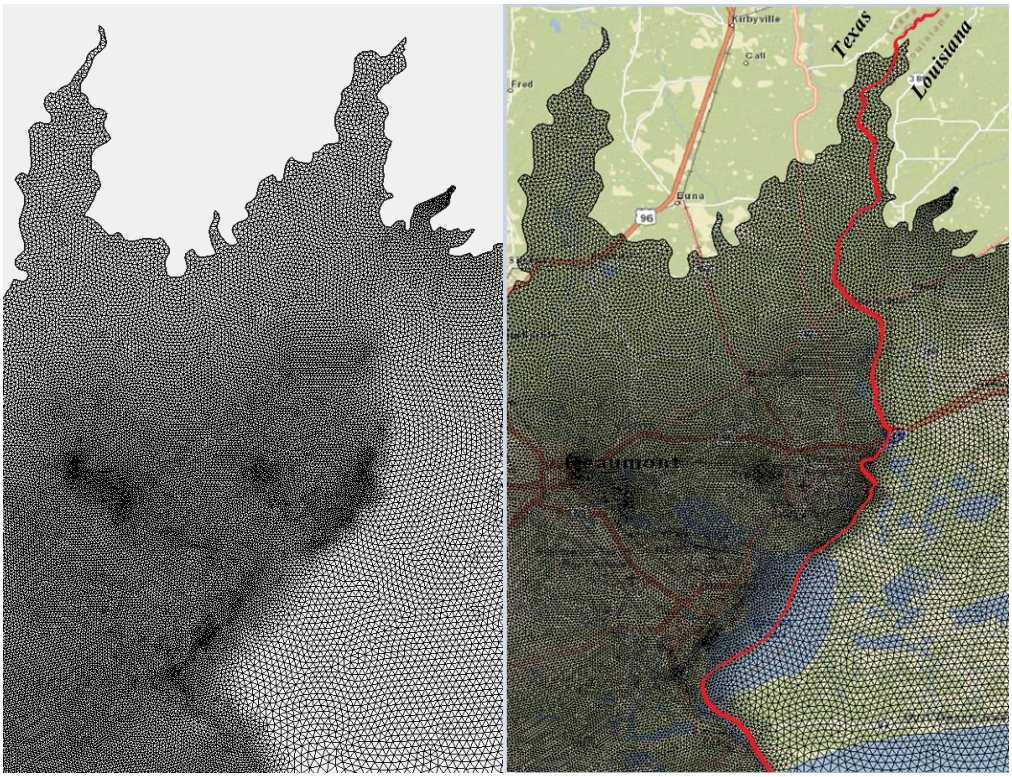

Figure 12-6. Comparison of node spacing between Texas and Louisiana with no background imagery on the left and World Street Maps on the right. Red line in image indicates the boundary between mesh sources; NOMAD on the left and SURA-IOOS on the right.

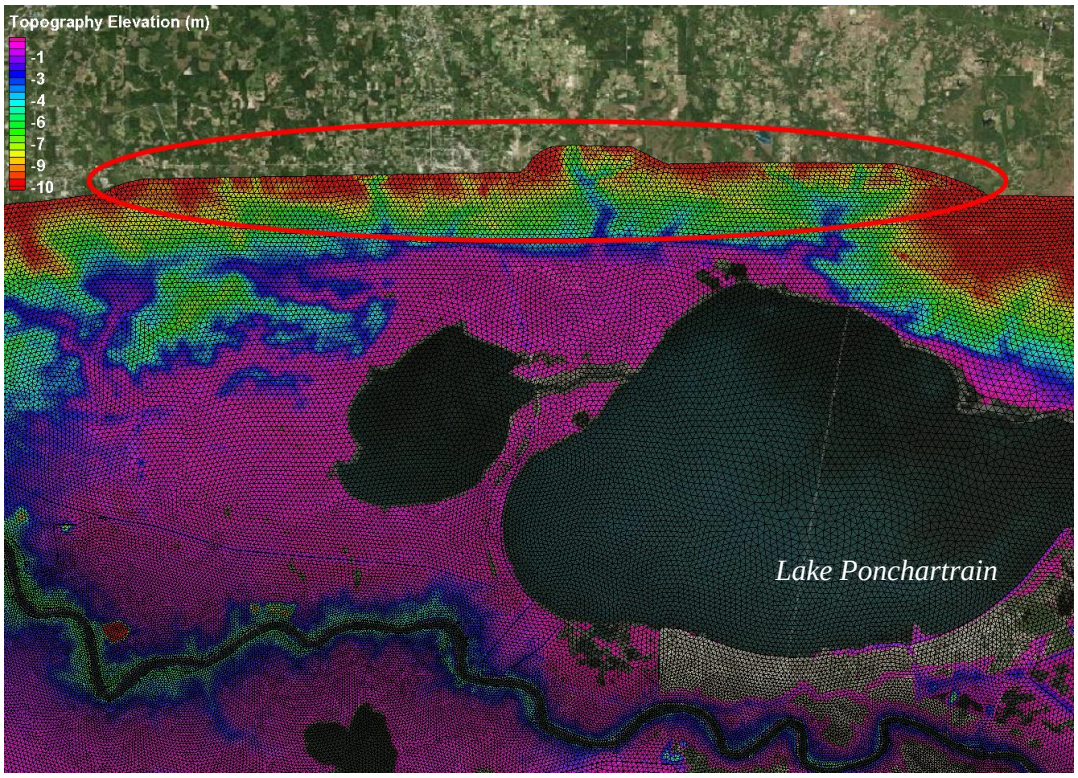

Figure 12-7. Inland extension of SURA-IOOS mesh north of Lake Pontchartrain, Louisiana.

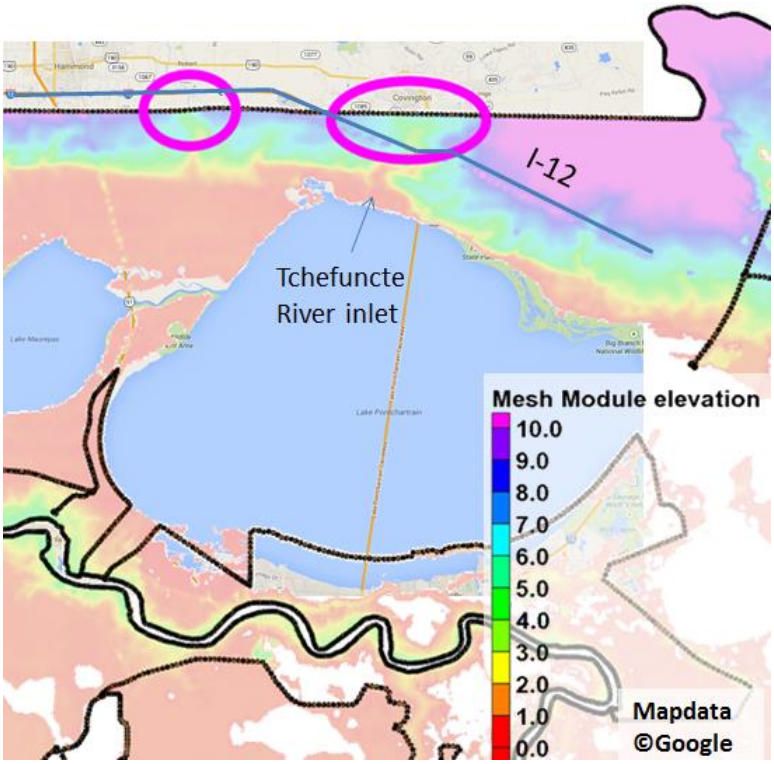

Figure 12-8: Magenta outlines highlight two areas of SURA-IOOS mesh requiring extension to include elevations up to 10 meters.

A final mesh incorporated in this project was developed for detailed storm surge studies in Puerto Rico and the US Virgin Islands (PR_new_boundary_2.grd provided by Joannes Westerink and Juan Gonzales-Lopez from the University of Notre Dame). This mesh was more detailed than necessary for this project with a minimum node spacing of 14 meters, so the inland boundary was extracted and then smoothed using a large node-to-node spacing. This boundary was used to develop the overland portion of the mesh for Puerto Rico and the US Virgin Islands and was "patched" into the larger ExEC2001 mesh. Figure 12-9 shows this area in the PR_new_boundary_2.grd and the NOMAD mesh developed for this project.

One advantage of using a model like ADCIRC is the ability to vary the mesh size relatively quickly to allow very large elements in the offshore area and very small elements in the area of interest. The final node-to-node spacing for this project ranged from a minimum of approximately 160 meters to a maximum of 46 kilometers. For the nearshore and overland areas of the mesh, an average node-to-node spacing of 400 to 500 meters was used. In order to preserve some narrow flow paths, the minimum node spacing was allowed to decrease to 200 meters. This was done in areas where the flow paths were hydraulically significant such as major waterways, areas that tied together two large water bodies, or areas that would provide a conduit to extensive inland flooding behind major flow barriers. Some highly populated areas were also modeled with a finer-scale mesh. More specifics on these highly detailed fine mesh areas will be discussed in the sections below. Figure 12-10 shows the mesh spacing across the US East and Gulf coasts.

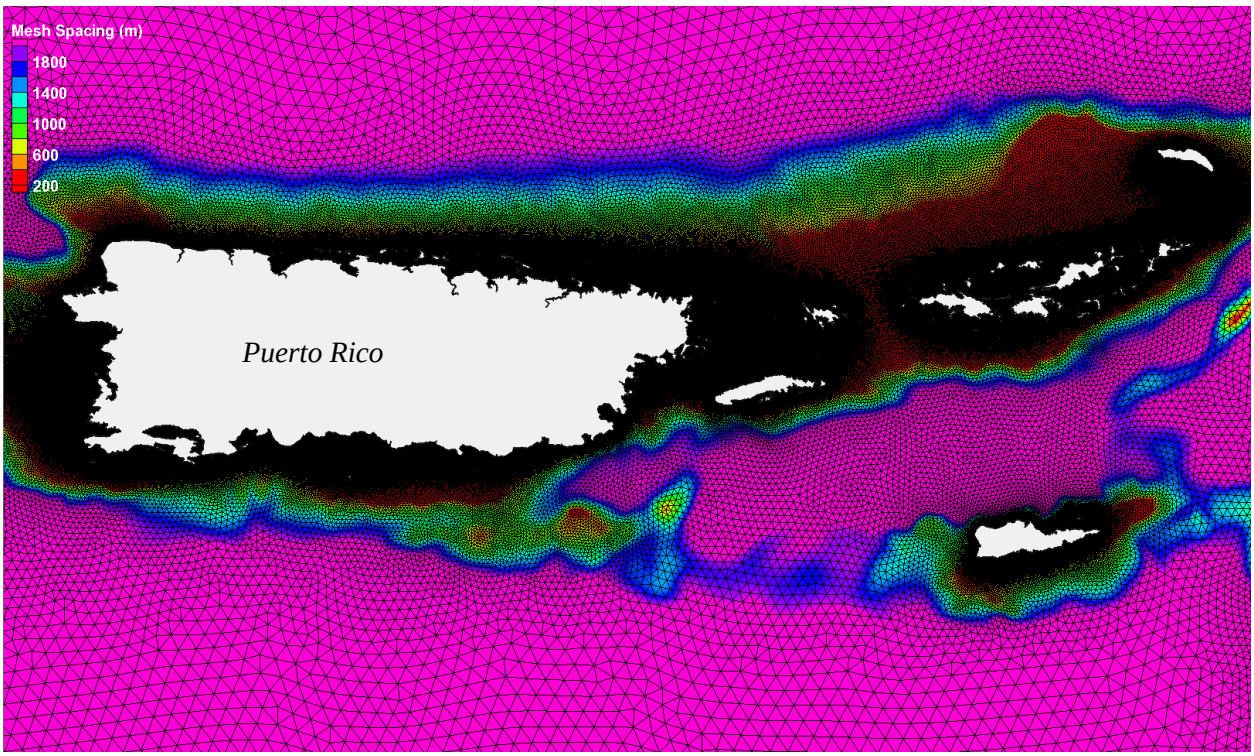

Figure 12-9. PR_new_boundary_2.grd mesh on the top and NOMAD mesh on the bottom with colors showing mesh spacing in the area of Puerto Rico and the US Virgin Islands Mesh Spacing.

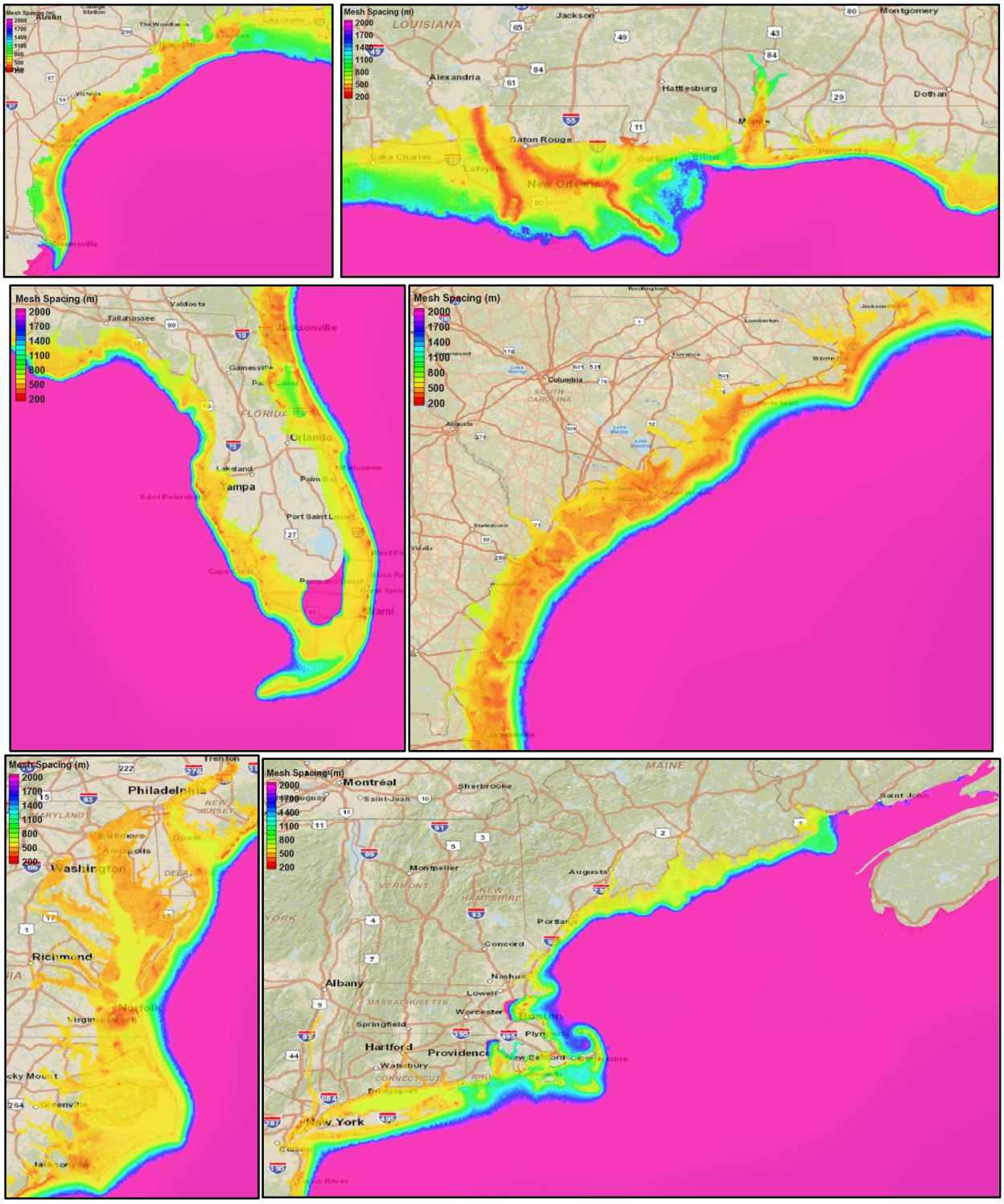

Figure 12-10. Mesh spacing along US Atlantic and Gulf coasts.

12.5 Flow Path Guidance

The goal of the ADCIRC mesh development was to represent major flow pathways and major flow barriers. Elevation data was examined and the mesh developers created a series of lines along critical flow features, which they wanted to explicitly include in the mesh.

When the elements were created using the Surface Water Modeling System (SMS) software program, triangles were generated that allowed at least three wet nodes across the face of the stream. For narrower rivers where only two wet nodes would be placed to represent the channel, an arc was generally drawn along one side of the stream. Figure 12-11 shows an area in Texas with arcs placed both down the sides of the channel and just in the middle of the channels. Figure 12-12 shows the same area with the final mesh (with bathymetric elements colored in shades of blue).

Figure 12-11. Sample arcs in Texas.

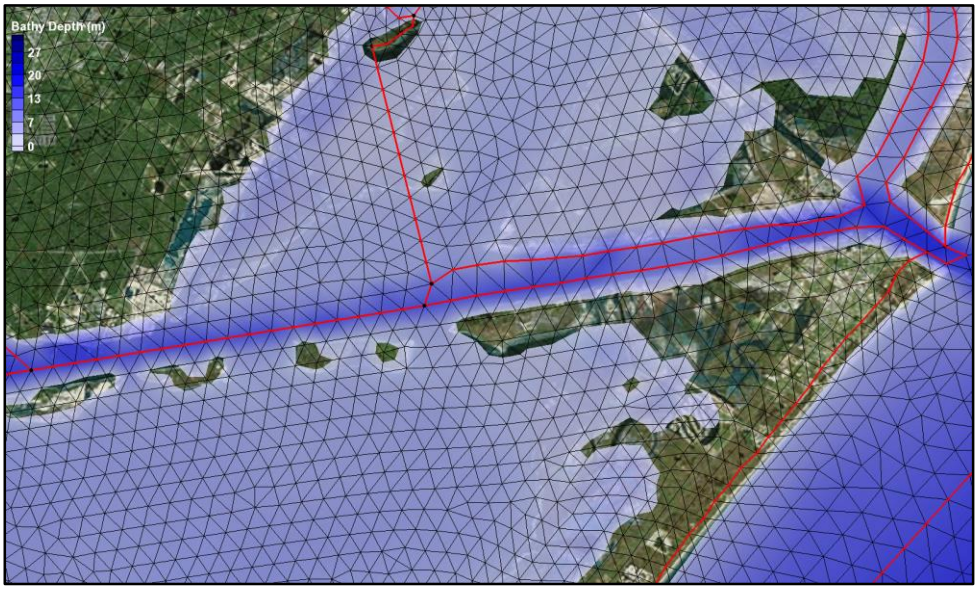

Figure 12-12. Final mesh in area shown in Figure 12-11.

In cases where key flow paths narrowed down to a width less than 400 to 500 meters, a decrease to a minimum node-to-node spacing (down to a minimum of 200 meters) was used to better represent flow channels deemed important to this project. If this decrease was not enough to maintain at least two wet nodes across the channel, but the flow path was deemed essential, some changes to the cross-section geometry were allowed to attempt to maintain the same cross-sectional area while increasing the channel width.

In general, "v-notch" channels (or channels that would only have one wet node in between two dry nodes) were avoided as this type of configuration may not properly convey flow and has been the cause of ADCIRC model instability issues in other projects. Areas with isolated "wet" nodes or "ponded nodes" were reviewed. This issue is complicated by the tide as new isolated nodes can appear as the tide recedes. All ponded bathymetric nodes not identified as major inland water bodies will be set dry using ADCIRC input file parameters for the start of the run, which should help decrease the potential for instabilities in the model.

An example where two "wet" nodes were placed on land in order to capture a flow channel is in Point Judith Pond, Rhode Island shown in Figure 12-13. The narrow inlet was essentially widened to allow flow to the back channel. The arcs created to assist in the mesh development are shown in red in this figure, and the narrow inlet is highlighted in green.

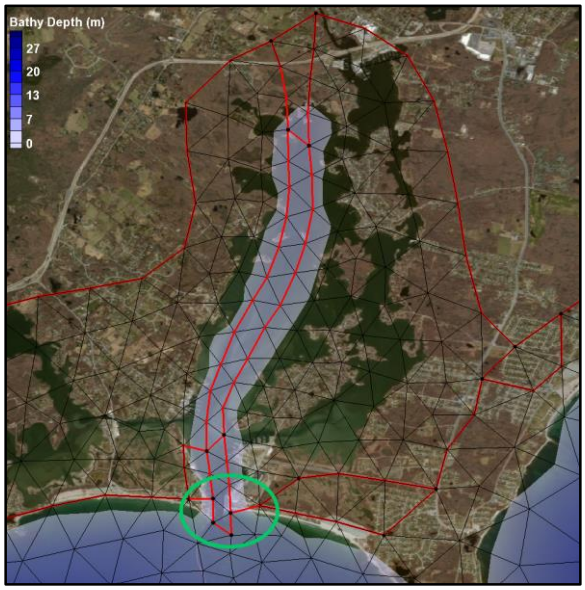

Figure 12-13. Flow channel for Point Judith Pond, Rhode Island.

During the mesh boundary development task, the project team reviewed areas where the National Weather Service is developing riverine HEC-RAS models. The following areas were identified for inclusion in the ADCIRC mesh at a resolution sufficient to provide information for creating a coupled riverine-coastal modeling system:

- Atchafalaya River, Mississippi
- Mississippi River, Louisiana
- St. John's River, Florida
- Waccamaw River, North Carolina

- Tar River, North Carolina
- Potomac River, Virginia, Maryland & Washington D.C.
- Hudson River, New Jersey & New York
- Connecticut River, Connecticut

These areas are shown in Figure 12-14 through Figure 12-20 below. In each figure, the mesh boundary is shown by dark purple lines, and the bathymetric areas are colored blue. (Note that some of the boundaries in the Louisiana area are along levees, which allow flow across the boundaries and are not inland boundaries, which do not allow flow past this boundary.)

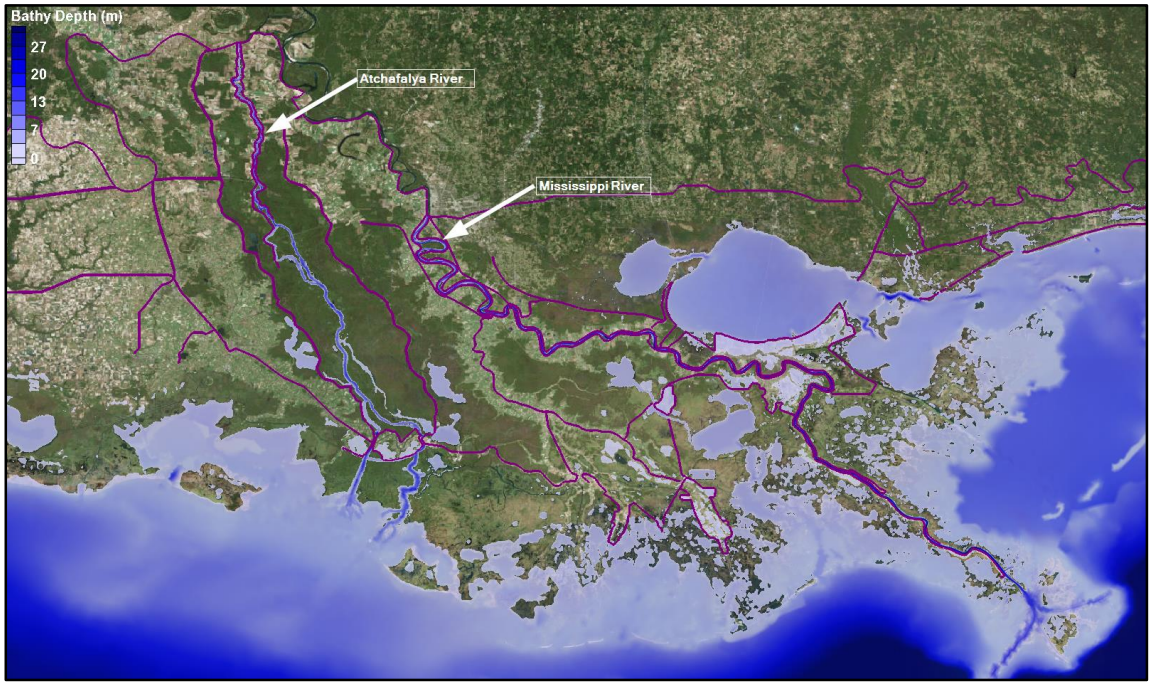

Figure 12-14. Atchafalaya River, Mississippi and Mississippi River, Louisiana.

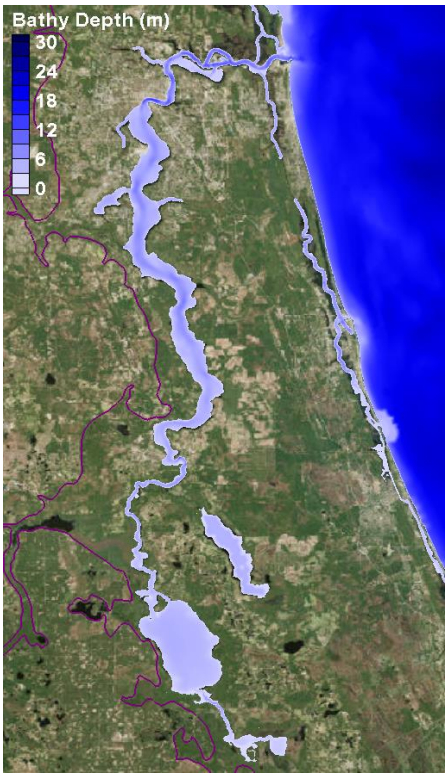

Figure 12-15. St. John's River, Florida.

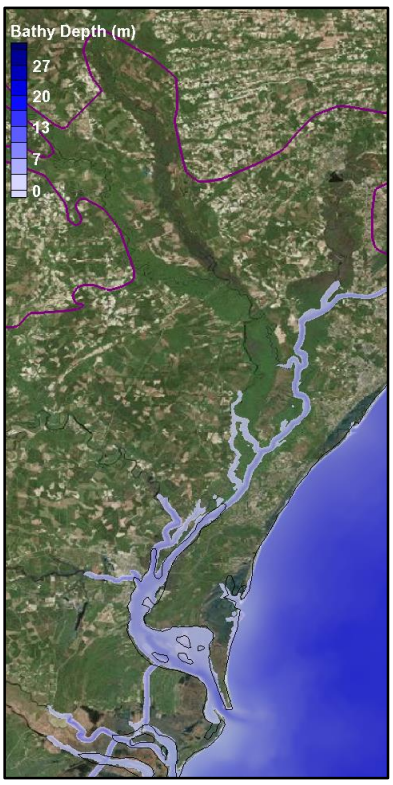

Figure 12-16. Waccamaw River, South Carolina.

Figure 12-17. Tar River, North Carolina.

Figure 12-18. Potomac River, Virginia, Maryland, and Washington D.C.

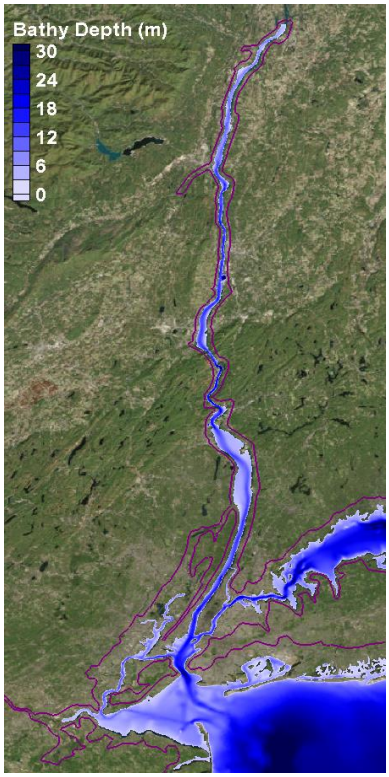

Figure 12-19. Hudson River, New Jersey and New York.

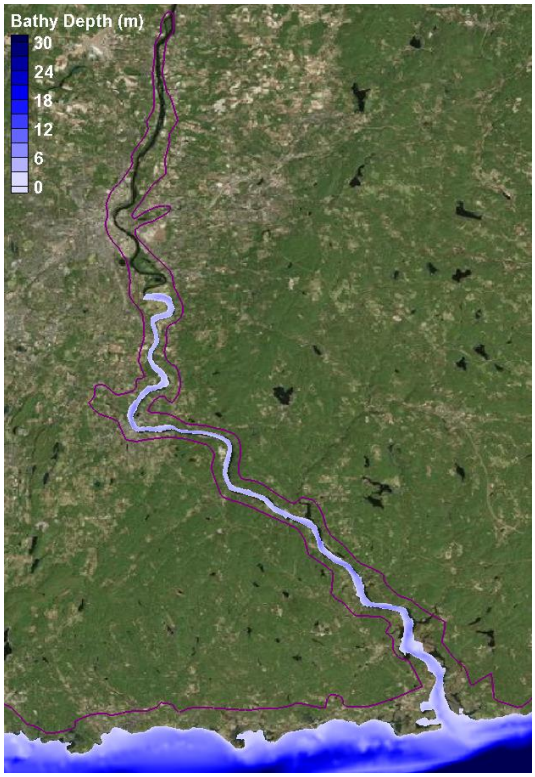

Figure 12-20. Connecticut River, Connecticut.

12.6 Flow Barrier Guidance

Flow barriers were determined primarily based on a review of topographic data and then compared to aerial imagery to confirm the existence of elevated features. Some information from other FEMA study meshes and the National Levee Database were reviewed to help identify major features. In order to simplify the mesh, some areas with steep gradients were not included if it was determined that excluding these features would not generally affect the modeling results. For example, if there were several sequential barriers running parallel to the shoreline, if the seaward-most barrier was high enough, landward barriers may not have been included in detail in the mesh because the seaward-most barrier would provide the most protection against storm surge. Large barriers were included almost everywhere, but small barriers in unpopulated areas were not specifically delineated with feature arcs.

12.7 Topographic Peak Elevation Assignment

The topographic data was reviewed visually to help the mesh developers identify high features. High features were delineated manually. A buffer was created along the high feature line, and focal statistics were applied to extract the elevations at points along the line. Using this technique, the final elevations along the line were smoothed to better capture the average elevation. Figure 12-21 shows a sample high feature where the green line shows the elevations extracted from the terrain data at the exact point location, and the purple line shows the smoothed elevations that were used for the final mesh. An example of peaks selected in Long Island, NY and the final mesh are shown in Figure 12-22.

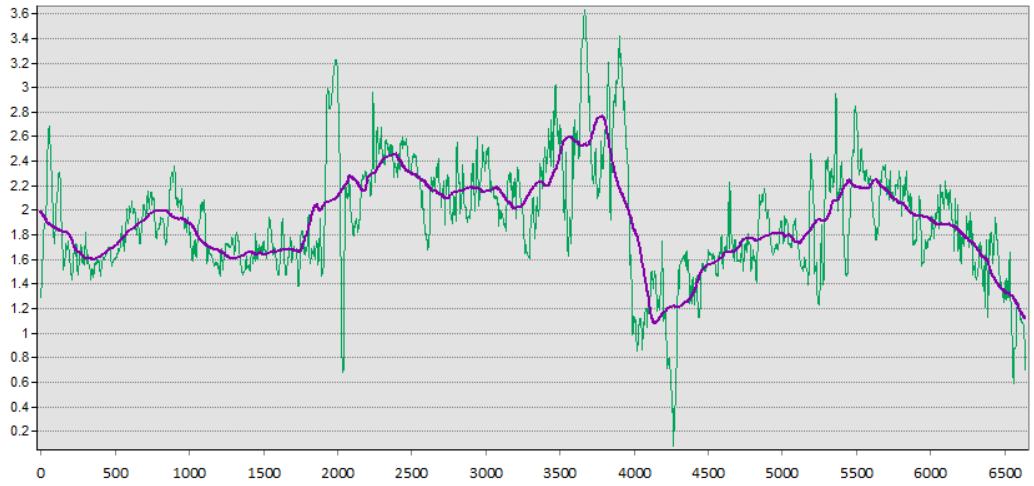

Figure 12-21. Exact elevations (green) and smoothed elevations (purple) along a sample high feature profile.

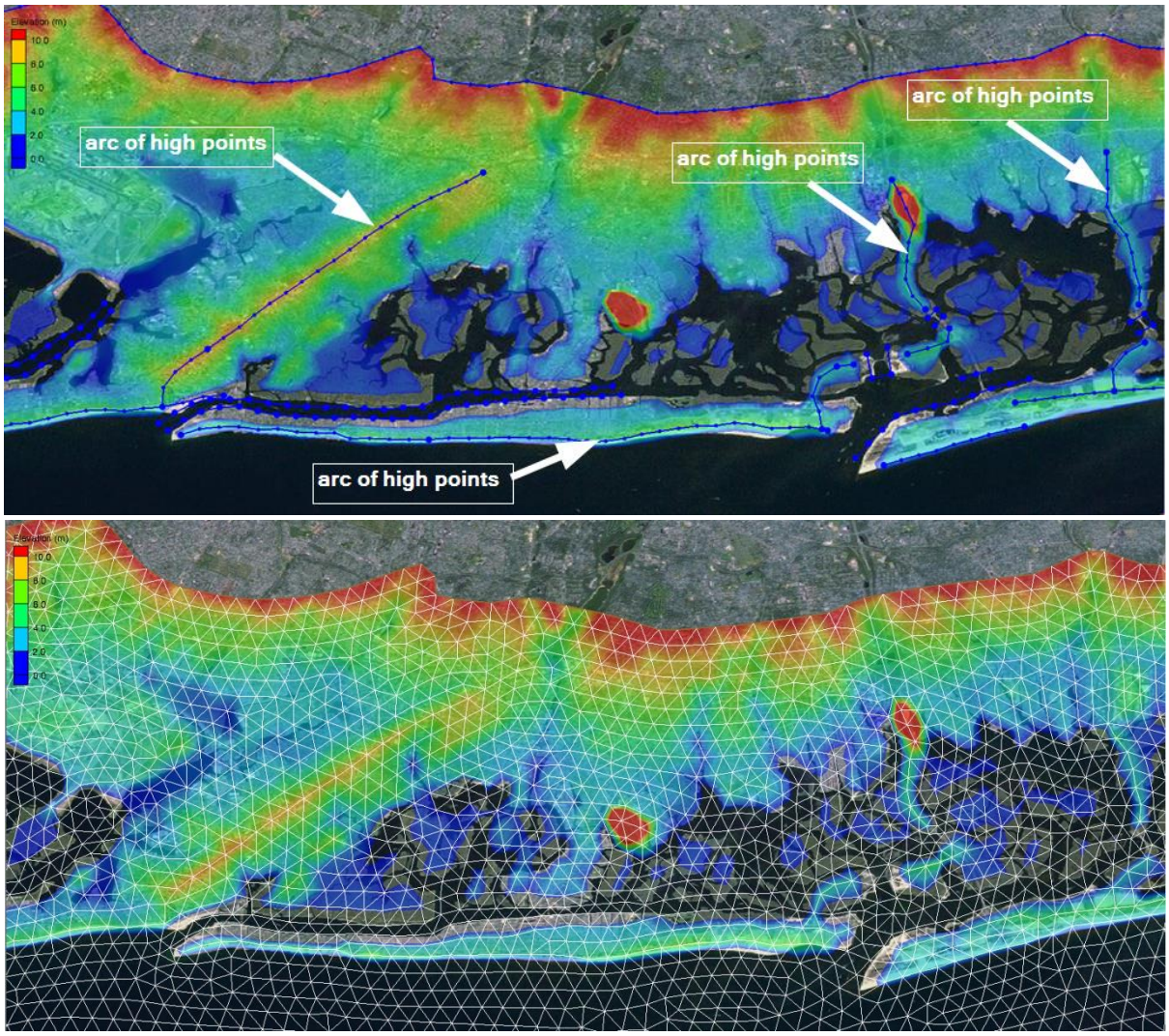

Figure 12-22. Example of feature arcs along high points in Long Island, New York (top image) and final mesh (bottom image).

12.8 General Elevation Assignment

For areas outside the peaks, the topographic data was smoothed using a circular averaging window with a radius of 100 to 300 meters via ArcGIS focal statistics. A Fortran program was used to assign elevations from the smoothed data to the mesh. Similar to the peak elevation assignment program, this program assigns the closest elevation data point from the smoothed topographic DEM to the mesh node.

12.9 Final Mesh

The final mesh has 1,813,443 nodes and 3,564,104 elements and is shown in Figure 12-23. This mesh, along with the feature arcs used for development, are found on the NOAA HPC storage system. Section 12.9.1 gives a number of displays of mesh bathymetry in Figure 12-24 through Figure 12-29. Section 12.9.2 presents the mesh spacing in Figure 12-30 through Figure 12-35.

12.9.1 ***NOMAD mesh topo-bathymetry***

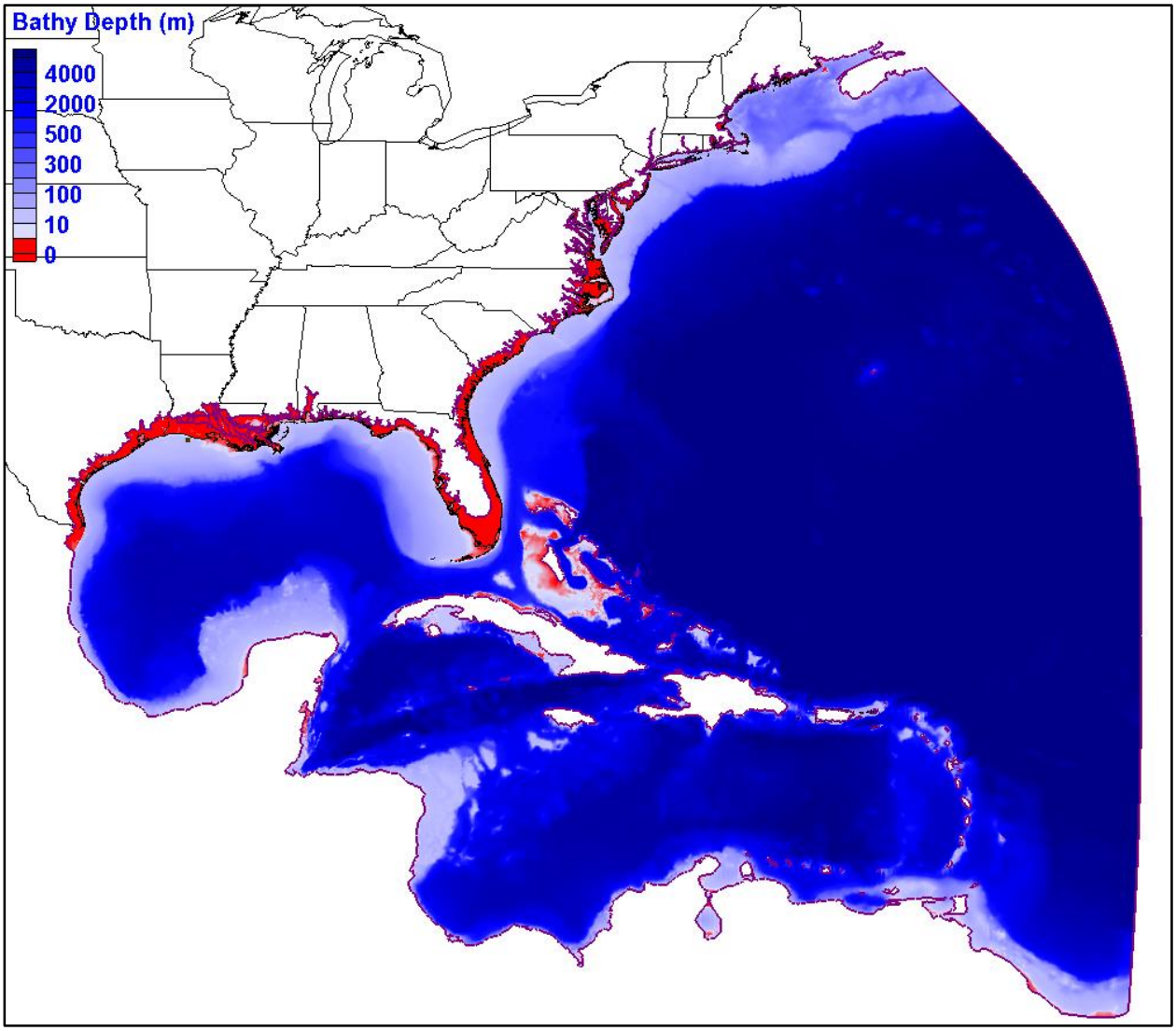

Figure 12-23. Final mesh with topography data in red and bathymetry data in shades of blue.

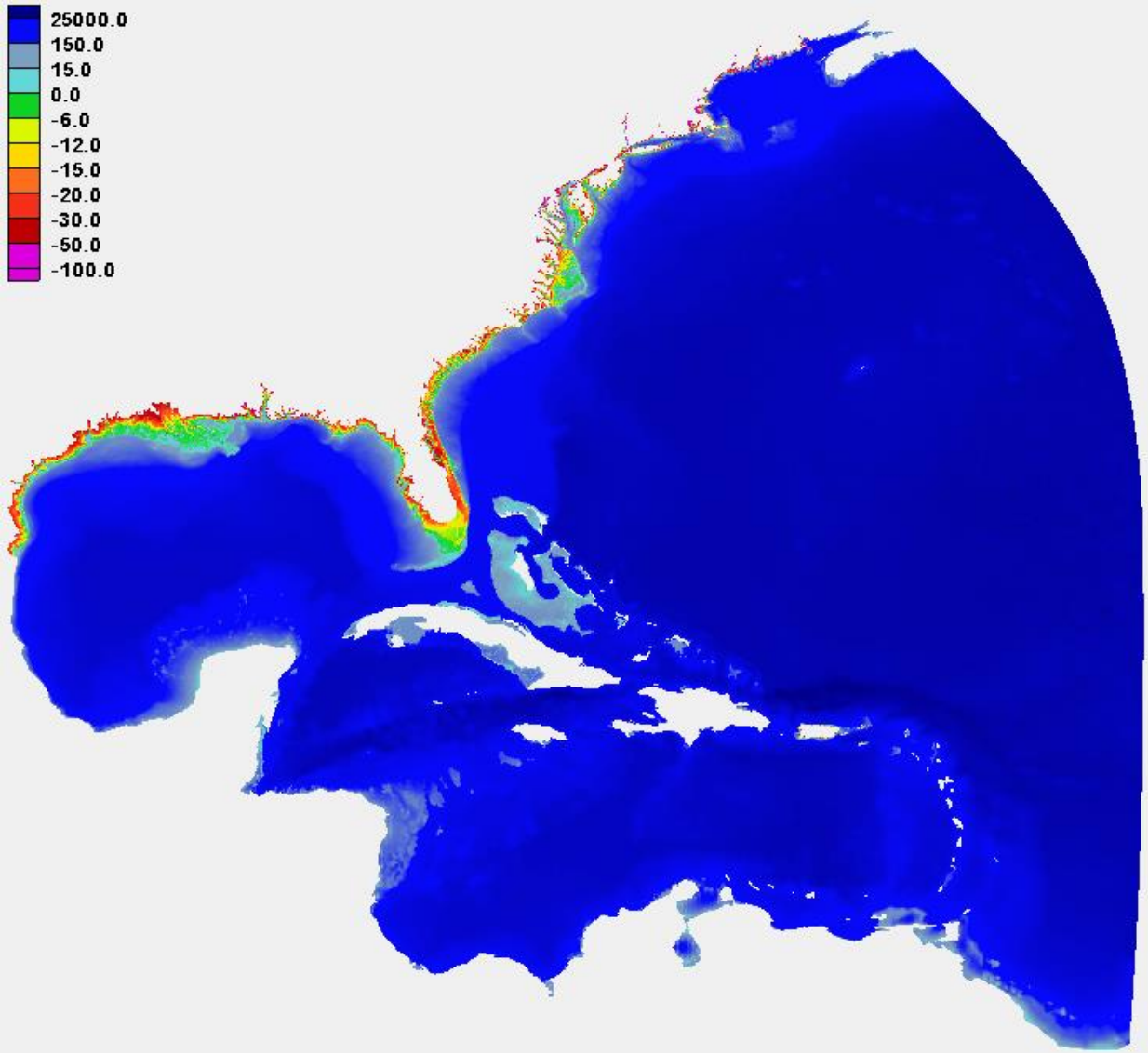

Figure 12-24: Overview of final NOMAD mesh topo-bathymetry (feet MSL)

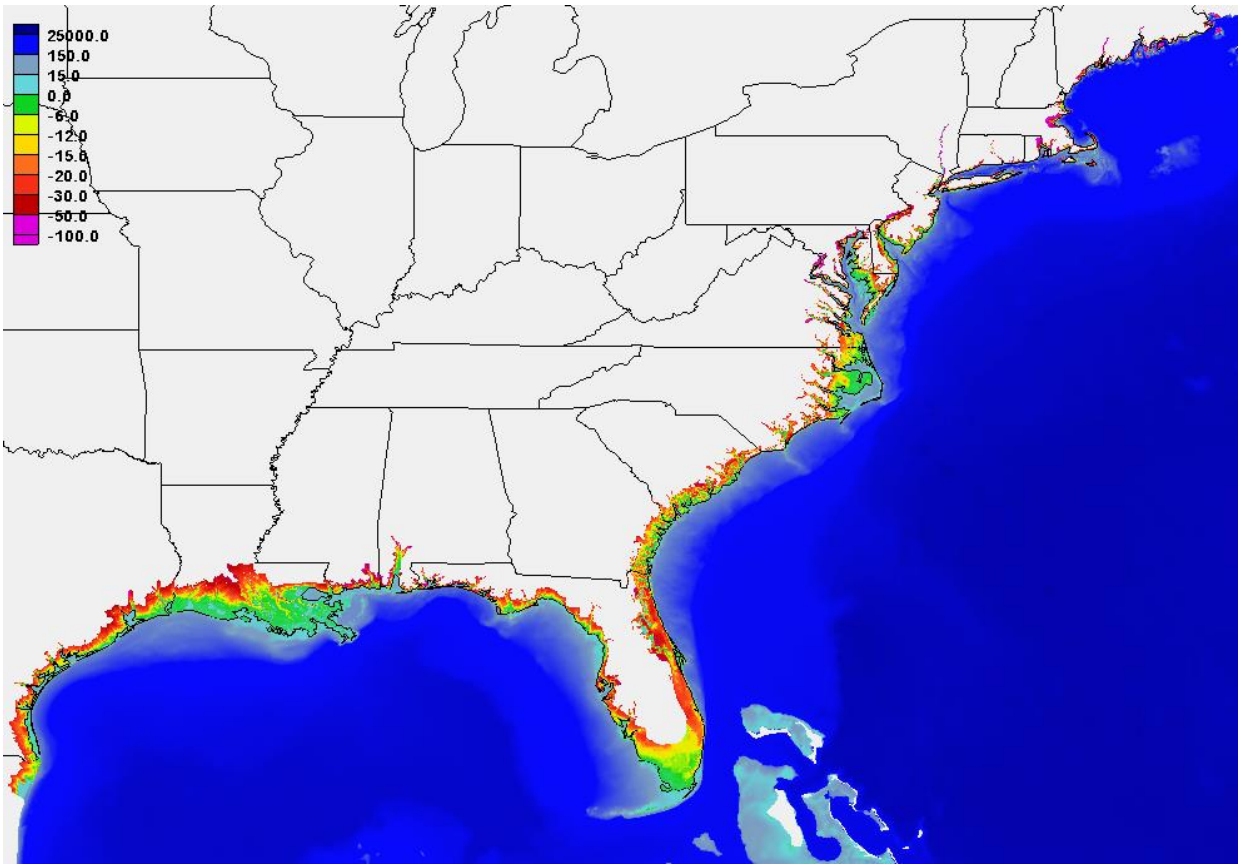

Figure 12-25: NOMAD mesh topo-bathymetry (feet MSL) for US coast

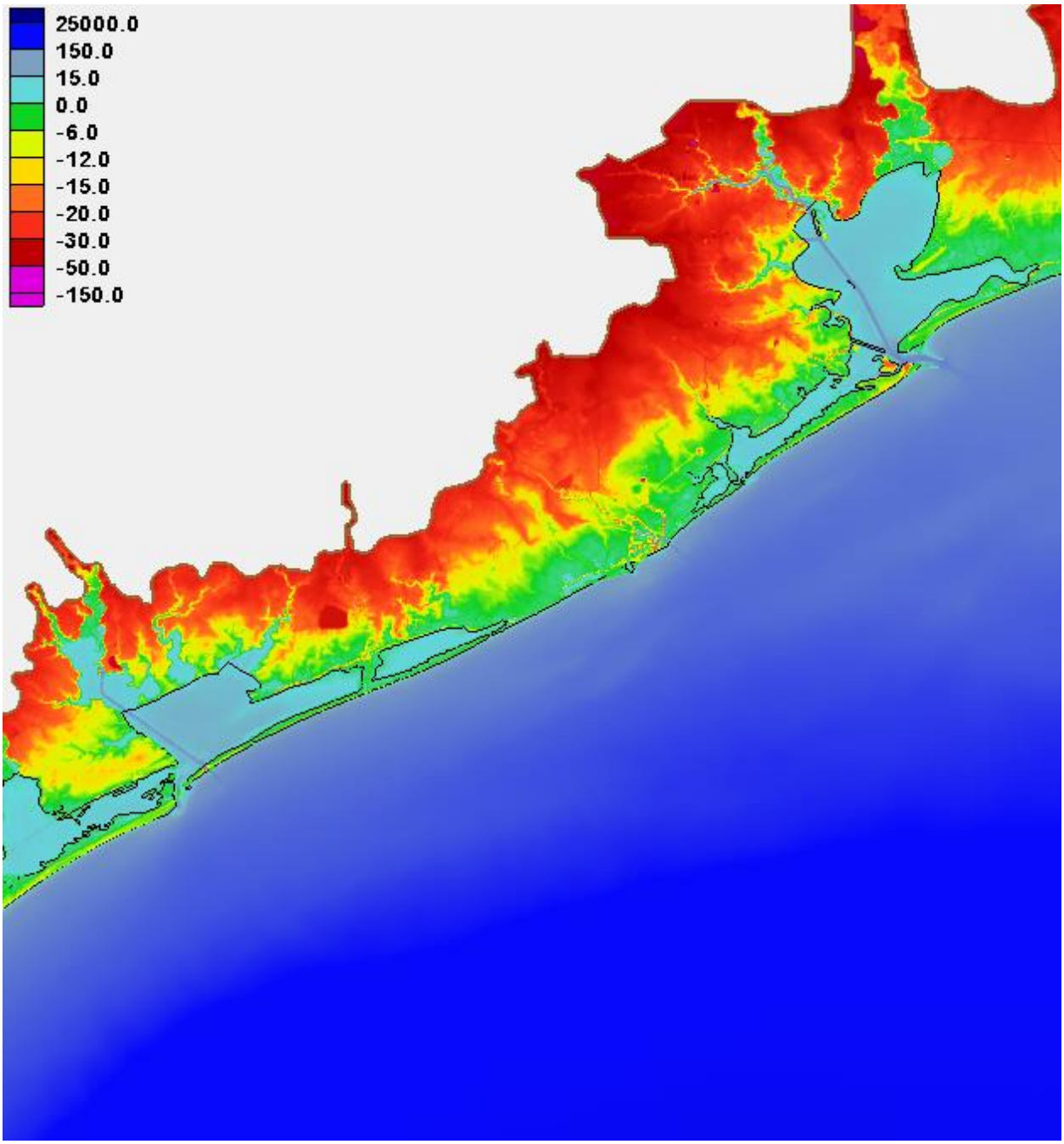

Figure 12-26: NOMAD mesh topo-bathymetry (feet MSL) on Texas coast.

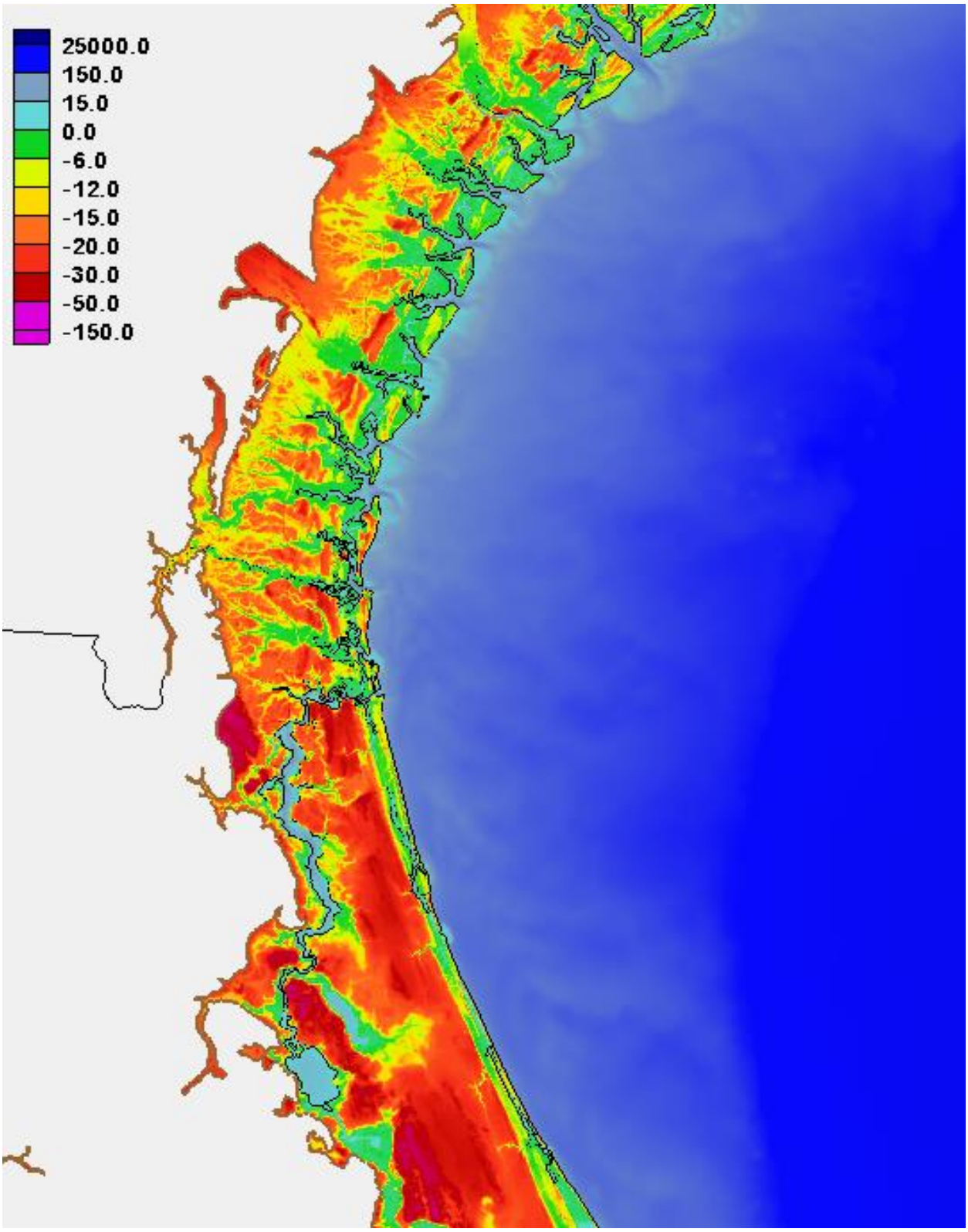

Figure 12-27: NOMAD mesh topo-bathymetry (feet MSL) along Georgia and Florida coast.

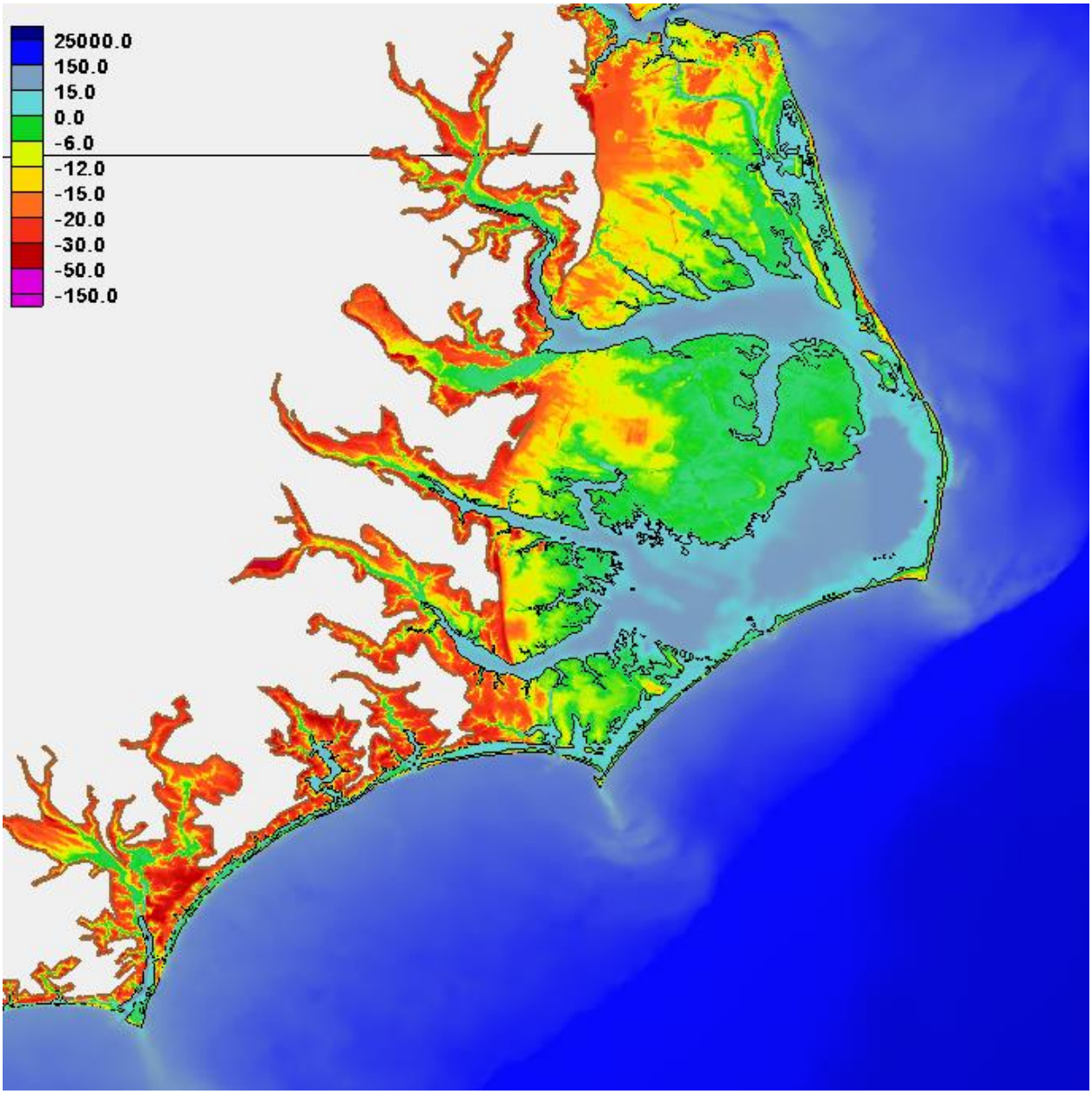

Figure 12-28: NOMAD mesh topo-bathymetry (feet MSL) along Virginia, North Carolina, and South Carolina coast.

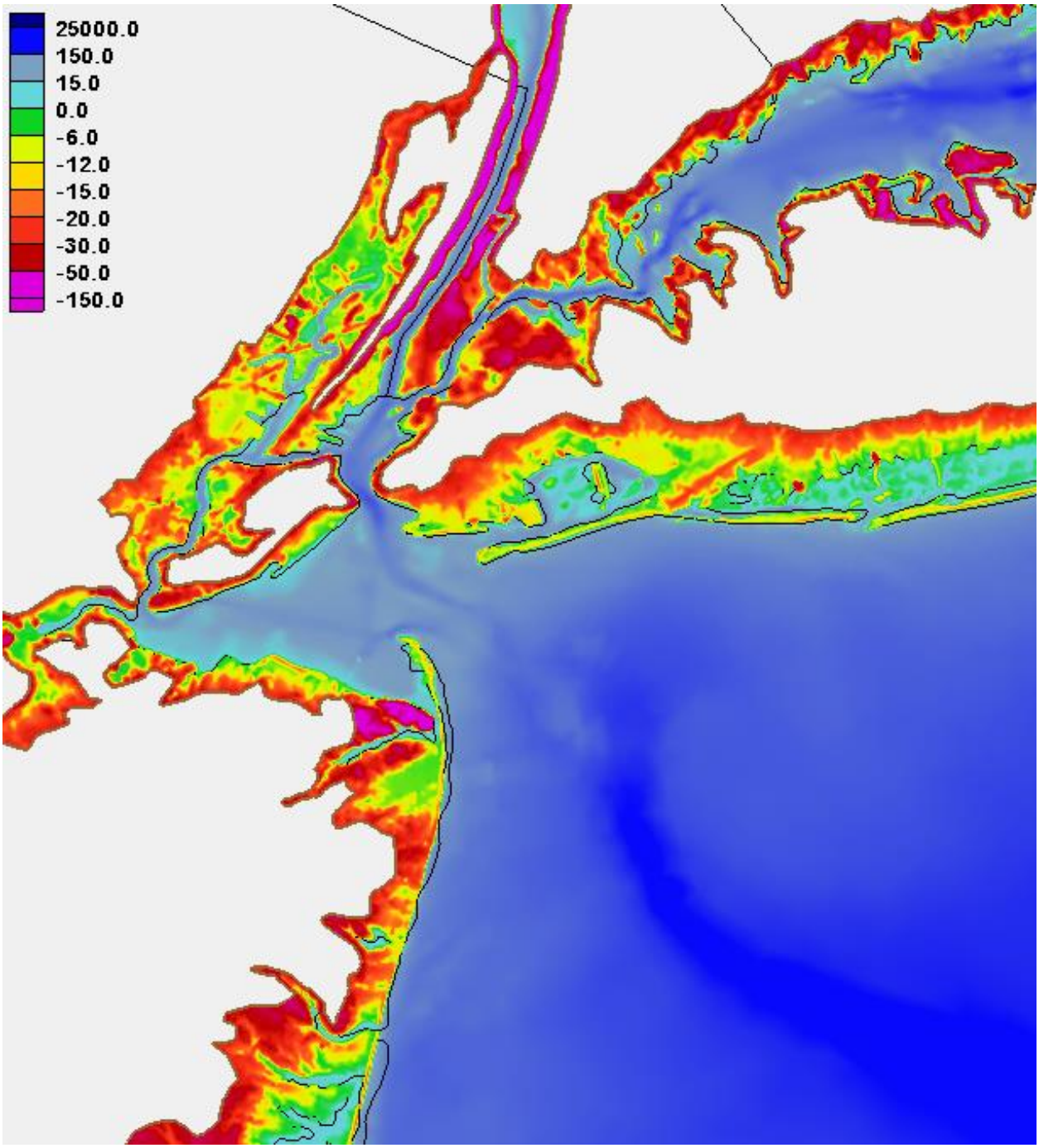

Figure 12-29: NOMAD mesh topo-bathymetry (feet MSL) in the area of New York City.

12.9.2 *NOMAD mesh node spacing*

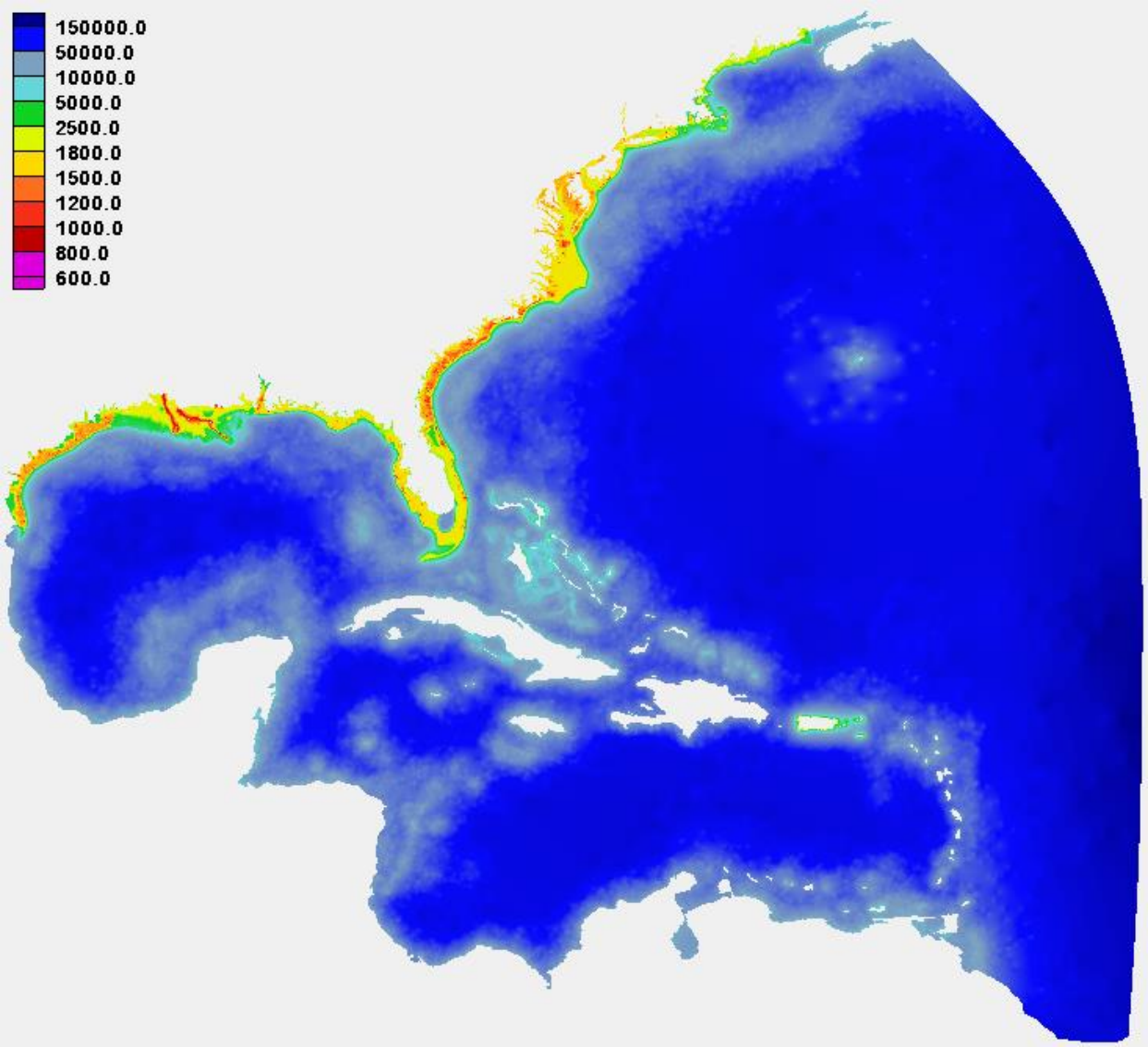

Figure 12-30: Overview of NOMAD mesh node spacing (feet).

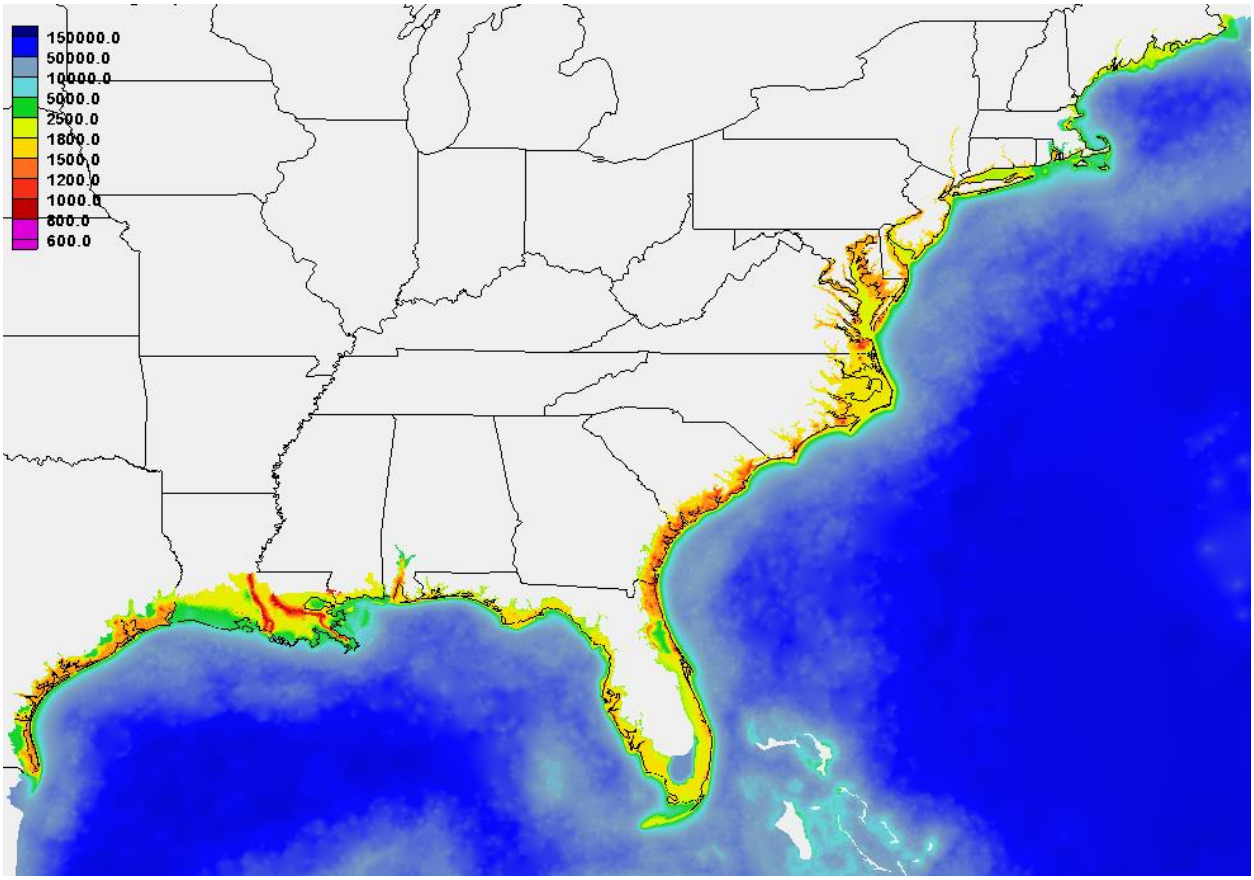

Figure 12-31: NOMAD mesh node spacing (feet) along US coast.

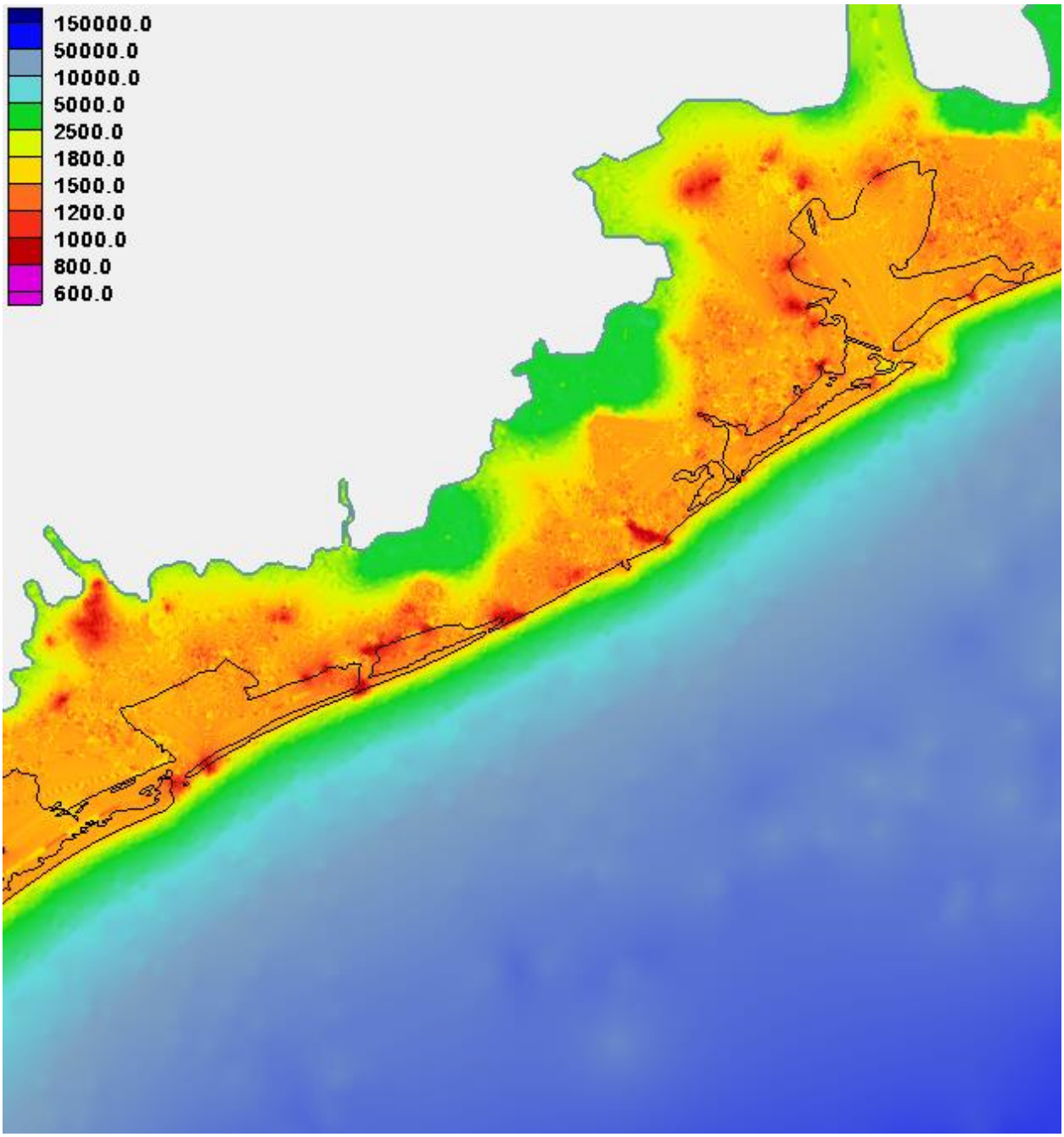

Figure 12-32: NOMAD mesh node spacing (feet) on Texas coast.

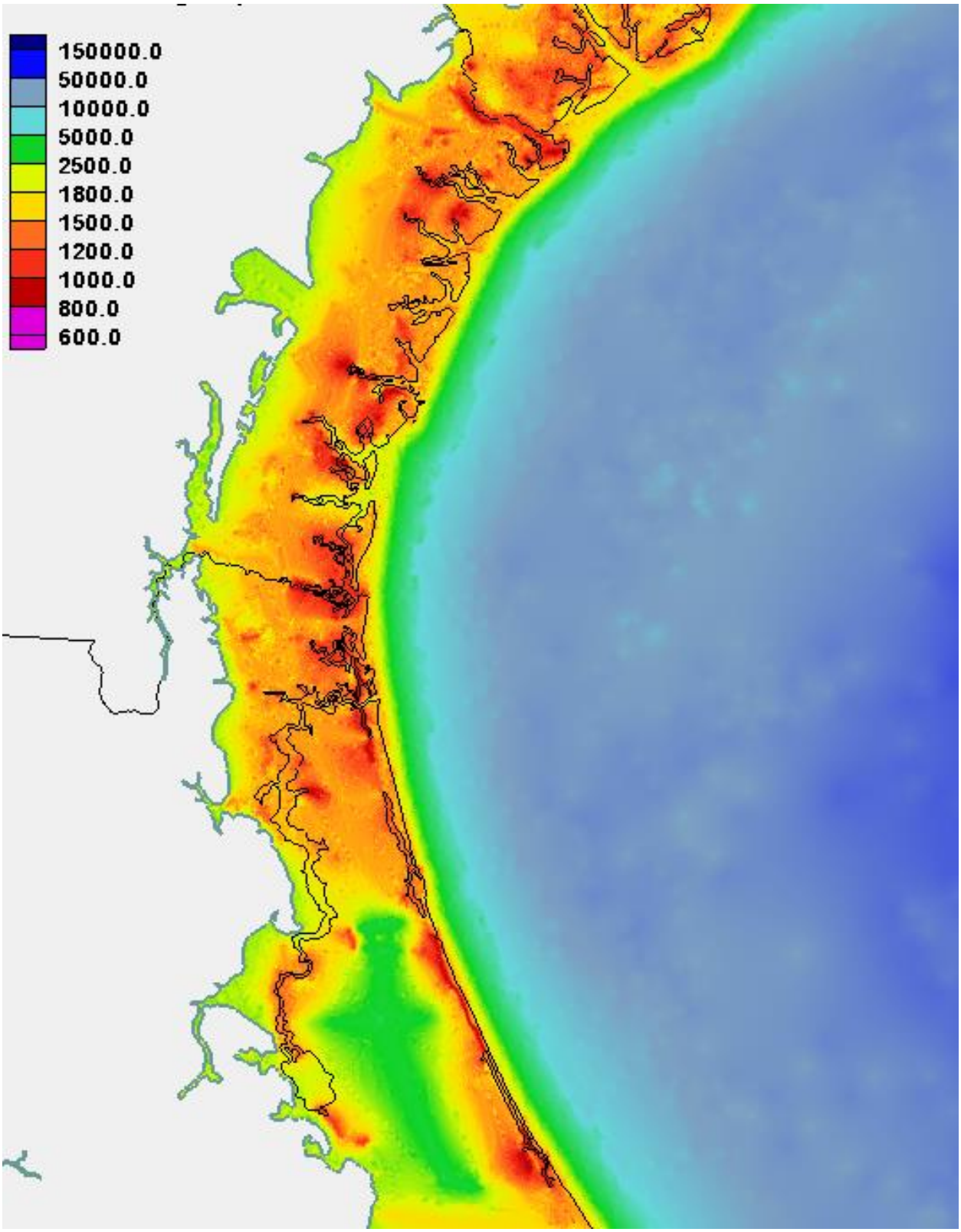

Figure 12-33: NOMAD Mesh node spacing (feet) along Georgia and Florida coast.

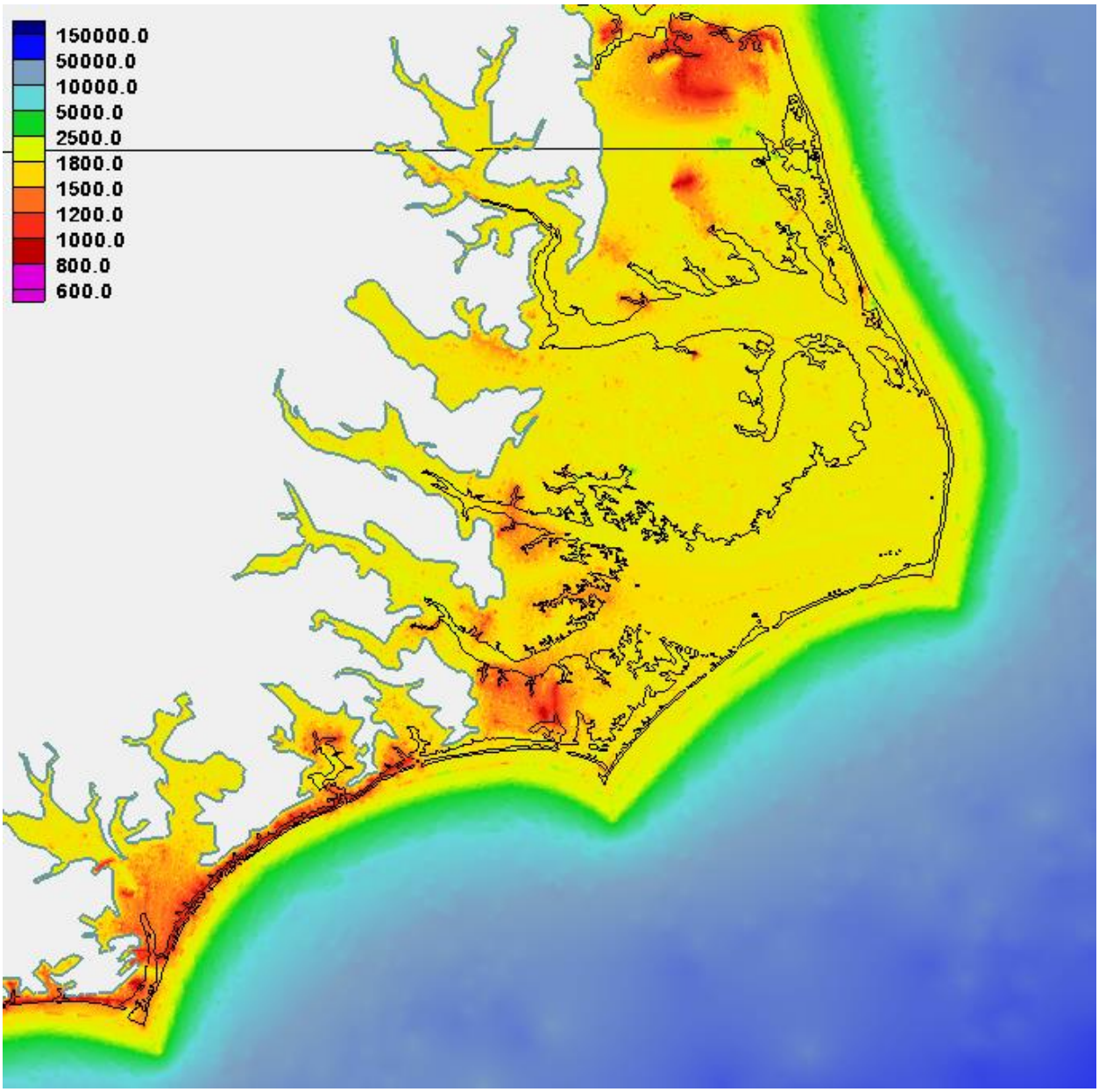

Figure 12-34: NOMAD mesh node spacing (feet) along Virginia, North Carolina, and South Carolina coast.

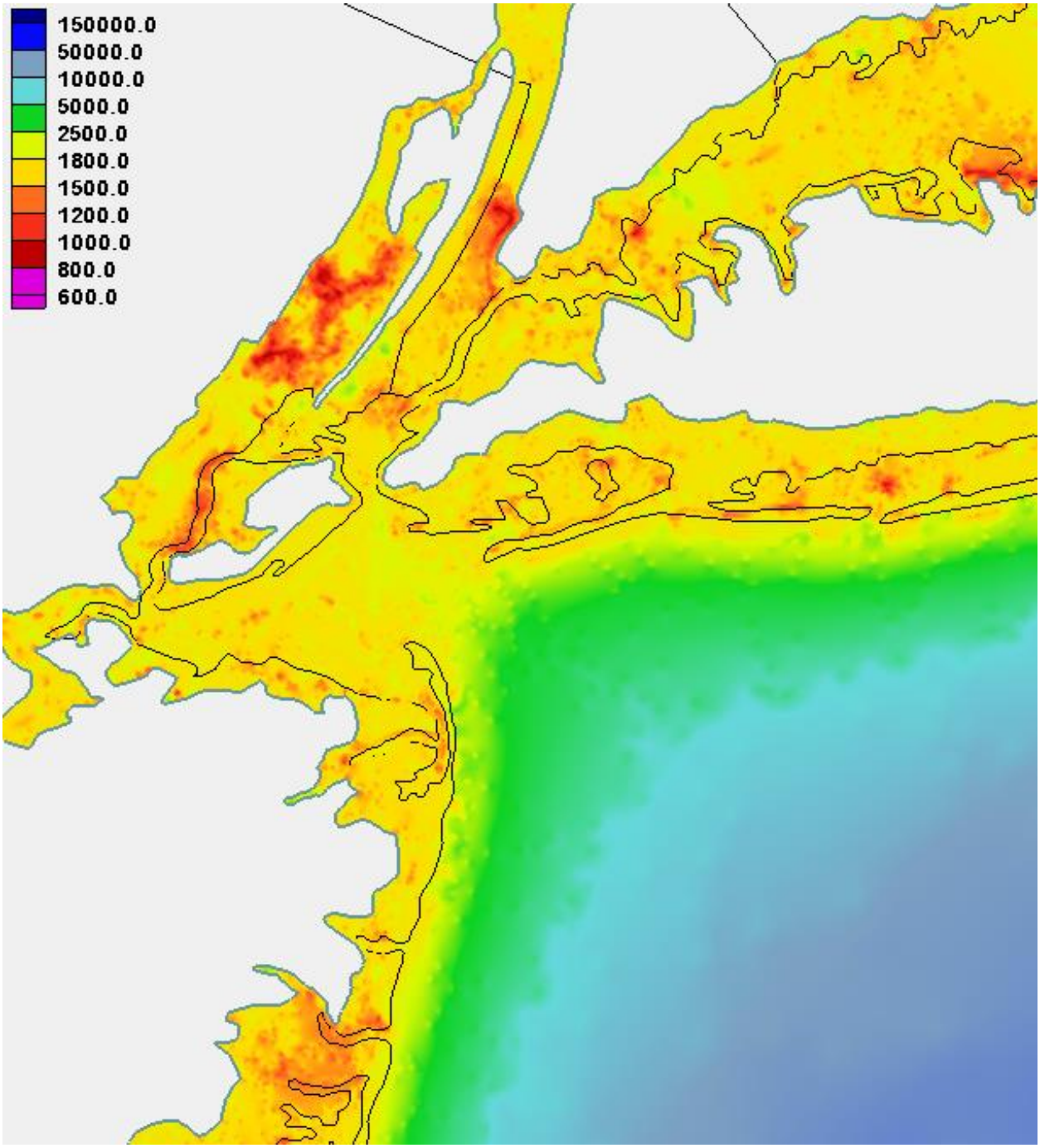

Figure 12-35: NOMAD mesh node spacing (feet) in the area of New York City.

13. **APPENDIX C – LIST OF STATIONS FOR SKILL ASSESSMENT**

The following table documents which stations from the Szpilka database were used for skill assessment. Some of the stations had only 1 hour data available as noted in the table.

Lon	Lat	Station ID	Name	Tidal	Ike	Katrina	Dennis	Charley	Hugo	Floyd	Isabel	Sandy	1938	1991
-64.7033	32.3734	2695540	BERMUDA ESSO PIER, ST. GEORGES ISLAND	T										
-66.9829	44.9046	8410140	EASTPORT, PASSAMAQUODDY BAY	T						6				
-67.1084	44.8705	8410714	COFFIN POINT, COFFIN NECK (moved 11/16 was -67.1083 44.87)	T										
-67.13	44.9233	8410715	GARNET POINT, HERSEY NECK	T										
-67.1438	45.1289	8410834	PETTEGROVE POINT, DOCHET ISLAND (mvd 11/16 was -67.14467 45.12844)	T										
-67.1517	44.8233	8410864	GRAVELLY PT., WHITING BAY	T										
-67.2092	44.6564	8411060	CUTLER FARRIS WHARF, LITTLE RIVER (mvd 11/6 was -67.21 44.65670)	T										
-67.2967	44.6417	8411250	CUTLER NAVAL BASE, MACHIAS BAY	T						6				
-67.875	44.54	8412581	MILBRIDGE, NARRAGUAGUS RIVER	T										
-68.205	44.3917	8413320	BAR HARBOR, FRENCHMAN BAY	T						6				
-68.435	44.17	8413825	MACKEREL COVE, SWANS ISLAND	T										
-68.6209	44.1923	8414249	OCEANVILLE, DEER ISLAND	T										
-68.7719	44.7877	8414612	BANGOR, PENOBSCOT RIVER (mvd 11/16 was -68.7667 44.785)	T										
-68.8133	44.4717	8414721	FORT POINT, PENOBSCOT RIVER	T										
-68.8884	44.1608	8414888	PULPIT HARBOR, PENOBSCOT BAY (mvd 11/16 was -68.8867 44.1567)	T										
-69.1017	44.105	8415490	ROCKLAND	T										
-69.1817	44.0714	8415709	THOMASTON, ST GEORGE RIVER (mvd 11/16 was -69.1817 44.0717)	T										
-69.785	43.755	8417177	HUNNIWELL POINT, KENNEBEC RIVER	T										
-69.7971	44.0872	8417208	RICHMOND, KENNEBEC RIVER (mvd 11/16 was -69.7983 44.0883)	T										
-69.8088	43.925	8417227	BATH, KENNEBEC RIVER (mvd 11/16 was -69.815 43.925)	T										
-70.246	43.6561	8418150	PORTLAND, CASCO BAY (mvd 11/16 was -70.2467 43.6567)	T						6			1h	
-70.3333	43.54	8418445	PINE POINT, SCARBOROUGH RIVER (mvd 11/16 was -70.3333 43.545)	T										
-70.3817	43.4617	8418606	CAMP ELLIS, SACO RIVER	T										
-70.563	43.3197	8419317	WELLS, WEBHANNET RIVER (mvd 11/16 was -70.56331 43.32)	T										
-70.7417	43.08	8419870	SEAVEY ISLAND, PORTSMOUTH HARBOR	T										
-70.7117	43.0718	8423898	FORT POINT, NEWCASTLE ISLAND (mvd 11/16 was -70.7117 43.0717)	T										
-70.908	42.836	8440273	SALISBURY POINT, MERRIMACK RIVER (mvd 11/16 was -70.9083 42.8383)	T										
-70.82	42.8167	8440452	PLUM ISLAND, MERRIMACK RIVER ENTRANCE	T										
-70.8733	42.815	8440466	NEWBURYPORT, MERRIMACK RIVER	T										
-70.6151	42.6603	8441551	ROCKPORT HARBOR (mvd 11/16 was -70.615 42.65830)	T										
-70.8765	42.523	8442645	SALEM, SALEM HARBOR (mvd 11/16 was -70.8767 42.5233)	T										
-70.9433	42.4583	8443187	LYNN, LYNN HARBOR	T										
-71.0472	42.3575	8443970	BOSTON, BOSTON HARBOR (mvd 11/16 was -71.0534 42.3548)	T						6			1h	1h
-70.8917	42.3283	8444162	BOSTON LIGHT, BOSTON HARBOR	T										
-70.9533	42.28	8444525	NUT ISLAND, QUINCY BAY	T										
-70.9667	42.2483	8444788	SHIPYARD POINT, WEYMOUTH FORE RIVER	T										
-70.7248	42.201	8445138	SCITUATE, SCITUATE HARBOR (mvd 11.16 was -70.7267 42.2017)	T										
-70.6387	42.0833	8446009	BRANT ROCK, GREEN HARBOR RIVER (mvd 11/16 was -70.6467 42.0833)	T										
-70.1822	42.0496	8446121	PROVINCETOWN, CAPE COD	T										
-70.6679	42.0383	8446166	DUXBURY, DUXBURY HARBOR (mvd 11/16 was -70.67 42.0383)	T										
-70.6617	41.96	8446493	PLYMOUTH, PLYMOUTH HARBOR	T										
-70.535	41.775	8447173	SAGAMORE, CAPE COD CANAL (STA. 115)	T										
-70.5617	41.77	8447191	BOURNEDALE, CAPE COD CANAL (STA. 200)	T										
-70.1555	41.756	8447241	SESUIT HARBOR, EAST DENNIS (mvd 11/16 was -70.155 41.7517)	T										
-70.5934	41.7459	8447259	BOURNE BRIDGE, CAPE COD CANAL (STA. 320) (mvd 11/16 was -70.5933 1.745)	T										
-70.6167	41.7417	8447270	BUZZARDS BAY (RR BRIDGE), CAPE COD CANAL	T										
-70.6243	41.735	8447295	GRAY GABLES, BUZZARDS BAY	T										
-70.715	41.7117	8447368	GREAT HILL	T										
-71.1655	41.7058	8447386	FALL RIVER, HOPE BAY (mvd 11/16 was -71.1641 41.7043)	T										
-70.7194	41.6958	8447416	PINEY POINT, WINGS COVE (mvd 11/16 was -70.72 41.695)	T										
-69.9489	41.6885	8447435	CHATHAM, LYDIA COVE (mvd 11/16 was -69.95108 41.68847)	T										
-70.0567	41.6648	8447495	SAQUATUCKET HARBOR (mvd 11/16 was -70.0567 41.6683)	T										
-70.8998	41.5929	8447712	NEW BEDFORD, CLARKS POINT (mvd 11/16 was -70.9 41.5933)	T										
-70.9283	41.5383	8447842	ROUND HILL POINT	T										
-70.6717	41.5233	8447930	WOODS HOLE, BUZZARDS BAY	T						6				1h
-70.5987	41.4583	8448157	VINEYARD HAVEN, VINEYARD HVN HBR (mvd 11/16 was -70.6 41.4583)	T										
-70.5115	41.3882	8448558	EDGARTOWN, MARTHA'S VINEYARD (mvd 11/16 was -70.5117 41.3883)	T										
-70.768	41.3546	8448725	MENEMSHA HARBOR	T										
-70.0944	41.285	8449130	NANTUCKET ISLAND, NANTUCKET SOUND (mvd 11/16 was -70.0967 41.285)	T						6				1h
-71.255	41.6367	8451552	BRISTOL FERRY	T										
-71.3267	41.505	8452660	NEWPORT, NARRAGANSETT BAY	T						6			1h	1h
-71.3433	41.7167	8452944	CONIMICUT LIGHT, NARRAGANSETT BAY	T										
-71.3867	41.4967	8453742	WEST JAMESTOWN	T										
-71.3998	41.8079	8454000	PROVIDENCE, PROVIDENCE RIVER (mvd 11/16 was -71.4012 41.8071)	T						6				1h
-71.411	41.5868	8454049	QUONSET POINT	T										
-71.4435	41.5738	8454538	WICKFORD, NARRAGANSETT BAY (mvd 11/16 was -71.445 41.5717)	T										
-71.49	41.3633	8455083	POINT JUDITH, HARBOR OF REFUGE	T										1h
-71.7617	41.3283	8458022	WEEKAPAUG POINT, BLOCK ISLAND SOUND	T										
-71.5562	41.174	8459338	BLOCK ISLAND HARBOR, OLD HARBOR (mvd 11/16 was -71.5567 41.1733)	T										
-71.58	41.2283	8459479	SANDY POINT, BLOCK IS, SOUND	T										

-71.6106	41.1633	8459681	BLOCK ISLAND, SW END, BLOCK ISLAND SOUND	T												
-72.0898	41.3611	8461490	NEW LONDON, THAMES RIVER (mvd 11/16 was -72.08997 41.36139)	T						6			1h	1h
-72.5317	41.2683	8463701	CLINTON, CLINTON HARBOR	T										
-72.9083	41.2833	8465705	NEW HAVEN, NEW HAVEN HARBOR	T										
-73.1817	41.1733	8467150	BRIDGEPORT, BRIDGEPORT HARBOR	T						6				1h
-73.2133	41.1567	8467373	BLACK ROCK HARBOR, CEDAR CREEK	T										
-73.2829	41.1325	8467726	SOUTHPORT, SOUTHPORT HARBOR (mvd 11/16 was -73.2833 41.1333)	T										
-73.48	41.0383	8468799	LONG NECK POINT, LONG ISLAND SOUND	T										
-71.8559	41.072	8510321	MONTAUK POINT LIGHT	T										
-71.935	41.0733	8510448	U.S. COAST GUARD STATION, LAKE MONTAUK	T										
-71.96	41.0483	8510560	MONTAUK, FORT POND BAY	T						6				1h
-72.0319	41.2579	8510719	SILVER EEL POND, FISHERS IS.	T										
-72.19	41.035	8511171	THREEMILE HARBOR ENTRANCE	T										
-72.2052	41.1713	8511236	PLUM ISLAND PLUM GUT HARBOR	T										
-72.3067	41.1367	8511671	ORIENT, ORIENT HARBOR	T										
-72.5617	41.015	8512668	MATTITUCK INLET, LONG ISLAND	T										
-72.5817	40.9347	8512735	SOUTH JAMESPORT, GREAT PECONIC BAY	T										
-72.5867	40.8183	8512769	SHINNECOCK YACHT CLUB, PENNIMAN CREEK (mvd 3/2014 - was -72.5833)	T										
-72.645	40.9817	8512987	NORTHVILLE FUEL DOCK, LONG ISLAND	T										
-72.8683	40.7383	8513825	SMITH POINT BRIDGE, NARROW BAY	T										
-73	40.7478	8514322	PATCHOGUE, PATCHOGUE RIVER	T										
-73.0433	40.965	8514422	CEDAR BEACH	T										
-73.3533	40.9	8515586	NORTHPORT, NORTHPORT BAY	T										
-73.4	40.9533	8515786	EATONS NECK, HUNTINGTON BAY	T										
-73.4317	40.91	8515921	LLOYD HARBOR LIGHTHOUSE	T										
-73.47	40.8733	8516061	COLD SPRINGS HARBOR	T										
-73.55	40.9033	8516299	BAYVILLE BRIDGE, OYSTER BAY	T										
-73.655	40.8633	8516614	GLEN COVE YACHT CLUB, LONG ISLAND	T										
-73.7033	40.8317	8516761	PORT WASHINGTON, MANHASSSET BAY	T										
-73.7649	40.8103	8516945	KINGS POINT, LONG ISLAND SOUND	T						6		6		
-73.7817	40.7933	8516990	WILLETS POINT, LITTLE BAY, EAST RIVER	T									1h	1h
-73.8567	40.7833	8517276	COLLEGE PT, FT. OF 110TH ST, LI	T										
-73.9952	40.7037	8517847	BROOKLYN BRIDGE, EAST RIVER	T										
-73.6717	40.9617	8518091	RYE BEACH, AMUSEMENT PARK	T										
-73.9063	40.8013	8518639	PORT MORRIS, EAST 138TH ST.	T										
-73.9417	40.7767	8518668	HORNS HOOK, E. 90TH STREET, HELL GATE	T										
-73.9583	40.7583	8518687	QUEENSBORO BRIDGE, EAST RIVER	T										
-73.9696	40.7117	8518699	WILLIAMSBURG BRIDGE	T										
-74.0144	40.7002	8518750	THE BATTERY, NEW YORK HARBOR	T						6		6	1h	1h
-73.925	40.8783	8518903	SPUYTEN DUYVIL CK, ENT., HUDSON R,	T										
-73.9167	40.9033	8518905	RIVERDALE, HUDSON RIVER	T										
-73.9633	41.2183	8518924	HAVERSTRAW BAY	T										
-74.1423	40.6398	8519483	BERGEN POINT WEST REACH, KILL VAN KULL	T						6		6		1h
-74.0094	40.4669	8531680	SANDY HOOK	T						6		6	1h	1h
-74.4183	39.355	8534720	ATLANTIC CITY, ATLANTIC OCEAN	T						6	6	6	1h	1h
-74.4767	39.335	8534770	VENTNOR CITY, FISHING PIER	T										1h
-74.5333	39.3083	8534836	LONGPORT, RISELY CHANNEL	T										
-74.96	38.9683	8536110	CAPE MAY, CAPE MAY CANAL, DELAWARE BAY	T						6	6	6		1h
-74.8917	39.1283	8536581	BIDWELL CREEK ENTRANCE, DELAWARE BAY	T										
-75.175	39.2383	8536931	FORTESCUE CREEK	T										
-75.375	39.305	8537121	SHIP JOHN SHOAL, DELAWARE RIVER	T							6	6		
-75.043	40.0119	8538886	TACONY-PALMYRA BRIDGE	T							6	6		
-74.8697	40.0817	8539094	BURLINGTON, DELAWARE RIVER	T							6	6		
-74.7367	40.1367	8539487	FIELDSBORO, DELAWARE RIVER	T										
-74.755	40.1883	8539993	TRENTON MARINE TERMINAL	T										1h
-75.41	39.8117	8540433	MARCUS HOOK	T							6	6		
-75.1409	39.9333	8545240	PHILADELPHIA (USCG STA.), DELAWARE RIVER	T						6	6	6		1h
-75.1383	39.9533	8545530	PHILADELPHIA (PIER 11 NORTH), DEL. RIVER	T									1h	
-74.7517	40.1367	8548989	NEWBOLD, DELAWARE RIVER	T							6	6		
-75.5883	39.5817	8551762	DELAWARE CITY, DELAWARE RIVER	T							6	6		
-75.5733	39.5587	8551910	REEDY POINT, C&D CANAL	T						6	6	6		1h
-75.4	39.185	8554399	MAHON RIVER ENTRANCE, DELAWARE BAY	T										
-75.1133	38.9867	8555889	BRANDYWINE SHOAL LIGHT, DELAWARE BAY	T							6	6		
-75.12	38.782	8557380	LEWES, FT. MILES	T						6	6	6		1h
-75.07	38.61	8558690	INDIAN RIVER INLET	T										
-75.0833	38.3267	8570280	OCEAN CITY, FISHING PIER	T										1h
-75.0917	38.3283	8570283	OCEAN CITY INLET	T							6	6		
-75.1891	38.2152	8570536	SOUTH POINT, SINEPUXENT NECK, CHINC. BAY	T										
-75.285	38.1483	8570649	PUBLIC LANDING, CHINCOTEAGUE BAY	T										
-75.8633	37.9767	8571091	CRISFIELD	T										
-76.029	37.9983	8571117	EWELL, SMITH ISLAND	T										
-76.0383	38.22	8571421	BISHOPS HEAD, HOOPERS STRAIT	T								6		
-76.005	38.3	8571559	MCCREADYS CREEK, FISHING BAY	T										
-76.265	38.3417	8571579	BARREN ISLAND, CHESAPEAKE BAY	T										
-75.8193	38.484	8571773	VIENNA, NANICOKE RIVER	T										
-76.0682	38.5735	8571892	CAMBRIDGE, CHOPTANK RIVER	T						6	6	6		1h
-76.3733	38.8367	8572467	KENT POINT, CHESAPEAKE BAY	T										
-75.945	38.9167	8572669	HILLSBORO, TUCKAHOE CREEK	T										
-76.355	38.9567	8572770	MATAPEAKE	T										
-76.3011	39.0317	8572955	LOVE POINT PIER, KENT ISLAND	T										
-75.925	39.245	8573349	CRUMPTON, CHESTER RIVER	T										
-76.2458	39.2133	8573364	TOLCHESTER BEACH, CHESAPEAKE BAY	T						6	6	6		
-76.0633	39.3717	8573704	BETTERTON, SASSAFRAS RIVER	T										
-75.9167	39.5033	8573903	TOWN POINT WHARF	T										1h

-75.81	39.5277	8573927	CHESAPEAKE CITY	T							6	6			
-76.09	39.5367	8574070	HAVRE DE GRACE, CHESAPEAKE BAY	T											1h
-76.255	39.3883	8574459	POND POINT (ABERDEEN P.G.), BUSH RIVER	T											
-76.5783	39.2667	8574680	BALTIMORE, FORT MCHENRY, PATAPSCO RIVER	T						6	6	6	1h	1h	
-76.585	39.2617	8574683	FORT MCHENRY MARSH, PATAPSCO RIVER	T											
-76.481	38.9844	8575512	U.S. NAVAL ACADEMY, SEVERN R., CHES. BAY	T						6	6	6	1h	1h	
-76.4726	38.4658	8577004	LONG BEACH, CHESAPEAKE BAY	T											
-76.3964	38.3934	8577188	COVE POINT	T											
-76.4517	38.3167	8577330	SOLOMONS ISLAND, PATUXENT RIVER	T						6	6	6		1h	
-76.6833	38.655	8579542	LOWER MARLBORO, PATUXENT RIVER	T											
-77.0217	38.8733	8594900	WASHINGTON, POTOMAC RIVER	T						6	6	6	1h	1h	
-75.4052	37.907	8630308	CHINCOTEAGUE CHANNEL, SOUTH END	T											
-75.9884	37.1652	8632200	KIPTOPEKE, CHESAPEAKE BAY	T						6	6	6			
-76.0245	37.2633	8632366	CAPE CHARLES HBR (U.S. G. WHARF)	T											
-76.015	37.5383	8632837	RAPPAHANNOCK LIGHT	T											
-75.9167	37.5567	8632869	GASKINS PT., OCCOHANNOCK CREEK	T											
-75.9929	37.8293	8633532	TANGIER ISLAND, CHESAPEAKE BAY	T											
-76.96	38.2517	8635150	COLONIAL BEACH, POTOMAC RIVER	T							6				
-77.243	38.2133	8635257	RAPPAHANNOCK BEND	T											
-76.4644	37.9959	8635750	LEWISETTA, POTOMAC RIVER	T						6	6	6			
-76.7833	37.8733	8635985	WARES WHARF, RAPPAHANNOCK RIVER	T											
-76.29	37.6144	8636580	WINDMILL POINT, RAPPAHANNOCK RIVER	T						6	6	6			
-76.2733	37.3467	8637289	NEW POINT	T											
-76.2217	37.2567	8637590	NEW POINT, COMFORT SHOAL	T											
-76.5	37.2467	8637624	GLOUCESTER POINT, YORK RIVER	T						6	6				
-76.4783	37.2267	8637689	YORKTOWN USCG TRAINING CENTER, YORK R.	T								6			
-76.3991	36.8232	8638339	WESTERN BRANCH	T											
-76.6683	37.0567	8638421	BURWELL BAY, JAMES RIVER	T											
-76.6633	37.22	8638424	KINGSMILL, JAMES RIVER	T							6				
-76.7833	37.185	8638433	SCOTLAND, JAMES RIVER	T							6				
-76.9117	37.4033	8638445	LANEXA, CHICAHOMINY RIVER	T											
-76.9433	37.2399	8638450	TETTINGTON, JAMES RIVER	T											
-76.33	36.9467	8638610	SEWELLS POINT, HAMPTON ROADS	T						6	6		1h	1h	
-76.292	36.8217	8638660	PORTSMOUTH, NORFOLK NAVAL SHIPYARD	T											
-76.1133	36.9667	8638863	CHESAPEAKE BAY BRIDGE TUNNEL	T						6	6			1h	
-75.9698	36.8318	8639207	INSIDE CHANNEL, RUDEE INLET	T											
-76.3017	36.778	8639348	MONEY POINT, S. BR. ELIZABETH RIVER	T						6	6				
-75.7467	36.1833	8651370	DUCK, FRF PIER	T					1h	6	6			1h	
-75.7689	35.9037	8652247	MANNS HARBOR, CROATAN SOUND	T											
-75.6565	35.8448	8652437	OYSTER CREEK, CROATAN SOUND	T											
-75.7	35.8117	8652547	ROANOKE MARSHES LIGHT, CROATAN SOUND	T											
-75.5494	35.7943	8652587	OREGON INLET MARINA, PAMLICO SOUND	T						6	6				
-75.635	35.2233	8654400	CAPE HATTERAS FISHING PIER	T					1h	6	6			1h	
-75.7042	35.2095	8654467	USCG STATION HATTERAS, PAMLICO SOUND	T											
-75.9895	35.1156	8654792	OCRACOKE ISLAND	T											
-76.3433	34.875	8655875	SEA LEVEL, CORE SOUND	T											
-76.67	34.72	8656483	BEAUFORT, DUKE MARINE LAB	T						6	6				
-76.7117	34.6933	8656590	ATLANTIC BEACH TRIPLE S PIER	T						6					
-77.9533	34.2267	8658120	WILMINGTON, CAPE FEAR RIVER	T					1h	6	6		1h	1h	
-77.7857	34.2133	8658163	WRIGHTSVILLE BEACH	T											
-78.0183	33.915	8659084	SOUTHPORT	T											
-78.0817	33.9017	8659182	OAK ISLAND, ATLANTIC OCEAN	T											
-78.5067	33.865	8659897	SUNSET BEACH PIER, ATLANTIC OCEAN	T											
-78.9183	33.655	8661070	SPRINGMAID PIER, ATLANTIC OCEAN	T					1h	6	6			1h	
-79.9214	33.0088	8664022	GEN. DYNAMICS PIER, COOPER R.	T											
-79.83	32.9267	8664545	CAINHOY, WANDO RIVER	T											
-79.7067	32.8567	8664941	SOUTH CAPERS ISLAND, CAPERS CREEK	T							6				
-80.0217	32.8367	8665099	I-526 BRIDGE, ASHLEY RIVER	T											
-79.9238	32.7817	8665530	CHARLESTON, COOPER RIVER ENTRANCE	T					1h	6	6				
-80.7841	32.5025	8667633	CLARENDON PLANTATION, WHALE BR.	T											
-80.465	32.34	8668498	HUNTING ISLAND PIER, FRIPPS INLET	T											
-80.7367	32.2667	8668918	RIBAUT ISLAND, SKULL CREEK	T											
-80.9017	32.0337	8670870	FORT PULASKI, SAVANNAH RIVER	T					1h	6					
-81.3967	31.1317	8677344	ST SIMONS LIGHTHOUSE, ST SIMONS ISLAND	T						6					
-81.5132	30.7978	8679511	KINGS BAY	T											
-81.4717	30.7633	8679758	DUNGENESS, SEACAMP DOCK	T											
-81.5483	30.72	8679964	ST. MARYS, ST. MARYS RIVER	T											
-81.465	30.7083	8720011	CUT 1N FRONT RANGE, ST MARYS RIVER ENTR	T											
-81.3017	30.7167	8720012	CUT 2N FRONT RANGE, ST MARYS RIVER ENTR	T											
-81.4654	30.6717	8720030	FERNANDINA BEACH, AMELIA RIVER	T						6					
-81.5233	30.6433	8720051	LANCEFORD CREEK, LOFTON	T											
-81.515	30.5683	8720098	NASSAUVILLE, NASSAU RIVER EAST	T											
-81.4133	30.4	8720211	WWTD, MAYPORT NAVAL STA., ST JOHNS RIVER	T											
-81.43	30.3967	8720218	BAR PILOTS DOCK, ST JOHNS RIVER	T											
-81.5583	30.3867	8720219	DAMES POINT, ST. JOHNS RIVER	T											
-81.4317	30.3933	8720220	MAYPORT (FERRY DEPOT), SAINT JOHNS RIVER	T					1h	6					
-81.6341	30.3834	8720225	PHOENIX PARK	T											
-81.62	30.36	8720242	LONGBRANCH (USE-DDP), ST JOHNS RIVER	T											
-81.3867	30.2833	8720291	JACKSONVILLE BEACH	T											
-81.6916	30.1917	8720357	I-295 BRIDGE, WEST END, ST JOHNS RIVER	T											
-81.6283	29.9783	8720503	RED BAY POINT, ST JOHNS RIVER	T						6					
-81.3	29.9167	8720554	VILANO BEACH (ICWW)	T											
-81.3067	29.8667	8720582	STATE ROAD 312, MATANZAS RIVER	T											
-81.2633	29.8567	8720587	ST. AUGUSTINE BEACH, ATLANTIC OCEAN	T						6					

-81.5483	29.8017	8720625	RACY POINT, ST JOHNS RIVER	T											
-81.2583	29.7683	8720651	CRESCENT BEACH, MATANZAS RIVER	T											
-81.2279	29.7045	8720692	STATE ROAD A1A BRIDGE	T											
-81.205	29.615	8720757	BINGS LANDING, MATANZAS RIVER	T											
-81.6817	29.595	8720767	BUFFALO BLUFF, ST. JOHNS RIVER	T											
-81.6317	29.6433	8720774	PALATKA, ST. JOHNS RIVER	T											
-81.6752	29.4768	8720832	WELAKA, ST. JOHNS RIVER	T							6				
-81.005	29.2283	8721020	DAYTONA BEACH (OCEAN)	T											
-80.5935	28.4158	8721604	TRIDENT PIER, PORT CANAVERAL	T				6		6					
-80.6015	28.4087	8721608	CANAVERAL HARBOR ENTRANCE	T											
-80.3717	27.6317	8722125	VERO BEACH, INDIAN RIVER	T											
-80.325	27.4717	8722208	NORTH BEACH CAUSEWAY, INDIAN RIVER	T											
-80.0667	26.8433	8722548	PGA BOULEVARD BRIDGE, PALM BEACH	T											
-80.051	26.77	8722588	PORT OF W. PALM BEACH, LAKE WORTH	T											
-80.0467	26.6133	8722669	LAKE WORTH INTRACOASTAL WATERWAY	T											
-80.0333	26.6117	8722670	LAKE WORTH PIER, ATLANTIC OCEAN	T											
-80.12	25.9033	8723080	HAULOVER PIER, N. MIAMI BEACH	T											
-80.1315	25.7683	8723170	MIAMI BEACH (CITY PIER)	T											
-80.13	25.7633	8723178	MIAMI BEACH, GOVERNMENT CUT	T											
-80.1618	25.7314	8723214	VIRGINIA KEY, BISCAYNE BAY	T				6							
-81.0167	24.7183	8723962	KEY COLONY BEACH	T											
-81.105	24.7117	8723970	VACA KEY, FLORIDA BAY	T				6							
-81.8079	24.5557	8724580	KEY WEST	T				6							
-81.8783	24.4533	8724635	SAND KEY LIGHTHOUSE	T											
-81.9215	24.7183	8724671	SMITH SHOAL LIGHT, FL	T											
-82.92	24.6317	8724698	LOGGERHEAD KEY, DRY TORTUGAS	T				6							
-81.8075	26.1317	8725110	NAPLES, GULF OF MEXICO	T	6			6							
-81.8712	26.6477	8725520	FORT MYERS, CALOOSAHATCHEE RIVER	T	6			6							
-82.76	27.6017	8726347	EGMONT KEY, TAMPA BAY	T											
-82.7267	27.615	8726364	MULLET KEY, TAMPA BAY	T											
-82.5621	27.6387	8726384	PORT MANATEE, TAMPA BAY	T	6			6							
-82.6269	27.7606	8726520	ST. PETERSBURG, TAMPA BAY	T	6			6							
-82.5538	27.8578	8726607	PORT TAMPA, OLD TAMPA BAY	T	6										
-82.425	27.9133	8726667	CSX ROCKPORT, MCKAY BAY ENTRANCE	T	6			6							
-82.8317	27.9783	8726724	CLEARWATER BEACH, GULF OF MEXICO	T	6	6		6							
-82.685	27.9883	8726738	SAFETY HARBOR, OLD TAMPA BAY	T											
-82.6383	28.6917	8727235	JOHNS ISLAND, CHASSAHOWITZKA BAY	T											
-82.6383	28.7617	8727274	MASON CREEK, HOMOSASSA BAY	T											
-82.6954	28.7717	8727277	TUCKERS ISLAND, HOMOSASSA RIVER	T											
-82.6033	28.8006	8727293	HALLS RIVER BRIDGE, HALLS RIVER	T											
-82.6583	28.825	8727306	OZELLO	T											
-82.6667	28.8633	8727328	OZELLO NORTH	T											
-82.7233	28.87	8727333	MSNGROVE POINT, CRYSTAL BAY	T											
-82.635	28.8817	8727336	DIXIE BAY	T											
-82.6383	28.9051	8727348	TWIN RIVERS MARINA, CRYSTAL RIVER	T											
-82.6917	28.9233	8727359	SHELL ISLAND, CRYSTAL RIVER	T											
-83.0317	29.135	8727520	CEDAR KEY, GULF OF MEXICO	T	6	6	6	6							
-84.29	30.0587	8728229	SHELL POINT, WALKER CREEK	T											
-84.5117	29.915	8728360	TURKEY POINT	T											
-84.9814	29.7267	8728690	APALACHICOLA, APALACHICOLA RIVER	T	6	6	6	6							
-85.6669	30.1523	8729108	PANAMA CITY, ST. ANDREW BAY	T	6	6	6	6							
-85.8783	30.2133	8729210	PANAMA CITY BEACH, GULF OF MEXICO	T		6	6	6							
-86.4933	30.5033	8729501	VALPARISO, BOGGY BAYOU	T											
-86.865	30.3767	8729678	NAVARRE BEACH	T											
-87.3567	30.4186	8729905	MILLVIEW, PERDIDO BAY	T											
-87.4288	30.3869	8729941	BLUE ANGELS PARK, PERDIDO BAY	T											
-87.6843	30.2798	8731439	GULF SHORES, ICWW	T											
-87.9345	30.4866	8733821	POINT CLEAR, MOBILE BAY	T											
-88.075	30.25	8735180	DAUPHIN ISLAND, MOBILE BAY	T	6	6	6								
-88.088	30.5652	8735391	STATE HIGHWAY 163 BRIDGE, DOG RIVER	T											
-88.0401	30.7083	8737048	MOBILE STATE DOCKS, MOBILE RIVER	T	6										
-88.5333	30.34	8741196	PASCAGOULA POINT, MISS. SOUND	T											
-88.6667	30.2383	8742221	HORN ISLAND, MISSISSIPPI SOUND	T		6	6								
-88.7983	30.3917	8743281	OCEAN SPRINGS	T		6	6								
-88.9033	30.4118	8744117	BILOXI, BAY OF BILOXI	T		6	6								
-89.0817	30.36	8745557	GULFPORT HARBOR, MISSISSIPPI SOUND	T	6	6									
-89.3258	30.3264	8747437	BAY WAVELAND YACHT CLUB, BAY ST. LOUIS	T	6										
-89.3667	30.2817	8747766	WAVELAND, MISSISSIPPI SOUND	T		6	6								
-89.0445	29.2008	8760417	DEVON ENERGY FACILITY, NORTH PASS	T	6										
-89.14	28.99	8760551	SOUTH PASS	T											
-89.2583	29.1783	8760721	PILOTTOWN	T											
-89.3512	29.2733	8760849	VENICE, GRAND PASS	T											
-89.4075	28.9322	8760922	PILOTS STATION EAST, SOUTHWEST PASS, LA	T	6	6									
-89.4183	28.925	8760943	PILOT STATION, SW PASS	T											
-89.6733	29.8681	8761305	SHELL BEACH, LAKE BORGNE	T	6										
-89.835	29.945	8761529	MARTELLO CASTLE, LAKE BORGNE	T											
-90.0383	29.4017	8761819	TEXACO DOCK, HACKBERRY BAY	T											
-90.1134	30.0272	8761927	USCG NEW CANAL STA., LAKE PONTCHARTRAIN	T	6										
-90.2086	29.1143	8762075	PORT FOURCHON, BELLE PASS	T	6	6	6								
-90.976	29.1739	8763535	TEXAS GAS PLATFORM, CAILLOU BAY	T											
-91.23	29.7433	8764025	STOUTS PASS AT SIX MILE LAKE	T											
-91.2375	29.6675	8764044	BERWICK, ATCHAFALAYA RIVER, LA	T	6	6									
-91.3381	29.455	8764227	LAWMA, AMERADA PASS	T											
-91.385	29.3717	8764311	EUGENE ISLAND	T											

-91.88	29.7134	8765251	CYPREMORT POINT	T	6	6								
-93.2217	30.2236	8767816	LAKE CHARLES, CALCASIEU RIVER	T										
-93.9313	29.8667	8770475	PORT ARTHUR, SABINE NACHES CANAL	T	6	6								
-93.8817	29.98	8770520	RAINBOW BRIDGE, NECHES RIVER	T	6	6								
-93.895	29.7667	8770539	MESQUITE POINT	T										
-94.6904	29.7133	8770559	ROUND POINT, TRINITY BAY	T										
-93.8701	29.7284	8770570	SABINE PASS NORTH	T	6	6								
-93.7217	30.0983	8770597	ORANGE (OLD NAVY BASE)	T										
-94.985	29.6817	8770613	MORGANS POINT, BARBOURS CUT	T	6									
-94.8683	29.68	8770625	UMBRELLA POINT, TRINITY BAY	T										
-95.0783	29.765	8770733	LYNCHBURG LANDING, SAN JACINTO RIVER	T										
-95.09	29.7567	8770743	BATTLESHIP TEXAS S.P, HOUSTON SHIP CHANN	T	6									
-95.2658	29.7258	8770777	MANCHESTER, HOUSTON SHIP CHANNEL	T	6									
-93.8369	29.6781	8770822	TEXAS POINT, SABINE PASS	T										
-95.0667	29.5633	8770933	CLEAR LAKE	T										
-94.5133	29.515	8770971	ROLLOVER PASS	T										
-94.9183	29.48	8771013	EAGLE POINT, GALVESTON BAY	T	6									
-93.64	29.4983	8771081	SABINE OFFSHORE	T										
-94.78	29.365	8771328	PORT BOLIVAR, BOLIVAR ROADS	T										
-94.7248	29.3573	8771341	GALVESTON BAY ENTRANCE, NORTH JETTY	T	6									
-94.7933	29.31	8771450	GALVESTON PIER 21, GALVESTON CHANNEL	T	6									
-94.7894	29.2853	8771510	GALVESTON PLEASURE PIER, GULF OF MEXICO	T	6									
-95.3083	28.9483	8772440	FREEPORT, DOW BARGE CANAL	T										
-95.3025	28.9431	8772447	USCG FREEPORT, FREEPORT ENTR CHANNEL	T										
-96.7117	28.408	8773037	SEADRIFT, SAN ANTONIO BAY	T										
-96.595	28.64	8773259	PORT LAVACA, LAVACA CAUSEWAY	T										
-96.3883	28.4517	8773701	PORT O'CONNOR, MATAGORDA BAY	T										
-97.0217	28.1183	8774513	COPANO BAY STATE FISHING PIER	T										
-97.0467	28.0217	8774770	ROCKPORT, ARANSAS BAY	T	6									
-97.475	27.8583	8775188	WHITE POINT BAY	T										
-97.0733	27.8389	8775237	PORT ARANSAS	T										
-97.05	27.8267	8775270	PORT ARANSAS, H. CALDWELL PIER	T										
-97.2033	27.8213	8775283	PORT INGLESIDE, CORPUS CHRISTI BAY	T										
-97.39	27.8117	8775296	TEXAS STATE AQUARIUM, CORPUS CHRISTI	T										
-97.28	27.705	8775421	CORPUS CHRISTI NAVAL AIR STATION	T										
-97.2367	27.6333	8775792	PACKERY CHANNEL	T										
-97.2167	27.58	8775870	CORPUS CHRISTI, GULF OF MEXICO	T	6									
-97.1767	26.0767	8779748	SOUTH PADRE ISLAND COAST GUARD STATION	T										
-97.1567	26.0683	8779750	PADRE ISLAND, BRAZOS SANTIAGO PASS	T										
-97.215	26.06	8779770	PORT ISABEL, LAGUNA MADRE	T	6									
-97.7805	22.262	9500966	MADERO, TAMPICO HARBOR, MEXICO	T										
-87.87	15.893	9650593	PUERTO CORTES	T										
-78.997	26.71	9710441	SETTLEMENT POINT, GRAND BAHAMAS	T										
-64.721	18.368	9751309	LEINSTER POINT, LEINSTER BAY, ST. JOHN'S	T										
-64.705	17.75	9751364	CHRISTIANSTED, ST. CROIX ISLAND	T										
-64.7148	18.3456	9751373	ST JOHN'S ISLAND, CORAL HARBOR	T										
-64.724	18.318	9751381	LAMESHUR BAY, ST. JOHN	T										
-64.7541	17.695	9751401	LIME TREE BAY, ST CROIX	T										
-64.804	18.6309	9751467	LOVANGO CAY, ST JOHN	T										
-64.818	18.297	9751494	DOG ISLAND, ST THOMAS	T										
-64.8691	18.3187	9751567	BENNER BAY	T										
-64.864	18.3487	9751583	WATER BAY, SAINT THOMAS	T										
-64.884	17.713	9751584	FREDERICKSTED, ST. CROIX ISLAND	T										
-64.9203	18.3357	9751639	CHARLOTTE AMALIE, ST. THOMAS	T										
-64.9627	18.3711	9751768	RUY POINT, ST THOMAS	T										
-65.035	18.363	9751774	BOTANY BAY, ST THOMAS	T										
-65.302	18.301	9752235	CULEBRA	T										
-65.444	18.153	9752619	ISABEL SEGUNDA, VIEQUES ISLAND	T										
-65.471	18.094	9752695	ESPERANZA, VIEQUES ISLAND	T										
-65.57	18.345	9752962	ISLA PALOMINOS	T										
-65.631	18.335	9753216	PLAYA DE FAJARDO	T										
-65.711	18.187	9753641	NAGUABO	T										
-65.833	18.055	9754228	YABUCOA HARBOR	T										
-66.116	18.459	9755371	SAN JUAN, LA PUNTILLA, SAN JUAN BAY	T										
-66.158	17.928	9755679	LAS MAREAS	T										
-66.407	17.9539	9756639	SANTA ISABEL	T										
-66.7021	18.4814	9757809	ARECIBO, PUERTO RICO	T										
-66.762	17.973	9758053	PENUELAS, PUNTA GUAYANILLA,CARIBBEAN SEA	T										
-67.046	17.97	9759110	MAGUEYES ISLAND, CARIBBEAN SEA	T										
-67.189	18.075	9759189	PUERTO REAL	T										
-67.197	17.951	9759197	BAHIA SALINAS	T										
-67.1608	18.2179	9759394	MAYAGUEZ, PUERTO RICO	T										
-67.165	18.457	9759412	AGUADILLA, CRASHBOAT BEACH	T										
-67.1853	18.165	9759421	PUNTA GUANAJABO, MAYAGUES	T										
-67.939	18.09	9759938	MONA ISLAND	T										
-61.821	17.5904	9761115	BARBUDA	T										
-93.3007	30.1903	8767961	Bulk Terminal #1											
-93.3429	29.7682	8768094	CALCASIEU PASS, EAST JETTY		6	6								
-77.3734	37.2669	8638489	PUDDLEDOCK, APPOMATTOX RIVER											
-77.4206	37.5245	8638495	RICHMOND RIVER LOCKS, JAMES RIVER											
-76.99	37.5833	8636653	LESTER MANOR											
-76.9392	38.9324	8579997	BLADENSBURG, ANACOSTIA RIVER											

14. APPENDIX D – NON-ZERO MEAN ELEVATION TREND

Investigation of model performance led to the identification of a persistent non-zero mean elevation trend in several rivers and sheltered water bodies. While the rivers might be expected to have a higher mean water level, the concern is that these tide-only, mean sea level simulations should not exhibit this behavior.

Stations exhibiting this behavior were identified by evaluating the ratio of the standard deviation and mean water elevations from modeled time series. Figure 14-1shows geographic locations of some of these locations surpassing a specified criterion. Table 14-1 lists names of several stations where the non-zero mean elevation trend was observed specifically.

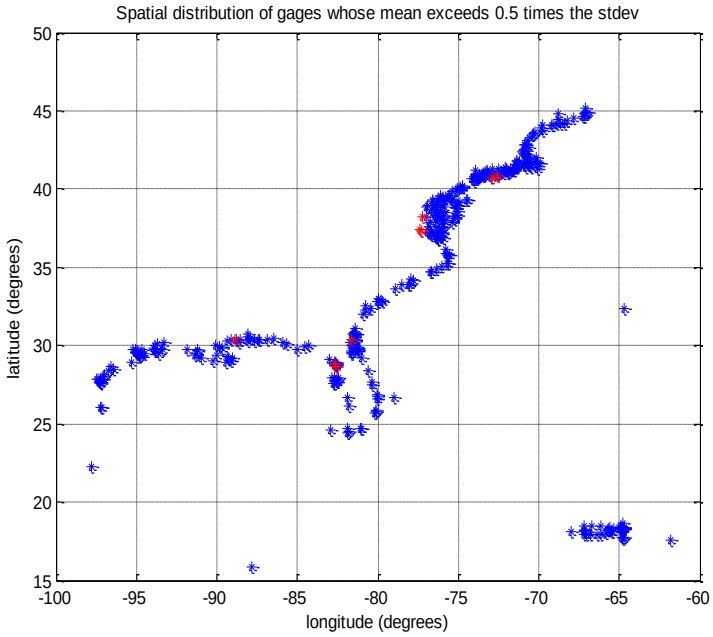

Figure 14-1: Red asterisks represent stations where mean water elevations are greater than 0.5 times the standard deviation of the water elevation and whose standard deviation is greater than 0.1 meters; blue asterisks are stations are within those tolerances.

In all instances, the stations are in narrow, sheltered waters away from the open coast and tend to be in areas with appreciable marsh or lowland coverage. Figure 14-2 shows the configuration of the St Johns River channel and the positioning of several of the gages exhibiting an increasing mean elevation trend. There is some periodicity of the mean elevation at roughly half a lunar cycle (about 14 days), indicating a potential relationship to the varying amplitudes of the tides that have the same period. Figure 14-3 through Figure 14-6 show several examples of the mean trend shift evident in 60-day time series from simulation results at stations in Florida (where the trend was first noticed and is largest), New York, Texas, Mississippi, and Louisiana. The Atlantic stations shown in the figures all have similar upward mean elevation trends with weak beat patterns. Stations in the Gulf of Mexico also have self-similar upward trends but have much stronger beat patterns than the Atlantic stations. Station time series shown in the figures for both basins show related periodicity of the tide beat and the mean elevation, with minima in both the signal envelope and in the mean elevation occurring around days 21, 34, and 49.

Table 14-1 Stations with identified non-zero mean elevation trend.

CO-OPS Station ID	*Station Name*	*State*	*Longitude*	*Latitude*
8720225	Phoenix Park	FL	-81.6309	30.38417
8720625	Racy Point, St Johns River	FL	-81.5494	29.80018
8720357	I-295 Bridge, West End, St Johns River	FL	-81.6873	30.19167
8514322	Patchogue, Patchogue River	NY	-73.0004	40.74627
8513825	Smith Point Bridge, Narrow Bay	NY	-72.8681	40.73851
8775188	White Point Bay	TX	-97.475	27.8583
8774770	Rockport, Aransas Bay	TX	-97.0463	28.02124
8774513	Copano Bay State Fishing Pier	TX	-97.0217	28.1183
8744117	Biloxi, Bay of Biloxi	MS	-88.9004	30.41646
8765251	Cypremort Point	LA	-91.88	29.7134
8761927	USCG New Canal Sta., Lake Pontchartrain	LA	-90.1134	30.0272

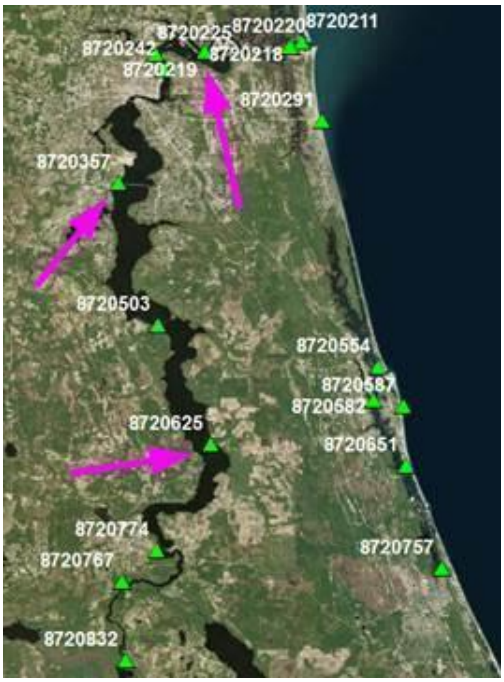

Figure 14-2: NOAA CO-OPS stations in the vicinity of the St. Johns River; arrows indicate stations plotted in Figure 14-3.

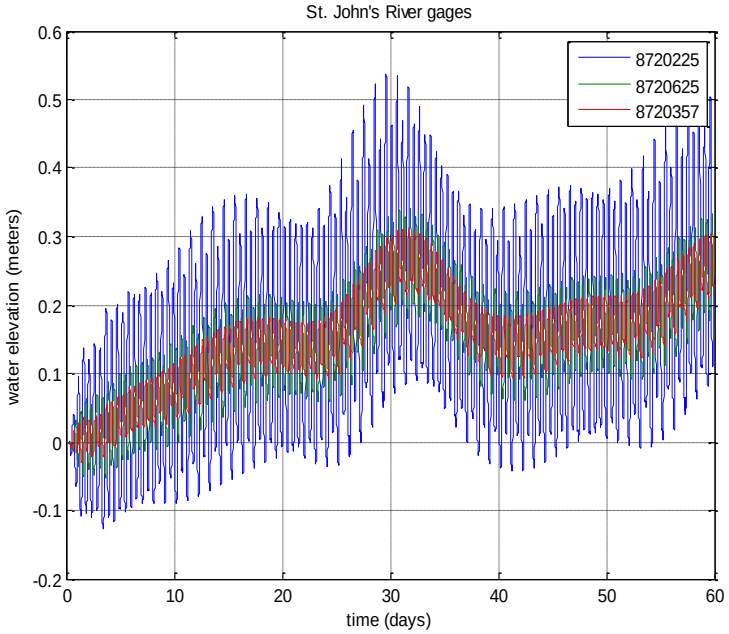

Figure 14-3: Time series of modeled water elevations along St. Johns River.

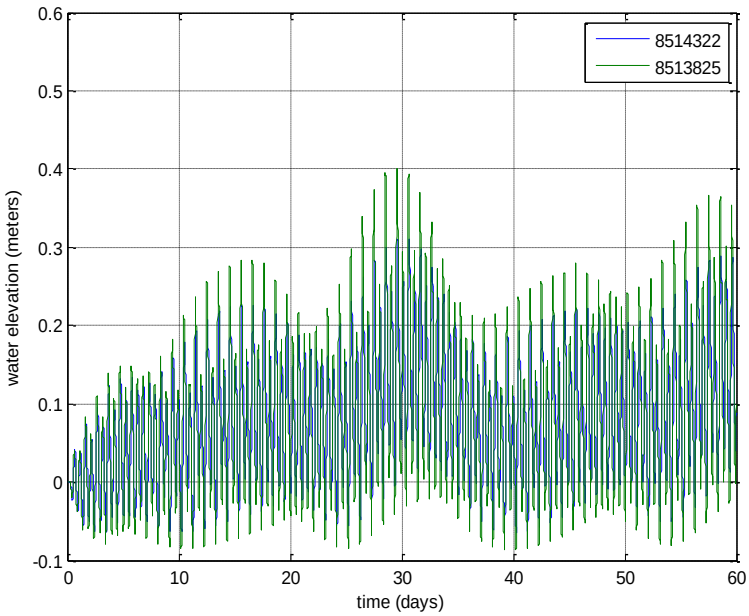

Figure 14-4: Sheltered southeastern Long Island stations exhibiting the beat pattern and non-zero trend.

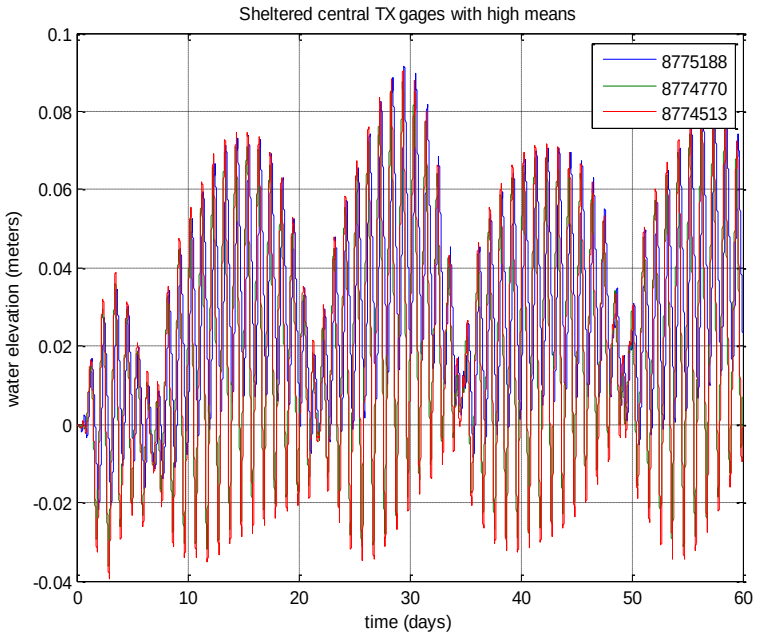

Figure 14-5: Sheltered Texas gages exhibiting the beat pattern and non-zero trend.

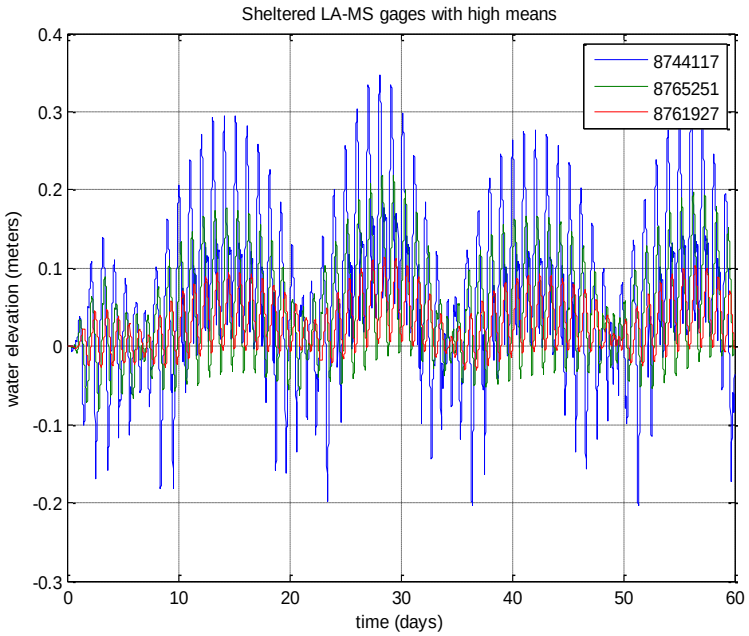

Figure 14-6: Sheltered Louisiana and Mississippi stations exhibiting the beat pattern and non-zero trend.

The non-zero mean trend was first noticed in the St. Johns River, due to the relatively large magnitude of the shift. Longer simulations showed a persistent positive mean elevation shift, though there are significant fluctuations and not a consistent upward trend as might be extrapolated from the last portion of the 60-day simulation time series shown above. A review of ADCIRC modeling in the St. Johns River region performed by the CHAMPS Lab at the University of Central Florida and also ADCIRC work done by the contractor performing the FEMA storm surge modeling in this area, showed the NOMAD mesh to be unique in exhibiting this behavior.

After detailed investigation (Dietrich et al. 2004, 2005), it was found that ADCIRC's wetting and drying algorithm is the cause of this issue. It is found in sections of the mesh with a broad, flat, low-lying area (such as a marsh or tidal flat) that is wetted during regular tidal cycles and is connected to deeper channels. As the tide goes out, water flows off of the high ground quickly, causing the water depth H to drop down below 0.8H0, where H0 is the user-input minimum depth. When this happens, ADCIRC adds mass to the system to bring the water depth back up to H=0.8H0 as diagrammed in Figure 14-7.

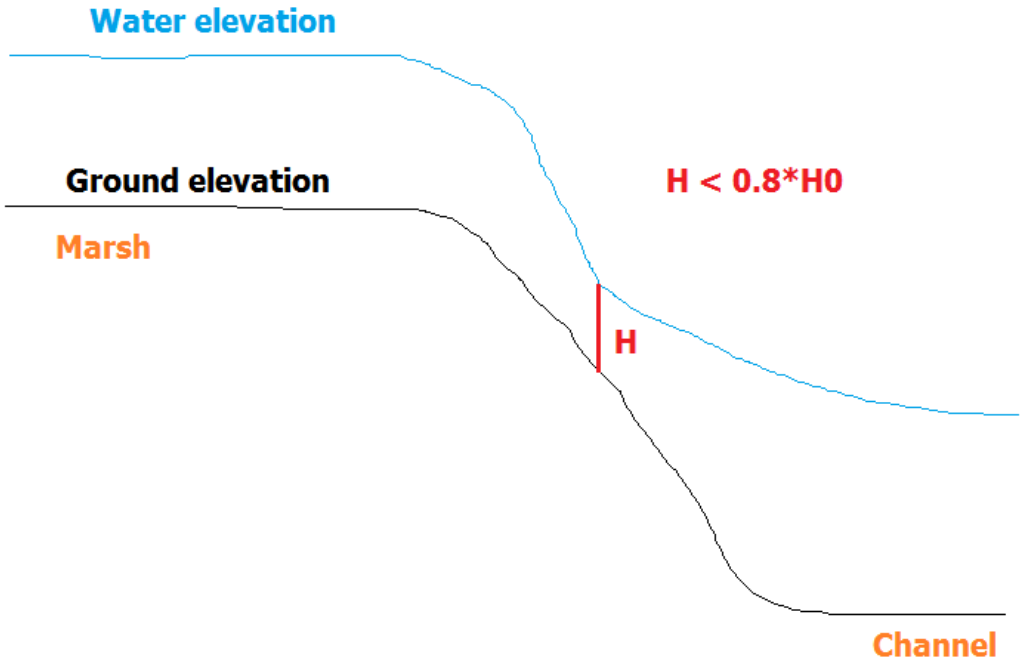

Figure 14-7 Schematic of wetting and drying issue.

This was noted in several areas, including the southern tip of the Delmarva Peninsula. As can be seen in Figure 14-8 and Figure 14-9, the model solution at a given time step corresponds only to the channel geometry, with water levels across the marshes staying artificially elevated. The transect profile demonstrates how the water elevation dips down to just below H0 as it transitions into the channel. The same pattern can be seen in several other areas as shown in Figure 14-10.

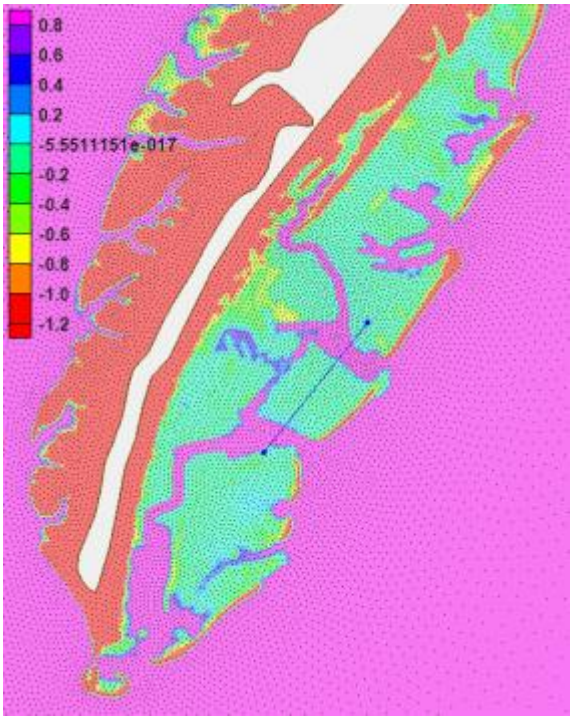

Figure 14-8 Topography in the Delmarva Peninsula, blue line is the transect line also shown in the following figure.

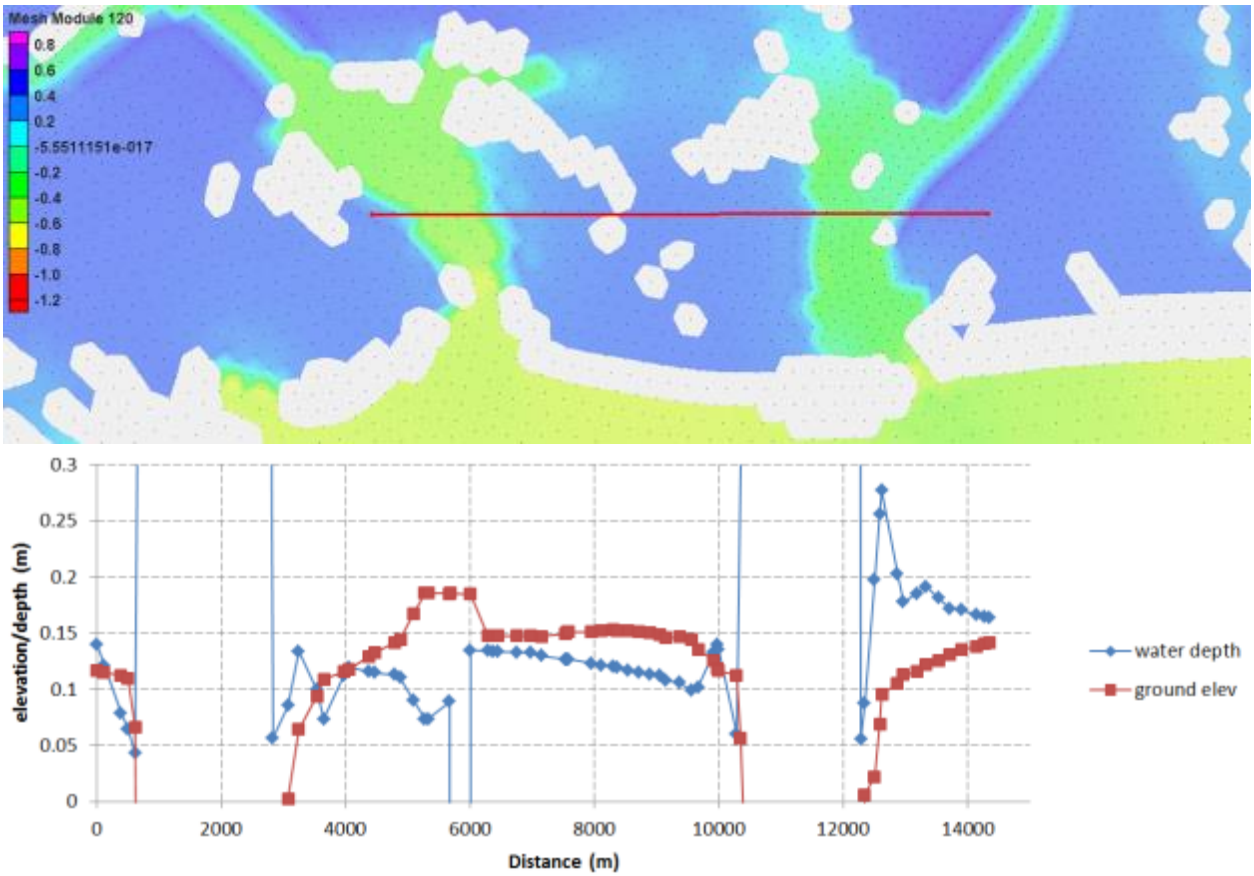

Figure 14-9 Water elevation solution at one time step and red transect line (top), profile plot along transect line of the water depth and ground elevation (bottom), H0=0.05 meters.

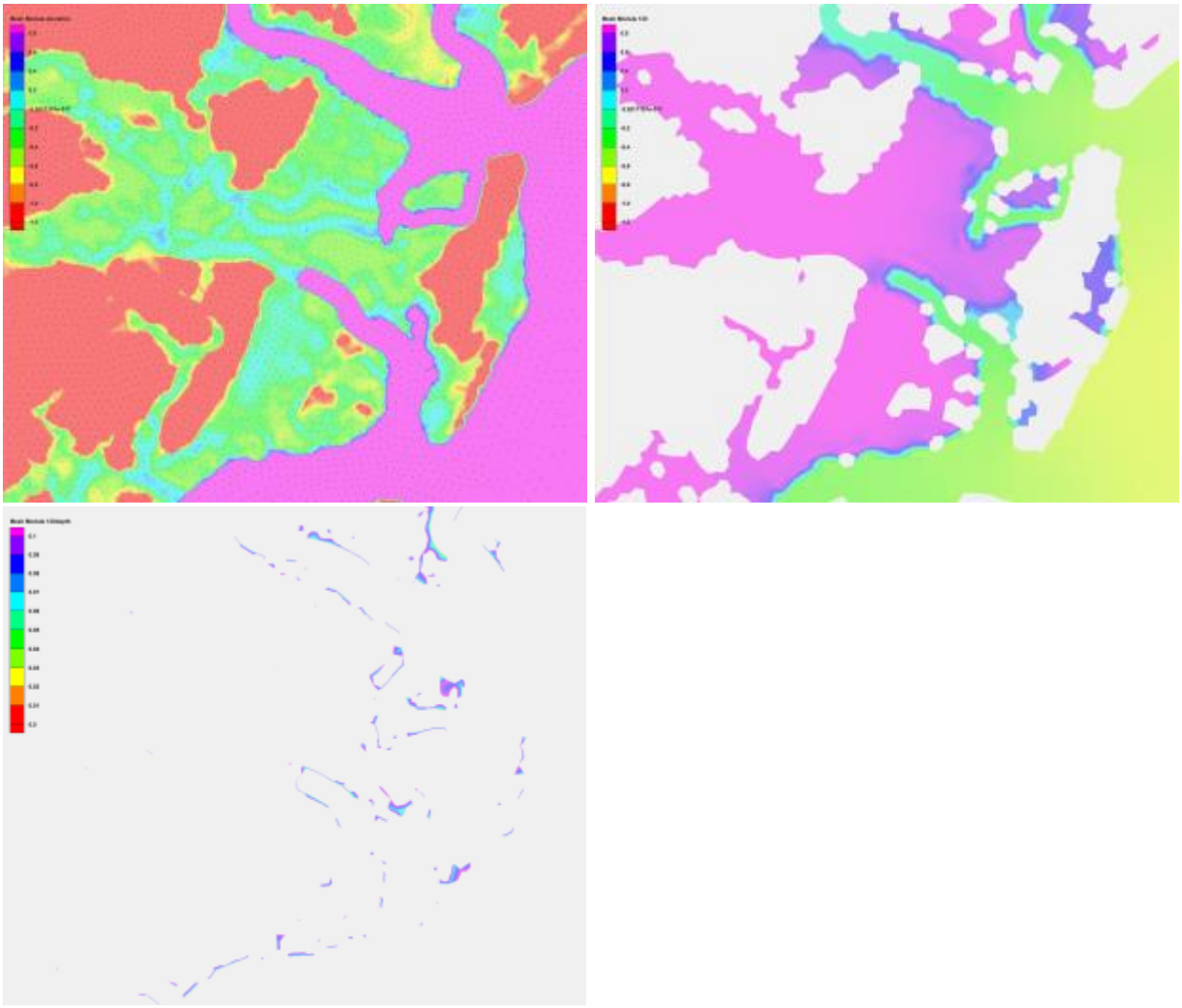

Figure 14-10 Sample area of topography (top left) indicates where wetting/drying issue will cause erroneous water elevations (right), and the corresponding areas of the water elevation solution whose depths are below the minimum wetting depth H0=0.1 m (bottom).

Although effect of the mean water elevation trend is largest in the St. John's, the root issue of areas staying wet artificially is most pervasive in the GA-SC area. It is also seen behind the barrier islands in southern NJ and parts of NC. The addition of mass into the system means that increasingly enclosed bodies will build up more mass than those that have easy access to the open ocean. If this effect is present near the mouth of a river or estuary, it will also artificially elevate the water level at the mouth, thereby partially preventing water from leaving the estuary. Elevated water levels are clearly visible in the Coastal marsh areas of from northern Florida, through Georgia, and into South Carolina as depicted in Figure 14-11.

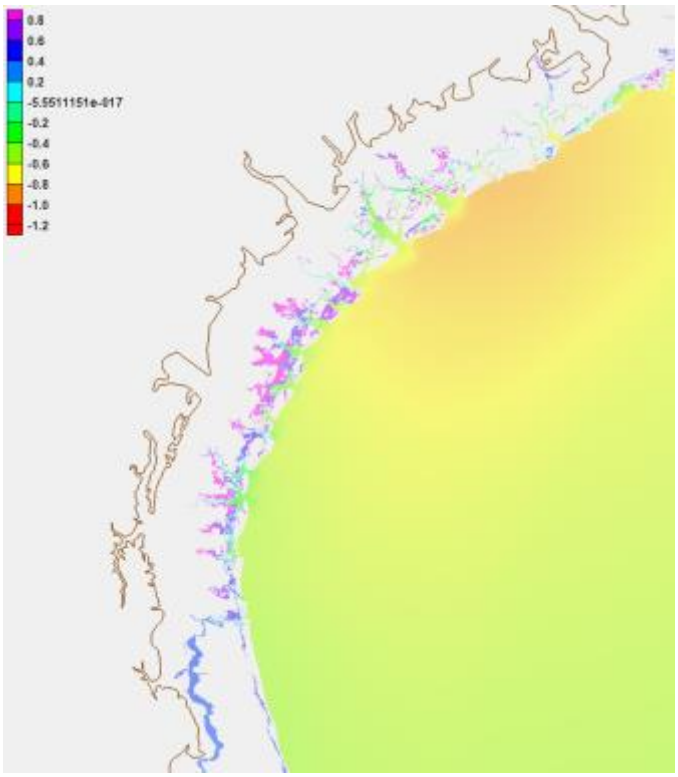

Figure 14-11 Water elevation at a single time step of a tidal run for the Florida-Georgia-South Carolina region; the St. John's River can be seen in the southern section of the figure, Bulls Bay is near the northern edge of the figure.